INTERNATIONAL DOCTORAL
SCHOOL OF THE USC

Marcos
Sánchez Carricoba

PhD Thesis

INTEGRAL ANALYSIS OF TIDAL STREAM ENERGY IN RIA DE ORTIGUEIRA

Santiago de Compostela, 2022

Doctoral Programme in Renewable Energy and Energy Sustainability

USC
UNIVERSIDADE
DE SANTIAGO
DE COMPOSTELA

DOCTORAL THESIS

INTEGRAL ANALYSIS OF TIDAL STREAM ENERGY IN RIA DE ORTIGUEIRA

Marcos Sánchez Carricoba

INTERNATIONAL PHD SCHOOL OF THE UNIVERSITY OF SANTIAGO DE COMPOSTELA

PHD PROGRAMME IN RENEWABLE ENERGY AND ENERGY SUSTAINABILITY

SANTIAGO DE COMPOSTELA

2022

USC
UNIVERSIDADE
DE SANTIAGO
DE COMPOSTELA

DECLARACIÓN DEL AUTOR DE LA TESIS

D. **Marcos Sánchez Carricoba**

Título de la tesis: **Integral analysis of tidal stream energy in Ria de Ortigueira**

Presento mi tesis, siguiendo el procedimiento adecuado al reglamento y declaro que:

1) La tesis abarca los resultados de la elaboración de mi trabajo.
2) De ser el caso, en la tesis se hace referencia a las colaboraciones que tuvo este trabajo.
3) Confirmo que la tesis no incurre en ningún tipo de plagio de otros autores ni de trabajos presentados por mí para la obtención de otros títulos.
4) La tesis es la versión definitiva presentada para su defensa y coincide la versión impresa con la presentada en formato electrónico.

Y me comprometo a presentar el Compromiso Documental de Supervisión en el caso que el original no esté depositado en la Escuela.

En Santiago de Compostela, mayo de 2022

Marcos Sánchez Carricoba
(Firma electrónica)

USC
UNIVERSIDADE
DE SANTIAGO
DE COMPOSTELA

AUTORIZACIÓN DE LOS DIRECTORES DE LA TESIS

INTEGRAL ANALAYSIS OF TIDAL STREAM ENERGY IN RIA DE ORTIGUEIRA

Prof. D Gregorio Iglesias Rodríguez
Dr. D. Rodrigo Carballo Sánchez

INFORMAN:

Que la presente tesis, se corresponde con el trabajo realizado por *D. Marcos Sánchez Carricoba*, bajo mi dirección/tutorización, y autorizo su presentación, considerando que reúne los requisitos exigidos en el Reglamento de Estudios de Doctorado de la USC, y que como director de esta no incurre en las causas de abstención establecidas en la Ley 40/2015.

De acuerdo con lo indicado en el Reglamento de Estudios de Doctorado, declara también que la presente tesis doctoral es idónea para ser defendida en base a la modalidad de *Monográfica con reproducción de publicaciones*, en los que la participación del doctorando fue decisiva para su elaboración y las publicaciones se ajustan al Plan de Investigación.

En Lugo, mayo de 2022

Prof. D. José Gregorio Iglesias Rodríguez
(Firma electrónica)

Dr. D. Rodrigo Carballo Sánchez
(Firma electrónica)

USC
UNIVERSIDADE
DE SANTIAGO
DE COMPOSTELA

LIST OF PAPERS INCLUDES IN THIS DOCTORAL THESIS

This thesis reproduces completely the following research papers:

Sanchez, M., Carballo, R., Ramos, V., & Iglesias, G. (2014). *Floating vs. bottom-fixed turbines for tidal stream energy: A comparative impact assessment* doi:https://doi.org/10.1016/j.energy.2014.05.096

Sánchez, M., Carballo, R., Ramos, V., & Iglesias, G. (2014a). *Energy production from tidal currents in an estuary: A comparative study of floating and bottom-fixed turbines* doi:https://doi.org/10.1016/j.energy.2014.09.053

USC
UNIVERSIDADE DE SANTIAGO DE COMPOSTELA

USC
UNIVERSIDADE
DE SANTIAGO
DE COMPOSTELA

ACKNOWLEDGEMENTS

First and foremost, I would like to express my sincere gratitude to my supervisors, Prof. Gregorio Iglesias and Prof. Rodrigo Carballo, for their invaluable advice, continuous support, and patience during my PhD study. Their immense knowledge and plentiful experience have encouraged me in all the time of my academic research and daily life.

I would also like to thank all my colleges of GICEMA, not only for their technical support on my day-to-day work, but also for sharing endless hours of amusement and entertainment during this period of my life.

Moreover, I cannot find words to express my gratitude to my family and my friends for their support. Without their tremendous understanding and encouragement in the past few years, it would be impossible for me to complete my study.

Finally, last but not least, I would like to express my sincerest thanks to Paula Varela for absolutely everything.

This Thesis is dedicated to all of them.

During this work the author of the Thesis have been supported by the *I2C grants PRE/2011/236* (Plan Galego de Investigación Innovación e Crecemento 2011–2015) of Xunta de Galicia and the *Grants for training university teachers – FPU* (Plan Estatal de Investigación Científica y Técnica y de Innovación 2013-2016) of Spanish Ministry of Education, Culture and Sports.

USC
UNIVERSIDADE
DE SANTIAGO
DE COMPOSTELA

INDEX

SUMMARY **13**
RESUMO **15**
RESUMEN **17**
RESUMO EXTENDIDO EN GALEGO **19**
RESUMEN EXTENDIDO EN ESPAÑOL **29**
1. INTRODUCTION **39**
2. OBJECTIVES **41**
3. ENERGY PRODUCTION FROM TIDAL CURRENTS IN AN ESTUARY: A COMPARATIVE STUDY OF FLOATING AND BOTTOM-FIXED TURBINES **43**
ABSTRACT 43
3.1. INTRODUCTION 44
3.2. METHODOLOGY 45
3.2.1. Three-dimensional hydrodynamics model 45
3.2.2. TSTs modelling 46
3.2.3. Performance analysis 47
3.3. APPLICATION TO RIA DE ORTIGUEIRA 48
3.3.1. Study site and proposed tidal plants 48
3.3.2. Model implementation 49
3.3.3. Model validation 51
3.4. POWER PERFORMANCE ANALYSIS 53
3.5. CONCLUSIONS 56
4. FLOATING VS. BOTTOM FIXED TURBINES FOR TIDAL STREAM ENERGY: A COMPARETIVE IMPACT ASSESMENT **59**
ABSTRACT 59
4.1. INTRODUCTION 60
4.2. STUDY AREA 61
4.3. NUMERICAL MODEL DESCRIPTION 63
4.3.1. Governing equations 63
4.3.2. Model set-up 64
4.4. RESULTS 66
4.4.1. Model validation 66

USC UNIVERSIDADE DE SANTIAGO DE COMPOSTELA

4.4.2. Assessment of the impacts on the estuarine circulation 69
4.5. CONCLUSIONS 73
5. EFFECTS OF TIDAL STREAM ENERGY EXPLOITATION ON ESTUARINE CIRCULATION AND ITS SEASONAL VARIABILITY 75
ABSTRACT 75
5.1. INTRODUCTION 75
5.2. STUDY AREA 77
5.3. MATERIALS AND METHODS 78
5.3.1. Field data 78
5.3.2. Numerical model (I): equations 79
5.3.3. Numerical model (II): implementation 80
5.3.4. Tide-driven residual circulation 83
5.3.5. Case studies 83
5.4. RESULTS AND DISCUSSION 84
5.4.1. Unaltered conditions 84
5.4.2. Altered conditions 88
5.5. CONCLUSIONS 92
6. CONCLUSIONS 95
REFERENCES 99
FIGURE INDEX 107
TABLE INDEX 108
APPENDIX I. ARTICLES INCLUDES IN THIS DOCTORAL THESIS 109
1. ENERGY PRODUCTION FROM TIDAL CURRENTS IN AN ESTUARY: A COMPARATIVE STUDY OF FLOATING AND BOTTOM-FIXED TURBINES. 111
2. FLOATING VS. BOTTOM-FIXED TURBINES FOR TIDAL STREAM ENERGY: A COMPARATIVE IMPACT ASSESSMENT. 121
APPENDIX II. PREVIOUS WORKS: DETERMINATION OF LOCATION FOR TIDAL STREAM ENERGY EXPLOITATION IN RIA DE ORTIGUEIRA 133
AUTORITATION OF THE PUBLISHER FOR USING THE ARTICLES IN THIS DOCTORAL THESIS 143
ACEPTATION OF THE COAUTHORS FOR USING THE ARTICLES IN THIS DOCTORAL THESIS 145

USC UNIVERSIDADE DE SANTIAGO DE COMPOSTELA

SUMMARY

Overall, the areas with the greatest potential for tidal stream energy exploitation are located in coastal regions with complex hydrodynamic patterns, such as estuaries or bays, which in turn correspond to regions of great environmental importance. Therefore, for decision-making on harnessing the tidal energy resource, in addition to the selection of the conversion system to be used and the determination of its production, it is of great importance to carry out a detailed assessment of the environmental impacts produced. In this sense, through this Doctoral Thesis several factors involved in the use of tidal energy in the Ría de Ortigueira are studied, including the determination of the most appropriate conversion system, based on the analysis of annual yields and their intra-annual variability, and the impacts derived from energy use on transient and residual circulations. For this purpose, a 3D high-resolution numerical model is implemented for simulate the hydrodynamics of the estuary during different periods, with different combinations of boundary conditions and different tidal power plants. As a result of these simulations, it is determined that the performances of floating and bottom-fixed TSTs in the same location can differ greatly, depending on the characteristics of the hydrodynamic conditions of the coastal zone in which they operate. In the case studied, as a result of higher velocities near the surface, floating TSTs provide better performance than bottom-fixed devices. Likewise, it is observed that tidal stream energy exploitation can cause important impacts on the transient estuarine circulation, without finding significant differences between the impacts produced by the different conversion systems considered. In both cases, slight appreciable reductions in speed up to a few km away from the plant are observed, with impacts of greater magnitude in the vicinity of the plant. Finally, it is determined that, in general, when any of the considered tidal power plants operates, regardless of its configuration and the forcings, the general residual circulation pattern does not undergo significant modifications, being limited the greatest modifications in the magnitude of the circulation to the vicinities of the plant. In addition, the use of tidal energy barely affects the upwelling phenomena.

The results obtained in this Doctoral Thesis allow us to continue advancing in the research and development of renewable energies in Galicia, more specifically, marine renewable energies, which have great potential in this territory due to its privileged location in the South Atlantic Region of Europe.

Keywords: tidal stream energy exploitation; 3D numerical model; impact assessment; residual circulation; seasonal variability.

USC
UNIVERSIDADE DE SANTIAGO DE COMPOSTELA

USC
UNIVERSIDADE
DE SANTIAGO
DE COMPOSTELA

RESUMO

En xeral, as áreas con maior potencial para o aproveitamento enerxético das correntes de marea atópanse en rexións costeiras con patróns hidrodinámicos complexos, como estuarios ou baías, que á súa vez se corresponden con rexións de gran importancia ambiental. Polo tanto, para a toma de decisións sobre a explotación do recurso enerxético mareomotriz, ademais da selección do sistema de conversión a empregar e da determinación da súa produción, é de gran importancia realizar unha avaliación detallada dos impactos ambientais derivados. Neste sentido, mediante esta Tese Doutoral estúdanse diversos factores que interveñen no aproveitamento da enerxía mareomotriz na Ría de Ortigueira, incluíndo a determinación do sistema de conversión máis adecuado, baseada na análise dos rendementos anuais e a súa variabilidade intraanual, e os impactos derivados do aproveitamento enerxético sobre as circulacións transitoria e residual. Para iso, impleméntase un modelo numérico 3D de alta resolución que simula a hidrodinámica da ría durante diferentes períodos, con diferentes combinacións de condicións de contorno e diferentes plantas mareomotrices. A raíz destas simulacións, determínase que os rendementos dos TSTs flotantes e fixos no fondo na mesma localización poden diferir moito segundo as características das condicións hidrodinámicas da zona costeira na que operan. No caso estudado, como resultado das velocidades máis altas preto da superficie, os TSTs flotantes brindan un mellor rendemento que os dispositivos fixos no fondo. Así mesmo, obsérvase que a explotación da enerxía das correntes de marea pode causar impactos importantes na circulación transitoria estuarina, sen que se atopen diferenzas significativas entre os impactos producidos polos distintos sistemas de conversión considerados. En ambos os casos obsérvanse lixeiras reducións da velocidade apreciables ata algúns km de distancia da planta, e impactos de maior magnitude nas proximidades da planta. Finalmente, determínase que, en xeral, cando opera algunha das plantas mareomotrices analizadas, independentemente da súa configuración e os forzamentos considerados, o patrón da circulación residual xeneral non experimenta modificacións significativas, limitándose tamén as maiores modificacións da magnitude da circulación residual ás proximidades da planta. Ademais, o aproveitamento da enerxía mareomotriz apenas afecta os fenómenos de *upwelling*.

Os resultados obtidos nesta Tese Doutoral permiten seguir avanzando na investigación e desenvolvemento das enerxías renovables en Galicia, máis concretamente, as enerxías renovables mariñas, que teñen un gran potencial neste territorio pola súa localización privilexiada na Rexión do Atlántico Sur de Europa.

Palabras clave: explotación enerxética da correntes de marea; modelo numérico 3D; avaliación de impactos; circulación residual; variabilidade estacional.

USC
UNIVERSIDADE DE SANTIAGO DE COMPOSTELA

USC
UNIVERSIDADE
DE SANTIAGO
DE COMPOSTELA

RESUMEN

En general, las áreas con mayor potencial para el aprovechamiento energético de las corrientes de marea se encuentran en regiones costeras con patrones hidrodinámicos complejos, como estuarios o bahías, que a su vez se corresponden con regiones de gran importancia ambiental. Por lo tanto, para la toma de decisiones sobre la explotación del recurso energético mareomotriz, además de la selección del sistema de conversión a emplear y de la determinación de su producción, es de gran importancia realizar una evaluación detallada de los impactos ambientales derivados. En este sentido, mediante esta Tesis Doctoral se estudian diversos factores que intervienen en el aprovechamiento de la energía mareomotriz en la Ría de Ortigueira, incluyendo la determinación del sistema de conversión más adecuado, basada en el análisis de los rendimientos anuales y su variabilidad intraanual, y los impactos derivados del aprovechamiento energético sobre las circulaciones transitorias y residuales. Para ello, se implementa un modelo numérico 3D de alta resolución que simula la hidrodinámica de la ría durante diferentes periodos, con diferentes combinaciones de condiciones de contorno y diferentes plantas mareomotrices. A raíz de estas simulaciones, se determina que los rendimientos de los TSTs flotantes y fijos en el fondo en la misma ubicación pueden diferir mucho según las características de las condiciones hidrodinámicas de la zona costera en la que operan. En el caso estudiado, como resultado de las velocidades más altas cerca de la superficie, los TSTs flotantes brindan un mejor rendimiento que los dispositivos fijos en el fondo. Asimismo, se observa que la explotación de la energía de las corrientes de marea puede causar impactos importantes en la circulación transitoria estuarina, sin que se encuentren diferencias significativas entre los impactos producidos por los distintos sistemas de conversión considerados. En ambos casos se observan ligeras reducciones de la velocidad apreciables hasta algunos km de distancia de la planta, e impactos de mayor magnitud en las proximidades de la planta. Finalmente, se determina que, en general, cuando opera alguna de las plantas mareomotrices consideradas, independientemente de su configuración y los forzamientos, el patrón de la circulación residual general no experimenta modificaciones significativas, limitándose también las mayores modificaciones de la magnitud de la circulación residual a las cercanías de la planta. Además, el aprovechamiento de la energía mareomotriz apenas afecta a los fenómenos de *upwelling*.

Los resultados obtenidos en esta Tesis Doctoral permiten seguir avanzando en la investigación y desarrollo de las energías renovables en Galicia, más concretamente, las energías renovables marinas, que tienen un gran potencial en este territorio por su ubicación privilegiada en la Región del Atlántico Sur de Europa.

Palabras clave: explotación energética de las corrientes de marea; modelo numérico 3D; evaluación de impactos; circulación residual; variabilidad estacional.

USC
UNIVERSIDADE DE SANTIAGO DE COMPOSTELA

USC
UNIVERSIDADE
DE SANTIAGO
DE COMPOSTELA

RESUMO EXTENDIDO EN GALEGO

Como resultado da crecente presión pública, do crecemento da lexislación baseada na mitigación dos efectos do cambio climático e, por suposto, do esgotamento dos combustibles fósiles, empresas e gobernos de todo o mundo traballan no desenvolvemento das enerxías renovables (Erdiwansyah, Mamat, Sani, & Sudhakar, 2019; European Commission, 2012; Fobissie, 2019; Herath & Tyner, 2019; Nicolli & Vona, 2019; Pischke et al., 2019). Dentro das distintas fontes de enerxías renovables existentes, cada rexión debe centrarse naquelas para as cales ten un maior potencial. En Galicia, debido á súa privilexiada localización na parte noroeste da Península Ibérica, son de especial interese as enerxías mariñas e, en particular, a enerxía mareomotriz, cuxo potencial nalgunhas rexións é moi importante (Álvarez et al., 2022; Carballo, Iglesias, & Castro, 2009a; Iglesias, Carballo, & Castro, 2008; Iglesias et al., 2009; Iglesias & Carballo, 2009b; Iglesias & Carballo, 2010b; Iglesias & Carballo, 2011b; Ramos & Iglesias, 2013a; Sánchez, Iglesias, Carballo, & Fraguela, 2013).

A enerxía mareomotriz vén sendo empregada para a xeración de enerxía eléctrica dende décadas atrás mediante grandes presas de marea (*tidal barrages*), como é o caso da central de La Rance, na Bretaña francesa, que leva en operación dende 1976. Con todo, a pesar de ser unha tecnoloxía suficientemente madura, non existen apenas proxectos de plantas dese tipo a nivel mundial, debido aos importantes impactos que causan sobre o medio mariño – a erosión do fondo mariño, a morte de peixes, a salinización das augas subterráneas ou a destrución de ecosistemas estuarinos son algúns destes impactos (Charlier, R. H. & Finkl, 2008).

Actualmente existe un novo enfoque para a explotación dá enerxía mareomotriz baseado no aproveitamento das correntes xeradas pola variación periódica do nivel do mar: a enerxía dás correntes de marea (Bahaj, A. S. & Myers, 2003; Carballo et al., 2009a; McCombes, Johnstone, & Grant, 2011). Este sistema de aproveitamento enerxético presenta numerosas vantaxes sobre outras enerxías renovables e sobre o sistema tradicional de explotación mareomotriz. Entre as vantaxes da enerxía das correntes de marea destacan: (i) predictibilidad dos fluxos debidos á marea e, consecuentemente, da potencia dispoñible; (ii) alto factor de carga debido á densidade do fluído (800 veces superior á densidade do aire); (iii) inexistencia de fluxos extremos que poderían poñer en perigo a supervivencia dos dispositivos; (iv) non ocupación de terra, eliminando os conflitos sobre o uso da mesma; (v) redución dos custos de instalación respecto das presas de marea (Bahaj, AbuBakr S., 2011; Carballo et al., 2009a; Sánchez, Carballo, Ramos, & Iglesias, 2014a).

O aproveitamento do recurso enerxético da corrente das mareas levase a cabo a través dos Convertedores de Enerxía das Mareas (TECs, polas súas siglas en inglés), que xeralmente se clasifican segundo o seu principio de funcionamento como dispositivos oscilantes ou xiratorios. Na actualidade, os dispositivos xiratorios (Hammar, Ehnberg, Mavume, Cuamba, & Molander, 2012; Khan, Bhuyan, Iqbal, & Quaicoe, 2009), tamén coñecidos como Turbinas de Corrente de Marea (TSTs, polas súas siglas en inglés), son os que presentan un nivel de desenvolvemento tecnolóxico máis alto (Segura, Morales, Somolinos, & López, 2017), existindo TSTs de terceira xeración deseñadas para operar en áreas pouco profundas (aprox. a partir de 1 m de profundidade) con velocidades de arranque relativamente baixas (aprox. 0,7 ms^{-1}) (Fouz,

Carballo, Ramos, & Iglesias, 2019). As TSTs pódense instalar de acordo con diferentes configuracións. Dependendo da súa posición na columna de auga, as TSTs poden clasificarse como: (i) TSTs flotantes, é dicir, dispositivos ancorados ao fondo do mar que flotan debaixo da superficie do mar, e que aproveitan a enerxía das capas superiores da columna de auga, e (ii) TSTs fixas no fondo, é dicir, convertedores rixidamente ancorados ao fondo do mar que aproveitan a enerxía dispoñible nas capas inferiores da columna de auga (Zhou, Benbouzid, Charpentier, Scuiller, & Tang, 2017).

As maiores velocidades das correntes de marea teñen lugar en rexións costeiras cunha carreira de marea importante e/ou cunhas características morfolóxicas que propician a circulación forzada a través de estreitas canles, provocando a existencia de importantes velocidades, susceptibles de ser aproveitadas para a xeración de enerxía eléctrica. En termos xerais, a explotación de correntes de marea é potencialmente de interese en áreas costeiras onde as velocidades máximas superan os 1,0 - 1,5 ms^{-1}(European Commission, 1996). Na Península Ibérica, as rexións con maior potencial para o aproveitamento enerxético das correntes de marea son as rías galegas, sendo a Ría de Ortigueira, onde se superan os 2.5 ms^{-1}, unha das máis destacadas (Sánchez et al., 2013; Sánchez, Carballo, Ramos, & Iglesias, 2014b).

Así mesmo, con carácter xeral, as rexións potencialmente adecuadas para a instalación dunha planta de aproveitamento enerxético das correntes mareas están situados en áreas costeiras con patróns hidrodinámicos complexos, como estuarios ou baías (Neill, Jordan, & Couch, 2012; Ramos, Carballo, Álvarez, Sánchez, & Iglesias, 2013; Ramos, Carballo, Sanchez, Veigas, & Iglesias, 2014), que á súa vez se corresponden con áreas de alta importancia ambiental, como é o caso da Ría de Ortigueira. Polo tanto, á hora da toma de decisións a cerca do aproveitamento do recurso mareomotriz dunha zona, é clave levar a cabo unha avaliación detallada do impacto ambiental producido, ademais da selección do sistema de conversión máis adecuado, que estará baseado na análise dos rendementos esperados.

DESCRICIÓN DA LOCALIZACIÓN

A Rexión Atlántica da Península Ibérica caracterízase pola presenza de extensos vales mergullados, unha clase específica de estuarios primarios, xeralmente coñecidos como rías, desenvoltos en costas con altos relevos asolagados durante o Holoceno (Dyer, Keith R., 1973; Evans & Prego, 2003). A ría analizada nesta Tese Doutoral, a Ría de Ortigueira é a máis occidental das Rías Altas Galegas (noroeste da Península Ibérica), delimitada polo Cabo Ortegal e Punta Estaca de Bares, cunha superficie aproximada de 85 km^2 e unha lonxitude de 18 km ao longo do seu eixo principal.

Respecto das mareas, o principal compoñente astronómico da marea é o harmónico M2, de igual modo que no resto de Europa (Pugh, 1996). Con todo, hai outros constituíntes semidirunos relevantes, como son o S2, o N2 e o K2, polo cal resulta ser unha rexión cun réxime de mareas semidiurno, cun factor de forma de 0.082.

Esta rexión costeira é unha área con gran potencial mareomotriz grazas á súa morfoloxía complexa, con numerosos estreitamentos, e a súa relativamente elevada carreira de marea, que alcanza os 4.5m. Traballos previos mostran que no estreitamento existente entre Punta Postiña e Punta Cabalar acádanse velocidades da corrente de aproximadamente 2.5 ms^{-1}, mostrando así a idoneidade da Ría de Ortigueira para a localización dunha planta de aproveitamento enerxético das correntes de marea (Iglesias, Sánchez, Carballo, & Fernández, 2012).

OBXECTIVOS

Na presente Tese Doutoral avánzase na análise da enerxía mareomotriz nas rías galegas mediante unha análise do potencial enerxético das correntes de marea na Ría de Ortigueira, que estuda dende unha óptica multifocal distintos factores implicados no aproveitamento deste recurso.

A identificación das áreas con maior potencial para a explotación das correntes de marea na Ria de Ortigueira é froito dun traballo previo realizada por persoal da Área de Enxeñaría Hidráulica da USC, no cal participou o autor da presente Tese Doutoral (Apéndice II). Neste traballo, impleméntase un modelo numérico 2D para resolver as condicións hidrodinámicas da ría, co fin de obter o patrón de velocidades, a partir do cal se estima, en primeira aproximación, o potencial enerxético na Ría de Ortigueira. A partir do patrón de velocidades e da profundidade de auga determínase a área óptima para o aproveitamento enerxético das correntes de marea.

O obxectivo final desta Tese Doutoral é realizar unha análise integral da enerxía das correntes de marea na Ría de Ortigueira, acadando así o coñecemento necesario para determinar o recurso potencialmente dispoñible e os efectos que a explotación deste suporía sobre a hidrodinámica da Ría. Para lograr este obxectivo, é necesario superar distintos obxectivos ou fases intermedias, que se corresponden con cadanseus capítulos que conforman o núcleo da presente Tese Doutoral. Estas fases intermedias son as seguintes:

a) Determinación do sistema de aproveitamento máis axeitado. Co fin de examinar as diferenzas no rendemento enerxético en condicións reais de operación de dúas plantas de aproveitamento das correntes de marea, unha delas composta por TSTs flotantes e outra por TSTs fixas no fondo, impleméntase un modelo numérico 3D de alta resolución na Ría de Ortigueira, que é validado con éxito a partir de medidas de campo de niveis e velocidade das correntes. Empregando este modelo, levase a cabo unha avaliación detallada do rendemento enerxético intraanual das plantas mareomotrices propostas, situadas no emprazamento en planta identificado como óptimo en traballos (Apéndice II). Deste xeito, determínase a importancia de seleccionar o tipo de TST que mellor funciona tendo en conta as condicións hidrodinámicas específicas da área de interese. **(Capítulo 3)**.

b) Análise do impacto derivado do aproveitamento enerxético sobre a circulación transiente. Analízanse os efectos producidos pola operación das dúas plantas de aproveitamento enerxético das correntes de marea estudadas en a) sobre a circulación transiente na Ría de Ortigueira. Con este fin, empregando o modelo numérico descrito no apartado anterior, realízanse distintas simulacións numéricas: (i) sen implementar planta de aproveitamento algunha, isto é, en condicións inalteradas; (ii) implementando unha planta formada por TSTs flotantes; e (iii) implementando unha planta composta por TSTs fixas no fondo. Posteriormente, realízase unha comparación entre os resultados obtidos coa operación de cada unha das plantas fronte aos resultados en ausencia de explotación enerxética mareomotriz. **(Capítulo 4)**.

c) Avaliación dos efectos sobre a circulación residual debidos ao aproveitamento enerxético das correntes de marea. De modo análogo á análise descrita no punto anterior, estúdanse tamén os efectos producidos por estas mesmas plantas pero, neste caso, sobre a circulación residual da Ría de Ortigueira, e sobre os fenómenos de *upwelling* e *downwelling*, responsables da gran produtividade oceánica nas Rías Galegas. **(Capítulo 5)**.

En suma, coa presente Tese Doutoral preténdese realizar un estudo dos factores implicados no aproveitamento da enerxía mareomotriz na Ría de Ortigueira, incluído o sistema de aproveitamento máis adecuado, o rendemento enerxético deste sistema e os impactos derivados

da explotación na circulación transiente e residual. Deste xeito, preténdese poñer de manifesto as posibilidades que ofrece a enerxía mareomotriz na fachada Atlántica da Península Ibérica, fomentando así a súa implementación nunha rexión na cal o grao de aproveitamento desta fonte enerxética ata o momento é nulo.

Máis aló do interese *per se* deste traballo, mediante esta Tese Doutoral preténdese establecer unha metodoloxía que poida ser aplicada en estudos posteriores no ámbito da enerxía mareomotriz realizados noutras rexións costeiras, e que sirva para realizar unha análise integral do recurso mareomotriz en calquera rexión do mundo con características similares.

METODOLOXÍA

Para acadar os obxectivos expostos no apartado anterior, impleméntase o modelo hidrodinámico Delft3D- FLOW na Ría de Ortigueira. O Delft3D- FLOW aproxima, por medio dun código de diferenzas finitas, as ecuacións de Navier Stokes (baixo os supostos de augas pouco profundas e Boussinesq) combinadas coa ecuación de transporte, o que permite o cálculo da circulación baroclínica e barotrópica (Deltares, 2010). Para poder estudar en detalle as diferenzas existentes ao longo da columna de auga, o modelo numérico impleméntase na súa forma 3D.

Este modelo numérico cobre toda a ría por medio dunha malla cartesiana que se estende cara á plataforma continental adxacente ata a isóbata de 150 m, a unha distancia de aprox. 10 km da costa. Esta malla está composta por 57.361 celas de tamaño variable da seguinte maneira: na ría interior e media adóptase unha resolución de malla de 50 x 50 m, decrecendo progresivamente en dirección norte, tendo unha resolución de 50 x 150 m no contorno de augas abertas. En canto á discretización vertical, utilízase un sistema de coordenadas σ composto por doce capas (Philips, 1957), establecendo os seguintes espesores de capa (porcentaxes de columna de auga) desde a superficie ata o fondo: 2, 3, 5, 10, 15, 15, 15, 15, 10, 5, 3 e 2 (Carballo, Iglesias, & Castro, 2009b; Iglesias & Carballo, 2009a; Ramos et al., 2014). Esta distribución de capas σ, que proporciona unha resolución máis alta preto da superficie e o leito mariño, garante un modelado adecuado en zonas superficiais, así como os fluxos da capa límite (Carballo et al., 2009b).

O modelo numérico valídase con éxito coas medicións de campo obtidas por medio dun ADCP (Perfilador de Corrente Doppler Acústico) e dous sensores de nivel despregados en dúas localizacións diferentes na ría interior e media durante un período de 19 días. Durante este período, o modelo é forzado ao longo dos límites oceánicos cos principais harmónicos de marea, condicións termohalinas, velocidade e dirección do vento; ademais da descargas fluvial do río Mera na ría interior. Obtense unha boa concordancia entre as series calculadas e observadas (tanto para niveis de auga como para velocidades das correntes), acadando valores altos do coeficiente de correlación R ($R \approx 0.99$ para niveis de auga e $R > 0.82$ para magnitude e dirección de fluxo en cada capa), e valores baixos de varios coeficientes estatísticos (diferenza media, *MD* e erro cuadrático medio, *MSE*).

A implementación das TSTs no modelo numérico levase a cabo mediante o método denominado de sumidoiro de momento (Defne, Haas, & Fritz, 2011; Ramos et al., 2013; Ramos et al., 2014); consistente en introducir un termo sumidoiro de cantidade de movemento na ecuación de conservación do *momentum* do modelo, mediante unha forza de retardo que compensa a forza de empuxe exercida polo fluxo sobre as TSTs (G.I. Shapiro, 2011). O modelo de TST seleccionada é unha turbina Evopod (Oceanflowenergy,), dada a súa idoneidade para zonas de augas pouco profundas, como é o caso da localización proposta na Ría de Ortigueira.

Ambas as plantas de aproveitamento consideradas, que están situados nos arredores do estreitamento entre Pt. Postiña e Pt. Cabalar, onde se atopan as correntes de marea máis fortes, teñen a mesma distribución, cunha superficie de ocupación en planta duns 1500 m^2. A primeira planta está composta por TSTs flotantes, que ocupan a parte superior da columna de auga, e a segunda planta está composta por TSTs das mesmas características, pero fixadas ao fondo, e que ocupan a parte inferior da columna de auga. Seguindo as recomendacións de distancia entre liñas de TSTs, consideráronse 30 turbinas cunha área de captación conxunta (área de varrido do rotor dentro da sección transversal da columna de auga) de aprox. 600 m^2, distribuídas en tres liñas aproximadamente perpendiculares á dirección principal do fluxo.

No capítulo 3, realízase a análise do rendemento de ambos parques de aproveitamento enerxético das correntes de marea en base a tres parámetros característicos que describen o funcionamento dos TSTs: a produción de enerxía eléctrica (E_e), o factor de dispoñibilidade (A_f) e o factor de capacidade (C_f), que pode ser expresado tamén a través das horas equivalentes (FLH).

No capítulo 4, analízanse tres escenarios para avaliar os impactos causados pola operación das dúas plantas mareomotrices consideradas sobre a circulación transiente. En primeiro lugar, calcúlanse as condicións de referencia, é dicir, as condicións hidrodinámicas na ría en ausencia de TSTs. A continuación, determínanse as condicións resultantes da operación de ambas plantas propostas. Os forzamentos do modelo nos contornos son os mesmos para as tres simulacións: os principais constituíntes das mareas, valores diarios de salinidade e temperatura nos límites abertos e descarga diaria do río na parte alta da ría.

Finalmente, no capítulo 5, levase a cabo unha avaliación detallada dos impactos sobre a circulación residual e o *upwelling* estuarino producidos por ambas plantas de aproveitamento enerxético propostas, tendo en conta as variacións estacionais. Para iso, realízanse varios casos de estudo (CS), co obxectivo de comparar as diferenzas entre condicións alteradas e inalteradas (é dicir, con e sen extracción de enerxía, respectivamente) para os diferentes escenarios considerados. O procedemento empregado para calcular a circulación residual inducida pola marea consiste en promediar no tempo as velocidades transitorias calculadas polo modelo numérico.

RESULTADOS

No capítulo 3 analízase o rendemento enerxético das plantas mareomotrices consideradas, unha formada por TSTs flotantes (P1), e a outra por TSTs fixas no fondo (P2), ao longo de todo un ano completo, observándose diferenzas significativas entre ambas. A produción anual de enerxía de P1 é de 2.425×10^3 MWh, mentres que a produción de P2 é ao redor dun 40% menor. Estes resultados demostran que as zonas costeiras con importantes diferenzas na velocidade do fluxo ao longo da columna de auga, como a área de estudo, poden presentar diferenzas significativas entre a produción enerxética das plantas compostas por TSTs flotantes ou fixas no fondo.

En canto ao tempo de operación anual, os valores do factor de dispoñibilidade (A_f) mostran que P1 e P2 operan durante o 63 % e 48 % do tempo, respectivamente. Isto implica que, no caso de que se requirise un sistema de almacenamento de enerxía, tería que ser substancialmente máis grande para P2, dado o seu menor tempo de operación. En canto ao factor de capacidade (C_f), as diferenzas son aínda maiores, aproximadamente un 64% (0,23 e 0,14 para P1 e P2, respectivamente), o que indica unha nova importante vantaxe de P1, xa que un maior factor de capacidade asóciase cunha mellor produción respecto do capital invertido.

Por outra banda, ambas plantas presentan un rendemento enerxético intraanual altamente variable. No caso da produción de enerxía, o mes con maior E_e é agosto (227,74 MWh e 143,44 MWh para P1 e P2, respectivamente); pola súa banda, novembro presenta unha E_e máis baixa (185,52 MWh para P1 e 112,76 para P2, preto dun 20% inferior ao de agosto). Así mesmo, lonxe do que cabería esperar, non é nos meses con maiores mareas, e por tanto de maiores picos de velocidade, cando a produción de enerxía é maior. A explicación radica en que nos meses con carreiras de mareas máis altas (marzo e setembro) existen diferenzas importantes entre ciclos de mareas (con velocidades máximas que van desde 2,2 ms^{-1} ata 0,5 ms^{-1}), mentres que noutros meses, por exemplo, xullo ou agosto, os ciclos das mareas son máis homoxéneos (con velocidades máximas que oscilan entre 1,5 ms^{-1} e 1 ms^{-1}).

Pola súa banda, no capítulo 4 analízase o impacto causado sobre a circulación transitoria debido á operación de cada planta mareomotriz considerada, en termos de diferenza entre as condicións alteradas e as de referencia ou inalteradas, durante media marea enchente e media marea baleirante dunha marea viva media.

En canto aos impactos durante a media marea enchente na circulación xeral da ría, cando P1 está en operación, os maiores efectos na capa superficial concéntranse nas proximidades da planta, con alteracións máximas de ao redor de 3×10^{-1} ms^{-1} que se poden observar dentro uns poucos centos de metros augas arriba e augas abaixo da planta. Tamén se pode observar unha redución xeral da orde de 10^{-3} ms^{-1} apreciables ata 8-7 km de distancia da planta. Doutra banda, os impactos producidos na capa inferior son menores que na superficie, non só na zona onde se sitúa a planta senón en toda a ría. Ademais, a área onde se concentran os efectos difire moito, estando agora restrinxida a uns 3-4 km de distancia da planta. Pola súa banda, os impactos causados por P2 na circulación xeral da ría en media marea enchente describen un patrón moi similar ao do caso de P1 (unha redución xeral de magnitude e área ocupada similares).

Respecto da avaliación detallada destes impactos na área ocupada polas plantas e os seus arredores, durante media marea enchente, os efectos resultantes da operación de P1 supoñen unha redución media de aprox. 0,25 ms^{-1} (con reducións de ata 0,36 ms^{-1} en puntos específicos) na capa superficial da sección ocupada polas TSTs. Pola contra, no tramo restante do estreitamento entre Pta. Postiña e Pta. Cabalar, ao sur da planta a velocidade aumenta ata 0,28 ms^{-1}, mentres que ao norte diminúe lixeiramente. Na capa inferior, a velocidade do fluxo aumenta en todo o tramo, localizándose os maiores efectos no tramo non ocupado polas TSTs (ata 0,22 ms^{-1}). Doutra banda, cando P2 está en operación, a presenza das TSTs na parte inferior da columna de auga provoca un aumento da velocidade na capa superficial dentro da sección ao sur das TSTs, onde as diferenzas entre o fluxo alterado e as condicións de referencia acadan valores de ata 0,30 ms^{-1}, así como unha lixeira diminución no tramo restante do estreitamento (tramo ocupado polas TSTs e ao norte destas). Na capa inferior, o fluxo decrece na sección ocupada polas TSTs ata 0,15 ms^{-1} en puntos específicos, aumenta cara ao sur da planta ata 0,27 ms^{-1} e mantense case invariable cara ao norte. En canto ás capas intermedias da columna de auga, as diferenzas entre o impacto causado por P1 e P2 son case desprezábeis. En ambos casos, a velocidade aumenta significativamente ao sur da planta (ata 0,28 ms^{-1}), e diminúe no mesmo orde de magnitude dentro da sección ocupada pola planta (ata 0,33 ms^{-1}); finalmente, cara ao norte, os efectos consisten nunha lixeira variación xa sexa de diminución ou de aumento.

Por outra banda, en canto aos impactos en media marea baleirante, o patrón xeral é bastante similar ao de media marea enchente, aínda que con dúas diferenzas significativas: os efectos son (i) un pouco maiores na localización da planta e as súas inmediacións, e (ii) menores dentro da área augas abaixo da planta (é dicir, ao leste). Neste caso, respecto aos efectos na parte

exterior da ría, só son significativos (da orde de $2\text{-}3\times10^{-3}$ ms^{-1}) a uns 4-5 e 2-3 kms da planta en capas superficiais e capas de fondo, respectivamente. Así mesmo, respecto do estudo de detalle da zona ocupada pola planta e as súas inmediacións, ademais do xa comentado lixeiro incremento xeneralizado da magnitude dos efectos producidos pola operación da localización da planta e os seus arredores, cando P2 está en operación a velocidade do fluxo aumenta lixeiramente cara ao norte da planta (ata 0,12 ms^{-1}).

No capítulo 5, realízase unha análise detallada dos efectos sobre a circulación residual na Ría de Ortigueira producidos polo funcionamento de ambas plantas de aproveitamento propostas, e as súas variacións estacionais. Para iso, en primeiro lugar estúdanse as condicións de referencia en ausencia de plantas de aproveitamento, ou condicións inalteradas, a través de catro casos de estudo (CS1 a CS4).

Os casos CS1 e CS2 describen a circulación residual dentro da Ría de Ortigueira en condicións de verán e inverno, respectivamente, en ausencia de ventos. En ambos casos, pódense distinguir dúas rexións diferentes en termos de patróns de circulación residual dentro da ría. Na ría interior (i), o patrón hidrodinámico é similar ao longo de toda a columna de auga, cun marcado fluxo de saída, aínda que con velocidades de fluxo algo máis fortes nas capas superficiais. As velocidades de fluxo máximas atópanse na contorna do estreitamento entre Pt. Postiña e Pt. Cabalar, acadándose uns 0,20 ms^{-1} e 0,15 ms^{-1} en capas superficiais e de fondo, respectivamente. Doutra banda, a ría media e exterior (ii) caracterízase por patróns típicos dunha circulación estuarina positiva (é dicir, entrada na capa inferior e saída na capa superficial), motivada pola descarga fluvial que flúe cara ao exterior polas capas superficiais. Polo tanto, obsérvase que, en ausencia de ventos, a estacionalidade dos axentes impulsores hidrodinámicos non provoca variacións significativas na circulación residual da Ría de Ortigueira, como consecuencia das relativamente baixas achegas fluviais a este estuario.

Pola súa banda, os casos CS3 e CS4 correspóndense coas condicións de contorno de CS1 e CS2, respectivamente, pero considerando a acción do vento do vento medio de SW de cada período, favorable ao *upwelling*. Os resultados obtidos son similares en ambos os casos, aínda que, debido á maior velocidade do vento e descargas, as correntes residuais inducidas son lixeiramente superiores en CS4, principalmente na capa superficial. A circulación resultante na ría media e exterior podería caracterizarse como unha circulación estuarina convencional de dúas capas, con fluxos de saída na capa superficial que acadan valores da orde de 0,25 ms^{-1} na ría interior na contorna do estreitamento entre Pt. Postiña e Pt. Cabalar. Finalmente, cabe mencionar que as masas de auga superficial tenden a saír da ría pola súa marxe dereita, o cal é probablemente o resultado da acción do vento, reforzado pola descarga fluvial, que tenden a desviar o caudal cara á dereita como consecuencia da Forza Coriolis.

Así mesmo, neste capítulo, estúdase tamén a circulación residual alterada pola explotación enerxética das correntes de marea, e compárase cos valores de referencia. Esta análise realizarse a través de catro casos de estudo adicionais (CS5 a CS8), que consideran diferentes combinacións de condicións de contorno e configuracións de planta maremotriz (P1 ou P2).

Os casos CS5 e CS7 estudan a circulación residual alterada con P1 operando en ausencia de vento e con vento medio de inverno do SW, respectivamente. Os resultados obtidos son moi similares en ambos casos, observándose unicamente pequenas diferenzas entre eles na magnitude da afección na circulación residual (diferenza entre condicións alteradas e inalteradas) na capa superficial. Os maiores cambios nas velocidades residuais sitúanse no estreitamento entre Pt. Postiña e Pt. Cabalar, como consecuencia da localización da planta proposta. Con todo, a magnitude destas variacións na circulación é realmente baixa en calquera

caso, limitándose principalmente á zona ocupada pola planta e aos seus arredores (aproximadamente a máis de 100-150 m de distancia), onde se acadan incrementos máximos de aprox. 0.05 ms^{-1} e reducións máximas de aprox. 0.02 ms^{-1}. Fóra desta zona de maior influencia da planta, as variacións na magnitude da circulación residual son inferiores a aprox. 0,01 ms^{-1}, e practicamente insignificante a certa distancia da granxa. As velocidades residuais máximas son do mesma orde que no caso das condicións inalteradas, aprox. 0,25 ms^{-1}.

Finalmente, nos casos CS6 e CS8 introdúcense no modelo as mesmas condicións de contorno que no caso de CS5 e C7, respectivamente, pero considerando agora a operación da planta P2. Os patróns hidrodinámicos son similares entre si e, á súa vez, similares tamén aos do caso da planta flotante. A principal diferenza observada en canto á afección sobre a circulación residual respecto dos casos CS5 e CS7 é que, na capa superficial os incrementos nas velocidades residuais son lixeiramente máis fortes e as reducións máis débiles; pola contra, na capa inferior, a situación é máis ou menos a contraria.

CONCLUSIÓNS

Nesta Tese Doutoral realizase un estudo de diversos factores implicados na explotación da enerxía mareomotriz na Ría de Ortigueira, incluíndo a determinación do sistema de aproveitamento máis adecuado, dos rendementos enerxéticos dos distintos sistemas analizados e dos impactos derivados da explotación enerxética sobre as circulacións transiente e residual. Para iso, impleméntase un modelo numérico 3D que se aplica para simular a hidrodinámica desta ría durante diferentes períodos, con diferentes combinacións de condicións de contorno e diferentes plantas de aproveitamento. As plantas consideradas neste estudo están compostas por Turbinas de Correntes de Marea (TSTs) e presentan a mesma distribución en planta; porén, unha delas, P1, está composta por TST flotantes e a outra, P2, por TSTs fixas no fondo.

A análise do rendemento basease en tres parámetros que permiten caracterizar a operación das plantas: produción de enerxía eléctrica, factor de dispoñibilidade e factor de capacidade; apreciándose diferenzas notables nos resultados obtidos para ambas plantas. A planta P1 presenta valores superiores en todos os parámetros considerados; en particular, a produción anual de enerxía eléctrica é case o dobre que a de P2. En canto ao factor de dispoñibilidade, as diferenzas son menos importantes (15%); con todo, a potencia de saída de P1 é máis homoxénea, o cal é unha vantaxe significativa á hora de instalar un sistema de almacenamento de enerxía. Ademais, na análise intraanual obsérvase que os parámetros mencionados tamén presentan unha importante variabilidade mensual. Un achado de especial interese é que, contrariamente ao que podería esperarse, os meses con maiores picos nas velocidades do fluxo non se corresponden con aqueles cos valores máis altos dos parámetros de rendemento, incluída a produción de enerxía.

Respecto dos efectos producidos pola operación de ambas plantas consideradas, P1 e P2, a pesar das diferenzas significativas existentes na produción anual de enerxía, observase que os impactos causados sobre a circulación transitoria xeral presentan grandes similitudes. Aínda que o seu funcionamento non é suficiente para modificar considerablemente a circulación ao longo de toda a ría, aprécianse alteracións da orde de 10^{-2} ms^{-1} a varios km de distancia das plantas. En canto aos efectos na localización da planta e os seus arredores, os resultados do modelo mostran que existe unha importante redución da velocidade da corrente. Con todo, non toda esta redución de velocidade provén da extracción de enerxía, senón tamén de que o fluxo se redirixe parcialmente cara á sección restante, co consecuente incremento da velocidade. En contraste coas fortes similitudes nas modificacións do patrón xeral causadas polas plantas P1 e P2, nesta zona si se aprecian importantes diferenzas, debido á súa configuración vertical

(ocupando unha porción diferente da vertical). Así mesmo, observase que os impactos poden diferir dos que inicialmente poderían esperarse (por exemplo, observase unha redución da velocidade nunha parte importante da capa superficial durante a operación das TSTs fixas no fondo).

Finalmente, analízanse un total de oito casos de estudo para obter unha avaliación detallada da estacionalidade dos impactos da explotación da enerxía das correntes de marea na circulación residual. En particular, estúdanse as condicións hidrodinámicas inalteradas e alteradas baixo escenarios típicos de verán e inverno, en ausencia da acción do vento e con ventos favorables ao *upwelling*.

Observase que a circulación residual inalterada é bastante similar en condicións de verán e inverno, mostrando como a relativamente baixa achega fluvial na ría non é capaz de inducir correntes residuais significativas. En ambos casos distínguense dúas rexións diferentes en termos de patróns de circulación residual ao longo da ría: (i) a ría interior presenta patróns hidrodinámicos similares en toda a columna de auga, con velocidades de fluxo algo máis fortes nas capas superficiais, acadando velocidades máximas da redor de 0,25 ms^{-1} e 0,15 ms^{-1} nas capas superficial e de fondo, respectivamente. Doutra banda, a ría media e exterior (ii) caracterízanse por patróns típicos dunha circulación estuarina positiva. Estes patróns vense reforzados cando se consideran os ventos típicos do SW, principalmente no caso típico de inverno, demostrando que a estacionalidade do réxime de ventos si ten un papel clave na circulación residual dentro da ría.

En xeral, cando funciona unha planta mareomotriz, as modificacións resultantes na circulación residual limítanse principalmente ao estreitamento entre Pt. Postiña e Pt. Cabalar, na área ocupada pola granxa e nos seus arredores (aproximadamente ata uns 100-150 m de distancia), independentemente da combinación de configuración de planta mareomotriz e condicións de contorno seleccionada. Os valores máximos da variación das velocidades residuais debido á explotación enerxética das correntes de marea por medio das plantas propostas son da orde de 0,05 ms^{-1} na área de influencia destas. Fóra desta zona, as variacións na magnitude da circulación residual son inferiores a aprox. 0,01 ms^{-1}, e practicamente imperceptibles a certa distancia da planta.

En resumo, mediante esta Tese Doutoral determínase que o rendemento enerxético das TSTs flotantes e fixas no fondo nun mesma localización pode diferir moito segundo sexan as características das condicións hidrodinámicas da área costeira na que operan. Isto pode verse agravado no caso de masas de auga con diferenzas significativas nas velocidades das correntes ao longo da columna de auga, como é o caso da zona de estudo (Ría de Ortigueira). Como resultado das velocidades máis altas preto da superficie, as TSTs flotantes brindan un rendemento moito mellor que os dispositivos fixos no fondo. Finalmente, observase unha importante variabilidade intraanual no rendemento enerxético, o que leva a concluír que a produción e o rendemento enerxético dunha planta mareomotriz debe analizarse en base a simulacións que cubran un ano completo, en lugar de extrapolar os resultados obtidos para un ciclo mareas vivas – mareas mortas.

Así mesmo este estudo demostra que a explotación enerxética das correntes de marea pode causar impactos importantes na circulación estuarina. Estes impactos cuantifícanse para dúas plantas de corrente de marea propostas, compostas de TSTs flotantes ou fixos no fondo. Os resultados mostran que case non existen diferenzas entre os impactos causados por ambas configuracións de TSTs sobre a circulación xeral da ría; pola contra, existen diferenzas significativas nos efectos na contorna das plantas. Ademais, nesta área os impactos difiren en

gran medida dos que poderían esperarse de antemán, o que resalta a importancia dunha análise específica do sitio.

Finalmente, neste traballo determínase o impacto potencial sobre a circulación residual na Ría de Ortigueira causado pola operación de diferentes configuracións de plantas mareomotrices baixo diferentes escenarios hidrodinámicos típicos, establecendo que estes impactos están tamén restrinxidos á contorna das plantas propostas, teñen unha magnitude moi limitada e apenas afectan os fenómenos de *upwelling*.

Máis aló do interese *per se* destes resultados para a área costeira aquí estudada, o procedemento presentado neste traballo podería usarse como unha metodoloxía de referencia para analizar o rendemento enerxético anual de diferentes TSTs noutras rexións costeiras semellantes, así como os seus efectos sobre as condicións hidrodinámicas. É importante ter en conta que estes impactos poden, á súa vez, xerar outros efectos ambientais que están fóra do alcance deste traballo, tales como modificacións nos patróns de transporte de sedimentos e dispersión de contaminantes. Estes efectos potenciais serán tratados como unha continuación desta liña de investigación.

Os resultados acadados como froito da realización desta Tese Doutoral permiten seguir avanzando na investigación e no desenvolvemento das enerxías renovables en Galicia, máis en concreto, das enerxías renovables mariñas, as cales teñen un gran potencial neste territorio dada a privilexiada localización na Rexión Sur-Atlántica de Europa.

USC
UNIVERSIDADE DE SANTIAGO DE COMPOSTELA

RESUMEN EXTENDIDO EN ESPAÑOL

Como resultado de la creciente presión pública, del crecimiento de la legislación basada en la mitigación de los efectos del cambio climático y, por supuesto, del agotamiento de los combustibles fósiles, empresas y gobiernos de todo el mundo trabajan en el desarrollo de las energías renovables (Erdiwansyah, et al., 2019; European Commission, 2012; Fobissie, 2019; Herath & Tyner, 2019; Nicolli & Vona, 2019; Pischke et al., 2019). Dentro de las distintas fuentes de energías renovables existentes, cada región debe centrarse en aquellas para las cuales tiene un mayor potencial. En Galicia, debido a su privilegiada localización en la parte noroeste de la Península Ibérica, son de especial interés las energías marinas y, en particular, la energía mareomotriz, cuyo potencial en algunas regiones es muy importante (Álvarez et al., 2022; Carballo et al., 2009a; Iglesias et al., 2008; Iglesias et al., 2009; Iglesias & Carballo, 2009b; Iglesias & Carballo, 2010b; Iglesias & Carballo, 2011b; Ramos & Iglesias, 2013a; Sánchez et al., 2013).

La energía mareomotriz viene siendo empleada para la generación de energía eléctrica desde décadas atrás mediante grandes presas de marea (*tidal barrages*), como es el caso de la central de La Rance, en la Bretaña francesa, que lleva en operación desde 1976. Sin embargo, pese a ser una tecnología suficientemente madura, no existen apenas proyectos de plantas de ese tipo a nivel mundial, debido a los importantes impactos que causan sobre el medio marino – la erosión del fondo marino, la muerte de peces, la salinización de las aguas subterráneas o la destrucción de ecosistemas estuarinos son algunos de estos impactos (Charlier, R. H. & Finkl, 2008).

Actualmente existe un nuevo enfoque para la explotación de la energía mareomotriz basado en el aprovechamiento de las corrientes generadas por la variación periódica del nivel del mar: la energía das corrientes de marea (Bahaj, A. S. & Myers, 2003; Carballo et al., 2009a; McCombes et al., 2011). Este sistema de aprovechamiento energético presenta numerosas ventajas sobre otras energías renovables y sobre el sistema de explotación mareomotriz tradicional. Entre las ventajas de la energía de las corrientes de marea destacan: (i) predictibilidad de los flujos debidos a la marea y, consecuentemente, de la potencia disponible; (ii) alto factor de carga debido a la densidad del fluido (800 veces superior a la densidad del aire); (iii) inexistencia de flujos extremos que podrían poner en peligro la supervivencia de los dispositivos; (iv) no ocupación de tierra, eliminando los conflictos sobre el uso de la misma; (v) reducción de los costes de instalación respeto de las presas de marea (Bahaj, AbuBakr S., 2011; Carballo et al., 2009a; Sánchez et al., 2014a).

El aprovechamiento del recurso energético de la corriente de las mareas se lleva a cabo a través de Convertidores de Energía de las Marea (TECs, por sus siglas en inglés), que generalmente se clasifican según su principio de funcionamiento como dispositivos oscilantes o giratorios (Hammar et al., 2012; Khan et al., 2009). En la actualidad, los dispositivos giratorios, también conocidos como Turbinas de Corriente de Marea (TSTs, por sus siglas en inglés), son los que presentan un nivel de desarrollo tecnológico más alto (Segura et al., 2017), existiendo TSTs de tercera generación que están diseñados para operar en áreas poco profundas (aprox. a partir de 1 m de profundidad) con velocidades de arranque relativamente bajas (aprox.

0,7 ms^{-1}) (Fouz et al., 2019). Las TSTs se pueden instalar de acuerdo con diferentes configuraciones. Dependiendo de su posición en la columna de agua, las TSTs pueden clasificarse como: (i) TSTs flotantes, es decir, dispositivos anclados al fondo del mar que flotan debajo de la superficie del mar, y que aprovechan la energía de las capas superiores de la columna de agua, y (ii) TSTs fijas en el fondo, es decir, convertidores rígidamente anclados al fondo del mar que aprovechan la energía disponible en las capas inferiores de la columna de agua (Zhou et al., 2017).

Las mayores velocidades de las corrientes de marea tienen lugar en regiones costeras con una carrera de marea importante y/o con unas características morfológicas que propician la circulación forzada a través de estrechos canales, provocando la existencia de importantes velocidades, susceptibles de ser aprovechadas para la generación de energía eléctrica. En términos generales, la explotación de corrientes de marea es potencialmente de interés en áreas costeras donde las velocidades máximas superan los 1,0 - 1,5 ms^{-1} (European Commission, 1996). En la Península Ibérica, las regiones con mayor potencial para el aprovechamiento energético de las corrientes de marea son las rías gallegas, siendo la Ría de Ortigueira, en donde se superan los 2.5 ms^{-1}, una de las más destacadas (Sánchez et al., 2013; Sánchez et al., 2014b).

Así mismo, con carácter general, las regiones potencialmente adecuadas para instalar una planta de aprovechamiento energético de las corrientes mareas están ubicadas en áreas costeras con patrones hidrodinámicos complejos, como estuarios o bahías (Neill et al., 2012; Ramos et al., 2013; Ramos et al., 2014), que a su vez se corresponden con áreas de alta importancia ambiental, como es el caso de la Ría de Ortigueira. Por lo tanto, a la hora de la toma de decisiones acerca del aprovechamiento del recurso mareomotriz de una zona, es clave llevar a cabo una evaluación detallada del impacto ambiental producido, además de la selección del sistema de conversión más adecuado, que estará basado en el análisis de los rendimientos esperados.

DESCRIPCIÓN DE LA LOCALIZACIÓN

La Región Atlántica de la Península Ibérica se caracteriza por la presencia de extensos valles sumergidos, una clase específica de estuarios primarios, generalmente conocidos como rías, desarrollados en costas con altos relieves anegados durante el Holoceno (Dyer, Keith R., 1973; Evans & Prego, 2003). La ría analizada en esta Tesis Doctoral, la Ría de Ortigueira es la más occidental de las Rías Altas Gallegas (noroeste de la Península Ibérica), delimitada por el Cabo Ortegal y la Punta Estaca de Bares, con una superficie aproximada de 85 km^2 y una longitud de 18 km a lo largo de su eje principal.

Al respecto de las mareas, el principal componente astronómico de la marea es el armónico M2, de igual modo que en el resto de Europa (Pugh, 1996). Además, hay otros constituyentes semidirunos relevantes, como son el S2, el N2 y el K2, resultando en una región con un régimen de mareas semidiurno, con un factor de forma de 0.082.

Esta región costera es un área con gran potencial mareomotriz gracias a su morfología compleja, con numerosos estrechamientos, y su relativamente elevada carrera de marea, que alcanza los 4.5 m. Trabajos previos muestran que en el estrechamiento existente entre Punta Postiña y Punta Cabalar se alcanzan velocidades de la corriente de aproximadamente 2.5 ms^{-1}, mostrando el interés de la Ría de Ortigueira para la ubicación de una planta de aprovechamiento energético de las corrientes de marea (Iglesias et al., 2012).

OBJETIVOS

En la presente Tesis Doctoral se avanza en el estudio de la energía mareomotriz en las rías gallegas mediante un análisis del potencial energético de las corrientes de marea en la Ría de Ortigueira, que aborda desde una óptica multifocal distintos factores implicados en el aprovechamiento de este recurso.

La identificación de las áreas con mayor potencial para la explotación de las corrientes de marea en la Ria de Ortigueira es fruto de un trabajo previo realizado por personal del Área de Ingeniería Hidráulica de la USC, en el cual ha participado el autor de la presente Tesis Doctoral (Apéndice II). En este trabajo, se implementa un modelo numérico 2D para resolver las condiciones hidrodinámicas de la ría, con el fin de obtener el patrón de velocidades, a partir del cual se estima, en primera aproximación, el potencial energético en la Ría de Ortigueira. A partir del patrón de velocidades y de la profundidad de agua se determina el área óptima para el aprovechamiento energético de las corrientes de marea.

El objetivo final de esta Tesis Doctoral es realizar un análisis integral de la energía de las corrientes de marea en la Ría de Ortigueira, alcanzando así el conocimiento necesario para determinar el recurso potencialmente disponible y los efectos que la explotación de este supondría sobre la hidrodinámica de la Ría. Para lograr este objetivo, es necesario alcanzar distintos objetivos o fases intermedias, que se corresponden con sendos capítulos que conforman el núcleo de la presente Tesis Doctoral. Estas fases intermedias son:

a) Determinación del sistema de aprovechamiento más adecuado. Con el fin de examinar las diferencias en el rendimiento energético en condiciones reales de operación de dos plantas de flujo de marea, una de ellas compuesta por TSTs flotantes y otra por TSTs fijas en el fondo, se implementa un modelo numérico 3D de alta resolución en la Ría de Ortigueira, que es validado con éxito a partir de medidas de campo de niveles y velocidad de las corrientes. Empleando este modelo, se lleva a cabo una evaluación detallada del rendimiento energético intraanual de las plantas mareomotrices propuestas, ubicadas en el emplazamiento en planta identificado como óptimo en trabajos previos (Apéndice II). De este modo, se determina la importancia de seleccionar el tipo de TSTs que mejor funcionan teniendo en cuenta las condiciones hidrodinámicas específicas del área de interés (**Capítulo 3)**.

b) Análisis del impacto derivado del aprovechamiento energético sobre la circulación transiente. Se analizan los efectos producidos por la operación de las dos plantas de aprovechamiento energético de las corrientes de marea estudiadas en a) sobre la circulación transiente en la Ría de Ortigueira. Con este fin, empleando el modelo numérico descrito en el apartado anterior, se realizan distintas simulaciones numéricas: (i) sin implementar planta de aprovechamiento alguna, o condiciones inalteradas; (ii) implementando una planta formada por TSTs flotantes; y (iii) implementando una planta compuesta por TSTs fijas en el fondo. Posteriormente, se realiza una comparación entre los resultados obtenidos con la operación de cada una de las plantas frente a los resultados en ausencia de explotación energética mareomotriz (**Capítulo 4).**

c) Evaluación de los efectos sobre la circulación residual debidos al aprovechamiento energético de las corrientes de marea. De modo análogo al análisis descrito en el punto anterior, se estudian también los efectos producidos por estas mismas plantas pero, en este caso, sobre la circulación residual de la Ría de Ortigueira, y sobre los fenómenos de *upwelling* y *downwelling*, responsables de la gran productividad oceánica en las Rías Gallegas (**Capítulo 5).**

En suma, con la presente Tesis Doctoral se pretende realizar un estudio de los factores implicados en el aprovechamiento de la energía mareomotriz en la Ría de Ortigueira, incluido el sistema de aprovechamiento más adecuado, el rendimiento energético de este sistema y los impactos derivados de la explotación en la circulación transiente y residual. De este modo, se pretende poner de manifiesto las posibilidades que ofrece la energía mareomotriz en la fachada Atlántica de la Península Ibérica, fomentando así su implementación en una región en la cual el grado de aprovechamiento de esta fuente energética hasta el momento es nulo.

Más allá del interés *per se* de este trabajo, mediante esta Tesis Doctoral se pretende establecer una metodología que pueda ser aplicada en estudios posteriores en el ámbito de la energía mareomotriz en otras regiones costeras, y que sirva para realizar un análisis integral del recurso mareomotriz en cualquier región del mundo con características similares.

METODOLOGÍA

Para alcanzar los objetivos expuestos en el apartado anterior, se implementa el modelo hidrodinámico Delft3D-FLOW en la Ría de Ortigueira. Delft3D-FLOW aproxima, por medio de un código de diferencias finitas, las ecuaciones de Navier Stokes (bajo los supuestos de aguas poco profundas y Boussinesq) combinadas con la ecuación de transporte, lo que permite el cálculo de la circulación baroclínica y barotrópica (Deltares, 2010). Para poder estudiar en detalle las diferencias existentes a lo largo de la columna de agua, el modelo numérico se implementa en su forma 3D.

Este modelo numérico cubre toda la ría por medio de una malla cartesiana que se extiende hacia la plataforma continental adyacente hasta la isóbata de 150 m, a una distancia de aprox. 10 km de la costa. Esta malla está compuesta por 57.361 celdas de tamaño variable de la siguiente manera: en la ría interior y media se adopta una resolución de malla de 50 x 50 m, decreciendo progresivamente en dirección norte, teniendo una resolución de 50 x 150 m en el contorno de aguas abiertas. En cuanto a la discretización vertical, se utiliza un sistema de coordenadas σ compuesto por doce capas (Philips, 1957), estableciendo los siguientes espesores de capa (porcentajes de columna de agua) desde la superficie hasta el fondo: 2, 3, 5, 10, 15, 15, 15, 15, 10, 5, 3 y 2 (Carballo et al., 2009b; Iglesias & Carballo, 2009a; Ramos et al., 2014). Esta distribución de capas σ, que proporciona una resolución más alta cerca de la superficie y el lecho marino, garantiza un modelado adecuado en zonas someras, así como los flujos de la capa límite (Carballo et al., 2009b).

El modelo numérico se valida con éxito con las mediciones de campo obtenidas por medio de un ADCP (Perfilador de Corriente Doppler Acústico) y dos sensores de nivel desplegados en dos ubicaciones diferentes en la ría interior y media durante un período de 19 días. Durante este período, el modelo es forzado a lo largo de los contornos oceánicos con los principales armónicos de marea, condiciones termohalinas, velocidad y dirección del viento; además de la descarga fluvial del río Mera en la ría interior. Se obtiene una buena concordancia entre las series calculadas y observadas (tanto para niveles de agua como para velocidades), alcanzando valores altos del coeficiente de correlación R ($R \approx 0.99$ para niveles de agua y $R > 0.82$ para magnitud y dirección de la corriente en cada capa), y valores bajos de varios coeficientes estadísticos (diferencia media, *MD* y error cuadrático medio, *MSE*).

La implementación de las TSTs en el modelo numérico se lleva a cabo mediante el método denominado de sumidero de momento (Defne et al., 2011; Ramos et al., 2013; Ramos et al., 2014). Este método consiste en introducir un término sumidero de cantidad de movimiento en la ecuación de conservación del *momentum* del modelo, mediante una fuerza de retardo que compensa la fuerza de empuje ejercida por el flujo sobre las TSTs (G.I. Shapiro, 2011). El

modelo de TST seleccionado es una turbina Evopod (Oceanflowenergy,), dada su idoneidad para zonas de aguas poco profundas, como es el caso de la ubicación propuesta en la Ría de Ortigueira.

Ambas plantas de aprovechamiento consideradas, que están ubicados en los alrededores del estrechamiento entre Pt. Postiña y Pt. Cabalar, donde se encuentran las corrientes de marea más fuertes, tienen la misma distribución, con una superficie de ocupación en planta de unos 1500 m^2. La primera planta está compuesta por TSTs flotantes que ocupan la parte superior de la columna de agua, y la segunda planta está compuesta por TSTs de las mismas características, pero fijadas al fondo, y que ocupan la parte inferior de la columna de agua. Siguiendo las recomendaciones de distancia entre líneas de TSTs, se consideraron un total de 30 turbinas con un área de captación conjunta (área de barrido del rotor dentro de la sección transversal de la columna de agua) de aprox. 600 m^2, distribuidas en tres líneas aproximadamente perpendiculares a la dirección principal del flujo.

En el capítulo 3, se realiza el análisis del rendimiento de ambos parques de aprovechamiento de corrientes de marea en base a tres parámetros característicos que describen el funcionamiento de las TSTs: la producción de energía eléctrica (E_e), el factor de disponibilidad (A_f) y el factor de capacidad (C_f), que puede ser expresado también a través de las horas equivalentes (*FLH*).

En el capítulo 4, se analizan tres escenarios para evaluar los impactos causados por la operación de las dos plantas mareomotrices consideradas sobre la circulación transiente. En primer lugar, se determinan las condiciones de referencia, es decir, las condiciones hidrodinámicas en la ría en ausencia de TSTs. A continuación, se determinan las condiciones resultantes de la operación de ambas plantas propuestas. Los forzamientos del modelo en los contornos son los mismos para las tres simulaciones: principales constituyentes de las mareas, valores diarios de salinidad y temperatura en los límites abiertos y descarga diaria del río en la parte alta de la ría.

Finalmente, en el capítulo 5, se lleva a cabo una evaluación detallada de los impactos sobre la circulación residual y el *upwelling* estuarino producidos por ambas plantas de aprovechamiento energético propuestas, considerando la variación estacional. Para ello, se analizan varios casos de estudio (CS), con el objetivo de comparar las diferencias entre condiciones alteradas e inalteradas (es decir, con y sin extracción de energía, respectivamente) para los diferentes escenarios considerados. El procedimiento empleado para determinar la circulación residual inducida por la marea consiste en promediar en el tiempo las velocidades transitorias calculadas por el modelo numérico.

RESULTADOS

En el capítulo 3 se analiza el rendimiento energético de las plantas mareomotrices consideradas, una formada por TSTs flotantes (P1), y la otra por TSTs fijas en el fondo (P2), a lo largo de un año completo, observándose diferencias significativas entre ambas. La producción anual de energía de P1 es de 2.425×10^3 MWh, mientras que la producción de P2 es alrededor de un 40% menor. Estos resultados demuestran que las zonas costeras con importantes diferencias en la velocidad del flujo a lo largo de la columna de agua, como el área de estudio, pueden presentar diferencias significativas entre la producción energética de las plantas compuestas por TST flotantes o fijas en el fondo.

En cuanto al tiempo de operación anual, los valores del factor de disponibilidad (A_f) muestran que P1 y P2 operan durante el 63 % y 48 % del tiempo, respectivamente. Esto implica

que, en caso de que se requiriera un sistema de almacenamiento de energía, tendría que ser sustancialmente más grande para P2, dado su menor tiempo de operación. En cuanto al factor de capacidad (C_f), las diferencias son aún mayores, aproximadamente un 64% (0,23 y 0,14 para P1 y P2, respectivamente), lo que indica una nueva importante ventaja de P1, ya que un mayor factor de capacidad se asocia con una mejor producción respecto del capital invertido.

Por otra parte, ambas plantas presentan un rendimiento energético intraanual altamente variable. En el caso de la producción de energía, el mes con mayor E_e es agosto (227,74 MWh y 143,44 MWh para P1 y P2, respectivamente); por su parte, noviembre presenta el E_e más bajo (185,52 MWh para P1 y 112,76 para P2, cerca de un 20% inferior al de agosto). Así mismo, lejos de lo que cabría esperar, no es en los meses con mayores mareas, y por tanto de mayores picos de velocidad, cuando la producción de energía es mayor. La explicación radica en que en los meses con carreras de mareas más altas (marzo y septiembre) existen diferencias importantes entre ciclos de mareas (con velocidades máximas que van desde 2,2 ms^{-1} hasta 0,5 ms^{-1}) mientras que, en otros meses, por ejemplo, julio o agosto, los ciclos de mareas son más homogéneos (con velocidades máximas que oscilan entre 1,5 ms^{-1} y 1 ms^{-1}).

Por su parte, en el capítulo 4 se analiza el impacto causado sobre la circulación transitoria debido a la operación de cada planta mareomotriz considerada, en términos de diferencia entre las condiciones alteradas y las de referencia o inalteradas, durante media marea llenante y media marea vaciante de una marea viva media.

En cuanto a los impactos durante media marea llenante en la circulación general de la ría, cuando P1 está en operación, los mayores efectos en la capa superficial se concentran en las cercanías de la planta, con alteraciones máximas de alrededor de 3×10^{-1} ms^{-1} que se pueden observar dentro unos pocos cientos de metros aguas arriba y aguas abajo de la planta. También se puede observar una reducción general del orden de 10^{-3} ms^{-1} apreciables hasta 8-7 km de distancia de la planta. Por otro lado, los impactos producidos en la capa inferior son menores que en la superficie, no solo en la zona donde se ubica la planta sino en toda la ría. Además, el área donde se concentran los efectos difiere mucho, estando ahora restringida a unos 3-4 km de distancia de la planta. Por su parte, los impactos causados por P2 en la circulación general de la ría en media marea llenante describen un patrón muy similar al del caso de P1 (una reducción general de magnitud y área ocupada similares).

Respecto de la evaluación detallada de estos impactos en el área ocupada por las plantas y sus alrededores, durante media marea llenante, los efectos resultantes de la operación de P1 suponen una reducción media de aprox. 0,25 ms^{-1} en la capa superficial en la sección ocupada por las TSTs (con reducciones de hasta 0,36 ms^{-1} en puntos específicos). Por el contrario, en el tramo restante del estrechamiento entre Pta. Postiña y Pta. Cabalar, al sur de la planta la velocidad aumenta hasta 0,28 ms^{-1}, mientras que al norte disminuye ligeramente. En la capa inferior, la velocidad del flujo aumenta en todo el tramo, localizándose los mayores efectos en el tramo no ocupado por las TST (hasta 0,22 ms^{-1}). Por otro lado, cuando P2 está en operación, la presencia de las TSTs en la parte inferior de la columna de agua provoca un aumento de la velocidad en la capa superficial dentro de la sección al sur de las TSTs, donde las diferencias entre el flujo alterado y las condiciones de referencia alcanzan valores de hasta 0,30 ms^{-1}, así como una ligera disminución en el tramo restante del estrechamiento (tramo ocupado por las TSTs y al norte de estas). En la capa inferior, el flujo decrece en la sección ocupada por las TSTs hasta 0,15 ms^{-1} en puntos específicos, aumenta hacia el sur de la planta hasta 0,27 ms^{-1} y se mantiene casi invariable hacia el norte. En cuanto a las capas intermedias de la columna de agua, las diferencias entre el impacto causado por P1 y P2 son casi despreciables. En ambos

casos, el flujo aumenta significativamente al sur de la planta (hasta 0,28 ms^{-1}), y disminuye en el mismo orden de magnitud dentro de la sección ocupada por la planta (hasta 0,33 ms^{-1}); finalmente, hacia el norte, los efectos consisten en una ligera variación ya sea de disminución o de aumento.

Por otra parte, en cuanto a los impactos en media marea vaciante, el patrón general es bastante similar al de media marea llenante, aunque con dos diferencias significativas: los efectos son (i) un poco mayores en la ubicación de la planta y sus inmediaciones, y (ii) menores dentro del área aguas abajo de la planta (es decir, al este). En este caso, respecto a los efectos en la parte exterior de la ría sólo son significativos (del orden de $2\text{-}3\times10^{-3}$ ms^{-1}) a unos 4-5 y 2-3 kms de la planta en capas superficiales y capas de fondo, respectivamente. Así mismo, respecto del estudio de detalle de la zona ocupada por la planta y sus inmediaciones, además del ya comentado ligero incremento generalizado de la magnitud de los efectos producidos por la operación de la ubicación de la planta y sus alrededores, cuando P2 está en operación la velocidad del flujo aumenta ligeramente hacia el norte de la planta (hasta 0,12 ms^{-1}).

En el capítulo 5, se realiza un análisis detallado de los efectos sobre la circulación residual en la Ría de Ortigueira producidos por el funcionamiento de ambas plantas de aprovechamiento propuestas, y sus variaciones estacionales. Para ello, en primer lugar se estudian las condiciones de referencia en ausencia de plantas de aprovechamiento, o condiciones inalteradas, a través de cuatro casos de estudio (CS1 a CS4).

Los casos CS1 y CS2 describen la circulación residual dentro de la Ría de Ortigueira en condiciones de verano e invierno, respectivamente, en ausencia de vientos. En ambos casos, se pueden distinguir dos regiones diferentes en términos de patrones de circulación residual dentro la ría. En la ría interior (i), el patrón hidrodinámico es similar a lo largo de toda la columna de agua, con un marcado flujo de salida, aunque con velocidades de flujo algo más fuertes en las capas superficiales. Las velocidades de flujo máximas se encuentran en el entorno del estrechamiento entre Pt. Postiña y Pt. Cabalar, alcanzándose unos 0,20 ms^{-1} y 0,15 ms^{-1} en capas superficiales y de fondo, respectivamente. Por otro lado, la ría media y exterior (ii) se caracteriza por patrones típicos de una circulación estuarina positiva (es decir, entrada en la capa inferior y salida en la capa superficial), motivada por la descarga fluvial que fluye hacia el exterior por las capas superficiales. Por tanto, se observa que, en ausencia de vientos, la estacionalidad de los agentes impulsores hidrodinámicos no provoca variaciones significativas en la circulación residual de la Ría de Ortigueira, como consecuencia de las relativamente bajas aportaciones fluviales en este estuario.

Por su parte, los casos CS3 y CS4 se corresponden con las condiciones de contorno de CS1 y CS2, respectivamente, pero considerando la acción del viento medio del SW de cada período, favorable al *upwelling*. Los resultados obtenidos son similares en ambos casos, aunque, debido a la mayor velocidad del viento y descargas, las corrientes residuales inducidas son ligeramente superiores en CS4, principalmente en la capa superficial. La circulación resultante en la ría media y exterior podría caracterizarse como una circulación estuarina convencional de dos capas, con flujos de salida en la capa superficial que alcanzando valores del orden de 0,25 ms^{-1} en la ría interior en el entorno del estrechamiento entre Pt. Postiña y Pt. Cabalar. Finalmente, cabe mencionar que las masas de agua superficial tienden a salir de la ría por su margen derecho, lo cual es probablemente el resultado de la acción del viento, reforzado por la descarga fluvial que tienden a desviar el caudal hacia la derecha como consecuencia de la Fuerza Coriolis.

Así mismo, en este capítulo, se estudia también la circulación residual alterada por la explotación energética de las corrientes de marea, y se compara con los valores de referencia.

Este análisis se realizar a través de cuatro casos de estudio adicionales (CS5 a CS8), que consideran diferentes combinaciones de condiciones de contorno y configuraciones de planta maremotriz (P1 o P2, flotante y fija en el fondo, respectivamente).

Los casos CS5 y CS7 estudian la circulación residual alterada con P1 operando en ausencia de viendo y con un viento medio de invierno del SW, respectivamente. Los resultados obtenidos son muy similares en ambos casos, observándose únicamente pequeñas diferencias entre ellos en la magnitud de la afección en la circulación residual (diferencia entre condiciones alteradas e inalteradas) en la capa superficial. Los mayores cambios en las velocidades residuales se ubican en el estrechamiento entre Pt. Postiña y Pt. Cabalar, como consecuencia de la ubicación de la planta propuesta. Sin embargo, la magnitud de estas variaciones en la circulación es realmente baja en cualquier caso, limitándose principalmente a la zona ocupada por la planta y en sus alrededores (aproximadamente a más de 100-150 m de distancia), donde se alcanzan incrementos máximos de aprox. 0.05 ms^{-1} y reducciones máximas de aprox. 0.02 ms^{-1}. Fuera de esta zona de mayor influencia de la planta, las variaciones en la magnitud de la circulación residual son inferiores a aprox. 0,01 ms^{-1}, y prácticamente insignificante a cierta distancia de la granja. Las velocidades residuales máximas son del mismo orden que en el caso de las condiciones inalteradas, aproximadamente 0,25 ms^{-1}.

Finalmente, en los casos CS6 y CS8 se introducen en el modelo las mismas condiciones de contorno que en el caso de CS5 y C7, respectivamente, pero considerando ahora la operación de la planta P2. Los patrones hidrodinámicos son similares entre sí y, a su vez, similares también a los del caso de la planta flotante. La principal diferencia observada en cuanto a la afección sobre la circulación residual respecto de los casos CS5 y CS7 es que, en la capa superficial los incrementos en las velocidades residuales son ligeramente más fuertes y las reducciones más débiles; por el contrario, en la capa inferior, la situación es prácticamente la contraria.

CONCLUSIONES

En esta Tesis Doctoral se realiza un estudio de diversos factores implicados en la explotación de la energía mareomotriz en la Ría de Ortigueira, incluyendo la determinación del sistema de aprovechamiento más adecuado, de los rendimientos energéticos de los distintos sistemas analizados y de los impactos derivados de la explotación energética sobre las circulaciones transiente y residual. Para ello, se implementa un modelo numérico 3D que se aplica para simular la hidrodinámica de esta ría durante diferentes períodos, con diferentes combinaciones de condiciones de contorno y diferentes plantas de aprovechamiento energético. Las plantas consideradas en este estudio están compuestas por Turbinas de Corrientes de Marea (TSTs) y presentan la misma distribución en planta; sin embargo, una de ellas, P1, está compuesto por TST flotantes y la otra, P2, por TST fijas en el fondo.

El análisis del rendimiento se basa en tres parámetros que permiten caracterizar la operación de las plantas: producción de energía eléctrica, factor de disponibilidad y factor de capacidad; apreciándose diferencias notables en los resultados obtenidos para ambas plantas. La planta P1 presenta valores superiores en todos los parámetros considerados; en particular, la producción anual de energía eléctrica es casi el doble que la de P2. En cuanto al factor de disponibilidad, las diferencias son menos importantes (15%); sin embargo, la potencia de salida de P1 es más homogénea, y esta es una ventaja muy significativa a la hora de instalar un sistema de almacenamiento de energía. Además, en el análisis intraanual se observa que los parámetros mencionados también presentan una importante variabilidad mensual. Un hallazgo de especial interés es que, contrariamente a lo que podría esperarse, los meses con mayores picos en las

velocidades del flujo no se corresponden con aquellos con los valores más altos de los parámetros de rendimiento, incluida la producción de energía.

Respecto de los efectos producidos por la operación de ambas plantas consideradas, P1 y P2, a pesar de las diferencias significativas existentes en la producción anual de energía, se observa que los impactos causados sobre la circulación transitoria general presentan grandes similitudes. Si bien su funcionamiento no es suficiente para modificar considerablemente la circulación a lo largo de toda la ría, se aprecian alteraciones del orden de 10^{-2} ms^{-1} a varios km de distancia de las plantas. En cuanto a los efectos en la ubicación de la planta y sus alrededores, los resultados del modelo muestran que existe una importante reducción de la velocidad de la corriente. Sin embargo, no toda esta reducción de velocidad proviene de la extracción de energía, sino también de que el flujo se redirige parcialmente hacia la sección restante, con el consecuente incremento de la velocidad. En contraste con las fuertes similitudes encontradas en las modificaciones del patrón general causadas por las plantas P1 y P2, en esta zona sí se aprecian importantes diferencias, debido a su configuración vertical (ocupando una porción distinta de la vertical). Así mismo, se observa que los impactos pueden diferir de los que inicialmente podrían esperarse (por ejemplo, se observa una reducción de la velocidad en una parte importante de la capa superficial durante la operación de las TSTs fijas en el fondo).

Finalmente, se analizan un total de ocho casos de estudio para obtener una evaluación detallada de la estacionalidad de los impactos derivados de la explotación de la energía de las corrientes de marea en la circulación residual. En particular, se analizan las condiciones hidrodinámicas inalteradas y alteradas bajo escenarios típicos de verano e invierno, en ausencia de acción del viento y con vientos favorables al *upwelling*.

Se observa que la circulación residual inalterada es bastante similar en condiciones de verano e invierno en ausencia de viento, mostrando cómo la relativa baja aportación fluvial en la ría no es capaz de inducir corrientes residuales significativas. En ambos casos se distinguen dos regiones diferentes en términos de patrones de circulación residual a lo largo de la ría: (i) la ría interior presenta patrones hidrodinámicos similares en toda la columna de agua, con velocidades de flujo algo más fuertes en las capas superficiales, alcanzando velocidades máximas de alrededor de 0,25 ms^{-1} y 0,15 ms^{-1} en las capas superficial y de fondo, respectivamente. Por otro lado, (ii) la ría media y exterior se caracterizan por patrones típicos de una circulación estuarina positiva. Estos patrones se ven reforzados cuando se consideran los vientos típicos del SW, principalmente en el caso típico de invierno, demostrando que la estacionalidad del régimen de vientos tiene un papel clave en la circulación residual dentro de la ría.

En general, las modificaciones resultantes en el flujo residual provocadas por la operación de una planta mareomotriz se limitan principalmente al área ocupada por la granja y en sus alrededores (aproximadamente hasta unos 100-150 m de distancia), independientemente de la combinación de configuración de planta mareomotriz y condiciones de contorno seleccionada. Los valores máximos de la variación de las velocidades residuales debido a la explotación energética de las corrientes de marea por medio de las plantas propuestas son del orden de 0,05 ms^{-1} en el área de influencia de estas. Fuera de esta zona, las variaciones en la magnitud de la circulación residual son inferiores a aprox. 0,01 ms^{-1}, y prácticamente imperceptibles a cierta distancia de la planta.

En resumen, mediante esta Tesis Doctoral se determina que el rendimiento energético de las TSTs flotantes y fijas en el fondo en una misma ubicación puede diferir en gran medida, según sean las características de las condiciones hidrodinámicas del área costera en la que

operan. Esto puede verse agravado en el caso de masas de agua con diferencias significativas en las velocidades de las corrientes a lo largo de la columna de agua, como es el caso de la zona de estudio (Ría de Ortigueira). Como resultado de las velocidades más altas cerca de la superficie, las TST flotantes brindan un rendimiento mucho mejor que los dispositivos fijos en el fondo. Finalmente, se observa una importante variabilidad intraanual en el rendimiento energético, lo que lleva a concluir que la producción y el rendimiento energético de una planta mareomotriz debe analizarse en base a simulaciones que cubran un año completo, en lugar de extrapolar los resultados obtenidos para un ciclo mareas vivas – mareas muertas.

Así mismo este estudio demuestra que la explotación energética de las corrientes de marea puede causar impactos importantes en la circulación transiente estuarina. Estos impactos se cuantifican para las dos plantas de corriente de marea propuestas en la Ría de Ortigueira. Los resultados muestran que casi no existen diferencias entre los impactos causados por ambas configuraciones de TSTs sobre la circulación general de la ría; por el contrario, existen diferencias significativas en los efectos en el entorno de las plantas. Además, en esta área los impactos difieren en gran medida de los que podrían esperarse de antemano, lo que resalta la importancia de un análisis específico del sitio.

Finalmente, en este trabajo se determina el impacto potencial sobre la circulación residual en la Ría de Ortigueira causado por la operación de diferentes configuraciones de plantas mareomotrices bajo diferentes escenarios hidrodinámicos típicos, estableciendo que estos impactos están restringidos al entorno de las plantas propuestas, tienen una magnitud muy limitada y apenas afectan a los fenómenos de *upwelling*.

Más allá del interés per se de estos resultados para el área costera aquí estudiada, el procedimiento presentado en este trabajo podría usarse como una metodología de referencia para analizar el rendimiento energético anual de diferentes TSTs en otras regiones costeras semejantes, tales como rías y estuarios, así como sus efectos sobre las condiciones hidrodinámicas. Es importante tener en cuenta que estos impactos pueden, a su vez, generar otros efectos ambientales que están fuera del alcance de este trabajo, tales como modificaciones en los patrones de transporte de sedimentos y dispersión de contaminantes. Estos efectos potenciales serán tratados como una continuación de esta línea de investigación.

Los resultados alcanzados como fruto de la realización de esta Tesis Doctoral permiten seguir avanzando en la investigación y en el desarrollo de las energías renovables en Galicia, más en concreto, de las energías renovables marinas, las cuales tienen un gran potencial en este territorio, dada su privilegiada localización en la Región Sur-Atlántica de Europa.

USC
UNIVERSIDADE DE SANTIAGO DE COMPOSTELA

1. INTRODUCTION

As a result of increasing public pressure, the growth of legislation based on mitigating the effects of climate change and the depletion of fossil fuels, companies and governments around the world are working on the development of renewable energies (Erdiwansyah, et al., 2019; European Commission, 2012; Fobissie, 2019; Herath & Tyner, 2019; Nicolli & Vona, 2019; Pischke et al., 2019). Within the various existing sources of renewable energy, each region should focus on those with the greatest potential. In Galicia, due to its privileged location in the northwest part of the Iberian Peninsula, marine energies are of special interest and, in particular, tidal energy, whose potential in some regions is very important (Álvarez et al., 2022; Carballo et al., 2009a; Iglesias et al., 2008; Iglesias et al., 2009; Iglesias & Carballo, 2009b; Iglesias & Carballo, 2010b; Iglesias & Carballo, 2011b; Ramos & Iglesias, 2013a; Sánchez et al., 2013).

Tidal energy has been used for the generation of electrical energy for decades through large tidal barrages, as is the case of the La Rance power plant in Brittany, France, which has been in operation since 1976. However, despite being a sufficiently mature technology, there are hardly any plant projects of this type worldwide, due to the significant impacts they cause on the marine environment – the erosion of the seabed, the death of fish, the salinization of waters underground or the destruction of estuarine ecosystems are some of these impacts.

Currently there is a new approach for the exploitation of tidal energy based on the use of currents generated by the periodic variation of sea level: tidal stream energy. This technique has numerous advantages over other renewable energies and over the traditional system of tidal exploitation. Among the advantages of tidal stream energy are: (i) predictability of the flows due to the tide and consequently of the available power; (ii) high load factor due to fluid density (800 times higher than air density); (iii) non-existence of extreme flows that could endanger the survival of the devices; (iv) non-occupation of land, eliminating conflicts over its use; (v) reduction of installation costs with respect to tidal dams (Bahaj, AbuBakr S., 2011; Blunden & Bahaj, 2006; Carballo et al., 2009a; Charlier, Roger H., 2003).

The harnessing of tidal stream energy resource is carried out through Tidal Energy Converters (TECs), which are usually classified according to their principle of operation as reciprocating or rotating devices (Hammar et al., 2012; Khan et al., 2009). Currently, rotating devices, also known as tidal stream turbines (TSTs), present a higher level of technological development, with third-generation TSTs that are designed to operate in shallow areas (approx. above 1 m depth) with relatively low cut-in velocities (approx. 0.7 ms^{-1}) (Fouz et al., 2019). TSTs can be installed according to different configurations. Depending on their position in the water column, TSTs can be classified as: (i) floating TSTs, i.e. devices anchored to the seabed that float below the sea surface, harnessing energy from the upper layers of the water column, and (ii) bottom-fixed TSTs, i.e., converters rigidly anchored to the seabed that harness the energy available in the bottom layers of the water column (Zhou et al., 2017).

USC
DE SANTIAGO
DE COMPOSTELA

The highest speeds of the tidal currents occur in coastal regions with an important tidal range and/or with morphological characteristics that encourage forced circulation through narrow channels, causing the existence of important flows that can be used for the generation of electrical energy. In general terms, the exploitation of tidal currents is potentially of interest

in coastal areas where maximum velocities exceed 1.0 - 1.5 ms^{-1} (European Commission, 1996). In the Iberian Peninsula, the regions with the greatest potential for harnessing energy from tidal currents are the Galician rías, being the Ría de Ortigueira, where 2.5 ms^{-1} is exceeded, one of the most prominent (Sánchez et al., 2013; Sánchez et al., 2014b).

However, the potentially suitable regions for installing a tidal stream farm are usually located in coastal areas with complex hydrodynamic patterns, such as estuaries or bays, which in turn correspond to areas of high environmental importance (Neill et al., 2012; Ramos et al., 2013; Ramos et al., 2014), as is the case of the Ria de Ortigueira. Therefore, for the decision-making about harnessing the tidal stream energy resource in an area of interest, it is of major importance, in addition to the selection of the most appropriate conversion system, to carry out a detailed assessment of the resulting environmental impact.

USC
UNIVERSIDADE
DE SANTIAGO
DE COMPOSTELA

2. OBJECTIVES

In this Doctoral Thesis, progress is made in the analysis of tidal energy in the Galician rías through an analysis of the energy potential of the tidal currents in the Ria de Ortigueira, which studies from a multifocal point of view different factors involved in tidal stream energy exploitation in this region.

The identification of the areas with the greatest potential for the exploitation of tidal currents in the Ria de Ortigueira is the result of previous work carried out by the Hydraulic Area of USC, with the participation of the author of this Doctoral Thesis (Appendix II). In this work, a 2D numerical model is implemented to solve the hydrodynamic conditions of the estuary, in order to obtain the velocity pattern, from which the energy potential in the Ortigueira estuary is determined, as a first approximation. Based on the pattern of velocities and water depth, the optimum area for tidal stream energy exploitation is determined.

The major objective of this Doctoral Thesis is to perform an integral analysis of tidal stream energy in Ría de Ortigueira, thus acquiring the necessary knowledge to determine the potentially available resource and the effects that its exploitation would produce on the hydrodynamics of the estuary. To achieve this objective, it is necessary to overcome different objectives or intermediate phases, which correspond with the chapters that make up the core of this Doctoral Thesis (chapters 3 to 5). These intermediate phases are:

a) Determination of the most appropriate harnessing system. In order to examine the differences in the energy performance under real operating conditions of two tidal stream plants, one of them composed of floating TSTs and the other of bottom-fixed TSTs, a high-resolution 3D numerical model is implemented in the Ria de Ortigueira. The different tidal stream energy plants studied are introduced numerically, non-concomitantly, by means of a momentum sink that emulates the effect of a tidal stream energy exploitation facility. Using this model, a detailed assessment of the intra-annual energy performance of the two proposed tidal power plants, located in plan view in the position identified as optimal in previous (Appendix II), is carried out. In this way, the importance of considering real operation conditions on the selection of the optimal TSTs is analysed. **(Chapter 3)**

b) Analysis of the impacts produced by energy use on transient circulation. The effects produced by the operation of the two proposed tidal stream energy plants in a) on the transient flow in the Ría de Ortigueira are analysed. For this purpose, using the numerical model described in the previous section, different numerical simulations are carried out: (i) without implementing any exploitation plant, i.e., unaltered conditions; (ii) implementing a plant composed by floating TSTs; and (iii) implementing a plant composed by bottom-fixed TSTs. Subsequently, the results obtained with the operation of each of the plants versus the results in the absence of tidal energy exploitation are compared. **(Chapter 4)**

c) Evaluation of the effects on the residual circulation due to tidal stream energy exploitation. Analogous to the analysis described in the previous point, the effects produced by these same plants are also studied, but in this case, on the residual circulation of the Ría de

Ortigueira, and on the *upwelling* and *downwelling* phenomena, responsible for the great oceanic productivity in the Galician Rías. **(Chapter 5)**

In short, this Doctoral Thesis studies several factors involved in the use of tidal energy in the Ría de Ortigueira, including the most appropriate use system, the energy performance of this system and the impacts derived from exploitation in transient and residual circulation. In this way, it is intended to highlight the possibilities offered by tidal energy in the Atlantic coast of the Iberian Peninsula, thus promoting its implementation in a country in which the degree of use of this energy source to date is zero.

Beyond the interest per se of this work, through this Doctoral Thesis it is intended to establish a methodology that can be applied in subsequent studies in the field of tidal energy carried out in other coastal regions, and that can be used to carry out an integral analysis of tidal stream resource in any region worldwide with similar characteristics

USC
UNIVERSIDADE
DE SANTIAGO
DE COMPOSTELA

3. ENERGY PRODUCTION FROM TIDAL CURRENTS IN AN ESTUARY: A COMPARATIVE STUDY OF FLOATING AND BOTTOM-FIXED TURBINES

This chapter reproduces completely the contents of the following research paper:

Title: *Energy production from tidal currents in an estuary: A comparative study of floating and bottom-fixed turbines*.

Journal: Energy, Volume 77 (1) December 2014, Pages 802-811

Doi: https://doi.org/10.1016/j.energy.2014.09.053

Authors: M. Sánchez [a], R. Carballo [a], V. Ramos [a], G. Iglesias [b]

Institution: *(a) University of Santiago de Compostela, Hydraulic Engineering, Campus Univ. s/n, 27002 Lugo, Spain*

(b) University of Plymouth, School of Marine Science and Engineering, Marine Building, Drakes Circus, Plymouth PL4 8AA, United Kingdom

ABSTRACT

In a tidal stream project, the selection of the most appropriate device is of major importance. The aim of this work is to investigate the differences between two tidal farms, one with floating Tidal Stream Turbines (TSTs), the other with bottom-fixed TSTs, in terms of annual performance and its monthly variability. This investigation is carried out considering real operational conditions in a case study: Ria de Ortigueira (NW Spain), a drowned river valleys which is one of the most promising sites for tidal stream energy exploitation in the Iberian Peninsula. A 3D, high-resolution numerical model is applied to simulate the hydrodynamics of the ria during an entire year with either the floating or bottom-fixed TSTs, and, on these grounds, determine the most representative performance parameters. Significant differences emerge in the performance of both plants; these are due to a great extent to the vertical variation in the flow velocity, which is relevant at many sites of interest for tidal stream energy exploitation such as Ria de Ortigueira. Finally, relevant variations were identified in the intra-annual performance which must be borne in mind in dimensioning the plant.

Keywords: Tidal stream energy; Tidal turbine; Ria de Ortigueira; Estuary; Numerical modelling.

3.1. INTRODUCTION

In the late 90s social pressure emerged claiming for a new, sustainable energy production and utilization model (World Commission on Environment and Development (WCED), 1987). This, together with a number of policies aimed at curbing greenhouse gas emissions and the realisation that the current energy model, with fossil fuels at its core, is necessarily limited in time, has resulted in companies and governments around the world being currently working intensively on the development and efficient utilization of new and renewable energy sources (European Commission, 2012).

Tidal stream energy is one of the most attractive and promising renewable energy sources owing to its advantages relative to other renewables: no land occupation, a high load factor (water density is ~ 800 times higher than air density), flow predictability and consequently power production predictability, inexistence of extreme flows (which might otherwise damage the conversion devices), etc. are some of the advantages of tidal stream energy exploitation (Bahaj, AbuBakr S., 2011; Blunden & Bahaj, 2006; Carballo et al., 2009a; Charlier, Roger H., 2003). However, due to the relatively recent interest in this type of energy (in comparison with other renewables such as wind or solar energy), only a few Tidal Energy Converters (TECs) have achieved at this point a commercial or pre-commercial stage (Fallon, Hartnett, Olbert, & Nash, 2014; Neill, Litt, Couch, & Davies, 2009). The conversion principle varies between the different TECs developed or in a development stage. Generally speaking, there exist two types of TECs, based on either the reciprocating or rotating principle. The latter, also known as Tidal Stream Turbines (TSTs), is the most popular. TSTs can be: (i) floating beneath the surface and anchored to the bottom by means of chains or cables (floating TSTs), or (ii) rigidly attached to the bottom by means of a structure (bottom-fixed TSTs) (Hammar et al., 2012; Khan et al., 2009). As a result of their different configuration, despite them being installed at the same coastal site, their performance may differ due to the varying hydrodynamic conditions throughout the water column (each type of TST is located at a different position within the water column). However, the implications for the power performance of opting for either floating or bottom-fixed devices have not been investigated as far as the authors are aware.

The aim of this study is to examine the differences in the power performance in real conditions of operation of two tidal stream plants, composed by either floating or bottom-fixed TSTs, proposed in a previous work (Sanchez, Carballo, Ramos, & Iglesias, 2014) where their impacts on the estuarine hydrodynamics were analysed. For this purpose, a 3D high-resolution numerical model is implemented in the Ria de Ortigueira, a drowned river valleys which is a promising site for tidal stream energy exploitation located in Galicia (NW Spain) (Figure 3.1). On the basis of the numerical results a detailed intra-annual power performance assessment of floating and bottom-fixed tidal plants have been conducted so as to investigate the importance of selecting the type of TST that performs best considering the specific hydrodynamic conditions of the area of interest.

USC
UNIVERSIDADE DE SANTIAGO DE COMPOSTELA

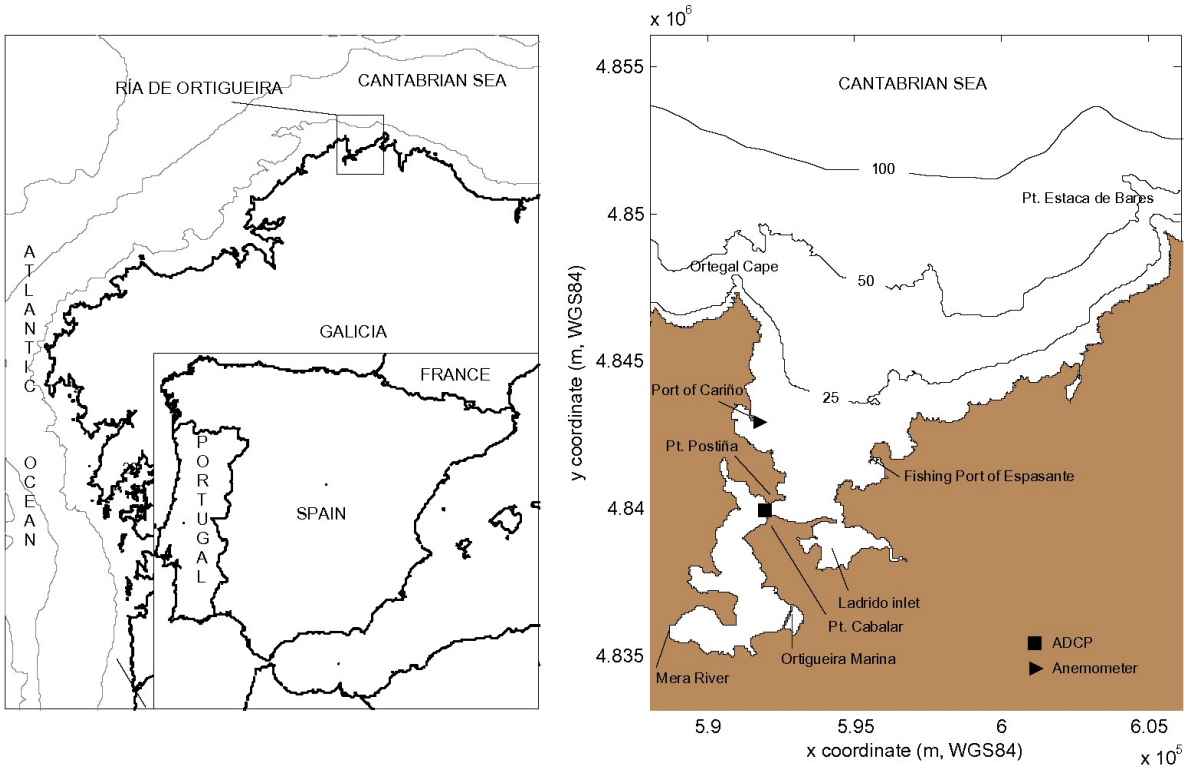


Figure 3.1. Situation of Ria de Ortigueira in the Iberian Peninsula (left-hand side plots) and detailed view of the ria (right-hand side plot)

3.2. METHODOLOGY

3.2.1. Three-dimensional hydrodynamics model

The 3D hydrodynamics model Delft3D-FLOW was used to compute the flow conditions in Ria de Ortigueira in the presence of a tidal stream farm. This model has been widely used to investigate coastal hydrodynamics in semi-enclosed water bodies (Bolle, Bing Wang, Amos, & De Ronde, 2010; Carballo et al., 2009a; Carballo et al., 2009b; Hu, Ding, Wang, & Yang, 2009; Iglesias & Carballo, 2010a; Iglesias & Carballo, 2011a; Iglesias et al., 2012; Ramos, Carballo, Álvarez, Sánchez, & Iglesias, 2014; Ramos et al., 2013). Given that the Galician Rias usually present a stratified flow pattern (e.g., (Iglesias & Carballo, 2009a; Ramos et al., 2014; Sánchez et al., 2014b), to properly analyse the ria's hydrodynamics, and as a result to conduct reliable energy computations, in this work a 3D model was implemented.

Delft3D-FLOW is a finite-difference code that solves the three-dimensional Navier-Stokes equations for incompressible free surface flow coupled to the transport equation (Deltares, 2010). In this manner baroclinic effects, which can be of great importance in the case of rias or estuaries (Dyer, K. E., 1997), can be taken into account. The model equations are as follows:

$$\frac{\partial u}{\partial x}+\frac{\partial v}{\partial y}+\frac{\partial w}{\partial z}=Q \tag{3.1}$$

USC UNIVERSIDADE DE SANTIAGO DE COMPOSTELA

$$\left.\begin{aligned}\frac{Du}{Dt} &= fv - g\frac{\partial\zeta}{\partial x} - \frac{g}{\rho_0}\int_{z'=z}^{z'=\zeta}\frac{\partial\rho}{\partial x}dz' + \upsilon_h\left(\frac{\partial^2 u}{\partial x^2}+\frac{\partial^2 u}{\partial y^2}\right)+\upsilon_v\left(\frac{\partial^2 u}{\partial z^2}\right)\\ \frac{Dv}{Dt} &= -fu - g\frac{\partial\zeta}{\partial y} - \frac{g}{\rho_0}\int_{z'=z}^{z'=\zeta}\frac{\partial\rho}{\partial y}dz' + \upsilon_h\left(\frac{\partial^2 v}{\partial x^2}+\frac{\partial^2 v}{\partial y^2}\right)+\upsilon_v\left(\frac{\partial^2 v}{\partial z^2}\right)\end{aligned}\right\} \quad (3.2)$$

$$\frac{\partial p}{\partial z} = -\rho g \quad (3.3)$$

$$\frac{Dc}{Dt} = D_h\left(\frac{\partial^2 c}{\partial x^2}+\frac{\partial^2 c}{\partial y^2}\right)+D_v\frac{\partial^2 c}{\partial z^2}-\lambda_d c + R_s \quad (3.4)$$

Equation (3.1) represents the conservation of mass under the assumption of incompressibility; Equation (3.2) represents the conservation of momentum in the *x*- and *y*-directions; Equation (3.3) expresses the conservation of momentum in the vertical direction which under the shallow-water assumption simplifies to the hydrostatic pressure distribution; finally, Equation (3.4) is the transport equation, which is solved in the present study for both salinity and temperature. In these equations, *x, y* and z represent the east, north and vertical directions, respectively and *u, v* and *w* the velocity components in the aforementioned directions; ζ is the free surface elevation above the datum; *Q* represents the intensity of mass sources per unit area; *f* is the Coriolis parameter; *g* is the gravitational acceleration, υ_h and υ_v are the horizontal and vertical eddy viscosity coefficients respectively, and ρ and ρ_0 are the density and the reference density of sea water, respectively. Finally, in the transport equation, *c* stands for salinity or temperature; D_h and D_v are the horizontal and vertical eddy diffusivity coefficients, respectively; λ_d represents the first order decay process; and R_s is the source term.

3.2.2. TSTs modelling

The flow conditions within a ria change as a result of the operation of the TSTs and the energy that they extract from the flow. If the flow at the locations of the TSTs and, consequently, their yield are to be accurately determined, it is therefore necessary to take them into account in the model. The operation of a turbine can be simulated by considering its effect on the flow, i.e., by adding a retarding force with the same magnitude as that exerted by the flow on the turbine but opposite direction. The common procedure for modelling this force is as a momentum sink (Ahmadian & Falconer, 2012; Ahmadian, Falconer, & Bockelmann-Evans, 2012; Defne et al., 2011; Ramos et al., 2013; Sánchez et al., 2014b). On this basis, in this study the retarding force was introduced into the model by adding the following sink terms to the right-hand side of the momentum equations (Equation 3.2) in the *x*- and *y*- directions:

$$\left.\begin{aligned}M_x &= -\frac{1}{2}\frac{C_T A}{V}Uu\\ M_y &= -\frac{1}{2}\frac{C_T A}{V}Uv\end{aligned}\right\}, \quad (3.6)$$

USC UNIVERSIDADE DE SANTIAGO DE COMPOSTELA

where M_x and M_y represent the momentum of the external forces per unit volume, V_c, in the *x*- and *y*- directions, respectively; *U* is the component of the effective flow velocity perpendicular to the turbine; A_t is the cross-sectional area of the turbine rotor; and C_T is the thrust coefficient (an aerodynamic coefficient given by the lift and drag coefficients) which is related to the power

coefficient, C_p (Bahaj, A. S., Molland, Chaplin, & Batten, 2007).The floating and bottom-fixed TSTs are modelled by introducing the retarding force in the vertical layers of the model corresponding to the water depth at which they operate.

3.2.3. Performance analysis

The analysis of the performance of a tidal stream farm can be based on three characteristic parameters describing the operation of the individual TSTs in the farm (Ramos & Iglesias, 2013a): electrical energy output, capacity factor and availability factor. The electrical energy output of the *i*-th TST of a tidal farm over the period from $t = 0$ to $t = t_1$ is given by

$$E_e{}^i = \int_0^{t_1} P_e(t)\ dt \tag{3.7}$$

where $P_e(t)$ is the electrical power output of the TST, which can be expressed as (Bahaj, A. S. & Myers, 2004)

$$P_e(t) = \frac{1}{2} C_p(v) \rho A_t [U(t)]^3 \tag{3.8}$$

where $C_p(v)$ is the power coefficient, defined as the ratio between the power available from the flow and the electrical power output. Its value varies with the flow velocity in a manner that is specific of each TST.

Therefore, the electrical energy output of the entire tidal farm is

$$E_e \quad = \sum_{i=1}^{n} E_e^i \tag{3.9}$$

where *n* is the number of TSTs of the farm.

The availability factor (A_f) is the ratio between the time during which the TST is actually generating power (T_g) – TSTs have a minimum (*cut-in*) and a maximum (*cut-off*) flow velocity, below and above which they do not generate electricity – and the total duration of the period considered (T_a):

$$A_f = \frac{T_g}{T_a} \tag{3.10}$$

The capacity factor (C_f) represents the ratio between the electrical energy output over a period of interest (E_e) and the electrical energy output the TST would have produced over the same period had it operated at rated power ($P_r T_a$):

$$C_f = \frac{E_e}{T_a P_r} \tag{3.11}$$

The information contained in the capacity factor can be expressed in terms of an annual cycle by means of the equivalent full-load hours:

USC UNIVERSIDADE DE SANTIAGO DE COMPOSTELA

$$FLH = \frac{E_e^a}{P_r} \tag{3.12}$$

where E_e^a is the annual electric energy output. The equivalent full-load hours represent the number of hours a turbine would have to operate at its rated power to produce the same amount of energy that it actually produced over a year.

To determine these parameters it is necessary, first, to define the location and characteristics of the tidal stream farm and, second, to implement a numerical model of the hydrodynamics in the area that taking into account the energy extracted by the farm. The implementation of the numerical model enables to obtain the perturbed flow velocities, which in turn are necessary for the computation of the aforementioned parameters.

3.3. APPLICATION TO RIA DE ORTIGUEIRA

3.3.1. Study site and proposed tidal plants

The rugged coastline of NW Spain is characterized by the rias, a specific type of primary estuary developed in high relief coasts drowned by the rise of sea level during Holocene (Dyer, Keith R., 1973; Evans & Prego, 2003), regarded as promising sites for tidal stream energy exploitation. These rias can be roughly divided into Rias Altas, or Higher Rias, Rias Centrales or Central Rias, and Rias Baixas or Lower Rías (Iglesias & Carballo, 2011a; Mendez & Rey, 2000). Owing to its complex geomorphology characteristics and its high tidal range, the Ria de Ortigueira (Figure 3.1), one of the Rias Altas, is amongst the most promising sites for tidal stream energy exploitation in the Iberian Peninsula (Iglesias et al., 2012; Sánchez et al., 2013).

Ria de Ortigueira is delimited by Cape Ortegal and Pt. Estaca de Bares (Figure 3.1). With an approximate area of 85 km and a length along its main axis of approx. 18 km, it is, by far, the largest of the Rias Altas. The tidal flow is strongest at two constrictions in its inner part where the highest current velocities occur. One of them is located to the East, between the main lobe of the ria and the Ladrido Inlet, and the other is located to the West, in the channel between Pt. Postiña and Pt. Cabalar. By applying the Tidal Stream Exploitability (TSE) index to this ria (Iglesias et al., 2012) the optimum site for the installation of a tidal stream farm was selected as follows. According to the TSE index values obtained, the former (eastern) constriction has a TSE of 0 owing to its insufficient water depth, and therefore it is considered inappropriate for tidal stream energy exploitation. By contrast, the TSE index value of the latter (western) constriction exceeds 5 – the largest value over the entire ria. Therefore, this area combines a substantial resource with an appropriate depth, implying that it is an appropriate site for an array of TSTs in Ria de Ortigueira (Figure 3.2).

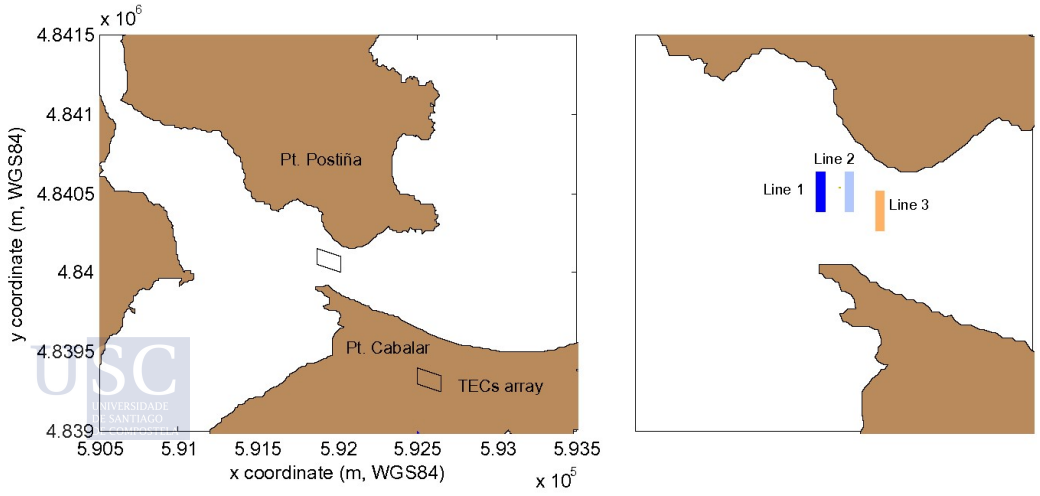


Figure 3.2. Area occupied by the proposed tidal stream plants (left-hand side plot) and their layout (right-hand side plot).

Two tidal stream farms were considered in this study, both composed of 30 turbines distributed in three lines roughly perpendicular to the main flow direction. The TST selected for the plants was an Evopod turbine (Oceanflowenergy,) in view of its appropriateness for shallow waters areas (Table 3.1). The surface occupied in plan view by each farm is about 1500 m^2, corresponding to a sweep area of approx. 600 m^2. Both arrays proposed are located at the same site and present the same layout (Figure 3.2) but differ in their vertical configuration. The first plant (P1) is composed of floating TSTs (Oceanflowenergy,) occupying roughly the upper 65 per cent of the water column; the second plant (P2) is composed by TSTs with exactly the same mechanical characteristics, but fixed to the bottom, occupying approximately the lower 65 per cent of the water column.

Table 3.1. Main technical specifications of the Evopod turbine [D, rotor diameter; Vci, cut-invelocity; V_r, rated velocity; V_{co}, cut-off velocity; P_r , rated power; A, swept area; C_{pNO}, power coefficient in normal operation; C_{pSC}, power coefficient in stall control]

D (m)	V_{ci} (ms^{-1})	V_r (ms^{-1})	V_{co} (ms^{-1})	A (m^2)	Pr (kW)	C_{pNO}	C_{pSC}
5	0.7	2.2	3.1	19.6	40	0.35	0.2

3.3.2. Model implementation

The numerical model previously described in sections 2.1 and 2.2 was implemented in Ria de Ortigueira. For this purpose, a Cartesian, varying-size numerical grid, with a total of 57361 cells was created covering the whole ria and extending up to the 150 m isobath. The grid size was finer (50 × 50 m) in the inner and middle ria than in the outer ria and on the shelf, where it decreased in the y-direction up to values of 50 × 150 m at the northern outer boundary. As regards the vertical grid discretization, a σ-coordinate system (Philips, 1957) with twelve layers was used. The layer thickness (% of water column) from surface to bottom was, as a percentage of the water column: 2, 3, 5, 10, 15, 15, 15, 15, 10, 5, 3 and 2. The resolution of the grid is higher near the seabed and surface in order to better resolve boundary layers flow. To close the turbulence the k-ε model (Rodi, 1987) was adopted. Finally, the bathymetry (Figure 3.3) was obtained from nautical charts 408 and 4083 from the Hydrographic Institute of the Spanish Navy (*Instituto Hidrografico de la Marina*) and interpolated onto the computational grid.

Table 3.2. Main tidal constituents in the Ria de Ortigueira

Constituent	Amplitude (cm)	Phase (º)
M2	122.79	90.15
S2	42.91	121.08
N2	25.98	70.39
K2	12.03	118.76
K1	7.35	73.49
O1	6.22	324.62
P1	2.22	65.15
Q1	2.11	271.31
M4	1.45	334.80

USC UNIVERSIDADE DE SANTIAGO DE COMPOSTELA

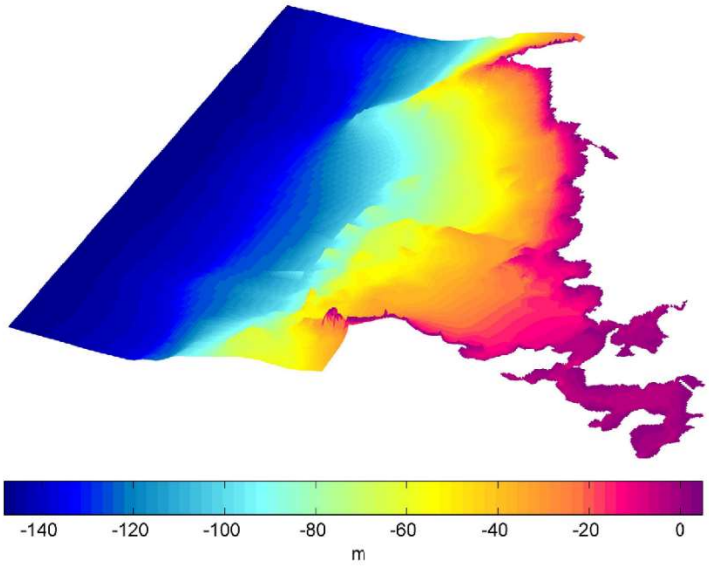


Figure 3.3. Three-dimensional representation of the bathymetry of Ria de Ortigueira.

With regard to the boundary conditions, Dirichlet conditions were imposed along the open boundary by prescribing the sea surface level based on the main tidal harmonics (Table 3.2) together with daily thermohaline conditions. At the land margins the forcings were null flow through the boundary and zero shear stress (free slip). On the other hand, the shear stress at the seabed, τ_{b3D}, induced by a turbulent flow is related to the current velocity above the bed:

$$\vec{\tau}_{b3D} = \frac{\rho_0 g \vec{u}_b \left|\vec{u}_b\right|}{C_{3D}^2} \tag{3.13}$$

where $\vec{u}_b$ is the magnitude of the horizontal velocity in the lowest layer (immediately above the bed) and C_{3D} is the 3D Chézy coefficient, given by

$$C_{3D} = C_{2D} + \frac{\sqrt{g}}{\kappa} ln\left(\frac{\Delta z_b}{2H}\right) \tag{3.14}$$

with κ the von Karman constant (κ = 0.41), Δz_b the vertical distance from the seabed to the nearest computational grid point, H the total water depth and C_{2D} the 2D Chézy coefficient, which can be determined based on Manning's coefficient, n, as follows:

$$C_{2D} = \frac{\sqrt[6]{H}}{n} \tag{3.15}$$

Manning's coefficient is assumed to be depth-dependent according to previous studies (Cheng, Casulli, & Gartner, 1993; Dias & Lopes, 2006; Iglesias & Carballo, 2010a); the value considered for each water depth range is shown in Table 3.3.

Finally, at the free surface the wind shear-stress, τ_s, is defined as

$$\vec{\tau}_s = \rho_a C_d U_{10}^2 \tag{3.16}$$

where ρ_a is the density of the air, U_{10} the wind speed at 10 m above the sea surface and C_d the wind drag coefficient, calculated following (Smith, 1980) and (Yelland et al., 1998).

Table 3.3. Value of Manning's coefficient function of water depth

H	n
$-2.5 \le H < -2.0$	0.042
$-2.0 \le H < -1.5$	0.038
$-1.5 \le H < 1.0$	0.034
$-1.0 \le H < -0.5$	0.030
$-0.5 \le H < 0.0$	0.027
$0.0 \le H < 0.5$	0.024
$0.5 \le H < 1.0$	0.022
$1.0 \le H < 3.0$	0.020
$3 \le H < 10$	0.018

The tidal stream plant was implemented in the model by using the momentum sink approach as described in section 3.2.2. In the case of P1 and P2, the retarding force affects the 7 upper or lower layers of the model, respectively. In both cases the value of C_T considered is 0.8, which corresponds to a value of the power coefficient, C_p, of 0.35 (Bahaj, A. S. et al., 2007).

3.3.3. Model validation

The numerical model was validated by comparing the numerical results with field data of water level and current velocity. For this purpose, an ADCP (Acoustic Doppler Current Profiler) Sontek Argonaut XR and two CTD (Conductivity Temperature a Depth) sensors Seabird Microcat 37 were deployed in Ria de Ortigueira (Figure 3.1) over a 19-day period. During the validation period, the numerical model was forced with the main tidal harmonics (Table 3.2) and daily conditions of salinity and temperature at the open boundaries, wind data every thirty minutes, and daily fluvial discharge data.

Table 3.4. Correlation coefficient between computed and measured time series of sea level (R_ζ) and flow velocity magnitude and direction (R_M and R_D respectively)

USC UNIVERSIDADE DE SANTIAGO DE COMPOSTELA

Water level		Current velocity			
			Surface layer	Middle layer	Bottom layer
R_ζ	0.9895	R_M	0.8965	0.8619	0.8439
		R_D	0.8509	0.8375	0.8215

The correlation coefficients between measured and computed time series of water level and current velocity direction and magnitude were computed (Table 3.4). It can be observed that the resulting correlation coefficients are close to the unit for both variables. The excellent agreement between measured and computed water level can be observed in Figure 3.4 over 9-day time series representation. In the same way the excellent agreement between time series of numerical and measured velocities can be observed in Figure 3.5 at three points of the water column: surface, mid-depth and bottom.

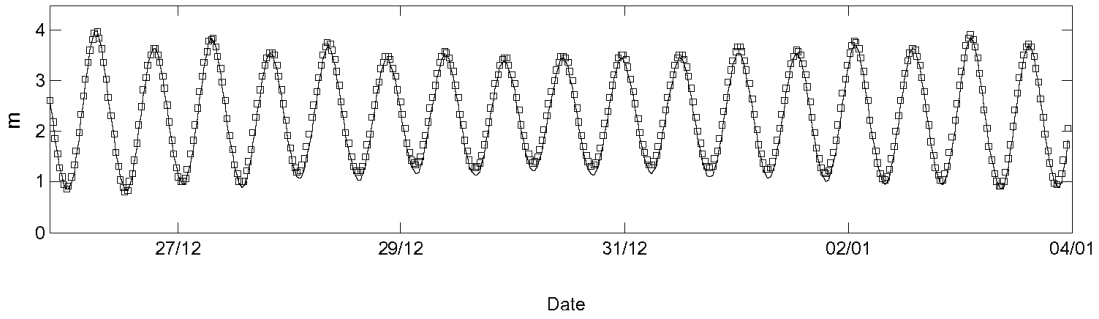


Figure 3.4. Comparison between computed (–) and measured (□) water levels in the ADCP location during the validation period

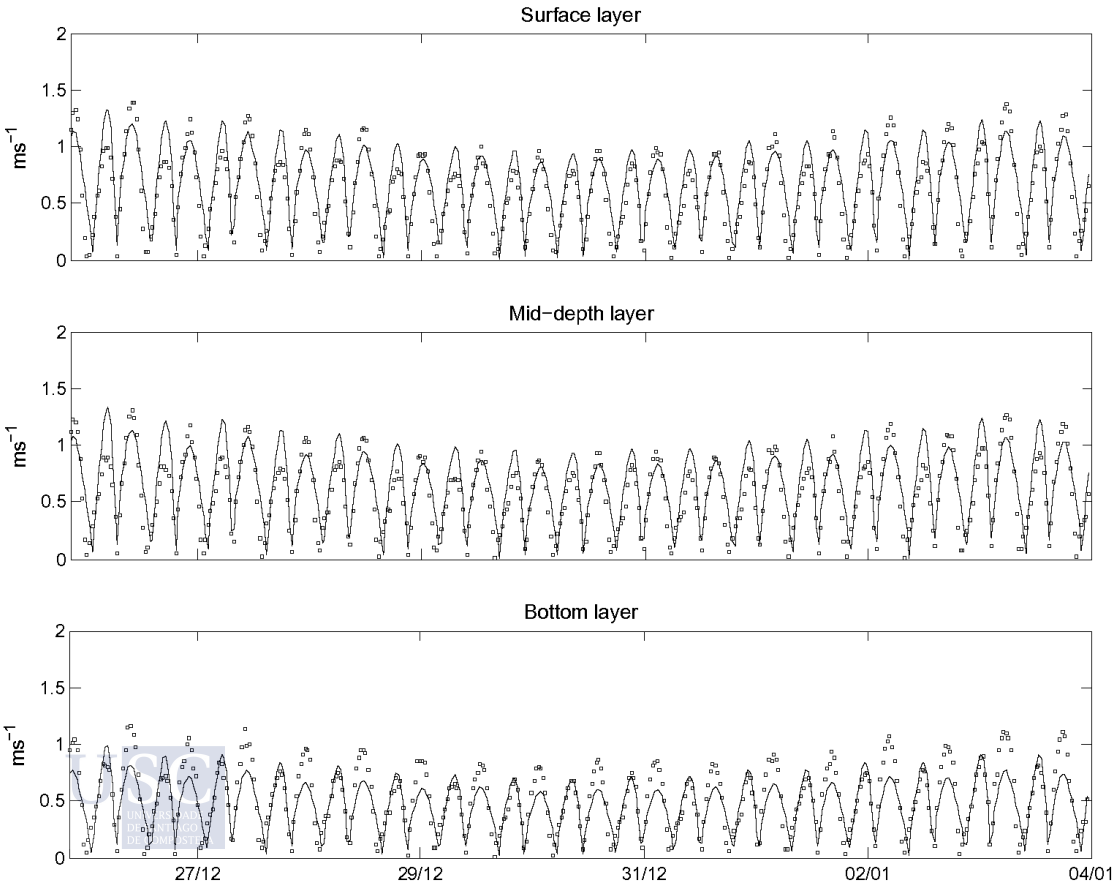


Figure 3.5. Comparison between computed (–) and measured (□) current speed for the surface, mid-depth and bottom layers in the ADCP location during the validation period

3.4. POWER PERFORMANCE ANALYSIS

Two long-term numerical simulations covering an entire year (Case 1 and Case 2, each of them considering a different tidal farm) were performed. In Case 1, the array introduced in the model is composed of floating TSTs (Plant P1), and in Case 2, of bottom-fixed TSTs (Plant P2). Next, on the basis of the numerical simulations and the characteristics of the turbine selected (Table 3.1 & Figure 3.6), the power performance throughout the entire year of the two tidal farms proposed was computed according to the parameters previously defined (section 2.3).

The forcing factors considered were the main tidal harmonics (Table 3.2), monthly averaged salinity and temperature conditions along the open boundary and monthly averaged river discharge. The velocity considered for electrical power generation is the velocity at rotor height, as in the case of wind generators, which varies depending on the case study (1 or 2) as a result of the different water depth at which the rotor is located.

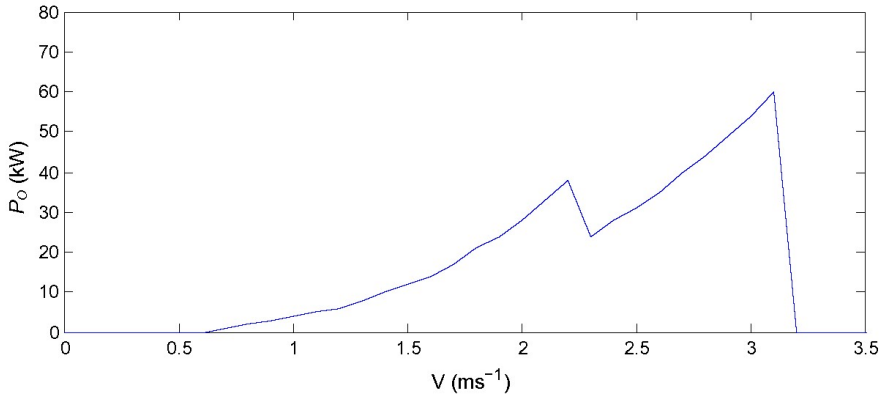


Figure 3.6. Power curve of the Evopod turbine [*v*, flow velocity; P_O, electrical power output]

The differences in the power performance of the two plants analysed are significant (Table 3.5). The annual energy production of P1 is 2.425×10^3 MWh, whereas the production of P2 is around 40% less. These differences are even larger in the case of the first row of TSTs (hereafter referred to as Line 1), whose energy production is almost double in the case of floating TSTs (P1) relative to bottom-fixed units (P2). These results prove that in a coastal area with significant differences in the flow speed throughout the water column, such as the study area, significant differences can arise between the power performance of plants composed of floating or bottom-fixed TSTs.

As a regard the operation time, the values of the availability factor (A_f) show that P1 and P2 operate during 63 % and 48% of the time, respectively. This would have implications if an energy storage system were required – it would have to be substantially larger for P2 given its lower operation time. Regarding the capacity factor (C_f), the differences are even higher, roughly 64% (0.23 and 0.64 for P1 and P2, respectively), indicating an important advantage of P1, for a higher capacity factor is associated with a better production to capital investment ratio. These important differences are directly transferred to the equivalent full-load hours (*FLH*): P1 has over 2000 *FLH*, and P2 only about 1250 *FLH*. Although a detailed study of the installation

costs would be necessary for an exhaustive analysis of the profitability of the proposed plant, the low *FLH* of P2 does not contribute to its economic viability.

Table 3.5. Annual parametric analyse of the different lines of the array

		Floating TSTs (P1)	Bottom-fixed TSTs (P2)
E_e(MWh)	Line 1	1.161×10^3	0.684×10^3
	Line 2	0.673×10^3	0.426×10^3
	Line 3	0.591×10^3	0.389×10^3
	Array	2.425×10^3	1.498×10^3
A_f	Line 1	0.63	0.53
	Line 2	0.53	0.41
	Line 3	0.50	0.39
	Array	0.63	0.53
C_f	Line 1	0.33	0.19
	Line 2	0.19	0.12
	Line 3	0.17	0.11
	Array	0.23	0.14
FLH	Line 1	2902	1710
	Line 2	1682	1065
	Line 3	1479	971
	Array	2021	1249

On the basis of the numerical simulations and the characteristics of the turbine selected, the monthly power performance parameters defined in section 2.3 were determined for P1 and P2 (Figures 3.7, 3.8, 3.9). The intra-annual power performance presents a significant variability, which should be analysed to ascertain the optimum tidal farm configuration. In the case of the energy production (Figure 3.7), the month with highest E_e is August (227.74 MWh and 143.44 MWh for P1 and P2, respectively); on the other hand, November presents the lowest E_e (185.52 MWh for P1 and 112.76 for P2, about 20% lower than that of August).

An important aspect that should be noted is that, far from what might be expected, it is not in the months with the largest tides, and therefore the strongest velocity peaks, that the energy production is largest – or, more generally, that the farm performance is best. The explanation lies in that in the months with highest tides (March and September) there exist important differences between tidal cycles (with peak velocities ranging from 2.2 ms^{-1} to 0.5 ms^{-1}) whereas in other months, e.g., July or August, the tidal cycles are more homogenous (with peak velocities ranging from 1.5 ms^{-1} to 1 ms^{-1}). This can be clearly observed in Figure 3.10, in which the flow velocity for P1 at the mid-depth layer is represented throughout a complete spring-neap cycle in March and July for P1 at mid-depth layer.

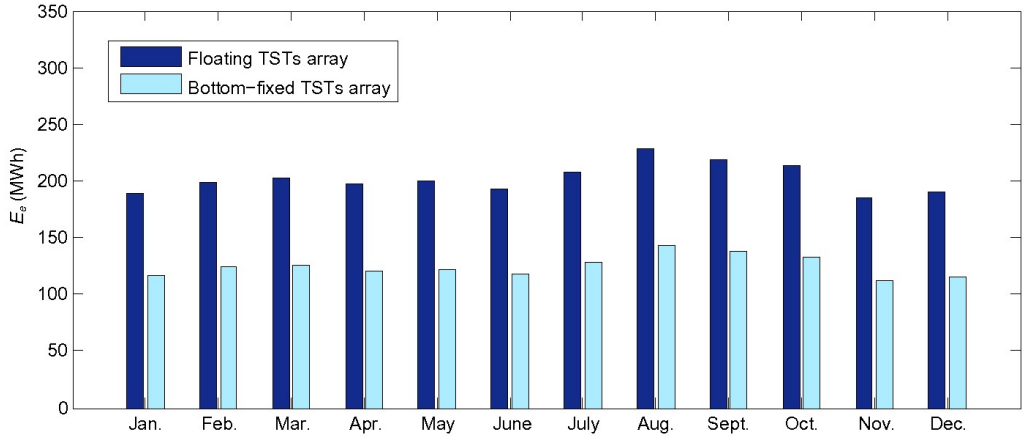


Figure 3.7. Monthly electrical energy output [E_e] of floating and bottom-fixed tidal plants.

The significant differences in the annual power performance parameters between both plants is also reflected in important differences in the monthly power performance parameters (Figures 3.7, 3.8, 3.9); the general trends of the performance of the two plants are, however, rather similar throughout the whole year. In the case of the power production, and in the case of capacity factor, the most important differences between both plants occur in December, when the production of P1 is 40 % higher, whereas the smallest differences occur in July and August, about 37 %.

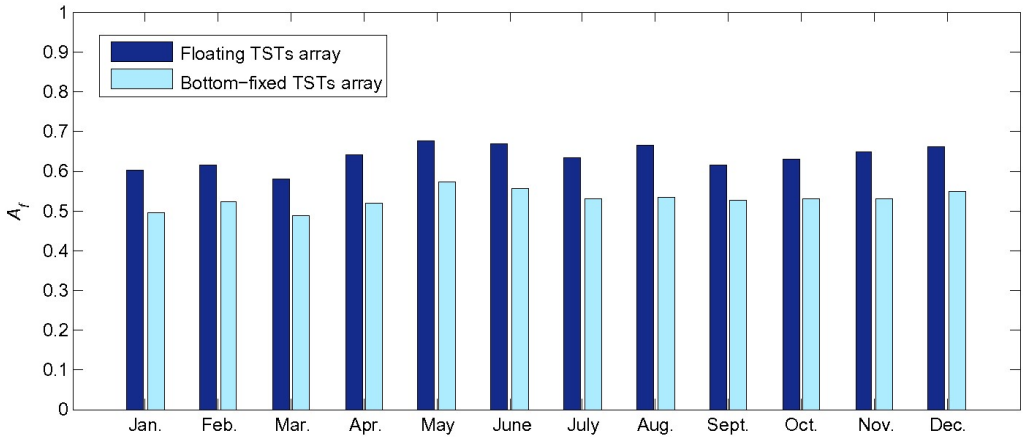


Figure 3.8. Monthly availability factor [A_f] of floating and bottom-fixed tidal plants.

Finally, as regards the availability factor (Figure 3.8), the monthly differences between both plants are less important than in the case of electrical energy output (Figure 3.7) and capacity factor (Figure 3.9). For P1 and P2 they are in the ranges 0.5 – 0.6 and 0.4 – 0.5, respectively. The months with highest and lowest operation time are May and March, respectively. This also helps to explain the fact that the energy production during these months is similar, in spite of the fact that the peak velocities are higher in March.

USC UNIVERSIDADE DE SANTIAGO DE COMPOSTELA

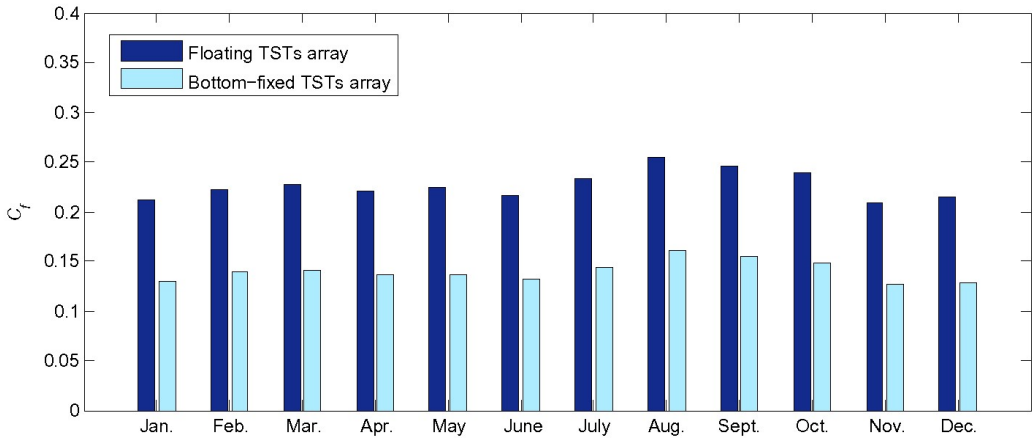


Figure 3.9. Monthly capacity factor [C_f] of floating and bottom-fixed tidal plants.

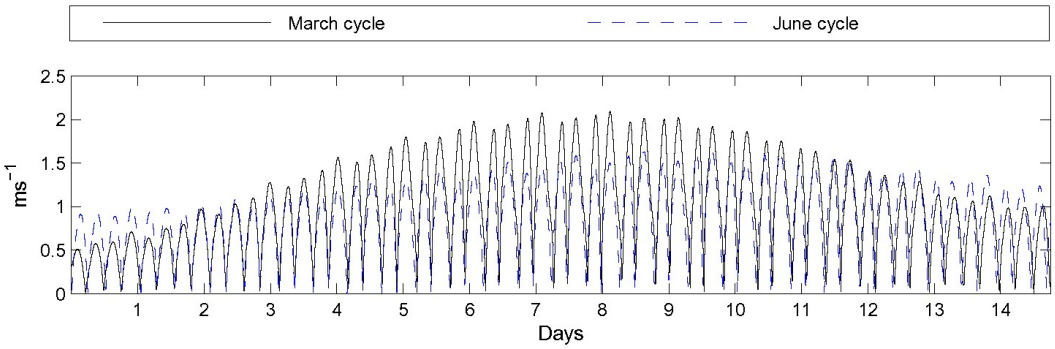


Figure 3.10. Comparison between flow velocities throughout two spring-neap cycles during March and June.

3.5. CONCLUSIONS

In this work a comparison of the intra-annual performance of floating and bottom-fixed TSTs was performed through a case study in Ria de Ortigueira, and its implications for tidal stream energy exploitation were addressed for the first time. For this purpose, a 3D numerical model was implemented and applied to simulate the hydrodynamics of this estuary during a complete year, taken into account the energy extracted from the flow by the tidal farms. Two options were considered for the latter, consisting of floating or bottom-fixed TSTs, referred to as plants P1 and P2, respectively. The tidal plants were modelled by introducing a momentum sink term in the vertical layers of the model corresponding to the area occupied by the rotors of the turbines. The computed velocity series were then used to conduct a thorough power performance analysis based on three performance parameters allowing the characterization of the operation of the plants: electric energy output, availability factor and capacity factor.

Remarkable differences in the power performance of both plants were found. Plant P1 presents higher values of the performance parameters considered; in particular, the annual electrical energy output is almost twice that of P2, and its capacity factors around 64% higher, showing that floating devices offer a better production to capital investment ratio. Regarding the availability factor, the differences are less important (15%); however, the power output of P1 is smoother, and this is an advantage that should not be disregarded – not least if an energy storage system is to be installed. In addition, it emerged from the intra-annual analysis that the aforementioned parameters also present a significant monthly variability. Their intra-annual

general trend is similar for both plants, i.e., the annual differences are roughly maintained throughout the whole year. A finding of special interest is that, contrary to what might be expected, the months with largest peak flow velocities are not those with the highest values of the power performance parameters, including energy output.

In sum, the power performance of floating and bottom fixed TSTs at the same location can differ greatly depending on the characteristics of the hydrodynamic conditions of the coastal area in which they operate. This can be exacerbated in the case of coastal bodies with significant differences in the current velocities throughout the water column, as is the case of the study area (Ria de Ortigueira). As a result of the higher velocities near the surface, floating TSTs provide a much better performance than bottom-fixed devices. Finally, a significant intra-annual variability in the power performance was observed, which leads to the conclusion that the energy output and performance of a tidal stream farm must be analysed based on simulations covering a complete year, rather than by extrapolating the results obtained for one spring-neap cycle, as it is done following the common procedure.

Beyond the interest of these results for the coastal area herein studied, the procedure presented in this work could be used to analyse the annual power performance of different tidal stream plants elsewhere. Furthermore, in addition to the performance, which is of undoubtedly importance in the decision-making regarding the installation of a tidal stream plant, other factors such as the impact on the hydrodynamics or the long-term coastal morphology should be considered before selecting the optimum farm configuration. These aspects will be dealt with as a continuation of this line of research.

USC
UNIVERSIDADE DE SANTIAGO DE COMPOSTELA

USC
UNIVERSIDADE
DE SANTIAGO
DE COMPOSTELA

4. FLOATING VS. BOTTOM FIXED TURBINES FOR TIDAL STREAM ENERGY: A COMPARETIVE IMPACT ASSESMENT

This chapter reproduces completely the contents of the following research paper:

Title: *Floating vs. bottom-fixed turbines for tidal stream energy: A comparative impact assessment*.

Journal: Energy, Volume 72 (1) August 2014, Pages 691-701

Doi: https://doi.org/10.1016/j.energy.2014.05.096

Authors: M. Sánchez [a], R. Carballo [a], V. Ramos [a], G. Iglesias [b]

Institutions: *(a) University of Santiago de Compostela, Hydraulic Engineering, Campus Univ. s/n, 27002 Lugo, Spain*

(b) University of Plymouth, School of Marine Science and Engineering, Marine Building, Drakes Circus, Plymouth PL4 8AA, United Kingdom

ABSTRACT

Tidal currents represent a promising energy source for electrical supply in Europe; however, nowadays there still exist important aspects to address regarding their exploitation prior to becoming a fully-fledged renewable energy. The accurate assessment of the available resource and the development of Tidal Energy Converters (TECs) are challenges which have been partially solved, but it is necessary to go further in the investigation of other aspects such as the impacts on the estuarine circulation. In this work, the impacts caused on the estuarine circulation in Ria de Ortigueira by the operation of two different tidal stream plants, one composed of floating and the other of bottom-fixed Tidal Stream Turbines (TSTs), were analysed by means of a three-dimensional model. Prior to using the model for assessing the impacts, it was validated based on field data at two measuring stations. Then, the tidal farms were implemented in the model as a momentum sink. The results show that there are no significant differences between the impacts caused on the general circulation by floating and bottom-fixed TSTs with slight reductions of the flow being apparent up to some km away the plant. Then again, strong differences were found in the vicinity of the plant.

Keywords: tidal currents, energy exploitation, 3D numerical model, impacts, floating TSTs, bottom-fixed TSTs

USC DE COMPOSTELA

4.1. INTRODUCTION

The interest of marine energy resources in Europe has been widely demonstrated over the last decades e.g. (Babarit et al., 2006; Iglesias & Carballo, 2010b; Iglesias & Carballo, 2011c; López, Andreu, Ceballos, Martínez de Alegría, & Kortabarria, 2013; Ramos & Iglesias, 2013b; Sánchez et al., 2013; Veigas, Carballo, & Iglesias, 2014). In particular, the exploitation of tidal energy was considered for the first time for energy supply in the 60's (O Rourke, Boyle, & Reynolds, 2010). Since then, lots of studies have dealt with this issue and several projects have been developed (O Rourke et al., 2010; Xia, Falconer, & Lin, 2010). Initially, the exploitation of tidal energy was based on the construction of tidal barrages but soon this system was abandoned due to its aggressiveness with the environment – large effects caused on the seabed, marine ecosystems, hydrodynamics, shipping, etc (Hooper & Austen, 2013). The efforts were then focused on the study of the exploitation of tidal currents. In this vein, two main lines of research dealing with the investigation of this new energy source can be distinguished: the assessment of the energy resource, e.g. (Brooks, 2006; Carballo et al., 2009a; Lim & Koh, 2010; O Rourke et al., 2010), and the development of new technologies capable of converting the kinetic energy into electric energy (Güney & Kaygusuz, 2010; Rourke, Boyle, & Reynolds, 2010). Both tasks constitute one of the major scientific challenges over the last decades and much work in these fields has been required to get successful results. Nevertheless, as a result of the large effort made, several regions with important tidal stream energy potential have been identified around the world and some Tidal Energy Converters (TECs) have achieved a commercial or pre-commercial stage (although a lot TECs are still in development stage). Overall, these TECs can be classified, according to its principle of operation, into reciprocating (Yavuz, Koç, & Kaynak, 2013) or rotating (Faez Hassan, Karim, & El-Shafie, 2012; Myers & Bahaj, 2010) devices. The latter, also known as Tidal Stream Turbines (TSTs), are the most popular and can be install with two different configurations: (i) floating beneath the surface and anchored to the bottom (floating TSTs), or (ii) rigidly attached to the bottom by means of a structure (bottom-fixed TSTs).

Despite both challenges being partially solved, there still exist important issues to be addressed and additional work is necessary. In this vein, it is important to note that tidal currents are almost negligible in the open ocean or along straight coasts, with the greatest tidal resource being usually located in estuaries, bays, and other coastal indentations (Carballo et al., 2009a; Ramos & Iglesias, 2013a; Work, Haas, Defne, & Gay, 2013) presenting complex hydrodynamics. Therefore, given the environmental importance that these coastal areas usually boast, the potential effects resulting from their exploitation should be carefully analysed before installing a tidal stream energy plant. With this aim, recent works have begun to study part of these potential effects (Ahmadian & Falconer, 2012; Ahmadian et al., 2012; Neill et al., 2009; Neill et al., 2012; Ramos et al., 2013; Ramos et al., 2014; Sánchez et al., 2014b).

In order to go further in the investigation of the impacts of tidal stream plants on the estuarine circulation, this work studies the effects resulting by the operation of two tidal stream plants in a specific region, Ria de Ortigueria (NW Spain), by means of a three-dimensional high resolution numerical model. Both plants have the same plan view layout but present a different vertical configuration: one is composed of floating and the other of bottom-fixed TSTs. As a result of their different configuration, despite them being installed at the same coastal site, the impacts caused by their operation may widely differ due to the varying hydrodynamic conditions throughout the water column (each type of TST is located at a different position within the water column). Clearly, the differences in their impacts on the estuarine hydrodynamics may be a major issue in the selection of the most appropriated TST for a specific

area. Far beyond the interest of the results obtained for the coastal region herein studied, the final aim of this investigation is to establish a methodology which can be used in the analysis of the potential impacts on the estuarine circulation in other rias or estuaries with similar hydrodynamic conditions.

The structure of this article is as follows. In Section 4.2, information about the area of study is provided. In Section 4.3, the numerical model implemented for the simulation of the operation conditions of the tidal plants considered is described. Next, Section 4.4 deals about the impacts caused on the estuarine circulation by the proposed plants. Finally, in Section 4.5 the most relevant conclusions are drawn, stating the interest of determining the impacts caused on the estuarine hydrodynamics by different TSTs for the selection of the most appropriated turbine.

4.2. STUDY AREA

The most characteristic feature of the Atlantic Region of the Iberian Peninsula is the presence of large drowned river valleys, a specific type of primary estuary (Perillo, 1995), generally known as rias, developed in high relief coasts drowned by the rise of sea level during Holocene. Although the use of the term ria is more popular in this region, there exist estuaries with similar geomorphology conditions in other areas around the world such as Brittany in France, Devon and Cornwall in the British Isles, Korea, certain regions of the Chinese and the Argentina coasts. It is important to note that the morphology of the rias have not any Pleistocene glacial influence which makes them quite different from fjords (Castaing & Guilcher, 1995).

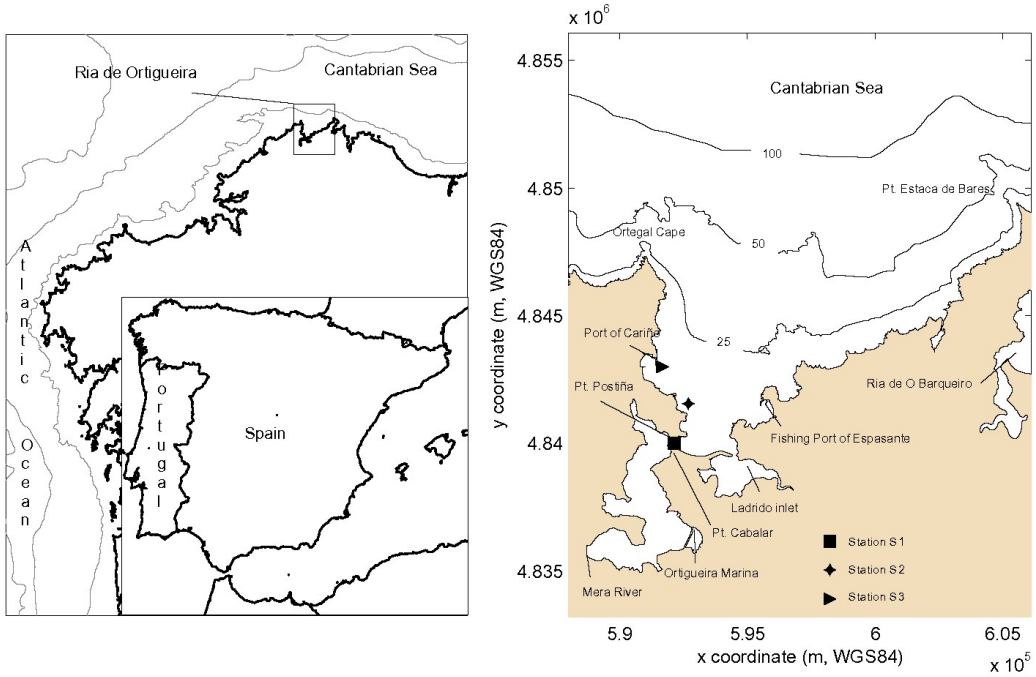


Figure 4.1. Location of Ria the Ortigueira (left-hand site). Detailed map of Ria the Ortigueira showing singular points and measuring stations (right-hand site).

The ria herein analysed, Ria the Ortigueira (Figure 4.1), is characterized by its irregular geomorphology. Flanked to the West by Cape Ortegal and to the East by Pt. Estaca de Bares, the northernmost point of the Iberian Peninsula, Ria the Ortigueira has an intricate main lobe presenting several curves and narrowings, and a secondary lobe, the Ladrido Inlet. The area occupied by the water mass covers 85 km^2 with its main axis extending approx. 18 km.

Furthermore, there exist several streams flowing into the ria, but only one of them presents a significant discharge, River Mera, with an average flow rate of 5.45 m^3s^{-1}. Regarding the tide, the main component of the astronomical tide is the M2 (Table 4.1), as in the rest of Europe. However, there are other semidiurnal relevant components in the area such as S2, N2 and K2 which results in a region with a semidiurnal tidal regime as it is stated by its *Form Factor* (*F=0.082*) (Pugh, 1996).

Table 4.1. Main tidal constituents in the Ria de Ortigueira

Constituent	Amplitude (cm)	Phase (º)
M2	122.79	90.15
S2	42.91	121.08
N2	25.98	70.39
K2	12.03	118.76
K1	7.35	73.49
O1	6.22	324.62
P1	2.22	65.15
Q1	2.11	271.31
M4	1.45	334.80

The narrowings of the main lobe together with the high tidal range (up to 4.5 m during spring tides) make tidal currents increase significantly; this causes Ria de Ortigueira being a promising region for tidal stream energy exploitation. According to previous works in this ria (Iglesias et al., 2012; Sánchez et al., 2013), tidal currents reach values up to 2.5 ms^{-1} in the narrow between Pt. Postiña and Pt. Cabalar. This strong current and its adequate water depth make this area the most appropriated site for tidal stream energy exploitation in Ria de Ortigueira (Iglesias et al., 2012). Consequently, the two tidal plants considered in this article are placed in this location. Furthermore, both plants have the same layout with an area of occupation in plan view of about 1500 m^2. The first plant (P1) is composed of floating TSTs occupying roughly the upper part of the water column and the second plant (P2) is composed of TSTs with exactly the same mechanical characteristics, but fixed to the bottom, occupying approximately the lower part of the water column.

The TST selected is an Evopod turbine (Oceanflowenergy,) in view of its appropriateness for shallow waters areas (Table 4.2), as it is the case of Ria de Ortigueira. Following the distance recommendations between lines of TSTs, 30 turbines with a sweep area of approx. 600 m^2, were distributed over three lines roughly perpendicular to the main flow direction within this area.

Table 4.2. Main technical specifications of the Evopod turbine [*D*, rotor diameter; V_{ci}, cut-invelocity; V_r, rated velocity; V_{co}, cut-off velocity; P_r , rated power; *A*, swept area; C_{pNO}, power coefficient in normal operation; C_{pSC}, power coefficient in stall control]

D (m)	V_{ci} (ms^{-1})	V_r (ms^{-1})	V_{co} (ms^{-1})	*A* (m^2)	*Pr* (kW)	C_{pNO}	C_{pSC}
5	0.7	2.2	3.1	19.6	40	0.35	0.2

4.3. NUMERICAL MODEL DESCRIPTION

4.3.1. Governing equations

The 3D hydrodynamics model Delft3D-FLOW (Deltares, 2010) was used to compute the flow conditions in Ria de Ortigueira with and without the presence of each of the studied tidal stream plans. This model was used in previous studies dealing with the investigation of coastal hydrodynamics in semi-enclosed water bodies (Bolle et al., 2010; Carballo et al., 2009a; Carballo et al., 2009b; Hu et al., 2009; Iglesias & Carballo, 2010a; Iglesias & Carballo, 2011a; Iglesias et al., 2012; Ramos et al., 2013).

The model is a finite-difference code solving the Navier-Stokes equations in their baroclinic form, i.e., coupled with the transport equation, which is solved for both salinity and temperature. Given that the Galician Rias usually present a stratified flow pattern (e.g., (Iglesias & Carballo, 2009a; Sánchez et al., 2014b)) and that the scopes of this work is the investigation of the impacts on the circulation caused by two tidal plants located at different positions in the water column, the model was implemented in its 3D form. The 3D model equations are:

$$\frac{\partial u}{\partial x}+\frac{\partial v}{\partial y}+\frac{\partial w}{\partial z}=Q \tag{4.1}$$

$$\left.\begin{aligned}\frac{Du}{Dt}&=fv-g\frac{\partial \zeta}{\partial x}-\frac{g}{\rho_0}\int_{z'=z}^{z'=\varsigma}\frac{\partial \rho}{\partial x}dz'+\upsilon_h\left(\frac{\partial^2 u}{\partial x^2}+\frac{\partial^2 u}{\partial y^2}\right)+\upsilon_v\left(\frac{\partial^2 u}{\partial z^2}\right)\\ \frac{Dv}{Dt}&=-fu-g\frac{\partial \zeta}{\partial y}-\frac{g}{\rho_0}\int_{z'=z}^{z'=\varsigma}\frac{\partial \rho}{\partial y}dz'+\upsilon_h\left(\frac{\partial^2 v}{\partial x^2}+\frac{\partial^2 v}{\partial y^2}\right)+\upsilon_v\left(\frac{\partial^2 v}{\partial z^2}\right)\end{aligned}\right\} \tag{4.2}$$

$$\frac{\partial p}{\partial z}=-\rho g \tag{4.3}$$

$$\frac{Dc}{Dt}=D_h\left(\frac{\partial^2 c}{\partial x^2}+\frac{\partial^2 c}{\partial y^2}\right)+D_v\frac{\partial^2 c}{\partial z^2}-\lambda_d c+R_s \tag{4.4}$$

Equation (4.1) represents the conservation of mass under the assumption of incompressibility; Equation (4.2) represents the conservation of momentum in the *x*- and *y*-directions; Equation (4.3) expresses the conservation of momentum in the vertical direction which under the shallow-water assumption simplifies to the hydrostatic pressure distribution; finally, Equation (4.4) is the transport equation, which is solved in the present study for both salinity and temperature. In these equations, *x, y* and z represent the east, north and vertical directions, respectively, and *u, v* and *w* the velocity components in the aforementioned directions; ζ is the free surface elevation above the datum; Q represents the intensity of mass sources per unit area; f is the Coriolis parameter; g is the gravitational acceleration, υ_h and υ_v are the horizontal and vertical eddy viscosity coefficients, respectively, and ρ and ρ_0 are the density and the reference density of sea water, respectively. Finally, in the transport equation, c stands for salinity or temperature; D_h and D_v are the horizontal and vertical eddy diffusivity coefficients, respectively; λ_d represents the first order decay process; and R_s is the source term.

Regard to the turbine's implementation in the model, it can be simulated by considering its effect on the flow, or in other words, by introducing a retarding force with the same magnitude as the force exerted by the flow on the turbine but in the opposite direction. This force was

introduced in the model by adding a sink term to the right-hand side of the momentum equations (Equation 4.2) in the *x*- and *y*- directions:

$$\left.\begin{aligned} M_x &= -\frac{1}{2}\frac{C_T A}{V}Uu \\ M_y &= -\frac{1}{2}\frac{C_T A}{V}Uv \end{aligned}\right\}, \tag{4.5}$$

where M_x and M_y represent the momentum of the external forces per unit volume, V, in the *x*- and *y*- directions, respectively; U is the component of the effective flow velocity perpendicular to the turbine; A is the area occupied by the turbine; and C_T is the thrust coefficient (an aerodynamic coefficient given by the lift and drag coefficients) which is related to the power coefficient, C_p (Bahaj, A. S. et al., 2007).The floating and bottom-fixed TSTs are modelled by introducing this retarding force in the vertical layers of the model corresponding to the water depth at which they operate.

4.3.2. Model set-up

4.3.2.1. Model area

The model covers Ria the Ortigueira and stretches approx. 10 km offshore (roughly 150 m isobath). Horizontally, a varying-size numerical grid was implemented, with a total of 57,361 cells. The grid size was set constant (50 × 50 m) in the inner and middle ria, progressively decreasing in the outer ria in the y-direction up to values of 50 × 150 m at the northern outer boundary (Figure 4.2). Vertically, 12 σ-coordinate layers were used (Philips, 1957). The layers follow the bottom topography and are distributed symmetrically with respect to the midpoint in the vertical, increasing their resolution towards the surface and the bottom in order to better resolve boundary layers flow (Lynch, Davies, Gerritsen, & Mooers, 1995). The layer thickness (% of water column) was set to 2, 3, 5, 10, 15, 15, 15, 15, 10, 5, 3 and 2.

The bathymetry within the model area (Figure 4.3) was obtained from nautical charts 408 and 4083 from the Hydrographic Institute of the Spanish Navy (Instituto Hidrografico de la Marina) and interpolated onto the computational grid by means of Delft3D-QUICKIN, a Delft3D-FLOW tool. Given that these charts do not have enough resolution in the intertidal areas, detailed bathymetric and topographic information was obtained from cartographic maps provided by the Galician Regional Authority (Xunta de Galicia).

USC UNIVERSIDADE DE SANTIAGO DE COMPOSTELA

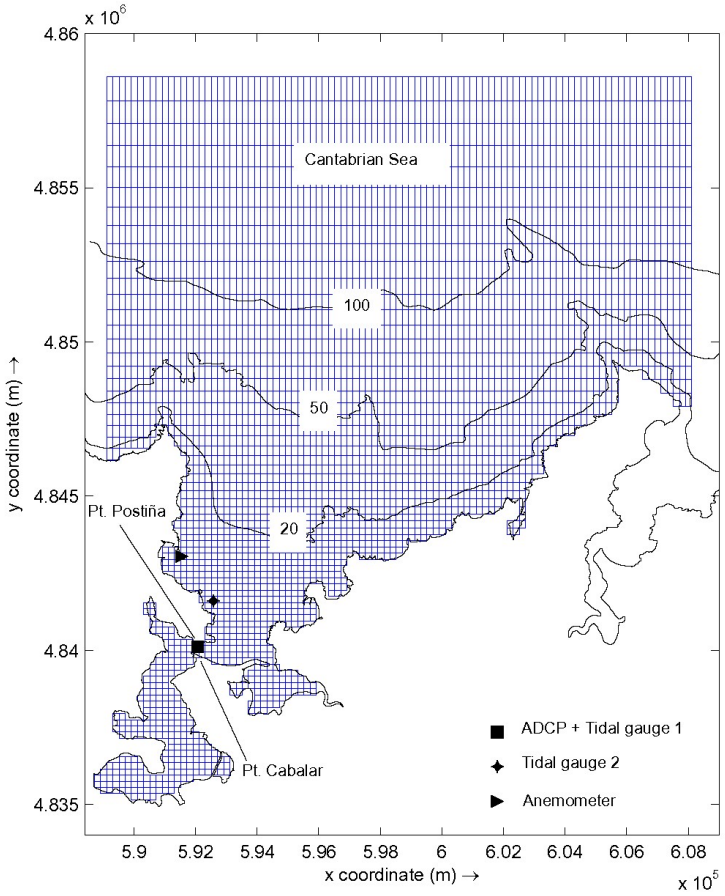


Figure 4.2. Computational grid of the model area [For a clearer understanding, the representation herein shown is derefined 4 times both *x*- and *y*- directions].

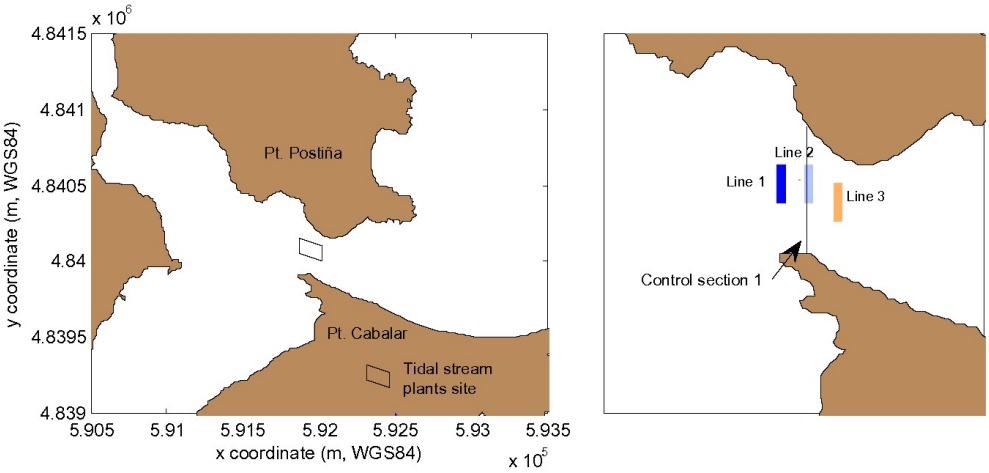


Figure 4.3. Location of the considered tidal stream plants (left-hand site). Layout in plan view of the plants (right-hand site).

USC UNIVERSIDADE DE SANTIAGO DE COMPOSTELA

4.3.2.2. Boundary conditions

Dirichlet conditions were imposed along the open boundary by prescribing the sea surface level based on the main tidal harmonics (Table 4.1) together with daily thermohaline conditions. At the land margins the forcings were null flow through the boundary and zero shear stress; at

the bottom, a stress, τ_{b3D}, induced by a turbulent flow which is related to the current velocity above the bed, was imposed:

$$\vec{\tau}_{b3D} = \frac{g\rho_0|\vec{u}_b|\vec{u}_b}{C_{3D}^2}, \tag{4.6}$$

where $\vec{u}_b$ is the magnitude of the horizontal velocity in the lowest layer (immediately above the bed) and C_{3D} is the 3D Chézy coefficient, given by

$$C_{3D} = C_{2D} + \frac{\sqrt{g}}{\kappa} ln\left(\frac{\Delta z_b}{2H}\right). \tag{4.7}$$

with κ the von Karman constant (κ = 0.41), Δz_b the vertical distance from the seabed to the nearest computational grid point, H the total water depth and C_{2D} the 2D Chézy coefficient, which can be determined based on Manning's coefficient, n, as:

$$C_{2D} = \frac{\sqrt[6]{H}}{n}. \tag{4.8}$$

Finally, at the free surface the wind shear-stress, $\vec{\tau}_s$, is defined as

$$\vec{\tau}_s = \rho_a C_d U_{10}^2, \tag{4.9}$$

where ρ_a is the density of the air, U_{10} the wind speed at 10 m above the sea surface and C_d the wind drag coefficient.

4.3.2.3. Numerical parameters

The model was run with a time step of 60 s. The horizontal eddy viscosity and eddy diffusivity were set to15 m^2s^{-1}, and the vertical eddy viscosity and eddy diffusivity to 1×10^{-5} m^2s^{-1} and 1×10^{-7} m^2s^{-1}, respectively (Skogseth, Sandvik, & Asplin, 2007). Manning's coefficient is assumed to be depth-dependent according to previous studies (Cheng et al., 1993; Dias & Lopes, 2006; Dias, Sousa, Bertin, Fortunato, & Oliveira, 2009; Iglesias & Carballo, 2010a). Finally, the drag coefficient for U_{10} up to 6 ms^{-1} is modelled following Smith (Smith, 1980)

$$C_d = 1.1 \times 10^{-3}, \tag{4.10}$$

and, for U_{10} above 6 ms^{-1}, following Yelland (Yelland et al., 1998),

$$C_d = (0.50 + 0.071U_{10}) \times 10^{-3}. \tag{4.11}$$

4.4. RESULTS

4.4.1. Model validation

The model was validated on the basis of measurements at stations S1 and S2 (Figure 4.1). At station S1, measures of water level and current speed were obtained since December 16th 2010 until January 4th 2011, whereas at station S2 only water level data was collected for the same period. So as to validate the numerical model, a simulation was run for the aforementioned period, using the previous 30 days as *spin-up* period. In this simulation the model was forced along the open boundaries with the main tidal constituents (Table 4.1) and salinity and temperature data. Moreover, wind stress acting on the sea surface and daily discharges of Mera

River were also considered. In the case of wind data, wind velocity and direction were recorded at station S3 every 30 min while river discharges were provided by the Regional Authority of Water Resources (*Augas de Galicia*) close to the river's mouth.

The visual comparison of the observed and computed water levels (Figure 4.4) and current velocity (Figure 4.5) time series indicates a good agreement between both series. However, to consider only a visual comparison may be a little subjective. So as to provide a more exhaustive (and more objective) comparison, the correlation coefficient (*R*) and the mean difference (*MD*) were calculated with Equations 4.12 and 4.13, respectively.

$$R = \frac{\sum_{i=1}^{N}(x_i^o - \overline{x^o})(x_i^m - \overline{x^m})}{\sqrt{\sum_{i=1}^{N}(x_i^o - \overline{x^o})^2 \sum_{i=1}^{N}(x_i^m - \overline{x^m})^2}}, \tag{4.12}$$

$$MD = \frac{\sum_{i=1}^{N}|x_i^o - x_i^m|}{N}, \tag{4.13}$$

where x_i represents the *i*-th value of either the water level or current velocity time series with N the total number of data points available, and the superscripts *o* and *m* the observed and modelled data, respectively. The values of these statistical parameters show the model's performance for reproducing the real hydrodynamic conditions on the estuary (Table 4.3).

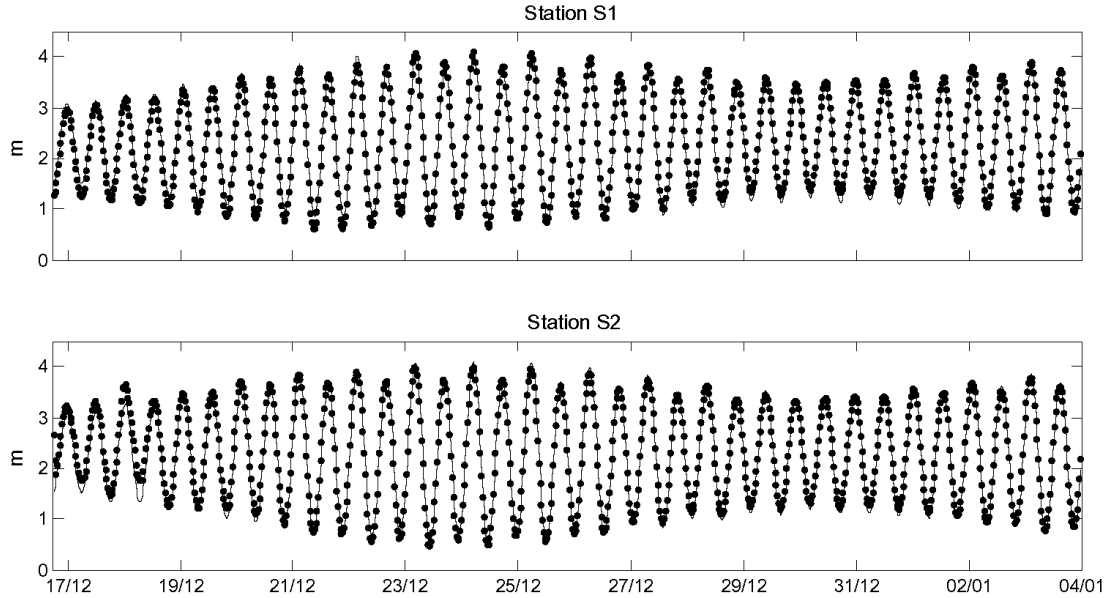


Figure 4.4. Comparison between computed (continuous line) and measured (dots) water level time series at measuring stations S1 and S2 during the validation period.

Table 4.3. Statistical coefficients for comparing measured and computed time series at stations S1 and S2.

	Station S1	Station S2

	Water level	Current speed			Water level
		Surface layer	Middle layer	Bottom layer	
MD	0.11	0.18	0.20	0.21	0.10
MSE	1.96×10^{-2}	2.25×10^{-2}	2.26×10^{-2}	3.24×10^{-2}	1.69×10^{-2}

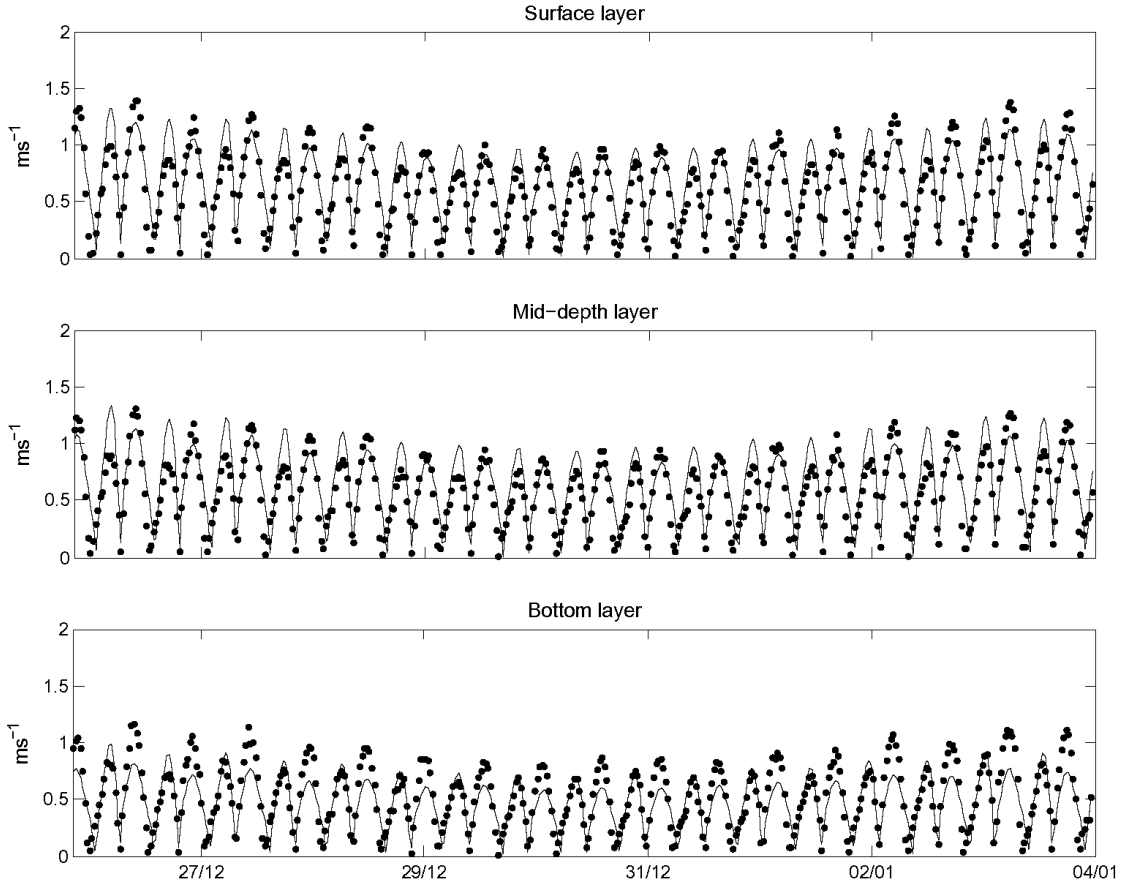


Figure 4.5. Comparison between modelled (continuous line) and measured (dots) current velocity time series for the surface, mid-depth and bottom layers at measuring station S1 during the validation period

Finally, a harmonic analysis of measured and modelled time series has been conducted and the results for the main tidal constituents compared. This analysis also show an excellent agreement between both time series (Table 4.4), especially for M2 and S2, which in turn are the most relevant tidal constituents in this location (Table 4.1).

In order to assess the impacts caused by the operation of both considered tidal stream plants, three simulations were performed. First of all, the reference conditions were calculated, i.e., the hydrodynamic conditions in the ria in the absence of TSTs. Then, two simulations were performed in order to determinate the conditions resulting from the operation of the plants (one simulation for each of the plants considered, P1 and P2). The model forcings were the same for the three simulations: main tidal constituents (Table 4.1), daily values of salinity and temperature at the open boundaries, and daily river discharge in the upper part of the ria.

Table 4.4. Comparison between observed and computed main tidal harmonics.

	Constituent	Observed amplitude (cm)	Modelled amplitude (cm)	Amplitude difference (cm)	Observed phase (º)	Modelled phase (º)	Phase difference (º)
Station S1	M2	119.3	116.7	2.6	93.0	97.0	4
	S2	54.1	43.4	10.7	116.8	119.9	3.1
	N2	22.6	23.7	1.1	76.8	73.7	3.1
	K2	24.3	18.1	6.2	127.6	117.2	10.4
Station S2	M2	117.2	123.1	5.9	100.4	97.4	3
	S2	43.7	43.2	0.5	152.9	128.4	24.5
	N2	26	26	0	86.2	77.4	8.8
	K2	12.5	12.3	0.2	219.6	126.1	93.5

4.4.2. Assessment of the impacts on the estuarine circulation

4.4.2.1. Energy extraction

Regarding the amount of energy extracted in the presence of the tidal plants, as it was described in section 3.1, the tidal stream plants were implemented in the model by using the momentum sink approach. The retarding force affects the upper layers of the model in the case plant P1, and the lower layers in the case of plant P2. In both cases the value of C_T considered is 0.8, which corresponds to a value of the power coefficient, C_p, of 0.35 (Bahaj, A. S. et al., 2007). According with this coefficient, the remaining turbine specifications (Table 4.2) and the perturbed velocities resulting from the existence of the aforementioned retarding force, the annual energy production of P1 and P2 would be 2.425×10^3 MWh and 1.498×10^3 MWh, respectively. This large difference is caused by the important variations in the flow velocities throughout the water column.

4.4.2.2. Impacts on the general circulation of the ria

The impact caused by the operation of each tidal plant was analysed in terms of the difference between altered and reference conditions, at mid-flood and mid-ebb of a mean spring tide. Regarding the impacts at mid-flood tide (Figure 4.6), important differences can be found between the effects caused on the estuarine circulation by the tidal plants considered. When plant P1 is in operation (left-hand side plots in Figure 4.6), the greatest effects on the surface layer are concentrated in the vicinity of the plant – with maximum alterations of about 3×10^{-1} ms^{-1} can be observed within a few hundreds of metres up and downstream of the plant – although a general reduction of the order of 10^{-3} ms^{-1} up to 8-7 km away the plant is also apparent. On the other hand, the impacts caused on the bottom layer are smaller than on the surface, not only in the area where the plant is located but also in the whole ria. Furthermore, the area where the effects are concentrated greatly differs, being now restricted to about 3-4 km away the plant. Finally, despite the impacts caused by plant P2 on the circulation of the whole ria at mid-flood describing a similar pattern as in the case of plant P1 (a general reduction of similar magnitude and occupying a similar area), in the area occupied by and next the plant they present strong differences. This issue is dealt with in detail in the next subsection.

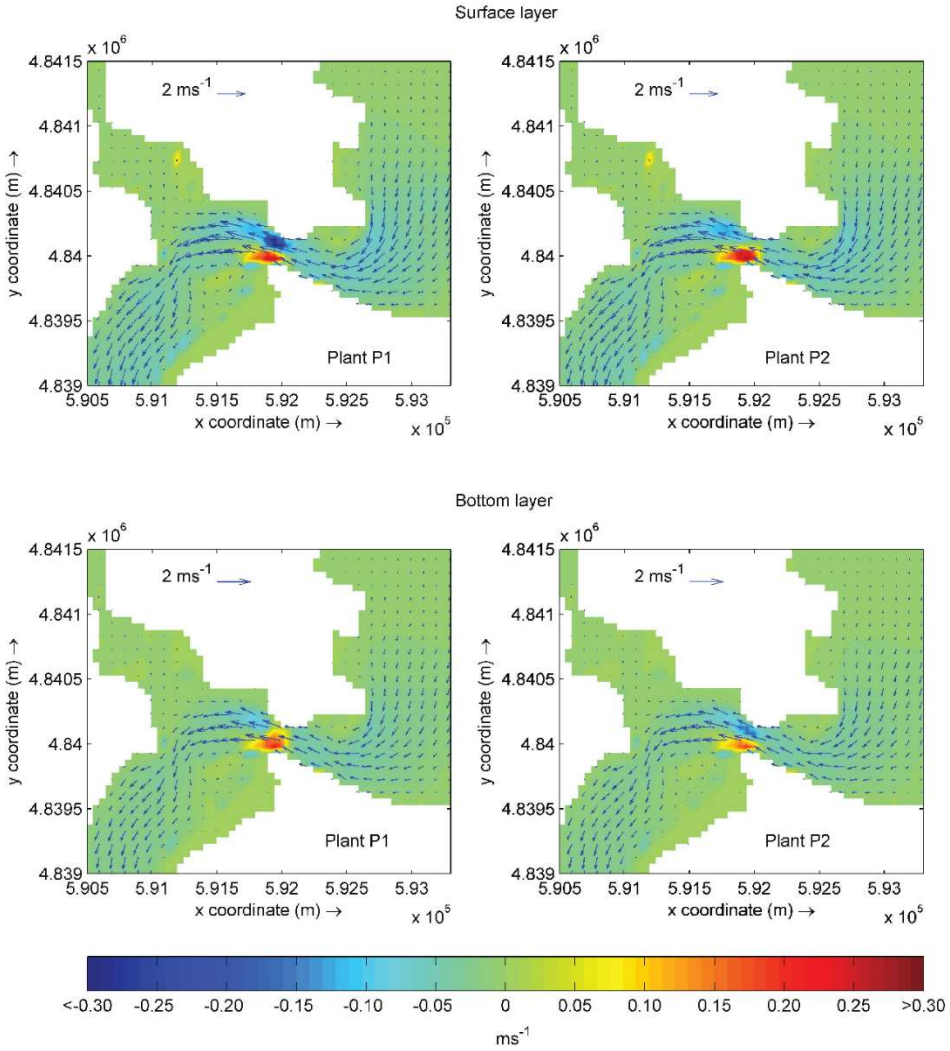


Figure 4.6. Differences between altered and reference flow velocities (colour map), and vectors showing the altered flow in the middle ria at mid-flood tide

Regard to the impacts at mid-ebb tide resulting by the operation of plants P1 and P2 (Figure 4.7), the general picture is rather similar to mid-flood tide, although with two significant differences: (i) the effects are a bit greater within and next the plant site and (ii) smaller within the area downstream the plant (i.e to the East). In this case, with respect to the effects on the outer part of the ria they are only significant (in the order of $2\text{-}3\times10^{-3}$ ms^{-1}) about 4-5 and 2-3 kms away the plant on surface and bottom layers, respectively.

USC UNIVERSIDADE DE SANTIAGO DE COMPOSTELA

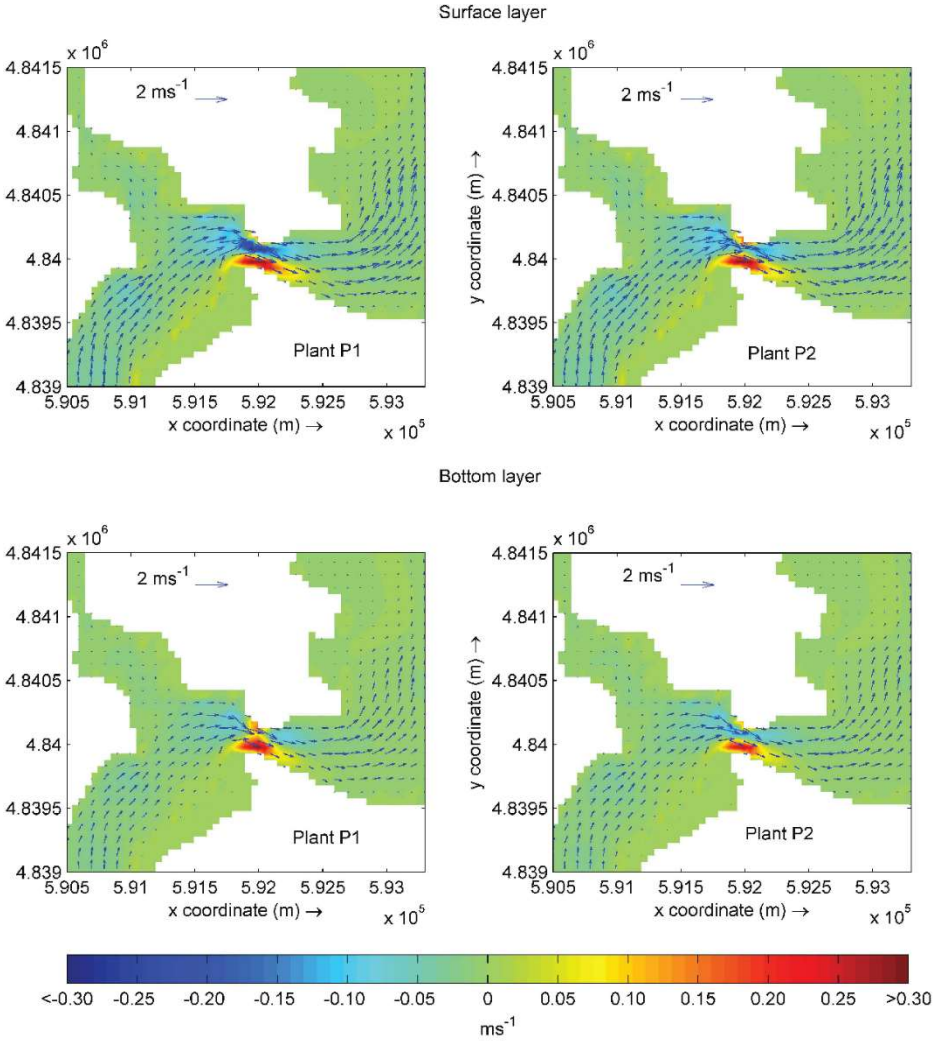


Figure 4.7. Differences between altered and reference flow velocities (colour map), and vectors showing the altered flow in the middle ria at mid-ebb tide

4.4.2.3. Detailed assessment of the impacts

In this section, a detailed assessment of the impacts was performed in the area occupied by and next to the proposed plants. For this purpose, a control section was defined in the narrowing where the plants are located (Figure 4.3) and the flow under the three simulated conditions (without plant, with plant P1 and with plant P2) analysed. As for the general circulation, the differences between altered and reference conditions at two representative tidal situations, mid-flood and mid-ebb, of a mean spring tide were considered.

At mid-flood tide (Figure 4.8), the effects resulting from the operation of P1 are as follows. In the surface layer in the section occupied by the TSTs it causes an average reduction of approx. 0.25 ms^{-1} (with reductions of up to 0.36 ms^{-1} at specific points). Regard to the remaining section of the narrowing, south of the plant (left hand side in Figure 4.8) the flow increases up to 0.28 ms^{-1}, whereas to the north (right hand side) it decreases slightly. With respect to the bottom layer, the flow increases throughout the whole section, with the greatest effects being located in the section non-occupied by the TSTs (up to 0.22 ms^{-1}). On the other hand, when plant P2 is in operation, the presence of the TSTs in the lower part of the water column results in an increase of the flow on the surface layer within the section to the south of

the TSTs where differences between altered and reference conditions reach values of up to 0.30 ms^{-1}, as well as in a slightly decrease in the remaining section of the narrowing (the section occupied by and north to the TSTs). In the bottom layer, the flow decreases in the section occupied by the TSTs up to 0.15 ms^{-1} at specific points, increases to the south of the plant up to 0.27 ms^{-1} and remains almost unchanged to the north. Regard to the mid-depth layer, the differences between the impact caused by plant P1 and P2 are almost negligible. In both cases the flow increases significantly to the south of the plant (up to 0.28 ms^{-1}), and decreases in the same order of magnitude within the section occupied by the plant (up to 0.33 ms^{-1}); finally, to the north, the effects consist on a slight variation either decrease or increase.

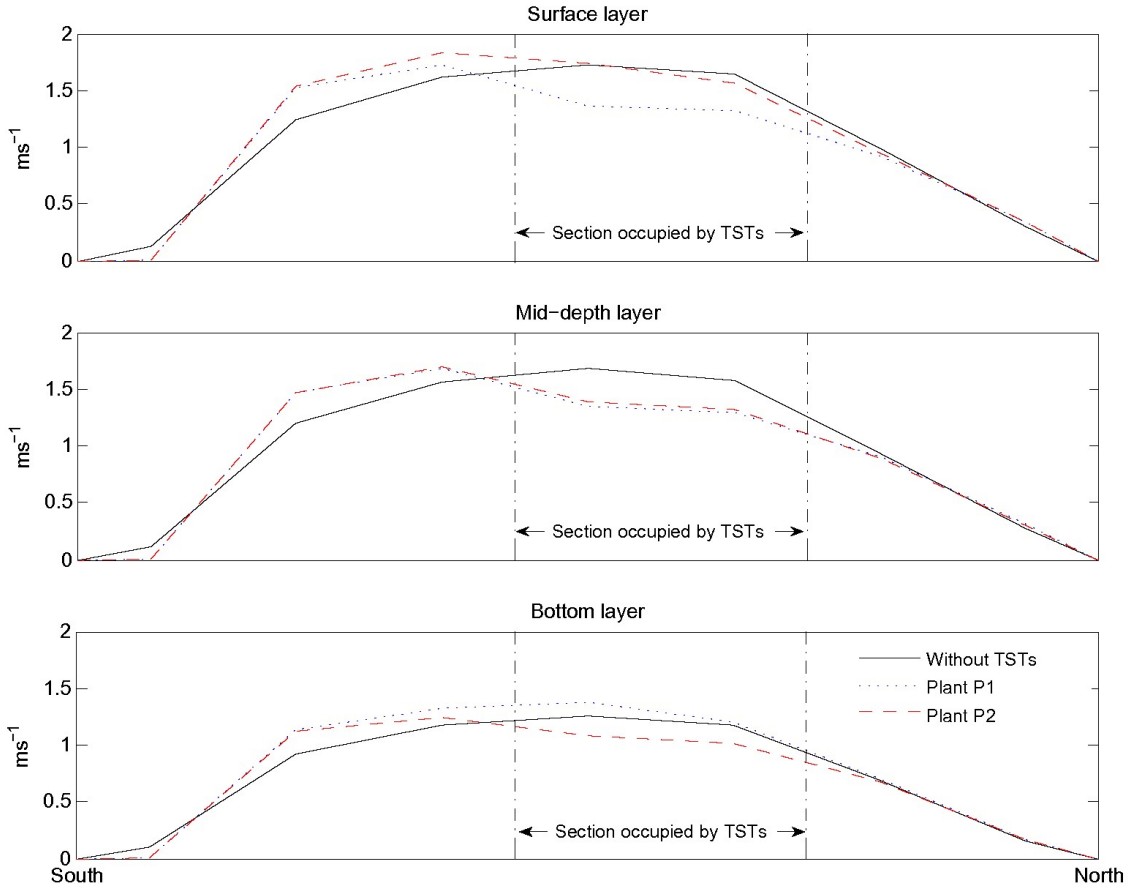


Figure 4.8. Magnitude of the current velocity on the control section at mid-flood situation of a mean spring tide

Regarding mid-ebb tide, the general pattern is rather similar to mid-flood situation (Figure 4.9) although with a somewhat different magnitude. On the surface layer, in the section occupied by the plant P1, the flow decreases up to 0.34 ms^{-1} whereas in the remaining section it increases up to 0.32 ms^{-1}. By contrast, on the bottom layer, the flow increases throughout the whole section, with modifications of up to 0.26 ms^{-1} being concentrated to the south of the plant. In the case of Plant P2, there exists an overall increase in the portion of the section non-occupied by the TSTs of up to 0.30 and 0.24 ms^{-1} on surface and bottom layers, respectively. On the other hand, within the area occupied by the turbines, the effects are almost the opposite; here, the flow decreases up to 0.08 and 0.14 ms^{-1} in the surface and bottom layers, respectively. Finally, as in the case of mid-flood situation, the effects of both plants on the mid-depth layer are similar. There exists a strong increase and decrease in the flow to the south (up to 0.30 ms^{-}

^{1}) and within the plant (up to 0.26 ms^{-1}), repectively. However, as opposed to mid-flood situation, in this case the flow increases slightly to the north of the plant (up to 0.12 ms^{-1})

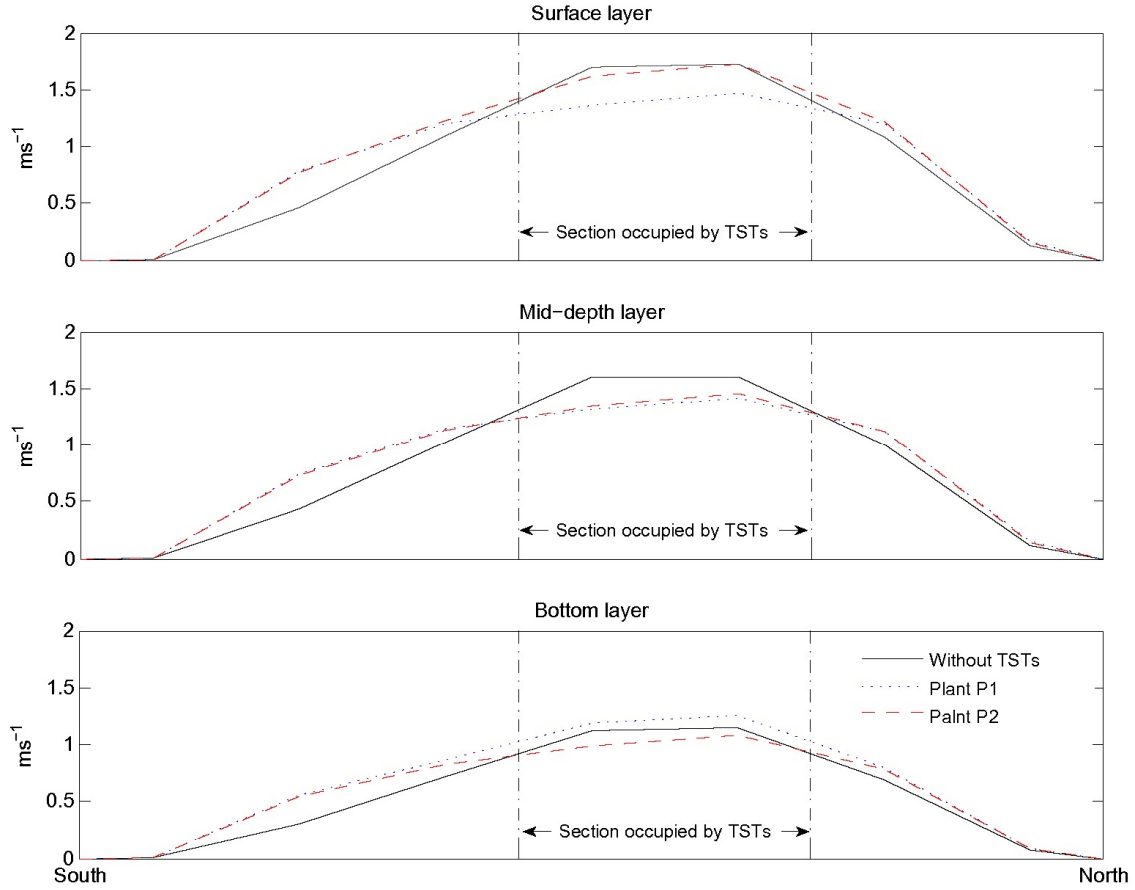


Figure 4.9. Magnitude of the current velocity on the control section at mid-ebb situation of a mean spring tide

4.5. CONCLUSIONS

The impacts caused by two tidal stream plants on the estuarine circulation of Ria de Ortigueira (NW Spain) were investigated by means of a three-dimensional hydro-environmental numerical model (Delft3D-FLOW). The plants analysed are composed of Tidal Stream Turbines (TSTs) and present the same plan view layout; however, one of them, plant P1, is composed of floating TSTs, and the other, plant P2, of bottom-fixed TSTs. The implementation of TSTs in the model was done by adding a sink term in the momentum equations representing the thrust force exerted by the flow in each turbine. This term is only considered in the vertical layers of the model corresponding to the area occupied by the rotors of the turbines (therefore affecting different layers in plants P1 and P2). First, the model was validated based on field data at two measuring stations, obtaining an excellent agreement between computed and measured water level and current velocity time series. Next, numerical simulations were performed in order to assess the potential impacts on the flow during mid-flood and mid-ebb of a mean spring tide.

Despite the significant differences in the annual energy production resulting from the operation of each tidal plant considered, it was found that the impacts caused on the general circulation present strong similarities. Although their operation is not sufficient for considerably modifying the flow throughout the whole ria, alterations of the order of 10^{-2} ms^{-1}

are apparent several km away the plants. Regard to the differences between mid-flood and mid-ebb situations, the general picture is virtually the same, with the main difference being the extension of the area affected to the east of the plant (smaller at mid-ebb tide). Regarding the plant site and its vicinities, the results of the model show that in this area there exists an important reduction of the current velocity. However, not all of this velocity reduction stems from the extraction of energy, but also from the flow being redirected towards the remaining section which results in an increase of the velocity within this area. In contrast with the strong similarities in the modifications of the general pattern caused by plants P1 and P2, significant differences were found in this area. This arises from the different vertical configuration (occupying a different portion of the vertical) which causes that the impacts greatly differ from those that could be initially expected (e.g. a velocity increase in the section non-occupied by the plant). In this vein, a reduction of the flow was found over an important part of the surface layer during the operation of bottom-fixed TSTs. This unpredictable behaviour of the flow modification highlights the importance of investigating the impacts caused by different plants in a tidal stream farm project under real conditions of operation.

In sum, this study has demonstrated that the energetic exploitation of tidal currents may cause important impacts on the estuarine circulation. These impacts were quantified for two proposed tidal stream plants, composed of floating or bottom-fixed TSTs. The results showed that there are almost no differences between the impacts caused by both configurations of TSTs on the general circulation; by contrast, there exist significant differences in the effects in the vicinity of the plants. Furthermore, in this area the impacts differ to a great extent from those that could be expected in advance, which highlights the importance of a site-specific analysis. Beyond the interest of these results for the area of study, the procedure herein implemented could be used to analyse the potential impacts caused by different TSTs on the hydrodynamics of other estuaries with similar hydrodynamic conditions. It is important to bear in mind that these impacts may, in turn, lead to other environmental effects that are outside the scope of this article, such as modifications to the sediment transport patterns and contaminant dispersion. These potential effects will be dealt with as a continuation of this line of research.

USC
UNIVERSIDADE DE SANTIAGO DE COMPOSTELA

5. EFFECTS OF TIDAL STREAM ENERGY EXPLOITATION ON ESTUARINE CIRCULATION AND ITS SEASONAL VARIABILITY

ABSTRACT

Residual flows are of major importance in coastal areas, driving environmental processes such as sediment transport or nutrient dispersion. Consequently, in those areas where a large tidal stream energy resource is available, prior to the installation of a tidal farm it is imperative to assess how energy extraction affects the residual flows. In this paper, the potential effects of different con-figurations of tidal stream farms on the residual circulation and its seasonality are analysed by means of a case study: Ria de Ortigueira, the westernmost of the Galician Rias Altas (NW Spain). For this purpose, a 3D numerical model was implemented and validated against field measurements. Next, a total of eight case studies, including the operation of bottom-fixed and floating converters under typical summer and winter scenarios, were studied. Overall, when a tidal farm operates, regardless of its configuration and the forcings considered, the resulting general residual flow pattern does not experience significant modifications. This pattern is characterized by a 2D circulation in the inner ria, and a positive estuarine circulation in the middle and outer ria. The largest modifications of the residual flow are apparent in the vicinities of the plant, with maximum values of about 0.05 ms^{-1}. Outside this area, the alteration is lower than 0.01 ms^{-1}, and virtually negligible at some distance from the farm.

5.1. INTRODUCTION

During the last decades, and especially since the late 80's, the interest in carbon-free energy sources has increased drastically (Bekun, Alola, & Sarkodie, 2019). In this context, a large number of policies have been implemented within different legal frameworks in order to achieve more ambitious quotas of renewable energy production (Erdiwansyah, et al., 2019; European Commission, 2012; Fobissie, 2019; Herath & Tyner, 2019; Nicolli & Vona, 2019; Pischke et al., 2019). In this regard, Marine Renewable Energies (MRE), and in particular tidal stream energy, stands out as one of the most promising alternatives to diversify the energy mix by means of zero emission technologies, principally due to the advantages that tidal stream energy presents in comparison with other types of renewable energies, such as its predictability, no land occupation or a high load factor, among others (Bahaj, AbuBakr S., 2011; Carballo et al., 2009a; Sánchez et al., 2014a).

Generally speaking, tidal stream exploitation is potentially of interest in coastal areas where peak velocities exceed 1.0 1.5 ms^{-1} (European Commission, 1996), resulting from different factors such as large tidal prisms and a constricted morphology (Iglesias et al., 2012; Zarzuelo, López-Ruiz, Díez-Minguito, & Ortega-Sánchez, 2017). These factors are sometimes reinforced by baroclinic flows and river discharges (Fouz et al., 2019). The harnessing of tidal stream energy resource is carried out through Tidal Energy Converters (TECs), which are usually classified according to their principle of operation as reciprocating (Liu, Qu, & Shi, 2019) or

rotating (Qian et al., 2019) devices. Rotating devices, also known as Tidal Stream Turbines (TSTs), present the highest Technology Readiness Level (TRL). Nowadays, third-generation TSTs (Segura et al., 2017) are designed to operate in shallow areas (approx. 1 m depth) with relatively low cut-in velocities (roughly 0.7 ms^{-1}) (Fouz et al., 2019). TSTs can be installed in different configurations, whose influence on the performance of a tidal farm was investigated in previous works (Sánchez et al., 2014a). Depending on their position in the water column, TSTs may be classified as (Zhou et al., 2017): (i) floating TSTs, i.e., devices anchored to the sea bottom floating below the sea surface, which harness the energy of the upper layers of the water column, and (ii) bottom fixed TSTs, i.e., converters rigidly anchored to the sea bottom, which harness the energy available in the bottom layers of the water column.

Suitable sites for installing a tidal farm are usually located in coastal areas driven by complex hydrodynamic patterns, such as estuaries or bays, which typically have high environmental value. This highlights the key role of an appropriate environmental impact assessment for informed decision-making when installing a tidal farm (Neill et al., 2012; Ramos et al., 2013; Ramos et al., 2014). In order to investigate the impacts of tidal stream energy exploitation over estuarine circulation, both transient and residual tidal flows were analysed in previous works by means of 3D numerical modelling (Sánchez et al., 2014b), including a comparison between floating and bottom-fixed TSTs (Sanchez et al., 2014). The results demonstrate that: (i) the impacts on the residual circulation extend their effects over wider regions than in the case of transient circulation (despite being of the same order in terms of percentage of velocity variation); and (ii) there are almost no differences regarding the impact on estuarine circulation between floating and bottom-fixed configurations, the most significant differences occurring in the vicinity of the plants, principally due to the different vertical configuration.

For all this extensive work, in areas suitable for tidal stream energy exploitation there are other circulation patterns to be considered, e.g., upwelling-downwelling systems, which have not been well studied in the vicinity of a tidal farm. An example of the effects of upwelling events can be found in the Galician Rias (NW Spain) – a region with one of the largest oceanic productivities worldwide (Duarte, Alvarez-Salgado, Fernández-Reiriz, Piedracoba, & Labarta, 2014). Galician Rias are flooded tectonic valleys, which are usually classified into Rias Altas and Rias Baixas according to the geographical location (north and south of Cape Fisterra, respectively). There are important tectonic and geomorphological differences between both groups (Díez, 1996): the Rias Baixas are larger, deeper and more homogeneous in their orientation (roughly NE-SW) than the Rias Altas. Upwelling events throughout the Rias Baixas have been extensively analysed in the scientific literature (Alvarez, Gomez-Gesteira, deCastro, & Novoa, 2008; Alvarez-Salgado, Roson, Perez, & Pazos, 1993; Blanton, Atkinson, Castillejo, & Lavin, 1984; deCastro et al., 2008; Gómez-Gesteira, deCastro, Prego, & Pérez-Villar, 2001; Herrera, Rosón, Varela, & Piedracoba, 2008; Souto, Gilcoto, Fariña-Busto, & Pérez, 2003; Villacieros-Robineau, Herrera, Castro, Piedracoba, & Roson, 2013), and their key role cooling and fertilizing surface waters was clearly highlighted (Prego, Barciela, & Varela, 1999). Ekman transport is the driver of upwelling processes, due to the incursion of Eastern North Atlantic Central Water (ENACW) into the Rias Baixas, that usually occurs during spring or summer in the presence of N-NE winds. As a result of the orientation of these rias (NE-SW), northerly winds cause a positive estuarine circulation, with an outflow of surface (riverine) water and an inflow of cold, laden ENACW, which ascends to the continental shelf and finally flows into the ria (Iglesias & Carballo, 2009a; Wooster, Bakun, & McLain, 1976).

The frequency and intensity of upwelling episodes are highly influenced by the orientation of the coast, which modifies the wind velocity and direction (Alvarez, Gomez-Gesteira, deCastro, Gomez-Gesteira, & Dias, 2010; Torres, Barton, Miller, & Fanjul, 2003). Several studies (Álvarez-Salgado, Labarta, Vinseiro, & Fernández-Reiriz, 2017; Duarte et al., 2014) remarked that the forcing factors driving the hydrodynamics in the Rias Altas are clearly dependent on the geographic orientation of a specific coastal system, being much more heterogeneous than in the case of the Rias Baixas. Taking this into account, and as a result of their different coastal orientation, upwelling-favourable conditions along the Rias Altas are not related to the spring summer NE winds typical of the Rias Baixas (Alvarez et al., 2010). In effect, the features of the upwelling episodes along this coastal region are partially unknown, with the specific orientation of each estuary playing a significant role in the hydrographical, biogeochemical and biological patterns during upwelling and downwelling events within Rias Altas (Ospina-Alvarez et al., 2010).

With this in view, and in order to go further into the analysis of the impacts of a tidal farm on the residual circulation and estuarine upwelling, this work studies the effects resulting from the operation of a tidal stream plant in a specific coastal area of the Rias Altas, the Ria de Ortigueira, by means of the implementation of a 3D high-resolution hydrodynamic numerical model.

This paper is structured as follows. First, in Section 5.2, a brief description of the study area, the Ria de Ortigueira, is presented. Next, in Section 5.3, the methodology used in this work for assessing the impacts of the operation of a tidal farm on the residual circulation and estuarine upwelling is thoroughly described. Then, in Section 5.4, results are presented and discussed focusing on two situations: unaltered and altered conditions (i.e., without and with energy extraction, respectively). Finally, in Section 5.5, conclusions are drawn.

5.2. STUDY AREA

The Ria de Ortigueira (Figure 5.1) is the westernmost of the Galician Rias Altas (NW Spain) delimited by Cape Ortegal and Pt. Estaca de Bares and presenting a total surface area of 85 km^2 and a length of 18 km along its main axis. This coastal area emerges as a promising region for tidal stream energy exploitation thanks to its complex geomorphology, with a number of constrictions, and its relatively high tidal range (maxima of 4.5 m). Previous works (Iglesias et al., 2012; Sánchez et al., 2013) show that tidal flows of approximately 2.5 ms^{-1} can be reached in the narrowing between Pt. Postiña and Pt. Cabalar, indicating the suitability of the Ria de Ortigueira to locate a tidal stream farm.

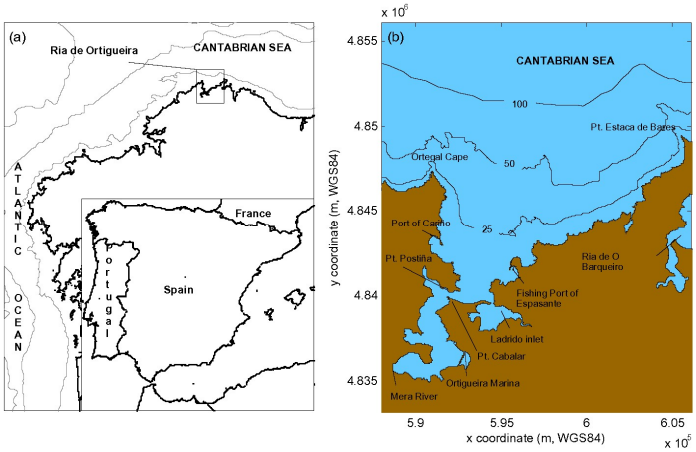


Figure 5.1. The Ria de Ortigueira (b) and its location in Galicia (NW Spain) (a).

USC UNIVERSIDADE DE SANTIAGO DE COMPOSTELA

Regarding the tidal regime of the Ria de Ortigueira, it is characterized by a predominance of semidiurnal components (Table 5.1), especially M2, as in the rest of the European Atlantic. In this regard, considering the main tidal constituents (M2, S2, K1 and O1) by means of a harmonic analysis, the tidal form factor (F) confirms the semidiurnal behaviour (F = 0.082) of this body of water (Pugh, 1996). However, even though the hydrodynamics of the Ria de Ortigueira are dominated by the tide, tides are not the only one relevant forcing factor within this estuarine area. There are other forcing factors that must be considered, such as: (i) wind regime, (ii) fluvial discharges, and (iii) thermohaline conditions. As a result of the interaction of the different forcing factors driving the hydrodynamics of the Ria de Ortigueira, this coastal location can be classified according to the salinity structure criterion as a well-mixed estuary (Iglesias et al., 2012).

Table 5.1. Main tidal constituents in the Ria de Ortigueira

Constituent	Amplitude (cm)	Phase (°)
M2	122.79	90.15
S2	42.91	121.08
N2	25.98	70.39
K2	12.03	118.76
K1	7.35	73.49
O1	6.22	324.62
P1	2.22	65.15
Q1	2.11	271.31
M4	1.45	334.80

Finally, with respect to its main geomorphological features, Ria de Ortigueira presents a gradual reduction in the width of its cross-sections from the mouth to the inner ria, ranging from more than 10 km at its ocean boundary to 150 200 m in the inner estuary. As far as the water depth is concerned, it presents an average value of 7.3 m (Cerdeira-Arias et al., 2018), but with strong variations throughout the estuary, varying from maximums of 30-35 m at its mouth to less than 5 m throughout extensive zones in the inner ria, including large intertidal areas.

5.3. MATERIALS AND METHODS

5.3.1. Field data

As was mentioned in Section 5.2, the tide is not the only one forcing factor capable of generating currents in the Ria de Ortigueira. Other relevant forcing factors, such as river discharge, wind regime and thermohaline conditions, are also considered in order to fully understand the hydrodynamics of the study area and the potential impacts on upwelling events resulting from the operation of a tidal energy farm.

USC DE SANTIAGO DE COMPOSTELA

Firstly, regarding river discharge data, though there are several fluvial courses flowing into this estuary, only the River Mera presents a significant flow rate (i.e., average annual discharge of 5.45 m^3s^{-1}) to be considered as a relevant hydrodynamics forcing agent in this coastal area. A seasonal analysis (Fouz et al., 2019) considering mean monthly flow rates since 1970 shows

that a marked intra-annual discharge variability is apparent, resulting in two different periods within the hydrological year (Table 5.2).

Next, regarding the wind regime, pronounced patterns of seasonality are found again, as in the case of river discharges. According to these seasonal patterns, the wind regime (in terms of wind velocity and occurrence) is highly dependent on the meteorological conditions of the different seasons; however, common trends are observed within two different large periods, as in the case of other Galician Rias (Iglesias & Carballo, 2010a; McClain, Chao, Atkinson, Blanton, & de Castillejo, 1986): (i) autumn-winter scenario (prevalence of W-SW winds) and (ii) spring-summer scenario (prevalence of NE winds), hereinafter referred for simplicity as winter and summer winds, respectively. Moreover, as mentioned in Section 5.1, in the Rias Altas the coastal orientation has a key role driving the upwelling-favourable winds. This feature should be taken into account in defining the wind conditions to be input to the numerical model for computing the upwelling-induced circulation in the Ria de Ortigueira. Considering the orientation of the shoreline in the Ria de Ortigueira (SSW-NNE), and despite NE winds being prevalent during spring-summer (upwelling favourable periods in other Galician Rias), SW winds are responsible for upwelling processes within this waterbody during both winter and summer scenarios. Upwelling episodes take place mainly during spring or summer, notwithstanding, they also occur during autumn or winter in both Rias Baixas (deCastro et al., 2008) and Rias Altas (Alvarez et al., 2009). With this in view, the average value of SW winds was considered for both autumn-winter and spring-summer scenarios, i.e., 3.32 ms^{-1} and 6.03 ms^{-1}, respectively.

Finally, with respect to the thermohaline conditions, and based on the previous results of river discharges, the average values of autumn-winter and spring-summer periods obtained by averaging daily field measurements are considered. The characteristics of the thermohaline conditions for these scenarios are shown in Table 5.2.

Table 5.2. Values of boundary conditions for spring-summer and autumn-winter scenarios.

Scenario	River discharge			Forcings in outer boundary		
	River flow (m^3s^{-1})	Salinity (ppm)	Temperature (˚C)	Tidal constituents	Salinity (ppm)	Temperature (˚C)
spring summer	-3.07	0.0508	15.60	M2	35.6849	15.51
autumn winter	-8.48	0.0508	11.10	M2	35.4821	13.17

5.3.2. Numerical model (I): equations

With the aim of analysing the impacts of tidal stream energy exploitation on the hydrodynamics of the Ria de Ortigueira, and more specifically on the upwelling events, the 3D hydrodynamic model Delft3D-FLOW is implemented in this estuarine area. Delft3D-FLOW approximates, by means of a finite-difference code, the Navier Stokes equations (under the shallow-water and Boussinesq assumptions) combined with the transport equation, allowing the computation of both the baroclinic and barotropic circulation (Deltares, 2010). In order to fully describe the resulting 3D flow structure during upwelling events (Iglesias & Carballo,

2009a) and how a tidal farm affects them, the numerical model is implemented in its 3D form. The model equations read:

$$\frac{\partial u}{\partial x}+\frac{\partial v}{\partial y}+\frac{\partial w}{\partial z}=Q \tag{5.1}$$

$$\left.\begin{aligned}\frac{Du}{Dt}&=fv-g\frac{\partial \zeta}{\partial x}-\frac{g}{\rho_0}\int_{z'=z}^{z'=\varsigma}\frac{\partial \rho}{\partial x}dz'+\upsilon_h\left(\frac{\partial^2 u}{\partial x^2}+\frac{\partial^2 u}{\partial y^2}\right)+\upsilon_v\left(\frac{\partial^2 u}{\partial z^2}\right)\\ \frac{Dv}{Dt}&=-fu-g\frac{\partial \zeta}{\partial y}-\frac{g}{\rho_0}\int_{z'=z}^{z'=\varsigma}\frac{\partial \rho}{\partial y}dz'+\upsilon_h\left(\frac{\partial^2 v}{\partial x^2}+\frac{\partial^2 v}{\partial y^2}\right)+\upsilon_v\left(\frac{\partial^2 v}{\partial z^2}\right)\end{aligned}\right\} \tag{5.2}$$

$$\frac{\partial p}{\partial z}=-\rho g \tag{5.3}$$

$$\frac{Dc}{Dt}=D_h\left(\frac{\partial^2 c}{\partial x^2}+\frac{\partial^2 c}{\partial y^2}\right)+D_v\frac{\partial^2 c}{\partial z^2}-\lambda_d c+R_s \tag{5.4}$$

Equation (5.1) represents the conservation of mass under the assumption of incompressibility (Boussinesq assumption); Equation (5.2) expresses the conservation of the momentum along *x*- and *y*- directions; Equation (5.3) represents the conservation of the momentum in the *z*- direction which are simplified to the hydrostatic pressure distribution according to the shallow-water assumption; lastly, Equation (5.4) stands for the transport equation, which is solved for salinity and temperature constituents. In these equations, u, v, and w are the velocity components in the *x*-, *y*- and *z*- directions, respectively; Q stands for the mass source intensity per unit area; t is the time; f represents the Coriolis parameter; g is the gravitational acceleration (≈ 9.81 ms^{-2}); ζ stands for the free surface elevation relative to $z = 0$, i.e., the water level; ρ_0 and ρ represent the reference density of sea water and the density, respectively; υ_h and υ_v represent the horizontal and vertical eddy viscosities, respectively; D_h and D_v stand for the horizontal and vertical eddy diffusivities, respectively; c represents the thermohaline conditions (i.e., salinity or temperature); λ_d stands for decay processes; finally R_s is the source term per unit area.

5.3.3. Numerical model (II): implementation

The numerical model covers the whole ria by means of a Cartesian grid extending towards the adjacent continental shelf up to the 150 m isobath, at a distance of approx. 10 km offshore. This grid (Figure 5.2) is composed of 57361 varying-size cells, being the grid size set as follows: in the inner and middle ria, a grid resolution of 50 x 50 m is adopted, progressively decreasing in the y-direction up to 50 x 150 m at the outer ria (northern boundary of the grid). Regarding the vertical discretisation, a σ- coordinate system composed of twelve layers is used(Philips, 1957), with the following layer thicknesses (percentages of water column) from surface to bottom: 2, 3, 5, 10, 15, 15, 15, 15, 10, 5, 3 and 2 (Carballo et al., 2009b; Iglesias & Carballo, 2009a; Ramos et al., 2014).This distribution of σ-layers, which provides a higher grid resolution near the surface and seabed, ensures an adequate modelling of boundary layer flows (Carballo et al., 2009b).

The bathymetric data of the Ria de Ortigueira and its surroundings were obtained from nautical charts #408 and #4083 from the Navy's Hydrography Institute (Instituto Hidrográfico de la Marina). Additionally, intertidal areas are fully described by using data from a 10 x 10 m resolution digital elevation model.

The initial conditions for the hydrodynamic numerical model are null free surface elevation and velocity at each node of the computational grid (cold start) (Iglesias & Carballo, 2011a). As far as the transport model is concerned, the initial thermohaline conditions are prescribed at the oceanic boundaries through field measurements (the reader is referred to Table 5.2 for a better understanding). Moreover, in order to avoid the influence of the initial conditions on the numerical results, a 30-day spin-up period is adopted to ensure their dynamical adjustment with the flow field (Souto et al., 2003; Torres López, Varela, & Delhez, 2001).

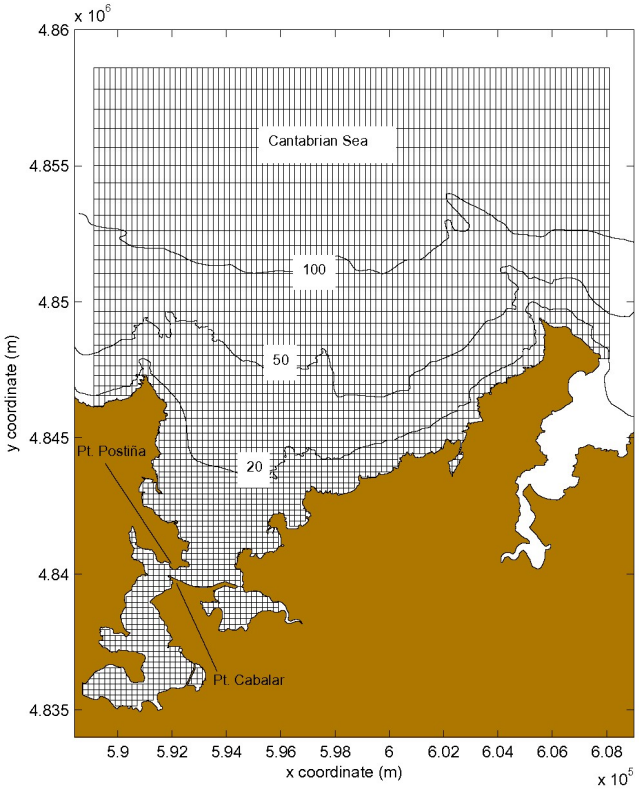


Figure 5.2. Numerical model grid.

Regarding the open boundary conditions, Dirichlet type conditions are imposed along the oceanic boundaries by considering the M2 constituent and the thermohaline conditions (Table 5.2). At the land-water transition, null flow through the boundary and zero shear stress are imposed. At the sea bottom boundary, the shear stress, $\vec{\tau}_{b3D}$, induced by a turbulent flow is computed by means of a quadratic law:

$$\vec{\tau}_{b3D} = \frac{g\rho_0|\vec{u}_b|\vec{u}_b}{C_{3D}^2}, \tag{5.5}$$

where $\vec{u}_b$ represents the magnitude of the horizontal velocity in the bottom layer and C_{3D} represents the 3D Chézy coefficient, which is computed as:

$$C_{3D} = C_{2D} + \frac{\sqrt{g}}{\kappa} ln\left(\frac{\Delta z_b}{2H}\right), \tag{5.6}$$

being k the von Karman constant ($k = 0.41$), Δz_b the distance from the sea bottom to the nearest grid node, H the water depth, and C_{2D} the 2D Chézy coefficient, which can be expressed as:

$$C_{2D} = \frac{\sqrt[6]{H}}{n}, \tag{5.7}$$

USC UNIVERSIDADE DE SANTIAGO DE COMPOSTELA

where n stands for the Manning's coefficient which is prescribed in this work as a function of the water depth (Dias & Lopes, 2006) in order to consider the full influence of the water depth on the seabed stress (Cheng & Gartner, 1985; Cheng et al., 1993).

Finally, the wind shear-stress, $\vec{\tau}_s$, at the free surface is given by:

$$\vec{\tau}_s = \rho_a C_d \left|\vec{U}_{10}\right| \vec{U}_{10}, \tag{5.8}$$

where ρ_a represents the density of the air, $\vec{U}_{10}$ stands for the wind velocity vector at 10 m height above the sea surface, and C_d is the wind drag coefficient computed following (Smith, 1980; Yelland et al., 1998). Moreover, regarding the main numerical and physical parameters of the numerical model, the horizontal advection terms in Equation (5.2) are calculated using the Cyclic method (Stelling & Leendertse, 1992); as regards the temporal discretisation, the model resorts to an alternating direction implicit (ADI) algorithm (Chung, 2002); finally, the k-ε model is adopted for the turbulence closure (Rodi, 1987).

The numerical model was successfully validated against field measurements obtained by means of an ADCP (Acoustic Doppler Current Profiler) and a tidal gauge deployed at two different locations in the inner and middle ria during a 19-day period. During this period, the model was forced along the oceanic boundaries with the main tidal harmonics, thermohaline conditions, wind velocity and direction and fluvial discharges of River Mera. A good agreement between computed and observed series (for both water levels and velocities) is obtained, reaching high values of the correlation coefficient R (i.e., $R \approx 0.99$ for water levels and $R > 0.82$ for flow magnitude and direction at each layer), and low values of several statistical coefficients (i.e., mean difference, *MD*, and mean square error, *MSE*). For further details of the numerical model validation, the reader is referred to previous works (Defne et al., 2011; Ramos et al., 2013; Ramos et al., 2014; Sanchez et al., 2014; Sánchez et al., 2014a; Sánchez et al., 2014b).

The implementation of the TSTs in the numerical model is conducted through the so-called momentum sink approach (Defne et al., 2011; Ramos et al., 2013; Ramos et al., 2014). It consists in introducing a momentum sink term into the right-hand side of Equation 5.2 by means of a retarding force which compensates the thrust force exerted by the flow on the TST (G.I. Shapiro, 2011). Considering this, the momentum sinks can be modelled as follows:

$$\left.\begin{aligned} M_x &= \frac{F_x}{\rho} \\ M_y &= \frac{F_y}{\rho} \end{aligned}\right\}, \tag{5.9}$$

being F_x and F_y the components of the retarding force per unit volume V along x- and y-directions, respectively. These components are opposite and equal to the thrust force, and therefore, they can be expressed as:

$$\left.\begin{aligned} M_x &= -\frac{1}{2}\frac{C_T A}{V} Uu \\ M_y &= -\frac{1}{2}\frac{C_T A}{V} Uv \end{aligned}\right\}, \tag{5.10}$$

where A represents the cross-section of a TST, U stands for the magnitude of the flow velocity and C_T is the thrust coefficient (Bahaj, A. S. et al., 2007).

USC UNIVERSIDADE DE SANTIAGO DE COMPOSTELA

Figure 5.3 shows the layout of the proposed tidal farms, which are located in the surroundings of the narrowing between Pt. Postiña and Pt. Cabalar where the strongest tidal currents are found (see Section 5.1). Both plants have the same layout with a surface area of about 1500 m^2. The first plant is composed of floating TSTs occupying roughly the upper part of the water column and the second plant is composed of TSTs of the same characteristics, but fixed to the bottom, and occupying the lower part of the water column.

The TST selected is an Evopod turbine in view of its appropriateness for shallow waters areas (Álvarez et al., 2022; Sanchez et al., 2014; Sánchez et al., 2014a), as is the case of the proposed location in the Ria de Ortigueira. Following the distance recommendations between lines of TSTs, 30 turbines with a sweep area of approx. 600 m^2, were distributed over three lines roughly perpendicular to the main flow direction.

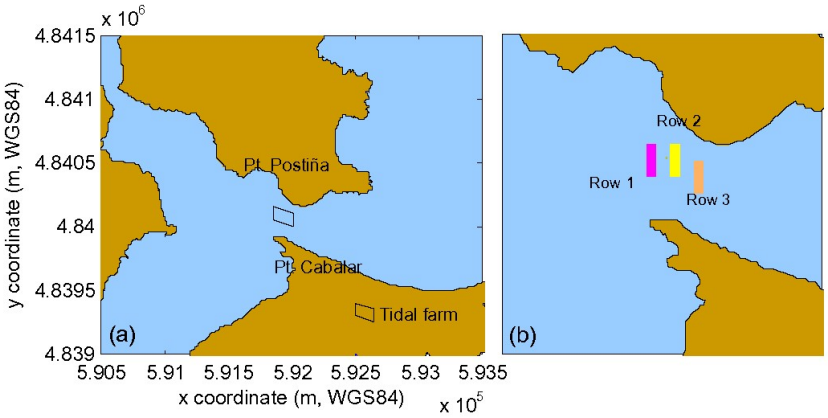


Figure 5.3. Location of the considered tidal stream plants (a). Layout in plan view of the plants (b).

5.3.4. Tide-driven residual circulation

The most usual procedure to compute the residual circulation induced by the tide consists in time-averaging or filtering the transient velocities computed by the numerical model (Umgiesser, 1997). There are other approaches, such as those based on the numerical solving of the so-called residual velocity evolution equations (Salas-de-León, Carbajal-Pérez, Monreal-Gómez, & Barrientos-MacGretor, 2003), which are not considered in the present application. The transient Eulerian horizontal velocity vector numerically computed (u, v), is decomposed into its periodic and residual components (u_p, v_p) and (u_r, v_r), respectively, as follows:

$$(u, v) = (u_p, v_p) + (u_r, v_r), \tag{5.11}$$

with the residual velocity vector computed as:

$$(u_r, v_r) = \frac{1}{T}\int_{-T/2}^{T/2} (u, v)dt, \tag{5.12}$$

where T represents the cut-off period of the averaging operator. A value of 12 h 25 min is adopted for this cut-off period in order to fully filter the variability of the semidiurnal tide prescribed by the dominance of the M2 tidal constituent.

5.3.5. Case studies

In this work, a detailed assessment of the impacts of tidal stream energy exploitation on the residual circulation and estuarine upwelling is conducted following a seasonal approach. To

this end, several case studies (CS) are undertaken with the aim of comparing the differences between altered and unaltered conditions (i.e., with and without energy extraction, respectively) for the different scenarios considered for the boundary conditions (i.e., winter and summer). Table 5.3 summarizes the case studies considered in this work.

Table 5.3. Summary of boundary conditions and the situations simulated in the different case studies analyzed

Case study	Tidal plant	Wind	Scenario
CS1	no plant	no wind	spring-summer
CS2	no plant	no wind	autumn-winter
CS3	no plant	SW mean summer wind (3.32 ms^{-1})	spring-summer
CS4	no plant	SW mean winter wind (6.03 ms^{-1})	autumn-winter
CS5	floating plant	no wind	autumn-winter
CS6	bottom plant	no wind	autumn-winter
CS7	floating plant	SW mean winter wind (6.03 ms^{-1})	autumn-winter
CS8	bottom plant	SW mean winter wind (6.03 ms^{-1})	autumn-winter

5.4. RESULTS AND DISCUSSION

5.4.1. Unaltered conditions

Unaltered hydrodynamic conditions (i.e., without considering energy extraction) in the Ria de Ortigueira are analysed through four case studies (CS1 to CS4), focusing this analysis on how the seasonality of river discharges and thermohaline conditions, in conjunction with the circulation induced by upwelling favourable SW winds, influence the estuarine residual circulation. With this aim, the results are provided in terms of the vectorial distribution of the unaltered residual circulation patterns throughout the estuary.

CS1 describes the residual circulation within the Ria de Ortigueira under summer conditions for fluvial discharges and thermohaline conditions in the absence of winds. Figure 5.4 shows the resulting unaltered residual circulation patterns in surface and bottom layers of the numerical grid. Two regions can be distinguished in terms of residual circulation patterns. In the inner ria (i), similar hydrodynamic patterns (i.e., a marked outflow) are present throughout the whole water column, including also a vortex rotating counterclockwise, with somewhat stronger flow velocities in surface layers (with peak velocities located in the surroundings of the narrowing between Pt. Postiña and Pt. Cabalar of about 0.20 ms^{-1} and 0.15 ms^{-1} in surface and bottom layers, respectively). On the other hand, the middle and outer ria (ii) are characterized by typical patterns of a positive estuarine circulation (i.e., inflow on the bottom layer and outflow on the surface layer) driven from river discharges flowing out in the surface layers.

USC UNIVERSIDADE DE SANTIAGO DE COMPOSTELA

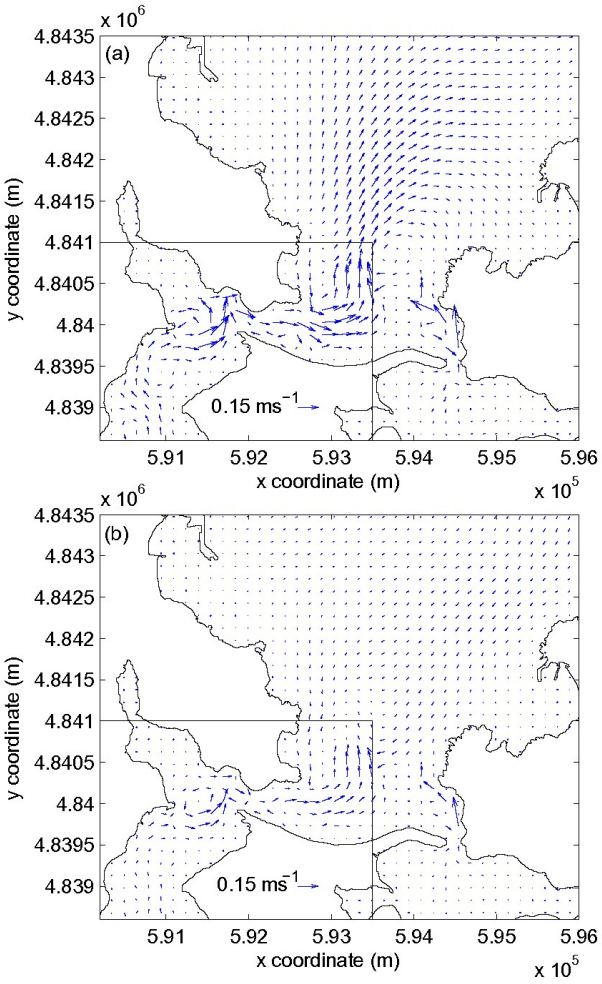


Figure 5.4. Residual flow pattern in Ria de Ortigueira under case study CS1 conditions. (a) Surface layer; (b) Bottom layer.

Regarding CS2, the same forcing factors as in CS1 are considered but now under winter conditions (Figure 5.5). As a result, the induced circulation is similar in both case studies, with somewhat greater velocities in the surface layer in the case of CS2, in particular in the middle and outer ria, due to the larger fluvial discharges. Therefore, it can be concluded that, in absence of winds, the seasonality of the hydrodynamic driving agents does not lead to significant variations in the residual circulation of the Ría de Ortigueira, as a consequence of the typical low riverine inputs to this estuary.

USC UNIVERSIDADE DE SANTIAGO DE COMPOSTELA

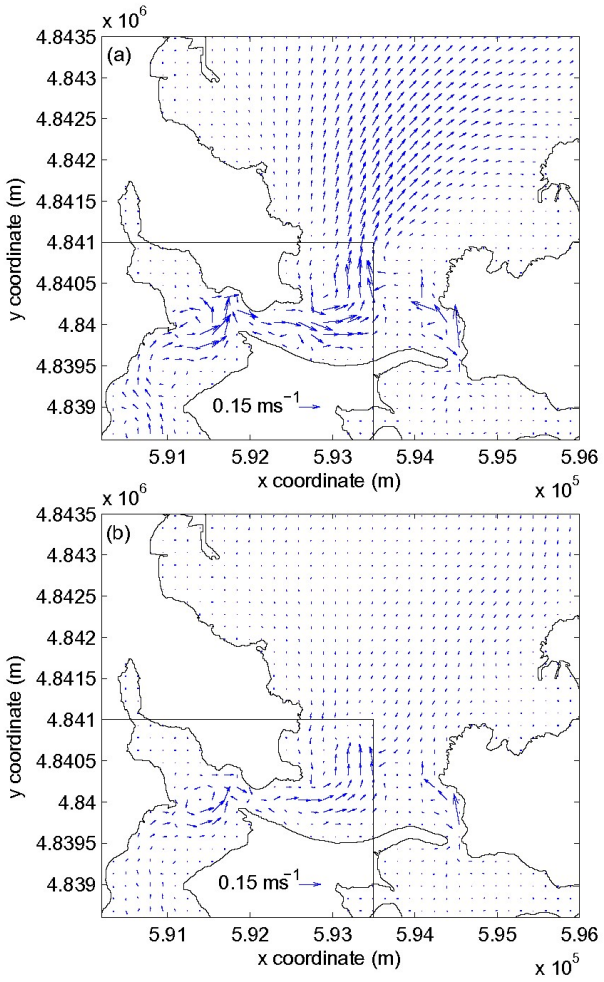


Figure 5.5. Residual flow pattern in Ria de Ortigueira under case study CS2 conditions. (a) Surface layer; (b) Bottom layer.

With respect to CS3, it corresponds to CS1 (i.e., summer conditions), but considering the action of the summer SW wind. The resulting circulation (Figure 5.6) could be characterized as a conventional two-layer estuarine circulation, reinforcing the residual patterns described in CS1 and CS2. In this case, the wind-induced outflow in the surface layer is strengthened, attaining values of about 0.25 ms^{-1} in the inner ria in the surroundings of the narrowing between Pt. Postiña and Pt. Cabalar, and increasing the shelf-water intrusion through the bottom layers. Finally, it is worthy of mention that surface water masses tend to leave the ria next to its right margin. This pattern, which is also apparent, although with less intensity, in CS1 and CS2, is probably the result of wind action, reinforced by the river discharges, which tend to deviate the flow to the right as a consequence of the Coriolis force.

USC UNIVERSIDADE DE SANTIAGO DE COMPOSTELA

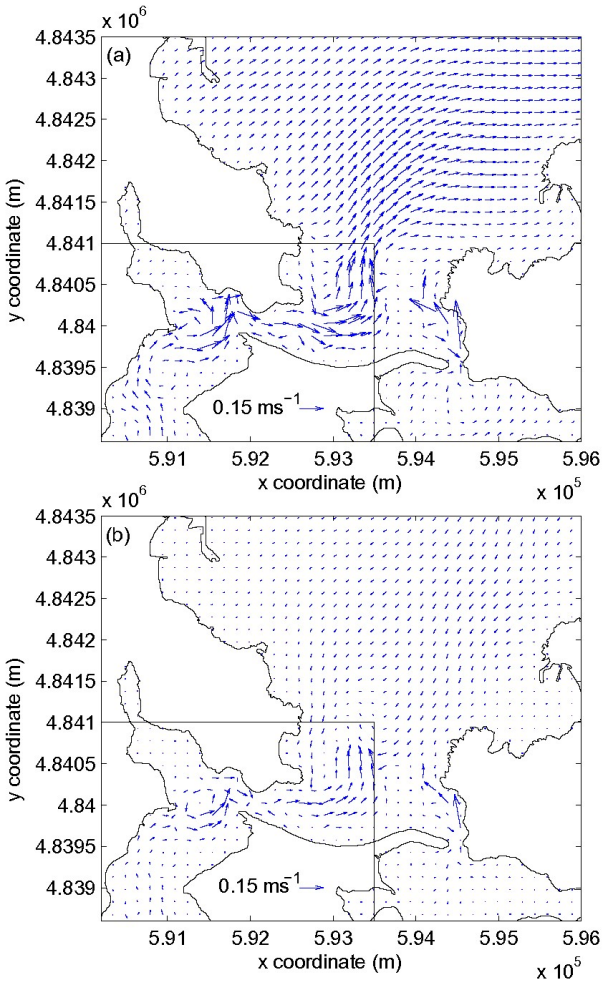


Figure 5.6. Residual flow pattern in Ria de Ortigueira under case study CS5 conditions. (a) Surface layer; (b) Bottom layer.

As far as CS4 is concerned, it considers the same forcing factors as in the case of CS3 but under the action of a winter SW wind. The results obtained (Figure 5.7) are similar to those obtained in CS3 (Figure 5.6). However, due to the larger wind velocity and fluvial discharges under winter conditions, the residual currents induced in CS4 are stronger than in CS3, in particular in the surface layer, which is more influenced by wind action and river discharges, reaching values of up to 0.25 ms^{-1}.

Overall, the aforementioned comparison of the case studies corresponding to unaltered conditions (CS1 to CS4) shows how the typical low fluvial inputs discharging into the Ria de Ortigueira are not capable of inducing significant residual currents; on the contrary, the seasonality of the wind regime plays a key role in the residual circulation within this semi-enclosed waterbody.

USC UNIVERSIDADE DE SANTIAGO DE COMPOSTELA

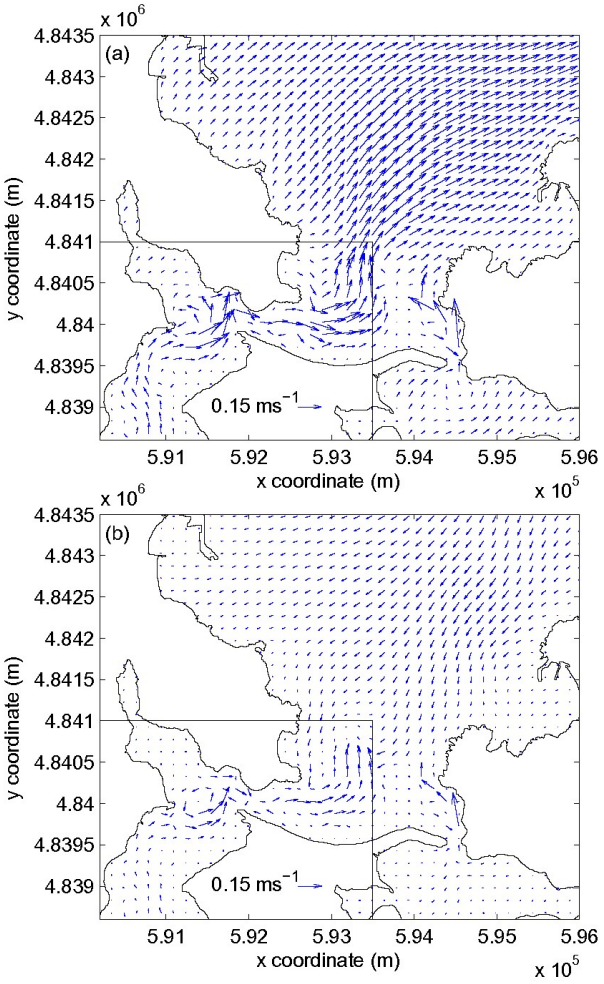


Figure 5.7. Residual flow pattern in Ria de Ortigueira under case study CS5 conditions. (a) Surface layer; (b) Bottom layer.

5.4.2. Altered conditions

The altered hydrodynamic conditions (i.e., considering energy extraction) in the Ria de Ortigueira which would result from the operation of a tidal farm are analysed through four additional case studies (CS5 to CS8), which consider different configurations (i.e., floating and bottom-fixed converters). As a consequence of the results provided by CS1 to CS4, which show the limited effects of the seasonality of thermohaline conditions and fluvial discharges on the resulting residual patterns, CS5 to CS8 only consider typical winter thermohaline and riverine conditions (summer scenarios are not retained) under no wind action and upwelling favourable winds.

With the aim of assessing the impacts of the energy extraction, the results are provided through a comparison with unaltered conditions case studies. In this way, the results provided by CS5 to CS8 (Figures 5.8 to 5.11) show the vectorial distribution of the altered residual circulation patterns (vectors) and the differences in the magnitude of the residual currents between altered and unaltered conditions (colormap) in the coastal area close to the location proposed for tidal energy exploitation (marked in Figures 5.4 to 5.7).

CS5 computes the altered residual circulation within the study area considering winter thermohaline and riverine conditions in absence of winds. Regarding the implementation of the

tidal farm and its energy extraction in the numerical model, it is conducted by considering a floating tidal farm, i.e., operating in the upper σ-layers of the grid. The results provided by CS5 (Figure 5.8) show that the major changes in the residual velocities are located in the constriction between Pt. Postiña and Pt. Cabalar, as a consequence of the location of the proposed farm (Figure 5.3). Resulting from the layout of the tidal farm, which is distributed in three different lines along a W-E axis, the changes in the residual velocities along this section are spatially distributed as follows:(i) in the westernmost part of the constriction, in the surroundings of row 1, there is an apparent increase in the residual velocities towards the N and S margins of the ria for both surface and bottom layers, attaining maximum increments up to 0.05 ms^{-1} in the case of the surface layer, where the differences between unaltered and altered conditions are somewhat higher; (ii) in the central section of the narrowing, in the surroundings of row 2, the situation is not homogenous, combining residual velocity increments (roughly 0.02 0.03 ms^{-1}) with weaker decrements (0.01-0.02 ms^{-1}) located W and E of row 2, respectively; finally, (iii) in the easternmost part of the constriction, in the surroundings of row 3, decrements towards the N (surface and bottom layers) and S margins (primarily in the surface layer) of the ria are apparent, along with a remarkable increase in the residual velocity within the central channel of this section (attaining maximum figures of approx. 0.05 ms^{-1}). Finally, the maximum residual velocities are of the same order than in the case of the unaltered conditions, roughly 0.25 ms^{-1}.

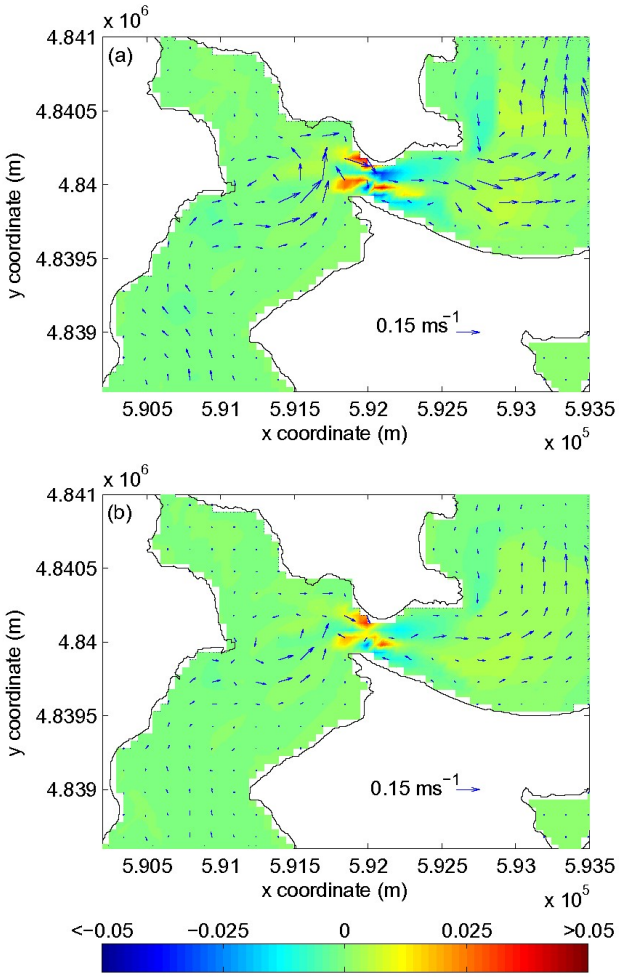


Figure 5.8. Residual flow pattern in Ria de Ortigueira under case study CS5 conditions (vectors); differences in the residual flow magnitude between altered flow and reference situation (CS5-CS2) (colour map). (a) Surface layer; (b) Bottom layer.

USC UNIVERSIDADE DE SANTIAGO DE COMPOSTELA

In CS6, the same forcing factors and conditions as in the case of CS5 (winter thermohaline and riverine conditions in absence of winds) are input to the model, but now considering a bottom-fixed tidal farm, i.e., operating in the lower σ-layers of the grid (Figure 5.9). The results show similar hydrodynamic patterns as in the case of the floating farm in CS5. With respect to the differences between unaltered and altered conditions, the spatial distribution of the effects of the energy extraction corresponds, in general, with those exposed in the case of CS5 (Figure 5.8); however, several peculiarities are now apparent: on the surface layer, the increments and decrements in the residual velocities are slightly stronger and weaker, respectively; on the contrary, on the bottom layer, the situation is roughly the opposite, although with even less differences with respect CS5. Moreover, as Figure 5.9 shows, there is an apparent decrement in the residual velocity (approx. 0.02 ms^{-1}) located in the surroundings of row 1, more specifically in the central channel of the ria, which is not present in the case of a floating plant.

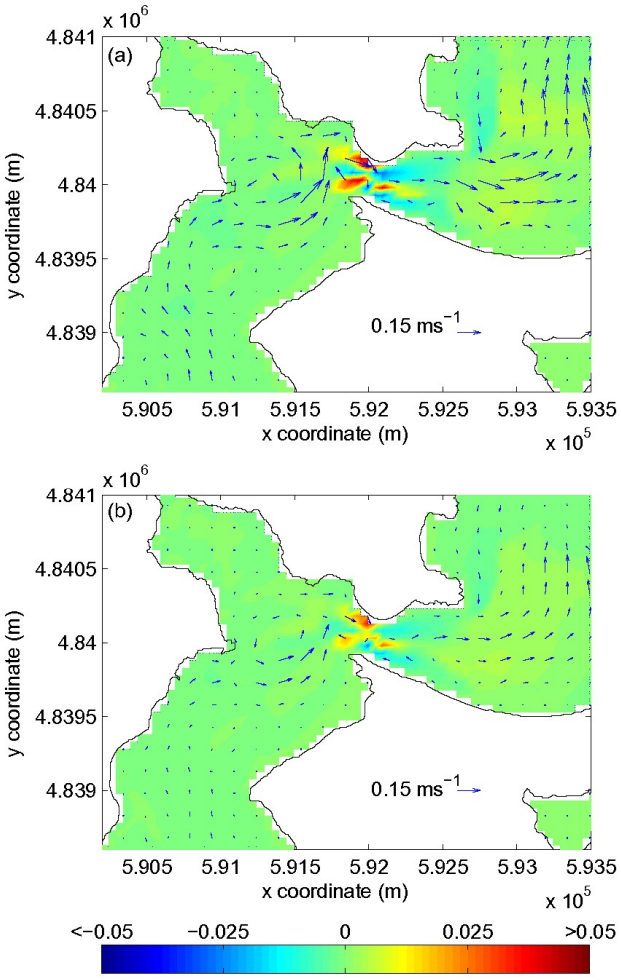


Figure 5.9. Residual flow pattern in Ria de Ortigueira under case study CS6 conditions (vectors); differences in the residual flow magnitude between altered flow and reference situation (CS6-CS2) (colour map). (a) Surface layer; (b) Bottom layer.

As far as CS7 is concerned, winter thermohaline and riverine conditions are considered under the action of SW upwelling favourable winds. Likewise, the effects of the energy extraction are modelled by means of a floating tidal farm as in the case of CS5. The results of CS7 (Figure 5.10) show the influence of SW winds on the surface layers, in which greater outflow residual velocities are attained (i.e., close to the maximum figures of about 0.25 ms-1) in comparison with previous altered conditions case studies in absence of winds. In the same

way, bottom layers also present outflow residual flows throughout the inner ria, although with weak residual velocity magnitudes. Regarding the spatial distribution of the impacts generated by the energy extraction in the vicinities of the farm, CS7 presents a similar pattern along the W-E axis as in the case of CS5 and CS6: (i) in the surroundings of row 1, there are two major areas, located towards the N and S margin of the channel, in which the greatest increase in the residual velocities (i.e., 0.03-0.04 ms^{-1}) for both surface and bottom layers is apparent; (ii) in the surroundings of row 2, there exists several areas characterized by increments (0.02-0.03 ms^{-1}) and decrements (0.01-0.02 ms^{-1}) in the residual velocities W and E of row 2, respectively; finally, (iii) in the surroundings of row 3, the largest reductions in the residual velocities are located within two major areas towards the N (surface and bottom layer) and S (surface layer) margin of the ria; on the contrary, the maximum increments in the residual velocities (0.04 ms^{-1}) are located within the central channel of the narrowing between Pt. Postiña and Pt. Cabalar.

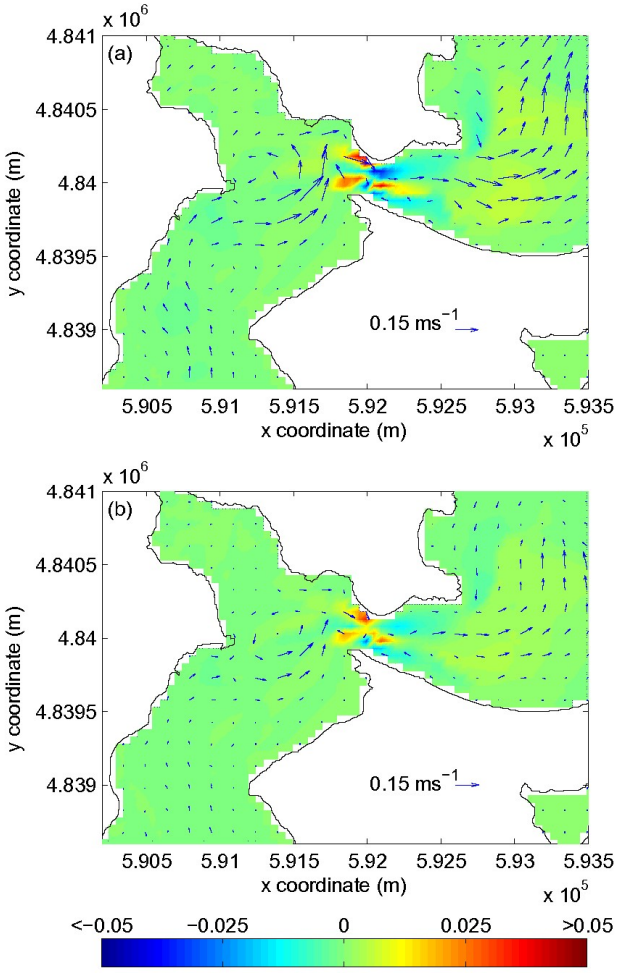


Figure 5.10. Residual flow pattern in Ria de Ortigueira under case study CS7 conditions (vectors); differences in the residual flow magnitude between altered flow and reference situation (CS7-CS4) (colour map). (a) Surface layer; (b) Bottom layer.

Finally, CS8 computes the altered residual circulation within the inner Ria de Ortigueira produced by the operation of a bottom-fixed tidal farm under winter riverine and thermohaline conditions, along with SW winds. The results obtained (Figure 5.11) are close, in terms of residual patterns, to those of CS6 in the absence of winds. Likewise, regarding the impacts of the energy extraction on the magnitude of the residual currents, the spatial distribution and magnitude of these impacts present, as in the case of other cases studies conducted (CS5 to

CS7), a clear spatial distribution in three different areas (corresponding with the surroundings of the different lines of TSTs) which alternate increments and decrements in residual velocities. Finally, Figure 5.11 confirms that, in the case of a bottom-fixed tidal farm, a clear reduction in the residual velocity in the surroundings of row 1 is observed, and more specifically in the central channel of the ria, which is not apparent in the case of a floating plant, as indicated in CS6 (Figure 5.9).

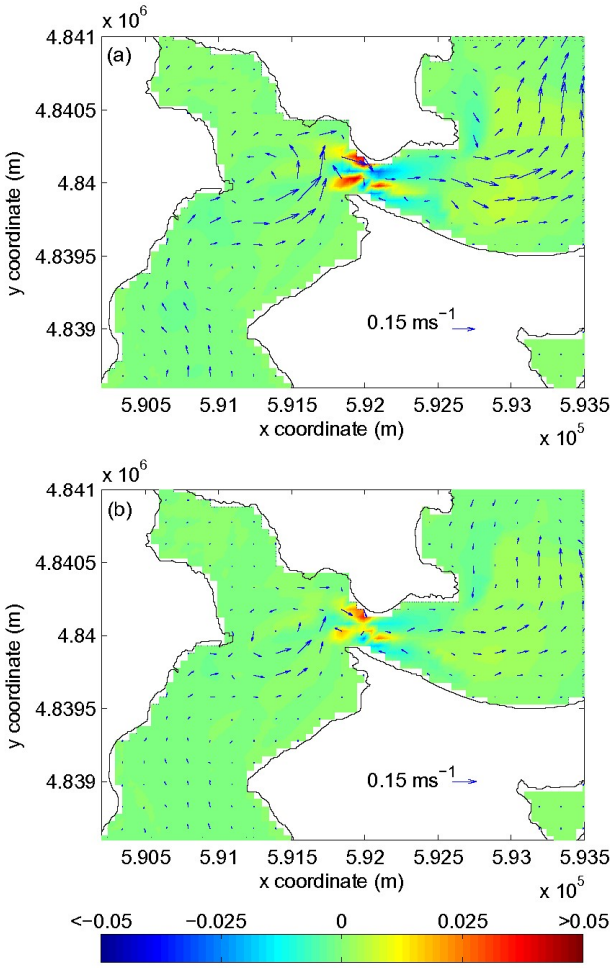


Figure 5.11. Residual flow pattern in Ria de Ortigueira under case study CS8 conditions (vectors); differences in the residual flow magnitude between altered flow and reference situation (CS8-CS4) (colour map). (a) Surface layer; (b) Bottom layer.

5.5. CONCLUSIONS

In this work, a 3D numerical model was implemented in the Ria de Ortigueira, the westernmost of the Galician Rias Altas (NW Spain), in order to study the potential effects of different configurations of tidal stream farms on the residual circulation, including the estuarine upwelling and its seasonality. First, the model was successfully validated against field measurements obtained by means of an ADCP (Acoustic Doppler Current Profiler) deployed at two different locations in the inner and middle ria during a 19-day period, obtaining correlation coefficients between model and measured data very close to unity. Next, a total of eight case studies (CS) were analysed in order to get a detailed seasonality assessment of the impacts of tidal stream energy exploitation on the residual flow. In particular, the unaltered hydrodynamic conditions (absence of tidal farm) and altered conditions (operation of floating

and bottom-fixed tidal farms), under typical summer and winter scenarios are analysed, including the absence of wind action and upwelling favourable winds.

The unaltered conditions in absence of wind action are rather similar under winter and summer conditions. In both cases, two different regions can be distinguished in terms of residual circulation patterns throughout the ria: (i) the inner ria presents similar hydrodynamic patterns throughout the whole water column, with somewhat stronger flow velocities in surface layers, reaching peak velocities of about 0.25 $ms^{-1}$and 0.15 ms^{-1} in surface and bottom layers, respectively. On the other hand, the middle and outer ria (ii) are characterized by typical patterns of a positive estuarine circulation.

When the summer SW wind is considered together with summer thermohaline conditions, the resulting circulation follows a conventional two-layer estuarine circulation, reinforcing the residual patterns described above, whit similar peak values. However, in the case of a typical winter SW wind, although the resulting circulation pattern is also similar, due to the larger wind velocity and fluvial discharges present, the residual currents induced are stronger, in particular in the surface layer.

Overall, when a tidal farm operates, the resulting modifications on the residual flow are primarily restricted to the narrowing between Pt. Postiña and Pt. Cabalar, in the area occupied by the farm and in its vicinities (roughly over 100-150 m distance), regardless of the combination of tidal farm configuration and boundary conditions selected. The maximum values of the variation in the residual velocities due to the tidal farm operation are of about 0.05 ms^{-1} in the influence area of the plant. Outside of this area, the variations on the residual flow magnitude are lower than approx. 0.01 ms^{-1}, and virtually negligible at a certain distance from the farm.

In general, and regardless of the combination of tidal farm configuration and hydrodynamic forcing factors, the residual flow velocity increases to the W of the plant and decreases to the E of the plant, both in the surface and bottom layers. In addition, in the bottom layer, the magnitude of the effects is quite similar in all the CS considered (bottom or floating plant, with and without wind action), and of less than 0.03 ms^{-1}. Although the pattern in the variations in the surface layer is also similar in the four CS, their magnitude is slightly greater when a bottom plant operates in the absence of wind, with increments in the residual flow velocities of around 0.05 ms^{-1} at the W of the plant.

This paper determined the potential impact on the residual flows in the Ría de Ortigueira caused by the operation of different tidal stream farms configurations under different typical hydrodynamic scenarios, establishing that these impacts are restricted to the surroundings of the proposed plants, and virtually do not affect the upwelling events. The procedure followed can be used to analyse the potential impacts on the hydrodynamics in other estuaries of interest for tidal stream energy operation.

USC UNIVERSIDADE DE SANTIAGO DE COMPOSTELA

USC
UNIVERSIDADE
DE SANTIAGO
DE COMPOSTELA

6. CONCLUSIONS

In this Doctoral Thesis, several factors involved in the exploitation of tidal stream energy in the Ría de Ortigueira are studied, including the determination of the most appropriate conversion system, the performance of the different systems analysed, and the impacts derived from the energy exploitation on transient and residual circulations. For this, a 3D numerical model is implemented and applied to simulate the hydrodynamics of this estuary during different periods, with different combinations of boundary conditions and different exploitation plants. The plants considered are composed by Tidal Stream Turbines (TSTs) and have the same layout in plan view; however, one of them, P1, is composed by floating TSTs and the other, P2, by bottom-fixed TSTs.

The performance analysis is based on three parameters that allowed the characterization of the operation of the plants: production of electrical energy, availability factor and capacity factor; appreciating notable differences in the results obtained for both plants. Plant P1 presents higher values in all the parameters considered; in particular, its annual electric power output is almost double that of P2, and its annual capacity factor is about 64% higher. Regarding the availability factor, the differences are less important (15%); however, the output power of P1 is more homogeneous, and this is an advantage that should not be overlooked, especially if an energy storage system is to be installed. In addition, the intra-annual analysis shows that the parameters mentioned also present a significant monthly variability, although their general trend is similar for both plants, that is, the annual differences remain approximately constant throughout the year. A finding of particular interest is that, contrary to what might be expected, the months with highest peak velocities are not those with the highest values of power performance parameters, including energy production.

Regarding the effects produced by the operation of both plants considered, P1 and P2, despite the significant differences existing in the annual energy production, it is observed that the impacts caused on the general transient circulation present great similarities. Although their operation is not sufficient to considerably modify the circulation throughout the estuary, alterations of the order of 10^{-2} ms^{-1} are observed several km away from the plants. As for the differences between the situations of mid-flood and mid-ebb tide, the general pattern is practically the same, the main difference being the extension of the affected area to the East of the plant (lesser in mid-ebb tide). Regarding the effects on the location of the plant and its vicinities, the results of the model show that there is a significant reduction in the speed of the current. However, not all this velocity reduction comes from energy extraction, but also from the fact that the flow is partially redirected towards the remaining section, with the consequent increase in current velocities. In contrast to the strong similarities in the modifications of the general pattern caused by plants P1 and P2, important differences were found in this zone, due to their vertical configuration (occupying a different portion in the water column). However, it has been observed that the impacts may differ from what might initially be expected (for example, a reduction in the flow was found over a significant part of the surface layer during the operation of the fixed bottom TSTs).

Finally, a total of eight case studies (CS) are analysed to obtain a detailed assessment of the seasonality of the impacts of tidal energy exploitation on the residual flow. In particular, the unaltered hydrodynamic conditions (absence of tidal power plants) and altered (operation of plants P1 and P2) are analysed under typical summer and winter scenarios, including the absence of wind action and favourable *upwelling* winds.

The unaltered residual circulation is quite similar in summer and winter conditions, showing how the relatively low fluvial contribution in the estuary is not capable of inducing significant residual currents. In both cases, two different regions are distinguished in terms of residual circulation patterns along the estuary: (i) the inner ria presents similar hydrodynamic patterns throughout the water column, with somewhat stronger flow velocities in the superficial layers, reaching maximum speeds of around 0.25 ms^{-1} and 0.15 ms^{-1} in the surface and bottom layers, respectively. On the other hand, the middle and outer estuary (ii) are characterized by typical patterns of a positive estuarine circulation. These patterns are reinforced when typical SW winds are considered, mainly in the typical winter case, showing that the seasonality of the wind regime itself plays a key role in the residual circulation in the estuary.

In general, when a tidal power plant operates, the resulting modifications in the residual flow are mainly limited to the narrowing between Pt. Postiña and Pt. Cabalar, in the area occupied by the farm and in its surroundings (approximately more than 100-150 m away), regardless of the combination of tide farm settings and boundary conditions selected. The maximum values of the variation of the residual velocities due to the operation of the tidal farm are of the order of 0.05 ms^{-1} in the area of influence of the plant. Outside this zone, the variations in the magnitude of the residual flow are less than approx. 0.01 ms^{-1}, and practically negligible at some distance from the farm.

In summary, through this Doctoral Thesis it is determined that the energy performance of floating and bottom-fixed TSTs in the same location can greatly differ depending on the characteristics of the hydrodynamic conditions of the coastal area in which they operate. This can be aggravated in the case of coastal masses with significant differences in current velocities throughout the water column, as is the case in the study area (Ría de Ortigueira). As a result of the higher speeds near the surface, floating TSTs provide better performance than bottom-fixed devices. Finally, a significant intra-annual variability in the energy yield is observed, which leads to the conclusion that it should be analysed based on simulations covering a complete year, instead of extrapolating the results obtained for a spring-neap cycle.

Likewise, this study shows that the energetic exploitation of tidal currents may cause important impacts on the estuarine circulation. These impacts were quantified for two proposed tidal stream energy plants, composed of floating or bottom-fixed TSTs. The results shows that there are almost no differences between the impacts on the general circulation caused by both TSTs configurations; on the contrary, there are significant differences in the effects in the plant site and its vicinities. Furthermore, impacts in this area greatly differ from what might be expected in advance, highlighting the importance of a site-specific analysis.

Finally, in this work the potential impact on the residual circulation in the Ria de Ortigueira caused by the operation of different configurations of tidal power plants under different typical hydrodynamic scenarios was determined. These impacts were found to be restricted to the area of the plants and its surroundings; they are of a very limited magnitude and hardly affect upwelling events.

Beyond the interest of these results for the coastal area herein studied, the procedure presented in this work could be used as a reference methodology to analyse the annual energy

yield of different TSTs in similar coastal regions, as well as their effects on coastal hydrodynamics. It is important to keep in mind that these impacts may generate other environmental effects that are beyond the scope of this work, such as changes in sediment transport patterns and dispersion of pollutants. These potential effects will be treated as a continuation of this line of research.

The results achieved in this Doctoral Thesis allow us to continue advancing in the research and development of renewable energies in Galicia, more specifically, marine renewable energies, which have great potential in our coast.

USC
UNIVERSIDADE
DE SANTIAGO
DE COMPOSTELA

USC
UNIVERSIDADE
DE SANTIAGO
DE COMPOSTELA

REFERENCES

Ahmadian, R., & Falconer, R. A. (2012). Assessment of array shape of tidal stream turbines on hydro-environmental impacts and power output. *Renewable Energy, 44*(0), 318-327. doi:10.1016/j.renene.2012.01.106

Ahmadian, R., Falconer, R., & Bockelmann-Evans, B. (2012). Far-field modelling of the hydro-environmental impact of tidal stream turbines. *Renewable Energy, 38*(1), 107-116. doi:10.1016/j.renene.2011.07.005

Alvarez, I., Gomez-Gesteira, M., deCastro, M., Gomez-Gesteira, J. L., & Dias, J. M. (2010). *Summer upwelling frequency along the western cantabrian coast from 1967 to 2007* doi:https://doi.org/10.1016/j.jmarsys.2009.09.004

Alvarez, I., Gomez-Gesteira, M., deCastro, M., & Novoa, E. M. (2008). *Ekman transport along the galician coast (NW, spain) calculated from QuikSCAT winds* doi:https://doi.org/10.1016/j.jmarsys.2007.01.013

Alvarez, I., Ospina-Alvarez, N., Pazos, Y., deCastro, M., Bernardez, P., Campos, M. J., . . . Prego, R. (2009). A winter upwelling event in the northern galician rias: Frequency and oceanographic implications. *Estuarine, Coastal and Shelf Science, 82*(4), 573-582. doi:10.1016/j.ecss.2009.02.023

Álvarez, M., Ramos, V., Carballo, R., López, I., Fouz, D. M., & Iglesias, G. (2022). Application of marine spatial planning tools for tidal stream farm micro-siting. *Ocean & Coastal Management, 220*, 106063. doi:https://doi.org/10.1016/j.ocecoaman.2022.106063

Alvarez-Salgado, X. A., Roson, G., Perez, F. F., & Pazos, Y. (1993). Hydrographic variability off the rias baixas (NW spain) during the upwelling season. *Journal of Geophysical Research, 98*(C8), 14,447-14,455.

Álvarez-Salgado, X. A., Labarta, U., Vinseiro, V., & Fernández-Reiriz, M. J. (2017). *Environmental drivers of mussels flesh yield in a coastal upwelling system* doi:https://doi.org/10.1016/j.ecolind.2017.04.039

Babarit, A., Ben Ahmed, H., Clément, A. H., Debusschere, V., Duclos, G., Multon, B., & Robin, G. (2006). Simulation of electricity supply of an atlantic island by offshore wind turbines and wave energy converters associated with a medium scale local energy storage. *Renewable Energy, 31*(2), 153-160. doi:https://doi.org/10.1016/j.renene.2005.08.014

Bahaj, A. S., Molland, A. F., Chaplin, J. R., & Batten, W. M. J. (2007). Power and thrust measurements of marine current turbines under various hydrodynamic flow conditions in a cavitation tunnel and a towing tank. *Renewable Energy, 32*(3), 407-426. doi:10.1016/j.renene.2006.01.012

Bahaj, A. S., & Myers, L. (2004). Analytical estimates of the energy yield potential from the alderney race (channel islands) using marine current energy converters. *Renewable Energy, 29*(12), 1931-1945. doi:10.1016/j.renene.2004.02.013

Bahaj, A. S., & Myers, L. E. (2003). Fundamentals applicable to the utilisation of marine current turbines for energy production. *Renewable Energy, 28*(14), 2205-2211. doi:10.1016/S0960-1481(03)00103-4

Bahaj, A. S. (2011). Generating electricity from the oceans. *Renewable and Sustainable Energy Reviews, 15*(7), 3399-3416. doi:10.1016/j.rser.2011.04.032

Bekun, F. V., Alola, A. A., & Sarkodie, S. A. (2019). *Toward a sustainable environment: Nexus between CO2 emissions, resource rent, renewable and nonrenewable energy in 16-EU countries* doi:https://doi.org/10.1016/j.scitotenv.2018.12.104

Blanton, J. O., Atkinson, L. P., Castillejo, F., & Lavin, A. (1984). Coastal upwelling off the rias bajas, galicia, northwest spain. *I.Hydrographic Studies.Réun.Cons.Int.Explor.Mer, 183*, 79-90.

Blunden, L. S., & Bahaj, A. S. (2006). Initial evaluation of tidal stream energy resources at portland bill, UK. *Renewable Energy, 31*, 121-132.

Bolle, A., Bing Wang, Z., Amos, C., & De Ronde, J. (2010). The influence of changes in tidal asymmetry on residual sediment transport in the western scheldt. *Continental Shelf Research, 30*(8), 871-882. doi:http://dx.doi.org/10.1016/j.csr.2010.03.001

Brooks, D. A. (2006). The tidal-stream energy resource in Passamaquoddy–Cobscook bays: A fresh look at an old story. *Renewable Energy, 31*(14), 2284-2295. doi:10.1016/j.renene.2005.10.013

Carballo, R., Iglesias, G., & Castro, A. (2009a). Numerical model evaluation of tidal stream energy resources in the ría de muros (NW spain). *Renewable Energy, 34*(6), 1517-1524. doi:10.1016/j.renene.2008.10.028

Carballo, R., Iglesias, G., & Castro, A. (2009b). Residual circulation in the ría de muros (NW spain): A 3D numerical model study. *Journal of Marine Systems, 75*(1-2), 130-130.

Castaing, P., & Guilcher, A. (1995). Chapter 4 geomorphology and sedimentology of rias. *Developments in Sedimentology, 53*, 69-111. doi:https://doi.org/10.1016/S0070-4571(05)80024-X

Cerdeira-Arias, J. D., Otero, J., Barceló, E., Río, G. d., Freire, A., García, M., . . . Álvarez-Salgado, X. A. (2018). *Hydrography of shellfish harvesting areas in the western cantabrian coast (rías altas, NW iberian peninsula)* doi:https://doi.org/10.1016/j.rsma.2018.06.005

Charlier, R. H., & Finkl, C. W. (2008). *Ocean energy: Tide and tidal power* Springer.

Charlier, R. H. (2003). A "sleeper" awakes: Tidal current power. *Renewable and Sustainable Energy Reviews, 7*(6), 515-529. doi:10.1016/S1364-0321(03)00079-0

Cheng, R. T., Casulli, V., & Gartner, J. W. (1993). Tidal, residual, intertidal mudflat (TRIM) model and its applications to san francisco bay, california. *Estuarine, Coastal and Shelf Science, 36*(3), 235-280.

Cheng, R. T., & Gartner, J. W. (1985). Harmonic analysis of tides and tidal currents in south san francisco bay, california. *Estuarine, Coastal and Shelf Science, 21*(1), 57-74.

Chung, T. J. (2002). *Computational fluid dynamics* Cambridge University Press.

deCastro, M., Gómez-Gesteira, M., Alvarez, I., Lorenzo, M., Cabanas, J. M., Prego, R., & Crespo, A. J. C. (2008). Characterization of fall-winter upwelling recurrence along the galician

western coast (NW spain) from 2000 to 2005: Dependence on atmospheric forcing. *Journal of Marine Systems, 72*(1-4), 145-158.

Defne, Z., Haas, K. A., & Fritz, H. M. (2011). Numerical modeling of tidal currents and the effects of power extraction on estuarine hydrodynamics along the georgia coast, USA. *Renewable Energy, 36*(12), 3461-3471. doi:10.1016/j.renene.2011.05.027

Deltares. (2010). *User manual Delft3D-FLOW* (Deltares ed.). Delft, The Netherlands:

Dias, J. M., & Lopes, J. F. (2006). Implementation and assessment of hydrodynamic, salt and heat transport models: The case of ria de aveiro lagoon (portugal). *Environmental Modelling and Software, 21*(1), 1-15.

Dias, J. M., Sousa, M. C., Bertin, X., Fortunato, A. B., & Oliveira, A. (2009). Numerical modeling of the impact of the ancão inlet relocation (ria formosa, portugal). *Environmental Modelling & Software, 24*(6), 711-725. doi:https://doi.org/10.1016/j.envsoft.2008.10.017

Díez, J. (1996). *Las costas* Alianza Editorial.

Duarte, P., Alvarez-Salgado, X. A., Fernández-Reiriz, M. J., Piedracoba, S., & Labarta, U. (2014). *A modeling study on the hydrodynamics of a coastal embayment occupied by mussel farms (ria de ares-betanzos, NW iberian peninsula)* doi:https://doi.org/10.1016/j.ecss.2014.05.021

Dyer, K. E. (1997). *Estuaries: A physical introduction*. New York: John Wiley.

Dyer, K. R. (1973). *Estuaries: A physical introduction*. London: Jhon Wiley & Sons.

Erdiwansyah, Mamat, R., Sani, M. S. M., & Sudhakar, K. (2019). *Renewable energy in southeast asia: Policies and recommendations* doi:https://doi.org/10.1016/j.scitotenv.2019.03.273

European Commission. (1996). *The exploitation of tidal marine currents.* (No. EUR16683EN).

Proposal for a directive amending directive 98/70/EC relating to the quality of petrol and diesel fuels and amending council directive 93/12/EC and amending directive 2009/28/EC on the promotion of the use of energy from renewable sources [COM(2012) 595], (2012).

Evans, G., & Prego, R. (2003). Rias, estuaries and incised valleys: Is a ria an estuary? *Marine Geology, 196*(3–4), 171-175. doi:http://dx.doi.org/10.1016/S0025-3227(03)00048-3

Faez Hassan, H., Karim, O. A., & El-Shafie, A. (2012). Tidal current turbines glance at the past and look into future prospects in malaysia. *Renewable and Sustainable Energy Reviews, 16*(8), 5707-5717. doi:10.1016/j.rser.2012.06.016

Fallon, D., Hartnett, M., Olbert, A., & Nash, S. (2014). The effects of array configuration on the hydro-environmental impacts of tidal turbines. *Renewable Energy, 64*(0), 10-25. doi:http://dx.doi.org/10.1016/j.renene.2013.10.035

Fobissie, E. N. (2019). *The role of environmental values and political ideology on public support for renewable energy policy in ottawa, canada* doi:https://doi.org/10.1016/j.enpol.2019.110918

Fouz, D. M., Carballo, R., Ramos, V., & Iglesias, G. (2019). *Hydrokinetic energy exploitation under combined river and tidal flow* doi:https://doi.org/10.1016/j.renene.2019.05.035

G.I. Shapiro. (2011). Effect of tidal stream power generation on the region-wide circulation in a shallow area. *Ocean Science, 7*, 165-174.

Gómez-Gesteira, M., deCastro, M., Prego, R., & Pérez-Villar, V. (2001). An unusual two layered tidal circulation induced by stratification and wind in the ría of pontevedra (NW spain). *Estuarine, Coastal and Shelf Science, 52*(5), 555-563.

Güney, M. S., & Kaygusuz, K. (2010). Hydrokinetic energy conversion systems: A technology status review. *Renewable and Sustainable Energy Reviews, 14*(9), 2996-3004. doi:https://doi.org/10.1016/j.rser.2010.06.016

Hammar, L., Ehnberg, J., Mavume, A., Cuamba, B. C., & Molander, S. (2012). Renewable ocean energy in the western indian ocean. *Renewable and Sustainable Energy Reviews, 16*(7), 4938-4950. doi:http://dx.doi.org/10.1016/j.rser.2012.04.026

Herath, N., & Tyner, W. E. (2019). *Intended and unintended consequences of US renewable energy policies* doi:https://doi.org/10.1016/j.rser.2019.109385

Herrera, J. L., Rosón, G., Varela, R. A., & Piedracoba, S. (2008). Variability of the western galician upwelling system (NW spain) during an intensively sampled annual cycle. an EOF analysis approach. *Journal of Marine Systems, 72*(1-4), 200-217.

Hooper, T., & Austen, M. (2013). Tidal barrages in the UK: Ecological and social impacts, potential mitigation, and tools to support barrage planning. *Renewable and Sustainable Energy Reviews, 23*, 289-298. doi:https://doi.org/10.1016/j.rser.2013.03.001

Hu, K., Ding, P., Wang, Z., & Yang, S. (2009). A 2D/3D hydrodynamic and sediment transport model for the yangtze estuary, china. *Journal of Marine Systems, 77*(1–2), 114-136. doi:http://dx.doi.org/10.1016/j.jmarsys.2008.11.014

Iglesias, G., & Carballo, R. (2009a). Seasonality of the circulation in the ría de muros (NW spain). *Journal of Marine Systems, 78*(1), 94-108. doi:10.1016/j.jmarsys.2009.04.002

Iglesias, G., & Carballo, R. (2009b). Wave energy potential along the death coast (spain). *Energy, 34*(11), 1963-1975. doi:http://dx.doi.org/10.1016/j.energy.2009.08.004

Iglesias, G., & Carballo, R. (2010a). Effects of high winds on the circulation of the using a mixed open boundary condition: The ría de muros, spain. *Environmental Modelling & Software, 25*(4), 455-466. doi:10.1016/j.envsoft.2009.10.013

Iglesias, G., & Carballo, R. (2010b). Wave energy resource in the estaca de bares area (spain). *Renewable Energy, 35*(7), 1574-1584. doi:10.1016/j.renene.2009.10.019

Iglesias, G., & Carballo, R. (2011a). Can the seasonality of a small river affect a large tide-dominated estuary? the case of the ria de viveiro, spain. *Journal of Coastal Research, 27*(6), 1170-1182.

Iglesias, G., & Carballo, R. (2011b). Choosing the site for the first wave farm in a region: A case study in the galician southwest (spain). *Energy, 36*(9), 5525-5531. doi:http://dx.doi.org/10.1016/j.energy.2011.07.022

Iglesias, G., & Carballo, R. (2011c). Wave resource in el hierro—an island towards energy self-sufficiency. *Renewable Energy, 36*(2), 689-698. doi:10.1016/j.renene.2010.08.021

Iglesias, G., Carballo, R., & Castro, A. (2008). Development of the WaveCat wave energy converter. Paper presented at the *31st Int. Conf. on Coastal Eng. (ICCE),* Hamburg. 3970-3982.

Iglesias, G., López, M., Carballo, R., Castro, A., Fraguela, J. A., & Frigaard, P. (2009). Wave energy potential in galicia (NW spain). *Renewable Energy, 34*(11), 2323-2333. doi:10.1016/j.renene.2009.03.030

Iglesias, G., Sánchez, M., Carballo, R., & Fernández, H. (2012). The TSE index – A new tool for selecting tidal stream sites in depth-limited regions. *Renewable Energy, 48*(0), 350-357. doi:10.1016/j.renene.2012.05.012

Khan, M. J., Bhuyan, G., Iqbal, M. T., & Quaicoe, J. E. (2009). *Hydrokinetic energy conversion systems and assessment of horizontal and vertical axis turbines for river and tidal applications: A technology status review* doi:https://doi.org/10.1016/j.apenergy.2009.02.017

Lim, Y. S., & Koh, S. L. (2010). Analytical assessments on the potential of harnessing tidal currents for electricity generation in malaysia. *Renewable Energy, 35*(5), 1024-1032. doi:10.1016/j.renene.2009.10.016

Liu, Z., Qu, H., & Shi, H. (2019). *Numerical study on hydrodynamic performance of a fully passive flow-driven pitching hydrofoil* doi:https://doi.org/10.1016/j.oceaneng.2019.01.055

López, I., Andreu, J., Ceballos, S., Martínez de Alegría, I., & Kortabarria, I. (2013). Review of wave energy technologies and the necessary power-equipment. *Renewable and Sustainable Energy Reviews, 27*(0), 413-434. doi:http://dx.doi.org/10.1016/j.rser.2013.07.009

Lynch, D., Davies, A., Gerritsen, H., & Mooers, C. (1995). Chapter 21. quantitative skill assessment for coastal ocean models. In Daniel R. Lynch,Alan M. Davies (Ed.), *Geomorphology and sedimentology of estuaries* (pp. 501-111) American Geophysical Union. doi:https://doi.org/10.1016/S0070-4571(05)80024-X

McClain, C. R., Chao, S. -., Atkinson, L. P., Blanton, J. O., & de Castillejo, F. F. (1986). Wind-driven upwelling in the vicinity of cape finisterre, spain. *Journal of Geophysical Research, 91*, 8470-8486.

McCombes, T., Johnstone, C., & Grant, A. (2011). Unsteady wake modelling for tidal current turbines. *IET Renewable Power Generation, 5*(4), 299-310.

Mendez, G., & Rey, D. (2000). An historical review of the geological studies of the galician rias. *Journal of Iberian Geology, 26*, 21-44.

Myers, L. E., & Bahaj, A. S. (2010). Experimental analysis of the flow field around horizontal axis tidal turbines by use of scale mesh disk rotor simulators. *Ocean Engineering, 37*(2-3), 218-227. doi:10.1016/j.oceaneng.2009.11.004

Neill, S. P., Jordan, J. R., & Couch, S. J. (2012). Impact of tidal energy converter (TEC) arrays on the dynamics of headland sand banks. *Renewable Energy, 37*(1), 387-397. doi:10.1016/j.renene.2011.07.003

Neill, S. P., Litt, E. J., Couch, S. J., & Davies, A. G. (2009). The impact of tidal stream turbines on large-scale sediment dynamics. *Renewable Energy, 34*(12), 2803-2812. doi:10.1016/j.renene.2009.06.015

Nicolli, F., & Vona, F. (2019). *Energy market liberalization and renewable energy policies in OECD countries* doi:https://doi.org/10.1016/j.enpol.2019.01.018

O Rourke, F., Boyle, F., & Reynolds, A. (2010). Tidal energy update 2009. *Applied Energy, 87*(2), 398-409. doi:https://doi.org/10.1016/j.apenergy.2009.08.014

Oceanflowenergy.Www.oceanflowenergy.com.

Ospina-Alvarez, N., Prego, R., Álvarez, I., deCastro, M., Álvarez-Ossorio, M. T., Pazos, Y., . . . Varela, M. (2010). *Oceanographical patterns during a summer upwelling–downwelling event in the northern galician rias: Comparison with the whole ria system (NW of iberian peninsula)* doi:https://doi.org/10.1016/j.csr.2010.04.018

Perillo, G. M. E. (1995). Chapter 2 definitions and geomorphologic classifications of estuaries. *Developments in Sedimentology, 53*, 17-47. doi:https://doi.org/10.1016/S0070-4571(05)80022-6

Philips, N. A. (1957). A co-ordinate system having some special advantages for numerical forecasting. *Journal of Meteorology, 14*, 184-185.

Pischke, E. C., Solomon, B., Wellstead, A., Acevedo, A., Eastmond, A., De Oliveira, F., . . . Lucon, O. (2019). *From kyoto to paris: Measuring renewable energy policy regimes in argentina, brazil, canada, mexico and the united states* doi:https://doi.org/10.1016/j.erss.2018.11.010

Prego, R., Barciela, M. d. C., & Varela, M. (1999). *Nutrient dynamics in the galician coastal area (northwestern iberian peninsula): Do the rias bajas receive more nutrient salts than the rias altas?* doi:https://doi.org/10.1016/S0278-4343(98)00099-5

Pugh, D. T. (1996). *Tides, surges, and mean sea-level/a handbook for engineers and scientists* John Wiley & Sons Inc.

Qian, P., Feng, B., Liu, H., Tian, X., Si, Y., & Zhang, D. (2019). *Review on configuration and control methods of tidal current turbines* doi:https://doi.org/10.1016/j.rser.2019.03.051

Ramos, V., Carballo, R., Álvarez, M., Sánchez, M., & Iglesias, G. (2014). A port towards energy self-sufficiency using tidal stream power. *Energy, 71*, 432-444.

Ramos, V., Carballo, R., Álvarez, M., Sánchez, M., & Iglesias, G. (2013). Assessment of the impacts of tidal stream energy through high-resolution numerical modeling. *Energy, 61*(0), 541-554. doi:http://dx.doi.org/10.1016/j.energy.2013.08.051

Ramos, V., Carballo, R., Sanchez, M., Veigas, M., & Iglesias, G. (2014). *Tidal stream energy impacts on estuarine circulation* doi:https://doi.org/10.1016/j.enconman.2014.01.027

Ramos, V., & Iglesias, G. (2013a). Performance assessment of tidal stream turbines: A parametric approach. *Energy Conversion and Management, 69*(0), 49-57. doi:10.1016/j.enconman.2013.01.008

Ramos, V., & Iglesias, G. (2013b). Wind power viability on a small island. *International Journal of Green Energy,* doi:10.1080/15435075.2013.823434

Rodi, W. (1987). Examples of calculation methods for flow and mixing in stratified fluids. *Journal of Geophysical Research, 92*(C5), 5305-5328.

Rourke, F. O., Boyle, F., & Reynolds, A. (2010). Marine current energy devices: Current status and possible future applications in ireland. *Renewable and Sustainable Energy Reviews, 14*(3), 1026-1036. doi:10.1016/j.rser.2009.11.012

Salas-de-León, D. A., Carbajal-Pérez, N., Monreal-Gómez, M. A., & Barrientos-MacGretor, G. (2003). Residual circulation and tidal stress in the gulf of california. *Journal of Geophysical Research, 108*(C10), 3317.

Sanchez, M., Carballo, R., Ramos, V., & Iglesias, G. (2014). *Floating vs. bottom-fixed turbines for tidal stream energy: A comparative impact assessment* doi:https://doi.org/10.1016/j.energy.2014.05.096

Sánchez, M., Carballo, R., Ramos, V., & Iglesias, G. (2014a). *Energy production from tidal currents in an estuary: A comparative study of floating and bottom-fixed turbines* doi:https://doi.org/10.1016/j.energy.2014.09.053

Sánchez, M., Carballo, R., Ramos, V., & Iglesias, G. (2014b). Tidal stream energy impact on the transient and residual flow in an estuary: A 3D analysis. *Applied Energy, 116*(0), 167-177. doi:http://dx.doi.org/10.1016/j.apenergy.2013.11.052

Sánchez, M., Iglesias, G., Carballo, R., & Fraguela, J. A. (2013). Power peaks against installed capacity in tidal stream energy. *IET Renewable Power Generation, 7*(6), 246-253.

Segura, E., Morales, R., Somolinos, J. A., & López, A. (2017). *Techno-economic challenges of tidal energy conversion systems: Current status and trends* doi:https://doi.org/10.1016/j.rser.2017.04.054

Skogseth, R., Sandvik, A. D., & Asplin, L. (2007). Wind and tidal forcing on the meso-scale circulation in storfjorden, svalbard. *Continental Shelf Research, 27*(2), 208-227. doi:https://doi.org/10.1016/j.csr.2006.10.001

Smith, S. D. (1980). Wind stress and heat flux over the ocean in gale force winds. *Journal of Physical Oceanography, 10*(5 , May 1980), 709-726.

Souto, C., Gilcoto, M., Fariña-Busto, L., & Pérez, F. F. (2003). Modeling the residual circulation of a coastal embayment affected by wind-driven upwelling: Circulation of the ría de vigo (NW spain). *Journal of Geophysical Research, 108*(C11), 4-1-4-18.

Stelling, G., & Leendertse, J. (1992). Approximation of convective processes by cyclic ADI methods. Paper presented at the *Proceedings 2nd ASCE Conference on Estuarine and Coastal Modelling,* Tampa.

Torres López, S., Varela, R. A., & Delhez, E. (2001). Residual circulation and thermohaline distribution of the ría de vigo: A 3-D hydrodynamic model. *Scientia Marina, 65*(1), 277-289.

Torres, R., Barton, E. D., Miller, P., & Fanjul, E. (2003). Spatial patterns of wind and sea surface temperature in the galician upwelling region. *Journal of Geophysical Research: Oceans, 108* doi:10.1029/2002JC001361

Umgiesser, G. (1997). Modelling the venice lagoon. *International Journal of Salt Lake Research, 6*, 177-199.

Veigas, M., Carballo, R., & Iglesias, G. (2014). Wave and offshore wind energy on an island. *Energy for Sustainable Development, 22*, 57-65.

Villacieros-Robineau, N., Herrera, J. L., Castro, C. G., Piedracoba, S., & Roson, G. (2013). *Hydrodynamic characterization of the bottom boundary layer in a coastal upwelling system (ría de vigo, NW spain)* doi:https://doi.org/10.1016/j.csr.2013.08.017

Wooster, W. S., Bakun, A., & McLain, D. R. (1976). Seasonal upwelling cycle along the eastern boundary of the north atlantic. *Journal of Marine Research, 34*(2), 131-141.

USC DE SANTIAGO DE COMPOSTELA

Work, P. A., Haas, K. A., Defne, Z., & Gay, T. (2013). Tidal stream energy site assessment via three-dimensional model and measurements. *Applied Energy, 102*(0), 510-519. doi:10.1016/j.apenergy.2012.08.040

World Commission on Environment and Development (WCED). (1987). Our common future.

Xia, J., Falconer, R. A., & Lin, B. (2010). Impact of different operating modes for a severn barrage on the tidal power and flood inundation in the severn estuary, UK. *Applied Energy, 87*(7), 2374-2391. doi:10.1016/j.apenergy.2009.11.024

Yavuz, T., Koç, E., & Kaynak, B. (2013). Hydrodynamics performance of hydrofoil-slat arrangements in 3D analysis. *Energy Conversion and Management, 75*, 44-50. doi:https://doi.org/10.1016/j.enconman.2013.05.041

Yelland, M. J., Moat, B. I., Taylor, P. K., Pascal, R. W., Hutchings, J., & Cornell, V. C. (1998). Wind stress measurements from the open ocean corrected for airflow distortion by the ship. *Journal of Physical Oceanography, 28*(7), 1511-1526.

Zarzuelo, C., López-Ruiz, A., Díez-Minguito, M., & Ortega-Sánchez, M. (2017). *Tidal and subtidal hydrodynamics and energetics in a constricted estuary* doi:https://doi.org/10.1016/j.ecss.2016.11.020

Zhou, Z., Benbouzid, M., Charpentier, J., Scuiller, F., & Tang, T. (2017). *Developments in large marine current turbine technologies – A review* doi:https://doi.org/10.1016/j.rser.2016.12.113

USC UNIVERSIDADE DE SANTIAGO DE COMPOSTELA

FIGURE INDEX

Figure 3.1. Situation of Ria de Ortigueira in the Iberian Peninsula (left-hand side plots) and detailed view of the ria (right-hand side plot) 45
Figure 3.2. Area occupied by the proposed tidal stream plants (left-hand side plot) and their layout (right-hand side plot). 48
Figure 3.3. Three-dimensional representation of the bathymetry of Ria de Ortigueira. ... 50
Figure 3.4. Comparison between computed (–) and measured (□) water levels in the ADCP location during the validation period 52
Figure 3.5. Comparison between computed (–) and measured (□) current speed for the surface, mid-depth and bottom layers in the ADCP location during the validation period 52
Figure 3.6. Power curve of the Evopod turbine [v, flow velocity; P_O, electrical power output] 53
Figure 3.7. Monthly electrical energy output [E_e] of floating and bottom-fixed tidal plants. 55
Figure 3.8. Monthly availability factor [A_f] of floating and bottom-fixed tidal plants..... 55
Figure 3.9. Monthly capacity factor [C_f] of floating and bottom-fixed tidal plants. 56
Figure 3.10. Comparison between flow velocities throughout two spring-neap cycles during March and June. 56
Figure 4.1. Location of Ria the Ortigueira (left-hand site). Detailed map of Ria the Ortigueira showing singular points and measuring stations (right-hand site). 61
Figure 4.2. Computational grid of the model area [For a clearer understanding, the representation herein shown is derefined 4 times both x- and y- directions]. 65
Figure 4.3. Location of the considered tidal stream plants (left-hand site). Layout in plan view of the plants (right-hand site). 65
Figure 4.4. Comparison between computed (continuous line) and measured (dots) water level time series at measuring stations S1 and S2 during the validation period. 67
Figure 4.5. Comparison between modelled (continuous line) and measured (dots) current velocity time series for the surface, mid-depth and bottom layers at measuring station S1 during the validation period 68
Figure 4.6. Differences between altered and reference flow velocities (colour map), and vectors showing the altered flow in the middle ria at mid-flood tide 70
Figure 4.7. Differences between altered and reference flow velocities (colour map), and vectors showing the altered flow in the middle ria at mid-ebb tide 71
Figure 4.8. Magnitude of the current velocity on the control section at mid-flood situation of a mean spring tide 72
Figure 4.9. Magnitude of the current velocity on the control section at mid-ebb situation of a mean spring tide 73
Figure 5.1. The Ria de Ortigueira (b) and its location in Galicia (NW Spain) (a). 77
Figure 5.2. Numerical model grid. 81
Figure 5.3. Location of the considered tidal stream plants (a). Layout in plan view of the plants (b). 83
Figure 5.4. Residual flow pattern in Ria de Ortigueira under case study CS1 conditions. (a) Surface layer; (b) Bottom layer. 85

Figure 5.5. Residual flow pattern in Ria de Ortigueira under case study CS2 conditions. (a) Surface layer; (b) Bottom layer. 86
Figure 5.6. Residual flow pattern in Ria de Ortigueira under case study CS5 conditions. (a) Surface layer; (b) Bottom layer. 87
Figure 5.7. Residual flow pattern in Ria de Ortigueira under case study CS5 conditions. (a) Surface layer; (b) Bottom layer. 88
Figure 5.8. Residual flow pattern in Ria de Ortigueira under case study CS5 conditions (vectors); differences in the residual flow magnitude between altered flow and reference situation (CS5-CS2) (colour map). (a) Surface layer; (b) Bottom layer. 89
Figure 5.9. Residual flow pattern in Ria de Ortigueira under case study CS6 conditions (vectors); differences in the residual flow magnitude between altered flow and reference situation (CS6-CS2) (colour map). (a) Surface layer; (b) Bottom layer. 90
Figure 5.10. Residual flow pattern in Ria de Ortigueira under case study CS7 conditions (vectors); differences in the residual flow magnitude between altered flow and reference situation (CS7-CS4) (colour map). (a) Surface layer; (b) Bottom layer. 91
Figure 5.11. Residual flow pattern in Ria de Ortigueira under case study CS8 conditions (vectors); differences in the residual flow magnitude between altered flow and reference situation (CS8-CS4) (colour map). (a) Surface layer; (b) Bottom layer. 92

TABLE INDEX

Table 3.1. Main technical specifications of the Evopod turbine [D, rotor diameter; Vci, cut-invelocity; V_r, rated velocity; V_{co}, cut-off velocity; P_r , rated power; A, swept area; C_{pNO}, power coefficient in normal operation; C_{pSC}, power coefficient in stall control] 49
Table 3.2. Main tidal constituents in the Ria de Ortigueira 49
Table 3.3. Value of Manning's coefficient function of water depth 51
Table 3.4. Correlation coefficient between computed and measured time series of sea level (R_ζ) and flow velocity magnitude and direction (R_M and R_D respectively) 51
Table 3.5. Annual parametric analyse of the different lines of the array 54
Table 4.1. Main tidal constituents in the Ria de Ortigueira 62
Table 4.2. Main technical specifications of the Evopod turbine [D, rotor diameter; V_{ci}, cut-invelocity; V_r, rated velocity; V_{co}, cut-off velocity; P_r , rated power; A, swept area; C_{pNO}, power coefficient in normal operation; C_{pSC}, power coefficient in stall control] 62
Table 4.3. Statistical coefficients for comparing measured and computed time series at stations S1 and S2. 67
Table 4.4. Comparison between observed and computed main tidal harmonics. 69
Table 5.1. Main tidal constituents in the Ria de Ortigueira 78
Table 5.2. Values of boundary conditions for spring-summer and autumn-winter scenarios. 79
Table 5.3. Summary of boundary conditions and the situations simulated in the different case studies analyzed 84

USC
UNIVERSIDADE DE SANTIAGO DE COMPOSTELA

APPENDIX I. ARTICLES INCLUDES IN THIS DOCTORAL THESIS

This thesis reproduces completely the following articles, which are include in the pages that follow:

1. Energy production from tidal currents in an estuary: A comparative study of floating and bottom-fixed turbines.

Journal: Energy, Volume 77 (1) December 2014, Pages 802-811

Doi: https://doi.org/10.1016/j.energy.2014.09.053

Impact factor (2014): 2014: 4.844

Position (2014): 12/89 in Energy & Fuels category (Q1) and 2/55 in Thermodynamics (Q1)

Authors: Marcos Sanchez (MS), Rodrigo Carballo (RC), Victor Ramos (VR), Gregorio Iglesias (GI)

Author Contributions: Conceptualization, M.S., R.C. and G.I.; methodology, M.S., V.R., R.C. and G.I.; software, M.S., and R.C.; validation, M.S., V.R. and R.C.; formal analysis, M.S. and R.C.; investigation, M.S. and R.C.; resources, M.S., V.R. and R.C.; data curation, M.S., V.R. and R.C.; writing—original draft preparation, M.S.; writing—review and editing, R.C. and G.I.; supervision, R.C. and G.I.

2. Floating vs. bottom-fixed turbines for tidal stream energy: A comparative impact assessment.

Journal: Energy, Volume 72 (1) August 2014, Pages 691-701

Doi: https://doi.org/10.1016/j.energy.2014.05.096

Impact factor (2014): 2014: 4.844

Position (2014): 12/89 in Energy & Fuels category (Q1) and 2/55 in Thermodynamics (Q1)

Authors: Marcos Sanchez (MS), Rodrigo Carballo (RC), Victor Ramos (VR), Gregorio Iglesias (GI)

Author Contributions: Conceptualization, M.S., R.C. and G.I.; methodology, M.S., V.R., R.C. and G.I.; software, M.S., and R.C.; validation, M.S., V.R. and R.C.; formal analysis, M.S. and R.C.; investigation, M.S. and R.C.; resources, M.S., V.R. and R.C.; data curation, M.S., V.R. and R.C.; writing—original draft preparation, M.S.; writing—review and editing, R.C. and G.I.; supervision, R.C. and G.I.

USC UNIVERSIDADE DE SANTIAGO DE COMPOSTELA

USC
UNIVERSIDADE
DE SANTIAGO
DE COMPOSTELA

1. ENERGY PRODUCTION FROM TIDAL CURRENTS IN AN ESTUARY: A COMPARATIVE STUDY OF FLOATING AND BOTTOM-FIXED TURBINES.

Energy 77 (2014) 802–811

Contents lists available at ScienceDirect

Energy

journal homepage: www.elsevier.com/locate/energy

Energy production from tidal currents in an estuary: A comparative study of floating and bottom-fixed turbines

M. Sánchez [a, *], R. Carballo [a], V. Ramos [a], G. Iglesias [b]

[a] University of Santiago de Compostela, Hydraulic Engineering, Campus Univ. s/n, 27002 Lugo, Spain
[b] University of Plymouth, School of Marine Science and Engineering, Marine Building, Drakes Circus, Plymouth PL4 8AA, United Kingdom

ARTICLE INFO

Article history:
Received 12 June 2014
Received in revised form
18 September 2014
Accepted 20 September 2014
Available online 12 October 2014

Keywords:
Tidal stream energy
Tidal turbine
Ria de Ortigueira
Estuary
Numerical modelling

ABSTRACT

In a tidal stream project the selection of the most appropriate device is of major importance. The aim of this work is to investigate the difference between two tidal farms, one with floating TSTs (Tidal Stream Turbines), the other with bottom-fixed TSTs, in terms of annual performance and its monthly variability. This investigation is carried out considering real operational conditions in a case study: Ria de Ortigueira (NW Spain), a drowned river valleys which is one of the most promising sites for tidal stream energy exploitation in the Iberian Peninsula. A 3D, high-resolution, numerical model is applied to simulate the hydrodynamics of the ria during an entire year with either the floating or bottom-fixed TSTs, and, on these grounds, determine the most representative performance parameters. Significant differences emerge in the performance of both plants; these are due to a great extent to the vertical variation in the flow velocity, which is relevant at many sites of interest for tidal stream energy exploitation such as Ria de Ortigueira. Finally, relevant variations were identified in the intra-annual performance which must be borne in mind in dimensioning the plant.

© 2014 Elsevier Ltd. All rights reserved.

1. Introduction

In the late 90's social pressure emerged claiming for a new, sustainable energy production and utilisation model [1]. This, together with a number of policies aimed at curbing greenhouse gas emissions and the realisation that the current energy model, with fossil fuels at its core, is necessarily limited in time, has resulted in companies and governments around the world being currently working intensively on the development and efficient utilisation of new and renewable energy sources [2].

Tidal stream energy is one of the most attractive and promising renewable energy sources owing to its advantages relative to other renewables: no land occupation, a high load factor (water density is ~800 times higher than air density), flow predictability and consequently power production predictability, inexistence of extreme flows (which might otherwise damage the conversion devices), etc. are some of the advantages of tidal stream energy exploitation [3–6]. However, due to the relatively recent interest in this type of energy (in comparison with other renewables such as wind or solar energy), only a few TECs (Tidal Energy Converters) have achieved at this point a commercial or pre-commercial stage [7,8]. The conversion principle varies between the different TECs developed or in a development stage. Generally speaking, there exist two types of TECs, based on either the reciprocating or rotating principle. The latter, also known as TSTs (Tidal Stream Turbines), is the most popular. TSTs can be: (i) floating beneath the surface and anchored to the bottom by means of chains or cables (floating TSTs), or (ii) rigidly attached to the bottom by means of a structure (bottom-fixed TSTs) [9,10]. As a result of their different configuration, despite them being installed at the same coastal site, their performance may differ due to the varying hydrodynamic conditions throughout the water column (each type of TST is located at a different position within the water column). However, the implications for the power performance of opting for either floating or bottom-fixed devices have not been investigated as far as the authors are aware.

The aim of this study is to examine the differences in the power performance in real conditions of operation of two tidal stream plants, composed by either floating or bottom-fixed TSTs, proposed in a previous work [11], where their impacts on the estuarine hydrodynamics were analysed. For this purpose, a 3D high-resolution numerical model is implemented in the Ria de Ortigueira, a drowned river valleys which is a promising site for tidal stream energy exploitation located in Galicia (NW Spain) (Fig. 1). On the basis of the numerical results a detailed intra-annual power performance assessment of floating and bottom-fixed tidal plants have

* Corresponding author. Tel.: +34 982823650; fax: +34 982285926.
E-mail address: marcos.sanchez@usc.es (M. Sánchez).

http://dx.doi.org/10.1016/j.energy.2014.09.053
0360-5442/© 2014 Elsevier Ltd. All rights reserved.

USC UNIVERSIDADE DE SANTIAGO DE COMPOSTELA

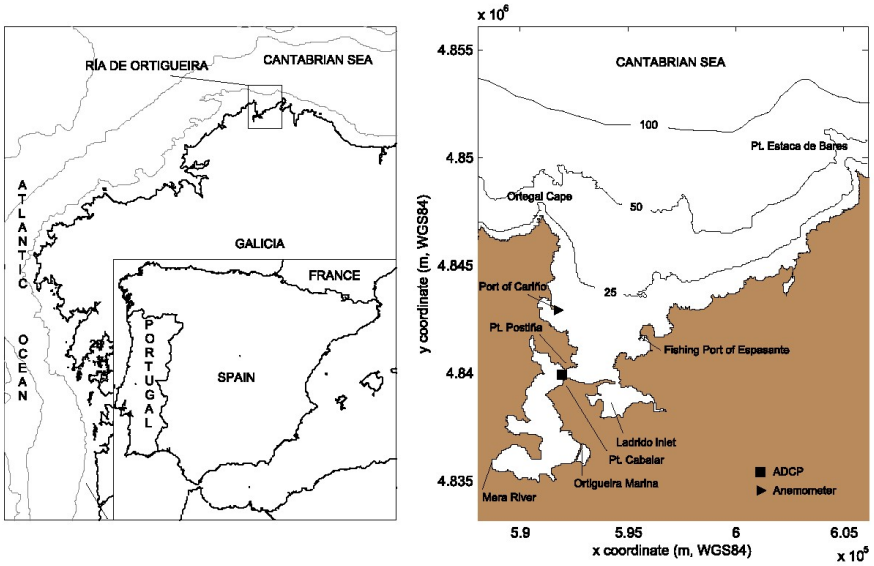


Fig. 1. Situation of Ria de Ortigueira in the Iberian Peninsula (left-hand side plots) and detailed view of the ria (right-hand side plot).

been conducted so as to investigate the importance of selecting the type of TST that performs best considering the specific hydrodynamic conditions of the area of interest.

2. Methodology

2.1. Three-dimensional hydrodynamics model

The 3D hydrodynamics model Delft3D-FLOW was used to compute the flow conditions in Ria de Ortigueira in the presence of a tidal stream farm. This model has been widely used to investigate coastal hydrodynamics in semi-enclosed water bodies [5,12–19]. Given that the Galician Rias usually present a stratified flow pattern (e.g. [20–22], to properly analyse the ria's hydrodynamics, and as a result to conduct reliable energy computations, in this work a 3D model was implemented.

Delft3D-FLOW is a finite-difference code that solves the three-dimensional Navier–Stokes equations for incompressible free surface flow coupled to the transport equation [23]. In this manner baroclinic effects, which can be of great importance in the case of rias or estuaries [24], can be taken into account. The model equations are as follows:

$$\frac{\partial u}{\partial x}+\frac{\partial v}{\partial y}+\frac{\partial w}{\partial z}=Q, \tag{1}$$

$$\left.\begin{aligned}\frac{Du}{Dt}&=fv-g\frac{\partial \zeta}{\partial x}-\frac{g}{\rho_0}\int_{z'-z}^{z'-\zeta}\frac{\partial \rho}{\partial x}dz'+\upsilon_h\left(\frac{\partial^2 u}{\partial x^2}+\frac{\partial^2 u}{\partial y^2}\right)+\upsilon_v\left(\frac{\partial^2 u}{\partial z^2}\right)\\ \frac{Dv}{Dt}&=-fu-g\frac{\partial \zeta}{\partial y}-\frac{g}{\rho_0}\int_{z'-z}^{z'-\zeta}\frac{\partial \rho}{\partial y}dz'+\upsilon_h\left(\frac{\partial^2 v}{\partial x^2}+\frac{\partial^2 v}{\partial y^2}\right)+\upsilon_v\left(\frac{\partial^2 v}{\partial z^2}\right)\end{aligned}\right\}, \tag{2}$$

$$\frac{\partial p}{\partial z}=-\rho g, \tag{3}$$

$$\frac{Dc}{Dt}=D_h\left(\frac{\partial^2 c}{\partial x^2}+\frac{\partial^2 c}{\partial y^2}\right)+D_v\frac{\partial^2 c}{\partial z^2}-\lambda_d c+R_s. \tag{4}$$

Equation (1) represents the conservation of mass under the assumption of incompressibility; Equation (2) represents the conservation of momentum in the x- and y-directions; Equation (3) expresses the conservation of momentum in the vertical direction which under the shallow-water assumption simplifies to the hydrostatic pressure distribution; finally, Equation (4) is the transport equation, which is solved in the present study for both salinity and temperature. In these equations, x, y and z represent the east, north and vertical directions, respectively and u, v and w the velocity components in the aforementioned directions; ζ is the free surface elevation above the datum; Q represents the intensity of mass sources per unit area; f is the Coriolis parameter; g is the gravitational acceleration, υ_h and υ_v are the horizontal and vertical eddy viscosity coefficients respectively, and ρ and ρ_0 are the density and the reference density of sea water, respectively. Finally, in the transport equation, c stands for salinity or temperature; D_h and D_v are the horizontal and vertical eddy diffusivity coefficients, respectively; λ_d represents the first order decay process; and R_s is the source term.

2.2. TSTs modelling

The flow conditions within a ria change as a result of the operation of the TSTs and the energy that they extract from the flow. If the flow at the locations of the TSTs and, consequently, their yield are to be accurately determined, it is therefore necessary to take them into account in the model. The operation of a turbine can be simulated by considering its effect on the flow, i.e., by adding a retarding force with the same magnitude as that exerted by the

USC UNIVERSIDADE DE SANTIAGO DE COMPOSTELA

flow on the turbine but opposite direction. The common procedure for modelling this force is as a momentum sink [18,21,25–27]. On this basis, in this study the retarding force was introduced into the model by adding the following sink terms to the right-hand side of the momentum equations (Equation (2)) in the x- and y-directions:

$$\left.\begin{aligned} M_x &= -\frac{1}{2}\frac{C_T A}{V}Uu \\ M_y &= -\frac{1}{2}\frac{C_T A}{V}Uv \end{aligned}\right\}, \tag{5}$$

where M_x and M_y represent the momentum of the external forces per unit volume, V_c, in the x- and y-directions, respectively; U is the component of the effective flow velocity perpendicular to the turbine; A_t is the cross-sectional area of the turbine rotor; and C_T is the thrust coefficient (an aerodynamic coefficient given by the lift and drag coefficients) which is related to the power coefficient, C_p [28].The floating and bottom-fixed TSTs are modelled by introducing the retarding force in the vertical layers of the model corresponding to the water depth at which they operate.

2.3. Performance analysis

The analysis of the performance of a tidal stream farm can be based on three characteristic parameters describing the operation of the individual TSTs in the farm [29]: electrical energy output, capacity factor and availability factor. The electrical energy output of the i-th TST of a tidal farm over the period from $t = 0$ to $t = t_1$ is given by

$$E_e^i = \int_0^{t_1} P_e(t)\,\mathrm{d}t, \tag{6}$$

where $P_e(t)$ is the electrical power output of the TST, which can be expressed as [30]

$$P_e(t) = \frac{1}{2}C_p(v)\rho A_t[U(t)]^3, \tag{7}$$

where $C_p(v)$ is the power coefficient, defined as the ratio between the power available from the flow and the electrical power output. Its value varies with the flow velocity in a manner that is specific of each TST.

Table 1
Main technical specifications of the Evopod turbine [D, rotor diameter; V_{ci}, cut-in velocity; V_n rated velocity; V_{co}, cut-off velocity; P_n rated power; A, swept area; C_{pNO}, power coefficient in normal operation; C_{pSC}, power coefficient in stall control].

D (m)	5
V_{ci} (ms^1)	0.7
V_r (ms^1)	2.2
V_{co} (ms^1)	3.1
A (m^2)	19.6
Pr (kW)	40
C_{pNO}	0.35
C_{pSC}	0.2

Therefore, the electrical energy output of the entire tidal farm is

$$E_e = \sum_{i-1}^{n} E_e^i, \tag{8}$$

where n is the number of TSTs of the farm.

The availability factor (A_f) is the ratio between the time during which the TST is actually generating power (T_g) – TSTs have a minimum (*cut-in*) and a maximum (*cut-off*) flow velocity, below and above which they do not generate electricity – and the total duration of the period considered (T_a):

$$A_f = \frac{T_g}{T_a}. \tag{9}$$

The capacity factor (C_f) represents the ratio between the electrical energy output over a period of interest (E_e) and the electrical energy output the TST would have produced over the same period had it operated at rated power ($P_r T_a$):

$$C_f = \frac{E_e}{T_a P_r}. \tag{10}$$

The information contained in the capacity factor can be expressed in terms of an annual cycle by means of the equivalent full-load hours:

$$FLH = \frac{E_e^a}{P_r}, \tag{11}$$

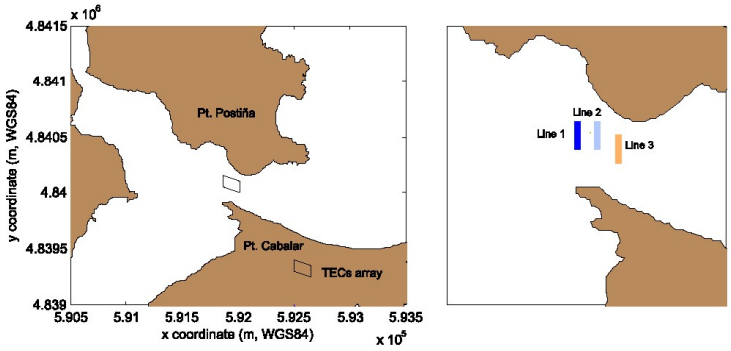


Fig. 2. Area occupied by the proposed tidal stream plants (left-hand side plot) and their layout (right-hand side plot).

USC UNIVERSIDADE DE SANTIAGO DE COMPOSTELA

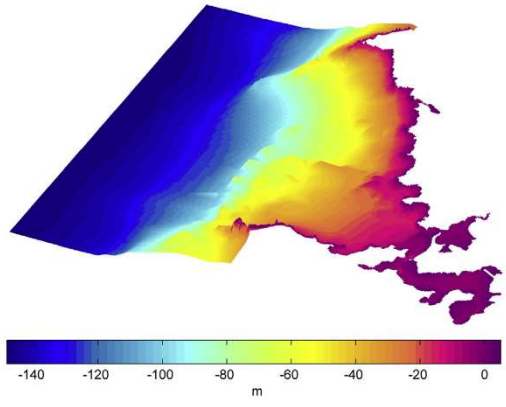


Fig. 3. Three-dimensional representation of the bathymetry of Ria de Ortigueira.

where E_e^a is the annual electric energy output. The equivalent full-load hours represent the number of hours a turbine would have to operate at its rated power to produce the same amount of energy that it actually produced over a year.

To determine these parameters it is necessary, first, to define the location and characteristics of the tidal stream farm and, second, to implement a numerical model of the hydrodynamics in the area that taking into account the energy extracted by the farm. The implementation of the numerical model enables to obtain the perturbed flow velocities, which in turn are necessary for the computation of the aforementioned parameters.

3. Application to Ria de Ortigueira

3.1. Study site and proposed tidal plants

The rugged coastline of NW Spain is characterised by the rias, a specific type of primary estuary developed in high relief coasts drowned by the rise of sea level during Holocene [31–33], regarded as promising sites for tidal stream energy exploitation. These rias can be roughly divided into Rias Altas, or Higher Rias, Rias Centrales or Central Rias, and Rias Baixas or Lower Rías [14,34]. Owing to its complex geomorphology characteristics and its high tidal range, the Ria de Ortigueira (Fig. 1), one of the Rias Altas, is amongst the most promising sites for tidal stream energy exploitation in the Iberian Pensinsula [15,35].

Ria de Ortigueira is delimited by Cape Ortegal and Pt. Estaca de Bares (Fig. 1). With an approximate area of 85 km and a length along its main axis of approx. 18 km, it is, by far, the largest of the Rias Altas. The tidal flow is strongest at two constrictions in its inner part where the highest current velocities occur. One of them is located to the East, between the main lobe of the ria and the Ladrido Inlet, and the other is located to the West, in the channel between Pt. Postiña and Pt. Cabalar. By applying the TSE (Tidal Stream Exploitability) index to this ria [15] the optimum site for the installation of a tidal stream farm was selected as follows. According to the TSE index values obtained, the former (eastern) constriction has a TSE of 0 owing to its insufficient water depth, and therefore it is considered inappropriate for tidal stream energy exploitation. By contrast, the TSE index value of the latter (western) constriction exceeds 5 – the largest value over the entire ria. Therefore, this area combines a substantial resource with an appropriate depth, implying that it is an appropriate site for an array of TSTs in Ria de Ortigueira (Fig. 2).

Two tidal stream farms were considered in this study, both composed of 30 turbines distributed in three lines roughly perpendicular to the main flow direction. The TST selected for the plants was an Evopod turbine [36] in view of its appropriateness for shallow waters areas (Table 1). The surface occupied in plan view by each farm is about 1500 m^2, corresponding to a sweep area of approx. 600 m^2. Both arrays proposed are located at the same site and present the same layout (Fig. 2) but differ in their vertical configuration. The first plant (P1) is composed of floating TSTs [36] occupying roughly the upper 65 per cent of the water column; the second plant (P2) is composed by TSTs with exactly the same mechanical characteristics, but fixed to the bottom, occupying approximately the lower 65 per cent of the water column.

Table 2
Main tidal constituents in the Ria de Ortigueira.

Constituent	Amplitude (cm)	Phase (°)
M2	122.79	90.15
S2	42.91	121.08
N2	25.98	70.39
K2	12.03	118.76
K1	7.35	73.49
O1	6.22	324.62
P1	2.22	65.15
Q1	2.11	271.31
M4	1.45	334.80

Table 3
Value of Manning's coefficient function of water depth.

H	n
$-2.5 \le H < -2.0$	0.042
$-2.0 \le H < -1.5$	0.038
$-1.5 \le H < 1.0$	0.034
$-1.0 \le H < -0.5$	0.030
$-0.5 \le H < 0.0$	0.027
$0.0 \le H < 0.5$	0.024
$0.5 \le H < 1.0$	0.022
$1.0 < H < 3.0$	0.020
$3 \le H < 10$	0.018
$10 < H$	0.015

3.2. Model implementation

The numerical model previously described in Sections 2.1 and 2.2 was implemented in Ria de Ortigueira. For this purpose a Cartesian, varying-size numerical grid, with a total of 57361 cells was created covering the whole ria and extending up to the 150 m isobath. The grid size was finer (50 × 50 m) in the inner and middle ria than in the outer ria and on the shelf, where it decreased in the y-direction up to values of 50 × 150 m at the northern outer boundary. As regards the vertical grid discretisation, a σ-coordinate

Table 4
Correlation coefficient between computed and measured time series of sea level (R_ζ) and flow velocity magnitude and direction (R_M and R_D respectively).

Water level		Current velocity			
			Surface layer	Middle layer	Bottom layer
R_ζ	0.9895	R_M	0.8965	0.8619	0.8439
		R_D	0.8509	0.8375	0.8215

USC UNIVERSIDADE DE SANTIAGO DE COMPOSTELA

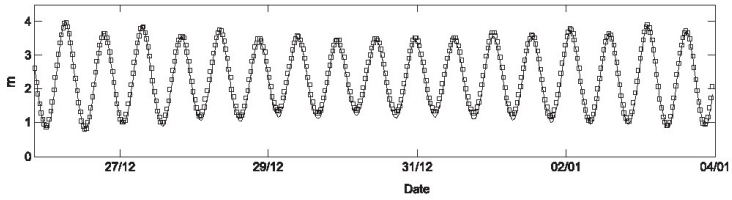


Fig. 4. Comparison between computed (–) and measured (□) water levels in the ADCP location during the validation period.

system [37] with twelve layers was used. The layer thickness (% of water column) from surface to bottom was, as a percentage of the water column: 2, 3, 5, 10, 15, 15, 15, 15, 10, 5, 3 and 2. The resolution of the grid is higher near the seabed and surface in order to better resolve boundary layers flow. To close the turbulence the k-ε model [38] was adopted. Finally, the bathymetry (Fig. 3) was obtained from nautical charts 408 and 4083 from the Hydrographic Institute of the Spanish Navy (*Instituto Hidrografico de la Marina*) and interpolated onto the computational grid.

With regard to the boundary conditions, Dirichlet conditions were imposed along the open boundary by prescribing the sea surface level based on the main tidal harmonics (Table 2) together with daily thermohaline conditions. At the land margins the forcings were null flow through the boundary and zero shear stress (free slip). On the other hand, the shear stress at the seabed, τ_{b3D}, induced by a turbulent flow is related to the current velocity above the bed:

$$\vec{\tau}_{b3D} = \frac{\rho_0 g \vec{u}_b |\vec{u}_b|}{C_{3D}^2}, \tag{12}$$

where $\vec{u}_b$ is the magnitude of the horizontal velocity in the lowest layer (immediately above the bed) and C_{3D} is the 3D Chézy coefficient, given by

$$C_{3D} = C_{2D} + \frac{\sqrt{g}}{\kappa} \ln\left(\frac{\Delta z_b}{2H}\right), \tag{13}$$

with κ the von Karman constant ($\kappa = 0.41$), Δz_b the vertical distance from the seabed to the nearest computational grid point, H the total water depth and C_{2D} the 2D Chézy coefficient, which can be determined based on Manning's coefficient, n, as follows:

$$C_{2D} = \frac{\sqrt[6]{H}}{n}. \tag{14}$$

Manning's coefficient is assumed to be depth-dependent according to previous studies [13,39–41]; the value considered for each water depth range is shown in Table 3.

Finally, at the free surface the wind shear-stress, τ_s, is defined as

$$\vec{\tau}_s = \rho_a C_d U_{10}^2 \tag{15}$$

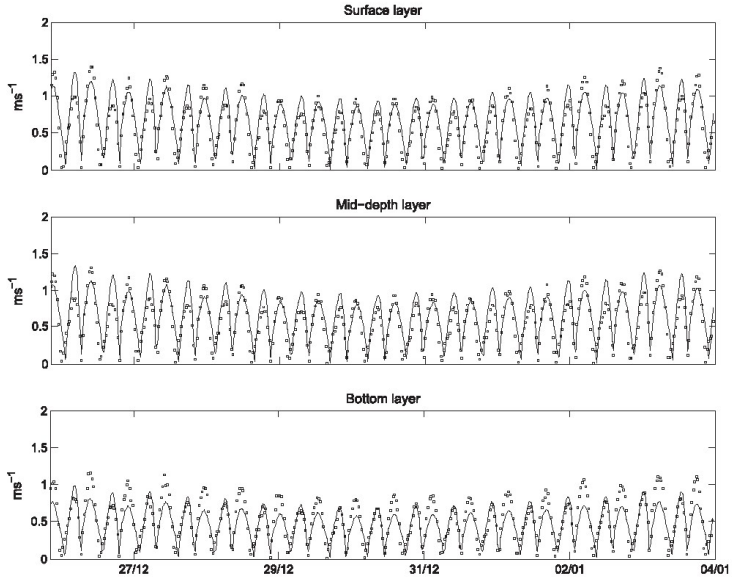


Fig. 5. Comparison between computed (–) and measured (□) current speed for the surface, mid-depth and bottom layers in the ADCP location during the validation period.

USC UNIVERSIDADE DE SANTIAGO DE COMPOSTELA

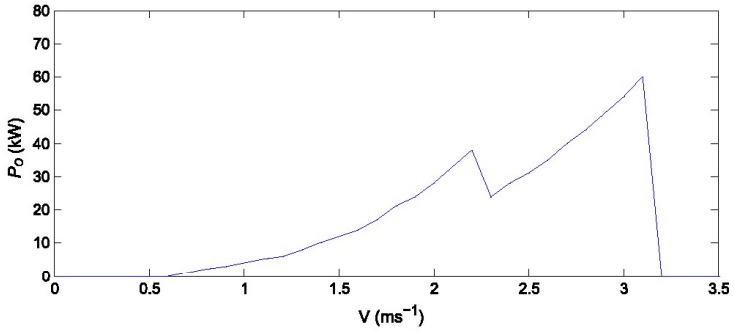


Fig. 6. Power curve of the Evopod turbine [*V*, flow velocity; P_O, electrical power output].

where ρ_a is the density of the air, U_{10} the wind speed at 10 m above the sea surface and C_d the wind drag coefficient, calculated following [42] and [43].

The tidal stream plant was implemented in the model by using the momentum sink approach as described in Section 2.2. In the case of P1 and P2, the retarding force affects the 7 upper or lower layers of the model, respectively. In both cases the value of C_T considered is 0.8, which corresponds to a value of the power coefficient, C_p, of 0.35 [28].

3.3. Model validation

The numerical model was validated by comparing the numerical results with field data of water level and current velocity. For this purpose, an ADCP (Acoustic Doppler Current Profiler) Sontek Argonaut XR and two CTD (Conductivity Temperature a Depth) sensors Seabird Microcat 37 were deployed in Ria de Ortigueira (Fig. 1) over a 19-day period. During the validation period, the numerical model was forced with the main tidal harmonics (Table 2) and daily conditions of salinity and temperature at the open boundaries, wind data every thirty minutes, and daily fluvial discharge data.

The correlation coefficients between measured and computed time series of water level and current velocity direction and magnitude were computed (Table 4). It can be observed that the resulting correlation coefficients are close to the unit for both variables. The excellent agreement between measured and computed water level can be observed in Fig. 4 over 9-day time series representation. In the same way the excellent agreement between time series of numerical and measured velocities can be observed in Fig. 5 at three points of the water column: surface, mid-depth and bottom.

Table 5
Annual parametric analyse of the different lines of the array.

		Floating TSTs (P1)	Bottom-fixed TSTs (P2)
E_e (MWh)	Line 1	1.161×10^3	0.684×10^3
	Line 2	0.673×10^3	0.426×10^3
	Line 3	0.591×10^3	0.389×10^3
	Array	2.425×10^3	1.498×10^3
A_f	Line 1	0.63	0.53
	Line 2	0.53	0.41
	Line 3	0.50	0.39
	Array	0.63	0.53
C_f	Line 1	0.33	0.19
	Line 2	0.19	0.12
	Line 3	0.17	0.11
	Array	0.23	0.14
FLH	Line 1	2902	1710
	Line 2	1682	1065
	Line 3	1479	971
	Array	2021	1249

4. Power performance analysis

Two long-term numerical simulations covering an entire year (Case 1 and Case 2, each of them considering a different tidal farm) were performed. In Case 1, the array introduced in the model is composed of floating TSTs (Plant P1), and in Case 2, of bottom-fixed TSTs (Plant P2). Next, on the basis of the numerical simulations and the characteristics of the turbine selected (Table 1 & Fig. 6), the power performance throughout the entire year of the two tidal farms proposed was computed according to the parameters previously defined (Section 2.3).

The forcing factors considered were the main tidal harmonics (Table 2), monthly averaged salinity and temperature conditions along the open boundary and monthly averaged river discharge. The velocity considered for electrical power generation is the velocity at rotor height, as in the case of wind generators, which varies depending on the case study (1 or 2) as a result of the different water depth at which the rotor is located.

The differences in the power performance of the two plants analysed are significant (Table 5). The annual energy production of P1 is 2.425×10^3 MWh, whereas the production of P2 is around 40% less. These differences are even larger in the case of the first row of TSTs (hereafter referred to as Line 1), whose energy production is almost double in the case of floating TSTs (P1) relative to bottom-fixed units (P2). These results prove that in a coastal area with significant differences in the flow speed throughout the water column, such as the study area, significant differences can arise between the power performance of plants composed of floating or bottom-fixed TSTs.

As a regard the operation time, the values of the availability factor (A_f) show that P1 and P2 operate during 63% and 48% of the time, respectively. This would have implications if an energy storage system was required – it would have to be substantially larger for P2 given its lower operation time. Regarding the capacity factor (C_f), the differences are even higher, roughly 64% (0.23 and 0.64 for P1 and P2, respectively), indicating an important advantage of P1, for a higher capacity factor is associated with a better production to capital investment ratio. These important differences are directly

USC UNIVERSIDADE DE SANTIAGO DE COMPOSTELA

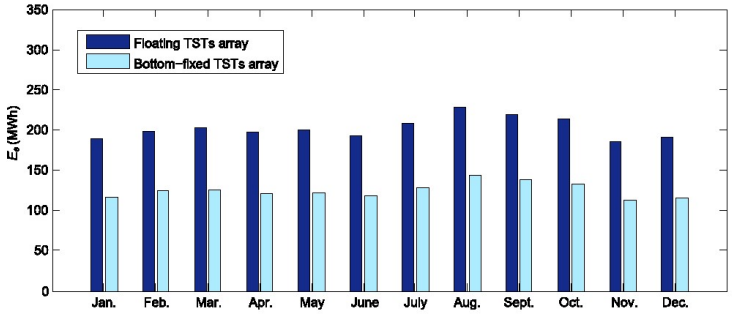


Fig. 7. Monthly electrical energy output [E_e] of floating and bottom-fixed tidal plants.

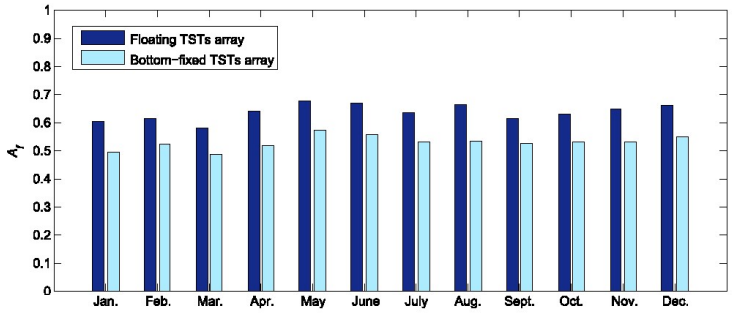


Fig. 8. Monthly availability factor [A_f] of floating and bottom-fixed tidal plants.

transferred to the equivalent *FLH* (full-load hours): P1 has over 2000 *FLH*, and P2 only about 1250 *FLH*. Although a detailed study of the installation costs would be necessary for an exhaustive analysis of the profitability of the proposed plant, the low *FLH* of P2 does not contribute to its economic viability.

On the basis of the numerical simulations and the characteristics of the turbine selected, the monthly power performance parameters defined in section 2.3 were determined for P1 and P2 (Figs. 7–9). The intra-annual power performance presents a significant variability, which should be analysed to ascertain the optimum tidal farm configuration. In the case of the energy production (Fig. 7), the month with highest E_e is August (227.74 MWh and 143.44 MWh for P1 and P2, respectively); on the other hand, November presents the lowest E_e (185.52 MWh for P1 and 112.76 for P2, about 20% lower than that of August).

An important aspect that should be noted is that, far from what might be expected, it is not in the months with the largest tides, and therefore the strongest velocity peaks, that the energy production is largest – or, more generally, that the farm performance is best. The explanation lies in that in the months with highest tides (March and September) there exist important differences between tidal cycles (with peak velocities ranging from 2.2 ms−1 to

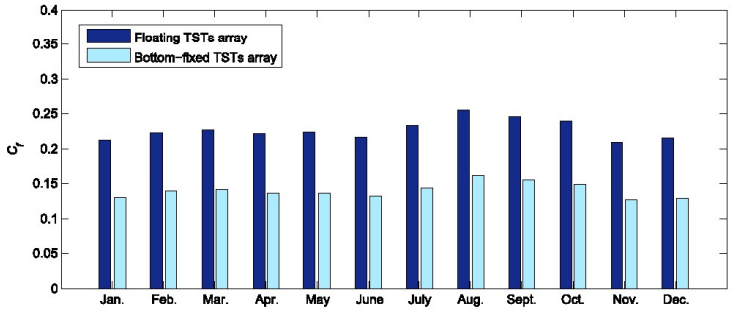


Fig. 9. Monthly capacity factor [C_f] of floating and bottom-fixed tidal plants.

USC UNIVERSIDADE DE SANTIAGO DE COMPOSTELA

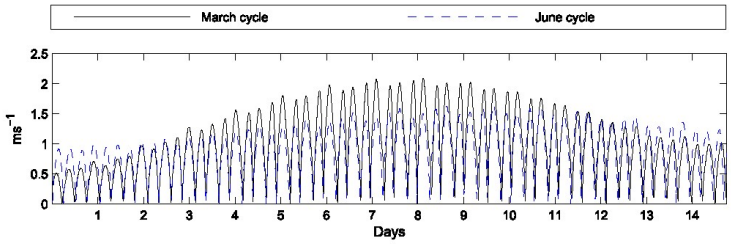


Fig. 10. Comparison between flow velocities throughout two spring-neap cycles during March and June.

0.5 ms−1) whereas in other months, e.g., July or August, the tidal cycles are more homogenous (with peak velocities ranging from 1.5 ms−1 to 1 ms−1). This can be clearly observed in Fig. 10, in which the flow velocity for P1 at the mid-depth layer is represented throughout a complete spring-neap cycle in March and July for P1 at mid-depth layer.

The significant differences in the annual power performance parameters between both plants is also reflected in important differences in the monthly power performance parameters (Figs. 7–9); the general trends of the performance of the two plants is, however, rather similar throughout the whole year. In the case of the power production, and in the case of capacity factor, the most important differences between both plants occur in December, when the production of P1 is 40% higher, whereas the smallest differences occur in July and August, about 37%.

Finally, as regards the availability factor (Fig. 8), the monthly differences between both plants are less important than in the case of electrical energy output (Fig. 7) and capacity factor (Fig. 9). For P1 and P2 they are in the ranges 0.5–0.6 and 0.4–0.5, respectively. The months with highest and lowest operation time are May and March, respectively. This also helps to explain the fact that the energy production during these months is similar, in spite of the fact that the peak velocities are higher in March.

5. Conclusions

In this work a comparison of the intra-annual performance of floating and bottom-fixed TSTs was performed through a case study in Ria de Ortigueira, and its implications for tidal stream energy exploitation were addressed for the first time. For this purpose, a 3D numerical model was implemented and applied to simulate the hydrodynamics of this estuary during a complete year, taken into account the energy extracted from the flow by the tidal farms. Two options were considered for the latter, consisting of floating or bottom-fixed TSTs, referred to as plants P1 and P2, respectively. The tidal plants were modelled by introducing a momentum sink term in the vertical layers of the model corresponding to the area occupied by the rotors of the turbines. The computed velocity series were then used to conduct a thorough power performance analysis based on three performance parameters allowing the characterisation of the operation of the plants: electric energy output, availability factor and capacity factor.

Remarkable differences in the power performance of both plants were found. Plant P1 presents higher values of the performance parameters considered; in particular, the annual electrical energy output is almost twice that of P2, and its capacity factors around 64% higher, showing that floating devices offer a better production to capital investment ratio. Regarding the availability factor, the differences are less important (15%); however, the power output of P1 is smoother, and this is an advantage that should not be disregarded – not least if an energy storage system is to be installed. In addition, it emerged from the intra-annual analysis that the aforementioned parameters also present a significant monthly variability. Their intra-annual general trend is similar for both plants, i.e., the annual differences are roughly maintained throughout the whole year. A finding of special interest is that, contrary to what might be expected, the months with largest peak flow velocities are not those with the highest values of the power performance parameters, including energy output.

In sum, the power performance of floating and bottom fixed TSTs at the same location can differ greatly depending on the characteristics of the hydrodynamic conditions of the coastal area in which they operate. This can be exacerbated in the case of coastal bodies with significant differences in the current velocities throughout the water column, as is the case of the study area (Ria de Ortigueira). As a result of the higher velocities near the surface, floating TSTs provide a much better performance than bottom-fixed devices. Finally, a significant intra-annual variability in the power performance was observed, which leads to the conclusion that the energy output and performance of a tidal stream farm must be analysed based on simulations covering a complete year, rather than by extrapolating the results obtained for one spring-neap cycle, as it is done following the common procedure.

Beyond the interest of these results for the coastal area herein studied, the procedure presented in this work could be used to analyse the annual power performance of different tidal stream plants elsewhere. Furthermore, in addition to the performance, which is of undoubtedly importance in the decision-making regarding the installation of a tidal stream plant, other factors such as the impact on the hydrodynamics or the long term coastal morphology should be considered before selecting the optimum farm configuration. These aspects will be dealt with as a continuation of this line of research.

Acknowledgements

This work was supported in part by project DPI2009-14546-C02-02 ("Assessment of Renewable Energy Resources") of Spain's Ministry of Science, and in part by the project "Marine Energies" (USC 2012-PP011). During this work M. Sanchez and V. Ramos have been supported by the I2C grants PRE/2011/236 (Plan Galego de Investigación Innovación e Crecemento 2011–2015) of Xunta de Galicia.

Nomenclature

Roman

A_t	cross-sectional area of turbine rotor [m^2]
A_f	availability factor

USC UNIVERSIDADE DE SANTIAGO DE COMPOSTELA

c	salinity or temperature (transported substance)
C_T	thrust coefficient
C_f	capacity factor
C_p	power coefficient
C_{pNO}	power coefficient in normal operation (Evopod turbine)
C_{pSC}	power coefficient in stall control (Evopod turbine)
C_{2D}	2D-Chézy coefficient
C_{3D}	3D-Chézy coefficient
C_d	wind drag coefficient
d	local water depth [m]
D	rotor diameter (Evopod turbine)
D_h	horizontal eddy diffusivity [m^2 s^{-1}]
D_v	vertical eddy diffusivity [m^2 s^{-1}]
E_e	electrical energy output [W h]
E_e^a	annual electrical energy output [W h]
f	Coriolis parameter
FLH	equivalent full load hours
F_x	x component of the flow retarding force per unit volume [N]
F_y	y component of the flow retarding force per unit volume [N]
g	gravitational acceleration [m s^{-2}]
H	total water depth [m]
M_x	x component of the momentum generated by an external force [N m]
M_y	y component of the momentum generated by an external force [N m]
n	Manning coefficient
P_e	electrical power output [W]
P_r	rated electrical power output [W]
Q	intensity of mass sources per unit area [m^2 s^{-1}]
R_s	source term per unit area
R_ζ	correlation coefficient between computed and measured time series of sea level
R_M	correlation coefficient between computed and measured time series of flow velocity magnitude
R_D	correlation coefficient between computed and measured time series of flow direction
T_a	reference period of time [h]
T_g	period of time with the tidal plant operating [h]
u	eastward component of the flow velocity [m s^{-1}]
U	component of the effective flow velocity perpendicular to the turbine [m s^{-1}]
$\overrightarrow{U_{10}}$	wind velocity at 10 m height above the sea surface [m s^{-1}]
$\overrightarrow{u_b}$	horizontal velocity in the bottom layer [m s^{-1}]
V_c	volume of control [m^3]
V_{ci}	cut-in velocity (Evopod turbine) [m s^{-1}]
V_{co}	cut-off velocity (Evopod turbine) [m s^{-1}]
V_r	rated velocity (Evopod turbine) [m s^{-1}]
v	northward component of the flow velocity [m s^{-1}]
w	vertical component of the flow velocity [m s^{-1}]
x	east direction
y	north direction
z	vertical direction

Greek

Δh	maximum tidal range [m]
Δz_b	vertical distance from the seabed to the computational grid [m]
κ	von Karman constant
ζ	water level [m]
λ_d	first-order decay process
ρ_0	water reference density [kg m^{-3}]
ρ	seawater density [kg m^{-3}]
ρ_a	air density [kg m^{-3}]
$\overrightarrow{\tau_s}$	wind stress on the sea surface [N m^{-2}]
$\overrightarrow{\tau_{b3D}}$	shear stress at the bottom [N m^{-2}]
υ_h	horizontal eddy viscosity [m^2 s^{-1}]
υ_v	vertical eddy viscosity [m^2 s^{-1}]

USC UNIVERSIDADE DE SANTIAGO DE COMPOSTELA

References

[1] World Commission on Environment and Development (WCED). Our common future. 1987.
[2] European Commission. Proposal for a directive amending Directive 98/70/EC relating to the quality of petrol and diesel fuels and amending Council Directive 93/12/EC and amending Directive 2009/28/EC on the promotion of the use of energy from renewable sources [COM(2012) 595]. 2012.
[3] Bahaj AS. Generating electricity from the oceans. Renew Sustain Energy Rev 2011;15(7):3399–416.
[4] Blunden LS, Bahaj AS. Initial evaluation of tidal stream energy resources at Portland Bill, UK. Renew Energy 2006;31(2):121–32.
[5] Carballo R, Iglesias G, Castro A. Numerical model evaluation of tidal stream energy resources in the Ría de Muros (NW Spain). Renew Energy 2009;34(6):1517–24.
[6] Charlier RH. A "sleeper" awakes: tidal current power. Renew Sustain Energy Rev 2003;7(6):515–29.
[7] Neill SP, Litt EJ, Couch SJ, Davies AG. The impact of tidal stream turbines on large-scale sediment dynamics. Renew Energy 2009;34(12):2803–12.
[8] Fallon D, Hartnett M, Olbert A, Nash S. The effects of array configuration on the hydro-environmental impacts of tidal turbines. Renew Energy 2014;64(0):10–25.
[9] Hammar L, Ehnberg J, Mavume A, Cuamba BC, Molander S. Renewable ocean energy in the Western Indian Ocean. Renew Sustain Energy Rev 2012;16(7):4938–50.
[10] Khan MJ, Bhuyan G, Iqbal MT, Quaicoe JE. Hydrokinetic energy conversion systems and assessment of horizontal and vertical axis turbines for river and tidal applications: a technology status review. Appl Energy 2009;86(10):1823–35.
[11] Sanchez M, Carballo R, Ramos V, Iglesias G. Floating vs. bottom-fixed turbines for tidal stream energy: a comparative impact assessment. Energy 2014;72(0):691–701.
[12] Carballo R, Iglesias G, Castro A. Residual circulation in the Ria de Muros (NW Spain): a 3D numerical model study. J Mar Syst 2009;75(1–2):130.
[13] Iglesias G, Carballo R. Effects of high winds on the circulation of the using a mixed open boundary condition: the Ría de Muros, Spain. Environ Model Softw 2010;25(4):455–66.
[14] Iglesias G, Carballo R. Can the seasonality of a small river affect a large tide-dominated estuary? the case of the Ria de Viveiro, Spain. J Coast Res 2011;27(6):1170–82.
[15] Iglesias G, Sánchez M, Carballo R, Fernández H. The TSE index – a new tool for selecting tidal stream sites in depth-limited regions. Renew Energy 2012;48(0):350–7.
[16] Bolle A, Bing Wang Z, Amos C, De Ronde J. The influence of changes in tidal asymmetry on residual sediment transport in the Western Scheldt. Cont Shelf Res 2010;30(8):871–82.
[17] Hu K, Ding P, Wang Z, Yang SA. 2D/3D hydrodynamic and sediment transport model for the Yangtze Estuary, China. J Mar Syst 2009;77(1–2):114–36.
[18] Ramos V, Carballo R, Álvarez M, Sánchez M, Iglesias G. Assessment of the impacts of tidal stream energy through high-resolution numerical modeling. Energy 1 November 2013;61:541–54.
[19] Ramos V, Carballo R, Álvarez M, Sánchez M, Iglesias G. A port towards energy self-sufficiency using tidal stream power. Energy 2014;71(0):432–44.
[20] Iglesias G, Carballo R. Seasonality of the circulation in the Ría de Muros (NW Spain). J Mar Syst 2009;78(1):94–108.
[21] Sánchez M, Carballo R, Ramos V, Iglesias G. Tidal stream energy impact on the transient and residual flow in an estuary: a 3D analysis. Appl Energy 2014;116(0):167–77.
[22] Ramos V, Carballo R, Sanchez M, Veigas M, Iglesias G. Tidal stream energy impacts on estuarine circulation. Energy Convers Manag 2014;80(0):137–49.
[23] User manual Delft3D-WAVE. Delft, The Netherlands: Deltares ed; 2010.
[24] Dyer KE. Estuaries: a physical introduction. New York: John Wiley; 1997.
[25] Defne Z, Haas KA, Fritz HM. Numerical modeling of tidal currents and the effects of power extraction on estuarine hydrodynamics along the Georgia coast, USA. Renew Energy 2011;36(12):3461–71.
[26] Ahmadian R, Falconer RA. Assessment of array shape of tidal stream turbines on hydro-environmental impacts and power output. Renew Energy 2012;44(0):318–27.
[27] Ahmadian R, Falconer R, Bockelmann-Evans B. Far-field modelling of the hydro-environmental impact of tidal stream turbines. Renew Energy 2012;38(1):107–16.
[28] Bahaj AS, Molland AF, Chaplin JR, Batten WMJ. Power and thrust measurements of marine current turbines under various hydrodynamic flow conditions in a cavitation tunnel and a towing tank. Renew Energy 2007;32(3):407–26.

[29] Ramos V, Iglesias G. Performance assessment of tidal stream turbines: a parametric approach. Energy Convers Manag 2013;69(0):49–57.
[30] Bahaj AS, Myers L. Analytical estimates of the energy yield potential from the Alderney Race (Channel Islands) using marine current energy converters. Renew Energy 2004;29(12):1931–45.
[31] Evans G, Prego R. Rias, estuaries and incised valleys: is a ria an estuary? Mar Geol 2003;196(3–4):171–5.
[32] Dyer KR. Estuaries: a physical introduction. London: John Wiley & Sons; 1973.
[33] Perillo GME. Chapter 2 Definitions and geomorphologic classifications of estuaries. Developments in sedimentology: Elsevier, 17–47.
[34] Mendez G, Rey D. An historical review of the geological studies of the Galician rias. J Iber Geol 2000;26:21–44.
[35] Sánchez M, Iglesias G, Carballo R, Fraguela JA. Power peaks against installed capacity in tidal stream energy. IET Renew Power Gener 2013;7(6):246–53.
[36] Oceanflowenergy. www.oceanflowenergy.com [accessed 10.07.14].
[37] Philips NA. A co-ordinate system having some special advantages for numerical forecasting. J Meteorol 1957;14:184–5.
[38] Rodi W. Examples of calculation methods for flow and mixing in stratified fluids. J Geophys Res 1987;92(C5):5305–28.
[39] Cheng RT, Casulli V, Gartner JW. Tidal, Residual, Intertidal Mudflat (TRIM) model and its applications to San Francisco Bay, California. Estuar Coast Shelf Sci 1993;36(3):235–80.
[40] Dias JM, Sousa MC, Bertin X, Fortunato AB, Oliveira A. Numerical modeling of the impact of the Ancão inlet relocation (Ria Formosa, Portugal). Environ Model Softw, In Press, Corrected proof.
[41] Dias JM, Lopes JF. Implementation and assessment of hydrodynamic, salt and heat transport models: the case of Ria de Aveiro Lagoon (Portugal). Environ Model Softw 2006;21(1):1–15.
[42] Smith SD. Wind stress and heat flux over the ocean in gale force winds. J Phys Oceanogr 5, May 1980;1980(10):709–26.
[43] Yelland MJ, Moat BI, Taylor PK, Pascal RW, Hutchings J, Cornell VC. Wind stress measurements from the open ocean corrected for airflow distortion by the ship. J Phys Oceanogr 1998;28(7):1511–26.

USC UNIVERSIDADE DE SANTIAGO DE COMPOSTELA

2. FLOATING VS. BOTTOM-FIXED TURBINES FOR TIDAL STREAM ENERGY: A COMPARATIVE IMPACT ASSESSMENT.

Energy 72 (2014) 691–701

Contents lists available at ScienceDirect

Energy

journal homepage: www.elsevier.com/locate/energy

Floating vs. bottom-fixed turbines for tidal stream energy: A comparative impact assessment

M. Sanchez [a, *], R. Carballo [a], V. Ramos [a], G. Iglesias [b]

[a] University of Santiago de Compostela, Hydraulic Engineering, Campus Univ. s/n, 27002 Lugo, Spain
[b] University of Plymouth, School of Marine Science and Engineering, Marine Building, Drakes Circus, Plymouth PL4 8AA, United Kingdom

ARTICLE INFO

Article history:
Received 20 March 2014
Received in revised form
16 May 2014
Accepted 24 May 2014
Available online 17 June 2014

Keywords:
Tidal currents
Energy exploitation
3D numerical model
Impacts
Floating TSTs
Bottom-fixed TSTs

ABSTRACT

Tidal currents represent a promising energy source for electrical supply in Europe; however, nowadays there still exist important aspects to address regarding their exploitation prior to becoming a fully-fledged renewable energy. The accurate assessment of the available resource and the development of TECs (Tidal Energy Converters) are challenges which have been partially solved, but it is necessary to go further in the investigation of other aspects such as the impacts on the estuarine circulation. In this work, the impacts caused on the estuarine circulation in Ria de Ortigueira by the operation of two different tidal stream plants, one composed of floating and the other of bottom-fixed TSTs (Tidal Stream Turbines), were analysed by means of a three-dimensional model. Prior to using the model for assessing the impacts, it was validated based on field data at two measuring stations. Then, the tidal farms were implemented in the model as a momentum sink. The results show that there are no significant differences between the impacts caused on the general circulation by floating and bottom-fixed TSTs with slight reductions of the flow being apparent up to some km away the plant. Then again, strong differences were found in the vicinity of the plant.

© 2014 Elsevier Ltd. All rights reserved.

1. Introduction

The interest of marine energy resources in Europe has been widely demonstrated over the last decades e.g. [1–7]. In particular, the exploitation of tidal energy was considered for the first time for energy supply in the 60's [8]. Since then, lots of studies have dealt with this issue and several projects have been developed [8,9]. Initially, the exploitation of tidal energy was based on the construction of tidal barrages but soon this system was abandoned due to its aggressiveness with the environment – large effects caused on the seabed, marine ecosystems, hydrodynamics, shipping, etc [10]. The efforts were then focused in the study of the exploitation of tidal currents. In this vein, two main lines of research dealing with the investigation of this new energy source can be distinguished: the assessment of the energy resource, e.g. Refs. [8,11–13], and the development of new technologies capable of converting the kinetic energy into electric energy [14,15]. Both tasks constitute one of the major scientific challenges over the last decades and much work in these fields has been required to get successful results. Nevertheless, as a result of the large effort made, several regions with important tidal stream energy potential have been identified around the world and some TECs (Tidal Energy Converters) have achieved a commercial or pre-commercial stage (although a lot TECs are still in development stage). Overall, these TECs can be classified, according to its principle of operation, into reciprocating [16] or rotating [17,18] devices. The latter, also known as TSTs (Tidal Stream Turbines), are the most popular and can be install with two different configurations: (i) floating beneath the surface and anchored to the bottom (floating TSTs), or (ii) rigidly attached to the bottom by means of a structure (bottom-fixed TSTs).

Despite both challenges being partially solved, there still exist important issues to be addressed and additional work is necessary. In this vein, it is important to note that tidal currents are almost negligible in the open ocean or along straight coasts, with the greatest tidal resource being usually located in estuaries, bays, and other coastal indentations [12,19,20] presenting complex hydrodynamics. Therefore, given the environmental importance that these coastal areas usually boast, the potential effects resulting from their exploitation should be carefully analysed before installing a tidal stream energy plant. With this aim, recent works have begun to study part of these potential effects [21–27].

In order to go further in the investigation of the impacts of tidal stream plants on the estuarine circulation, this work studies the effects resulting by the operation of two tidal stream plants in a

* Corresponding author. Tel.: +34 982823650; fax: +34 982285926.
E-mail address: marcos.sanchez@usc.es (M. Sanchez).

http://dx.doi.org/10.1016/j.energy.2014.05.096
0360-5442/© 2014 Elsevier Ltd. All rights reserved.

USC UNIVERSIDADE DE SANTIAGO DE COMPOSTELA

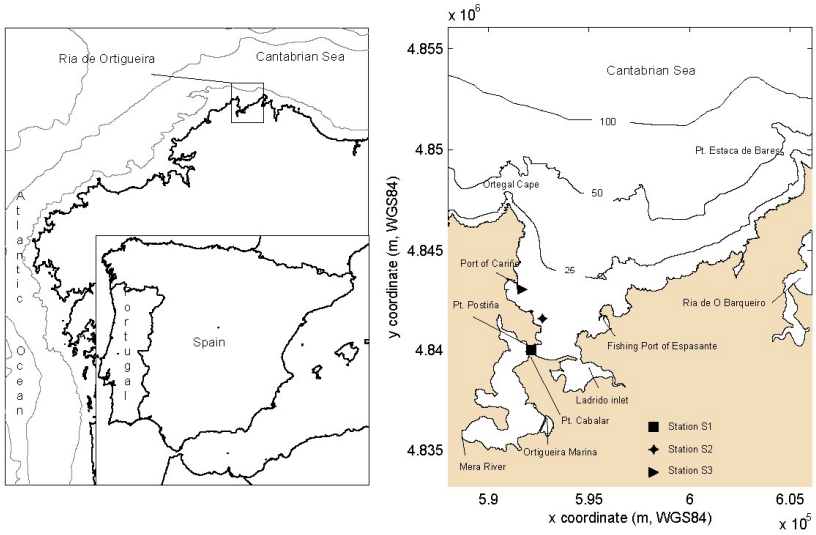


Fig. 1. Location of Ria the Ortigueira (left-hand site). Detailed map of Ria the Ortigueira showing singular points and measuring stations (right-hand site).

specific region, Ria de Ortigueria (NW Spain), by means of a three-dimensional high resolution numerical model. Both plants have the same plan view layout but present a different vertical configuration: one is composed of floating and the other of bottom-fixed TSTs. As a result of their different configuration, despite them being installed at the same coastal site, the impacts caused by their operation may widely differ due to the varying hydrodynamic conditions throughout the water column (each type of TST is located at a different position within the water column). Clearly, the differences in their impacts on the estuarine hydrodynamics may be a major issue in the selection of the most appropriated TST for a specific area. Far beyond the interest of the results obtained for the coastal region herein studied, the final aim of this investigation is to establish a methodology which can be used in the analysis of the potential impacts on the estuarine circulation in other rias or estuaries with similar hydrodynamic conditions.

The structure of this article is as follows. In Section 2, information about the area of study is provided. In Section 3, the numerical model implemented for the simulation of the operation conditions of the tidal plants considered is described. Next, Section 4 deals about the impacts caused on the estuarine circulation by the proposed plants. Finally, in Section 5 the most relevant conclusions are drawn, stating the interest of determining the impacts caused on the estuarine hydrodynamics by different TSTs for the selection of the most appropriated turbine.

2. Study area

The most characteristic feature of the Atlantic Region of the Iberian Peninsula is the presence of large drowned river valleys, a specific type of primary estuary [28], generally known as rias, developed in high relief coasts drowned by the rise of sea level during Holocene. Although the use of the term ria is more popular in this region, there exist estuaries with similar geomorphology conditions in other areas around the world such as Brittany in France, Devon and Cornwall in the British Isles, Korea, certain regions of the Chinese and the Argentina coasts. It is important to note that the morphology of the rias have not any Pleistocene glacial influence which makes them quite different from fjords [29].

The ria herein analysed, Ria the Ortigueira (Fig. 1), is characterised by its irregular geomorphology. Flanked to the West by Cape Ortegal and to the East by Pt. Estaca de Bares, the northernmost point of the Iberian Peninsula, Ria the Ortigueira has an intricate main lobe presenting several curves and narrowings, and a secondary lobe, the Ladrido Inlet. The area occupied by the water mass covers 85 km^2 with its main axis extending approx. 18 km. Furthermore, there exist several streams flowing into the ria, but only one of them presents a significant discharge, River Mera, with an average flow rate of 5.45 $m^3\ s^{-1}$. Regarding the tide, the main component of the astronomical tide is the M2 (Table 1), as in the rest of Europe. However, there are other semidiurnal relevant components in the area such as S2, N2 and K2 which results in a region with a semidiurnal tidal regime as it is stated by its *Form Factor* ($F = 0.082$) [30].

The narrowings of the main lobe together with the high tidal range (up to 4.5 m during spring tides) make tidal currents increase significantly; this causes Ria de Ortigueira being a promising region for tidal stream energy exploitation. According to previous works in this ria [6,31], tidal currents reach values up to 2.5 ms^{-1} in the narrow between Pt. Postiña and Pt. Cabalar. This strong current and

Table 1
Main tidal constituents in the Ria de Ortigueira

Constituent	Amplitude (cm)	Phase (°)
M2	122.79	90.15
S2	42.91	121.08
N2	25.98	70.39
K2	12.03	118.76
K1	7.35	73.49
O1	6.22	324.62
P1	2.22	65.15
Q1	2.11	271.31
M4	1.45	334.80

USC UNIVERSIDADE DE SANTIAGO DE COMPOSTELA

its adequate water depth make this area the most appropriated site for tidal stream energy exploitation in Ria de Ortigueira [31]. Consequently, the two tidal plants considered in this article are placed in this location. Furthermore, both plants have the same layout with an area of occupation in plan view of about 1500 m^2. The first plant (P1) is composed of floating TSTs occupying roughly the upper part of the water column and the second plant (P2) is composed of TSTs with exactly the same mechanical characteristics, but fixed to the bottom, occupying approximately the lower part of the water column.

The TST selected is an Evopod turbine [32] in view of its appropriateness for shallow waters areas (Table 2), as it is the case of Ria de Ortigueira. Following the distance recommendations between lines of TSTs, 30 turbines with a sweep area of approx. 600 m^2, were distributed over three lines roughly perpendicular to the main flow direction within this area.

3. Numerical model description

3.1. Governing equations

The 3D hydrodynamics model Delft3D-FLOW [33] was used to compute the flow conditions in Ria de Ortigueira with and without the presence of each of the studied tidal stream plans. This model was used in previous studies dealing with the investigation of coastal hydrodynamics in semi-enclosed water bodies [13,26,31,34–38].

The model is a finite-difference code solving the Navier–Stokes equations in their baroclinic form, i.e. coupled with the transport equation, which is solved for both salinity and temperature. Given that the Galician Rias usually present a stratified flow pattern (e.g. [25,39], and that the scopes of this work is the investigation of the impacts on the circulation caused by two tidal plants located at different positions in the water column, the model was implemented in its 3D form. The 3D model equations are:

$$\frac{\partial u}{\partial x}+\frac{\partial v}{\partial y}+\frac{\partial w}{\partial z}=Q, \tag{1}$$

$$\left.\begin{aligned}\frac{Du}{Dt}&=fv-g\frac{\partial \zeta}{\partial x}-\frac{g}{\rho_0}\int_{z'=z}^{z'=\varsigma}\frac{\partial \rho}{\partial x}dz'+\upsilon_h\left(\frac{\partial^2 u}{\partial x^2}+\frac{\partial^2 u}{\partial y^2}\right)+\upsilon_v\left(\frac{\partial^2 u}{\partial z^2}\right)\\ \frac{Dv}{Dt}&=-fu-g\frac{\partial \zeta}{\partial y}-\frac{g}{\rho_0}\int_{z'=z}^{z'=\varsigma}\frac{\partial \rho}{\partial y}dz'+\upsilon_h\left(\frac{\partial^2 v}{\partial x^2}+\frac{\partial^2 v}{\partial y^2}\right)+\upsilon_v\left(\frac{\partial^2 v}{\partial z^2}\right)\end{aligned}\right\}, \tag{2}$$

$$\frac{\partial p}{\partial z}=-\rho g, \tag{3}$$

$$\frac{Dc}{Dt}=D_h\left(\frac{\partial^2 c}{\partial x^2}+\frac{\partial^2 c}{\partial y^2}\right)+D_v\frac{\partial^2 c}{\partial z^2}-\lambda_d c+R_S. \tag{4}$$

Equation (1) represents the conservation of mass under the assumption of incompressibility; Equation (2) represents the conservation of momentum in the x- and y-directions; Equation (3) expresses the conservation of momentum in the vertical direction which under the shallow-water assumption simplifies to the hydrostatic pressure distribution; finally, Equation (4) is the transport equation, which is solved in the present study for both salinity and temperature. In these equations, x, y and z represent the east, north and vertical directions, respectively, and u, v and w the velocity components in the aforementioned directions; ζ is the free surface elevation above the datum; Q represents the intensity of mass sources per unit area; f is the Coriolis parameter; g is the gravitational acceleration, υ_h and υ_v are the horizontal and vertical eddy viscosity coefficients, respectively, and ρ and ρ_0 are the density and the reference density of sea water, respectively. Finally, in the transport equation, c stands for salinity or temperature; D_h and D_v are the horizontal and vertical eddy diffusivity coefficients, respectively; λ_d represents the first order decay process; and R_s is the source term.

Regard to the turbine's implementation in the model, it can be simulated by considering its effect on the flow, or in other words, by introducing a retarding force with the same magnitude as the force exerted by the flow on the turbine but in the opposite direction. This force was introduced in the model by adding a sink term to the right-hand side of the momentum equations (Equation (2)) in the x- and y-directions:

$$\left.\begin{aligned}M_x&=-\frac{1}{2}\frac{C_T A}{V}Uu\\ M_y&=-\frac{1}{2}\frac{C_T A}{V}Uv\end{aligned}\right\}, \tag{5}$$

where M_x and M_y represent the momentum of the external forces per unit volume, V, in the x- and y-directions, respectively; U is the component of the effective flow velocity perpendicular to the turbine; A is the area occupied by the turbine; and C_T is the thrust coefficient (an aerodynamic coefficient given by the lift and drag coefficients) which is related to the power coefficient, C_p [40].The floating and bottom-fixed TSTs are modelled by introducing this retarding force in the vertical layers of the model corresponding to the water depth at which they operate.

Table 2
Main technical specifications of the Evopod turbine [D, rotor diameter; V_{ci}, cut-in velocity; V_r, rated velocity; V_{co}, cut-off velocity; P_r, rated power; A, swept area; C_{pNO}, power coefficient in normal operation; C_{pSC}, power coefficient in stall control].

D (m)	V_{ci} (ms^{-1})	V_r (ms^{-1})	V_{co} (ms^{-1})	A (m^2)	Pr (kW)	C_{pNO}	C_{pSC}
5	0.7	2.2	3.1	19.6	40	0.35	0.2

3.2. Model set-up

3.2.1. Model area

The model covers Ria the Ortigueira and stretches approx. 10 km offshore (roughly 150 m isobath). Horizontally, a varying-size numerical grid was implemented, with a total of 57,361 cells. The grid size was set constant (50 × 50 m) in the inner and middle ria, progressively decreasing in the outer ria in the y-direction up to values of 50 × 150 m at the northern outer boundary (Fig. 2). Vertically, 12 σ-coordinate layers were used [41]. The layers follow the bottom topography and are distributed symmetrically with respect to the midpoint in the vertical, increasing their resolution towards the surface and the bottom in order to better resolve boundary layers flow [42]. The layer thickness (% of water column) was set to: 2, 3, 5, 10, 15, 15, 15, 15, 10, 5, 3 and 2.

The bathymetry within the model area (Fig. 3) was obtained from nautical charts 408 and 4083 from the Hydrographic Institute of the Spanish Navy (Instituto Hidrografico de la Marina) and interpolated onto the computational grid by means of Delft3D-QUICKIN, a Delft3D-FLOW tool. Given that these charts do not have enough resolution in the intertidal areas, detailed bathymetric and topographic information was obtained from cartographic maps provided by the Galician Regional Authority (Xunta de Galicia).

USC UNIVERSIDADE DE SANTIAGO DE COMPOSTELA

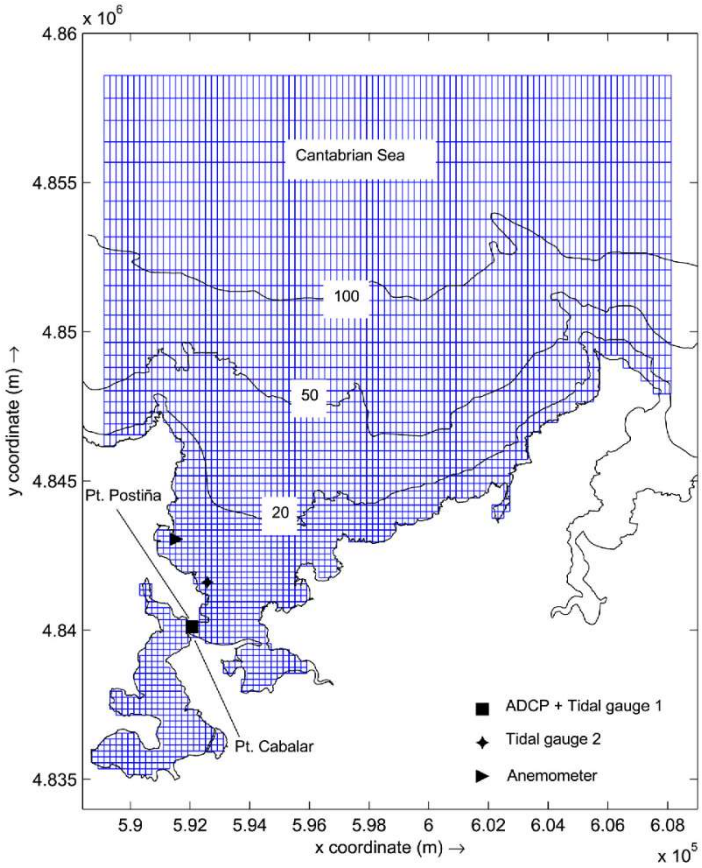


Fig. 2. Computational grid of the model area [For a clearer understanding, the representation herein shown is derefined 4 times both *x*- and *y*-directions].

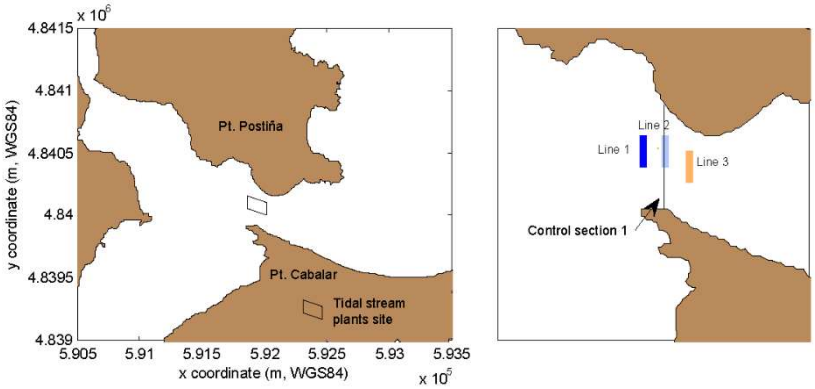


Fig. 3. Location of the considered tidal stream plants (left-hand site). Layout in plan view of the plants (right-hand site).

USC UNIVERSIDADE DE SANTIAGO DE COMPOSTELA

3.2.2. Boundary conditions

Dirichlet conditions were imposed along the open boundary by prescribing the sea surface level based on the main tidal harmonics (Table 1) together with daily thermohaline conditions. At the land margins the forcings were null flow through the boundary and zero shear stress; at the bottom, a stress, τ_{b3D}, induced by a turbulent flow which is related to the current velocity above the bed, was imposed:

$$\vec{\tau}_{b3D} = \frac{g\rho_0 |\vec{u}_b| \vec{u}_b}{C_{3D}^2}, \tag{6}$$

where $\vec{u}_b$ is the magnitude of the horizontal velocity in the lowest layer (immediately above the bed) and C_{3D} is the 3D Chézy coefficient, given by

$$C_{3D} = C_{2D} + \frac{\sqrt{g}}{\kappa} \ln\left(\frac{\Delta z_b}{2H}\right), \tag{7}$$

with κ the von Karman constant ($\kappa = 0.41$), Δz_b the vertical distance from the seabed to the nearest computational grid point, H the total water depth and C_{2D} the 2D Chézy coefficient, which can be determined based on Manning's coefficient, n, as:

$$C_{2D} = \frac{\sqrt[6]{H}}{n}. \tag{8}$$

Finally, at the free surface the wind shear-stress, $\vec{\tau}_s$, is defined as

$$\vec{\tau}_s = \rho_a C_d U_{10}^2 \tag{9}$$

where ρ_a is the density of the air, U_{10} the wind speed at 10 m above the sea surface and C_d the wind drag coefficient.

3.2.3. Numerical parameters

The model was run with a time step of 60 s. The horizontal eddy viscosity and eddy diffusivity were set to15 $m^2\ s^{-1}$, and the vertical eddy viscosity and eddy diffusivity to 1×10^{-5} $m^2\ s^{-1}$ and 1×10^{-7} $m^2\ s^{-1}$, respectively [43]. Manning's coefficient is assumed to be depth-dependent according to previous studies [35,44–46]. Finally, the drag coefficient for U_{10} up to 6 ms^{-1} is modelled following Smith [47]

$$C_d = 1.1 \times 10^{-3}, \tag{10}$$

and, for U_{10} above 6 ms^{-1}, following Yelland [48],

$$C_d = (0.50 + 0.071 U_{10}) \times 10^{-3}. \tag{11}$$

4. Results

4.1. Model validation

The model was validated on the basis of measurements at stations S1 and S2 (Fig. 1). At station S1, measures of water level and current speed were obtained since December 16th 2010 until January 4th 2011, whereas at station S2 only water level data was collected for the same period. So as to validate the numerical model, a simulation was run for the aforementioned period, using the previous 30 days as *spin-up* period. In this simulation the model was forced along the open boundaries with the main tidal constituents (Table 1) and salinity and temperature data. Moreover, wind stress acting on the sea surface and daily discharges of Mera River were also considered. In the case of wind data, wind velocity and direction were recorded at station S3 every 30 min while river discharges were provided by the Regional Authority of Water Resources (*Augas de Galicia*) close to the river's mouth.

The visual comparison of the observed and computed water levels (Fig. 4) and current velocity (Fig. 5) time series indicates a good agreement between both series. However, to consider only a visual comparison may be a little subjective. So as to provide a more exhaustive (and more objective) comparison, the correlation coefficient (R) and the mean difference (MD) were calculated with Equations (12) and (13), respectively.

$$R = \frac{\sum_{i=1}^{N}\left(x_i^o - \overline{x^o}\right)\left(x_i^m - \overline{x^m}\right)}{\sqrt{\sum_{i=1}^{N}\left(x_i^o - \overline{x^o}\right)^2 \sum_{i=1}^{N}\left(x_i^m - \overline{x^m}\right)^2}} \tag{12}$$

$$\mathrm{MD} = \frac{\sum_{i=1}^{N}|x_i^o - x_i^m|}{N} \tag{13}$$

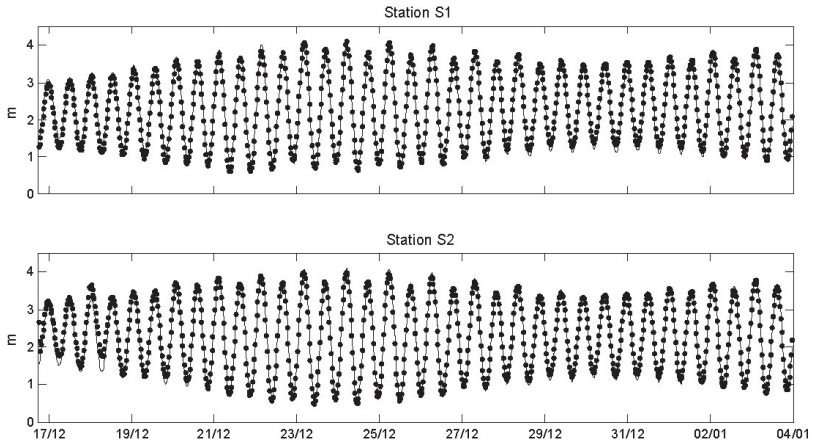


Fig. 4. Comparison between computed (continuous line) and measured (dots) water level time series at measuring stations S1 and S2 during the validation period.

USC UNIVERSIDADE DE SANTIAGO DE COMPOSTELA

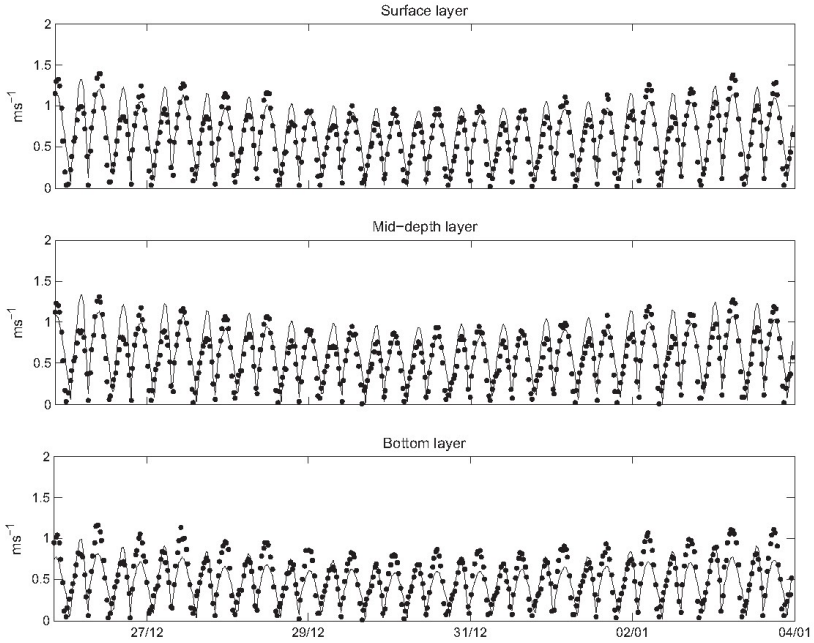


Fig. 5. Comparison between modelled (continuous line) and measured (dots) current velocity time series for the surface, mid-depth and bottom layers at measuring station S1 during the validation period.

where x_i represents the i-th value of either the water level or current velocity time series with N the total number of data points available, and the superscripts o and m the observed and modelled data, respectively. The values of these statistical parameters show the model's performance for reproducing the real hydrodynamic conditions on the estuary (Table 3).

Finally, a harmonic analysis of measured and modelled time series has been conducted and the results for the main tidal constituents compared. This analysis also show an excellent agreement between both time series (Table 4), especially for M2 and S2, which in turn are the most relevant tidal constituents in this location (Table 1).

4.2. Assessment of the impacts on the estuarine circulation

4.2.1. Energy extraction

In order to assess the impacts caused by the operation of both considered tidal stream plants, three simulations were performed. First of all, the reference conditions were calculated, i.e. the hydrodynamic conditions in the ria in the absence of TSTs. Then, two simulations were performed in order to determinate the conditions resulting from the operation of the plants (one simulation for each of the plants considered, P1 and P2). The model forcings were the same for the three simulations: main tidal constituents (Table 1), daily values of salinity and temperature at the open boundaries, and daily river discharge in the upper part of the ria.

Regarding the amount of energy extracted in the presence of the tidal plants, as it was described in Section 3.1, the tidal stream plants were implemented in the model by using the momentum sink approach. The retarding force affects the upper layers of the model in the case plant P1, and the lower layers in the case of plant P2. In both cases the value of C_T considered is 0.8, which corresponds to a value of the power coefficient, C_p, of 0.35 [40]. According with this coefficient, the remaining turbine specifications (Table 2) and the perturbed velocities resulting from the existence of the aforementioned retarding force, the annual energy production of P1 and P2 would be 2.425×10^3 MWh and 1.498×10^3 MWh, respectively. This large difference is caused by the important variations in the flow velocities throughout the water column.

Table 3
Statistical coefficients for comparing measured and computed time series at stations S1 and S2.

	Station S1				Station S2
	Water level	Current speed			Water level
		Surface layer	Middle layer	Bottom layer	
MD	0.11	0.18	0.20	0.21	0.10
MSE	1.96×10^{-2}	2.25×10^{-2}	2.26×10^{-2}	3.24×10^{-2}	1.69×10^{-2}

4.2.2. Impacts on the general circulation of the ria

The impact caused by the operation of each tidal plant was analysed in terms of the difference between altered and reference conditions, at mid-flood and mid-ebb of a mean spring tide. Regarding the impacts at mid-flood tide (Fig. 6), important differences can be found between the effects caused on the estuarine circulation by the tidal plants considered. When plant P1 is in operation (left-hand side plots in Fig. 6), the greatest effects on the surface layer are concentrated in the vicinity of the plant – with maximum alterations of about 3×10^{-1} ms $^{-1}$ can be observed within a few hundreds of metres up and downstream of the plant –

USC UNIVERSIDADE DE SANTIAGO DE COMPOSTELA

Table 4
Comparison between observed and computed main tidal harmonics.

	Constituent	Observed amplitude (cm)	Modelled amplitude (cm)	Amplitude difference (cm)	Observed phase (°)	Modelled phase (°)	Phase difference (°)
Station S1	M2	119.3	116.7	2.6	93.0	97.0	4
	S2	54.1	43.4	10.7	116.8	119.9	3.1
	N2	22.6	23.7	1.1	76.8	73.7	3.1
	K2	24.3	18.1	6.2	127.6	117.2	10.4
Station S2	M2	117.2	123.1	5.9	100.4	97.4	3
	S2	43.7	43.2	0.5	152.9	128.4	24.5
	N2	26	26	0	86.2	77.4	8.8
	K2	12.5	12.3	0.2	219.6	126.1	93.5

although a general reduction of the order of 10^{-3} ms^{-1} up to 8–7 km away the plant is also apparent. On the other hand, the impacts caused on the bottom layer are smaller than on the surface, not only in the area where the plant is located but also in the whole ria. Furthermore, the area where the effects are concentrated greatly differs, being now restricted to about 3–4 km away the plant. Finally, despite the impacts caused by plant P2 on the circulation of the whole ria at mid-flood describing a similar pattern as in the case of plant P1 (a general reduction of similar magnitude and occupying a similar area), in the area occupied by and next the plant they present strong differences. This issue is dealt with in detail in the next subsection.

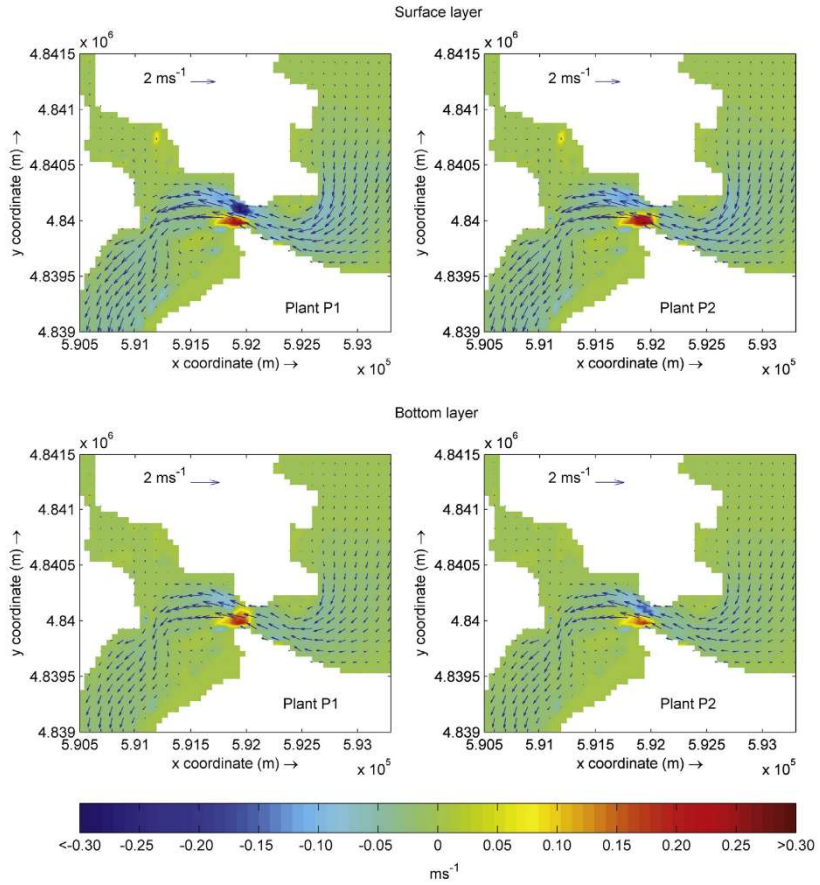


Fig. 6. Differences between altered and reference flow velocities (colour map), and vectors showing the altered flow in the middle ria at mid-flood tide. (For interpretation of the references to colour in this figure legend, the reader is referred to the web version of this article.)

USC UNIVERSIDADE DE SANTIAGO DE COMPOSTELA

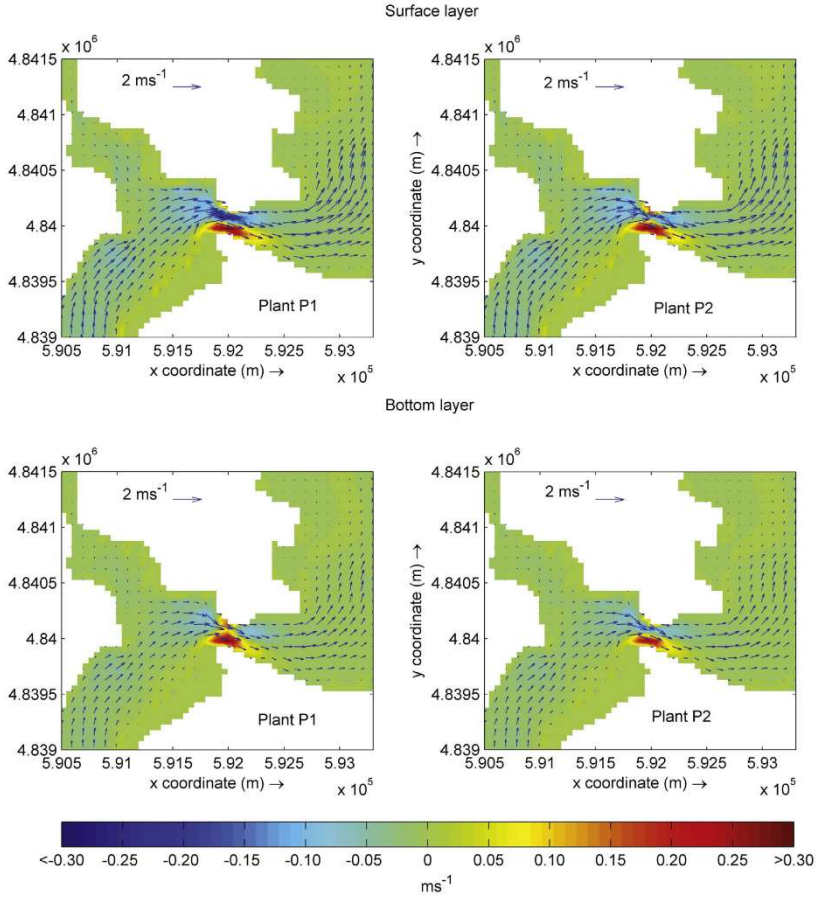


Fig. 7. Differences between altered and reference flow velocities (colour map), and vectors showing the altered flow in the middle ria at mid-ebb tide. (For interpretation of the references to colour in this figure legend, the reader is referred to the web version of this article.)

Regard to the impacts at mid-ebb tide resulting by the operation of plants P1 and P2 (Fig. 7), the general picture is rather similar to mid-flood tide, although with two significant differences: (i) the effects are a bit greater within and next the plant site and (ii) smaller within the area downstream the plant (i.e to the East). In this case, with respect to the effects on the outer part of the ria they are only significant (in the order of $2-3 \times 10^{-3}$ ms $^{-1}$) about 4–5 and 2–3 kms away the plant on surface and bottom layers, respectively.

4.2.3. Detailed assessment of the impacts

In this section, a detailed assessment of the impacts was performed in the area occupied by and next to the proposed plants. For this purpose, a control section was defined in the narrowing where the plants are located (Fig. 3) and the flow under the three simulated conditions (without plant, with plant P1 and with plant P2) analysed. As for the general circulation, the differences between altered and reference conditions at two representative tidal situations, mid-flood and mid-ebb, of a mean spring tide were considered.

At mid-flood tide (Fig. 8), the effects resulting from the operation of P1 are as follows. In the surface layer in the section occupied by the TSTs it causes an average reduction of approx. 0.25 ms $^{-1}$ (with reductions of up to 0.36 ms $^{-1}$ at specific points). Regard to the remaining section of the narrowing, south of the plant (left hand side in Fig. 8) the flow increases up to 0.28 ms^{-1}, whereas to the north (right hand side) it decreases slightly. With respect to the bottom layer, the flow increases throughout the whole section, with the greatest effects being located in the section non-occupied by the TSTs (up to 0.22 ms^{-1}). On the other hand, when plant P2 is in operation, the presence of the TSTs in the lower part of the water column results in an increase of the flow on the surface layer within the section to the south of the TSTs where differences between altered and reference conditions reach values of up to 0.30 ms $^{-1}$, as well as in a slightly decrease in the remaining section of the narrowing (the section

USC UNIVERSIDADE DE SANTIAGO DE COMPOSTELA

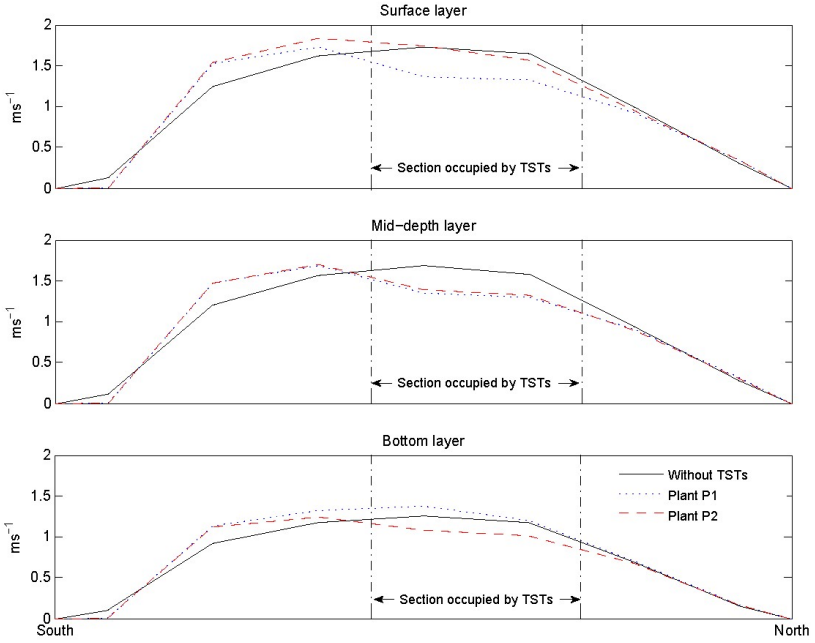


Fig. 8. Magnitude of the current velocity on the control section at mid-flood situation of a mean spring tide.

occupied by and north to the TSTs). In the bottom layer, the flow decreases in the section occupied by the TSTs up to 0.15 ms ^{1} at specific points, increases to the south of the plant up to 0.27 ms ^{1} and remains almost unchanged to the north. Regard to the mid-depth layer, the differences between the impact caused by plant P1 and P2 are almost negligible. In both cases the flow increases significantly to the south of the plant (up to 0.28 ms ^{1}), and decreases in the same order of magnitude within the section occupied by the plant (up to 0.33 ms ^{1}); finally, to the north, the effects consists on a slight variation either decrease or increase.

Regarding mid-ebb tide, the general pattern is rather similar to mid-flood situation (Fig. 9) although with a somewhat different magnitude. On the surface layer, in the section occupied by the plant P1, the flow decreases up to 0.34 ms ^{1} whereas in the remaining section it increases up to 0.32 ms ^{1}. By contrast, on the bottom layer, the flow increases throughout the whole section, with modifications of up to 0.26 ms ^{1} being concentrated to the south of the plant. In the case of Plant P2, there exists an overall increase in the portion of the section non-occupied by the TSTs of up to 0.30 and 0.24 ms ^{1} on surface and bottom layers, respectively. On the other hand, within the area occupied by the turbines, the effects are almost the opposite; here, the flow decreases up to 0.08 and 0.14 ms ^{1} in the surface and bottom layers, respectively. Finally, as in the case of mid-flood situation, the effects of both plants on the mid-depth layer are similar. There exists a strong increase and decrease in the flow to the south (up to 0.30 ms ^{1}) and within the plant (up to 0.26 ms ^{1}), repectively. However, as opposed to mid-flood situation, in this case the flow increases slightly to the north of the plant (up to 0.12 ms ^{1})

5. Conclusions

The impacts caused by two tidal stream plants on the estuarine circulation of Ria de Ortigueira (NW Spain) were investigated by means of a three-dimensional hydro-environmental numerical model (Delft3D-FLOW). The plants analysed are composed of Tidal Stream Turbines (TSTs) and present the same plan view layout; however one of them, plant P1, is composed of floating TSTs, and the other, plant P2, of bottom-fixed TSTs. The implementation of TSTs in the model was done by adding a sink term in the momentum equations representing the thrust force exerted by the flow in each turbine. This term is only considered in the vertical layers of the model corresponding to the area occupied by the rotors of the turbines (therefore affecting different layers in plants P1 and P2). First, the model was validated based on field data at two measuring stations, obtaining an excellent agreement between computed and measured water level and current velocity time series. Next, numerical simulations were performed in order to assess the potential impacts on the flow during mid-flood and mid-ebb of a mean spring tide.

Despite the significant differences in the annual energy production resulting from the operation of each tidal plant considered, it was found that the impacts caused on the general circulation present strong similarities. Although their operation is not sufficient for considerably modifying the flow throughout the whole ria, alterations of the order of 10 ^{2} ms ^{1} are apparent several km away the plants. Regard to the differences between mid-flood and mid-ebb situations, the general picture is virtually the same, with the main difference being the extension of the area affected to the east of the plant (smaller at mid-ebb tide). Regarding the plant site and its vicinities, the results of the model show that in this area there

USC UNIVERSIDADE DE SANTIAGO DE COMPOSTELA

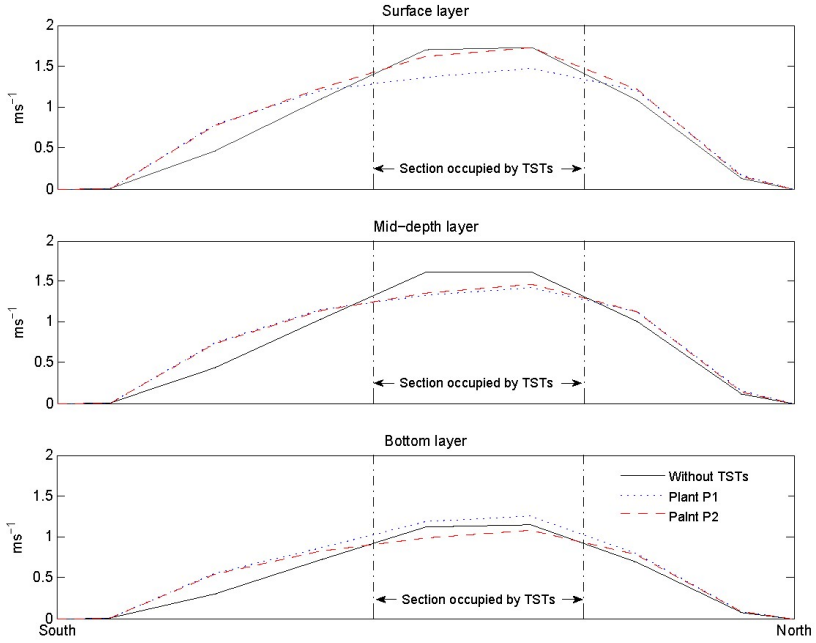


Fig. 9. Magnitude of the current velocity on the control section at mid-ebb situation of a mean spring tide.

exists an important reduction of the current velocity. However, not all of this velocity reduction stems from the extraction of energy, but also from the flow being redirected towards the remaining section which results in an increase of the velocity within this area. In contrast with the strong similarities in the modifications of the general pattern caused by plants P1 and P2, significant differences were found in this area. This arises from the different vertical configuration (occupying a different portion of the vertical) which causes that the impacts greatly differ from those that could be initially expected (e.g. a velocity increase in the section non-occupied by the plant). In this vein, a reduction of the flow was found over an important part of the surface layer during the operation of bottom-fixed TSTs. This unpredictable behaviour of the flow modification, highlights the importance of investigating the impacts caused by different plants in a tidal stream farm project under real conditions of operation.

In sum, this study has demonstrated that the energetic exploitation of tidal currents may cause important impacts on the estuarine circulation. These impacts were quantified for two proposed tidal stream plants, composed of floating or bottom-fixed TSTs. The results showed that there are almost no differences between the impacts caused by both configurations of TSTs on the general circulation; by contrast, there exist significant differences in the effects in the vicinity of the plants. Furthermore, in this area the impacts differ to a great extent from those that could be expected in advance, which highlights the importance of a site-specific analysis. Beyond the interest of these results for the area of study, the procedure herein implemented could be used to analyse the potential impacts caused by different TSTs on the hydrodynamics of other estuaries with similar hydrodynamic conditions. It is important to bear in mind that these impacts may, in turn, lead to other environmental effects that are outside the scope of this article, such as modifications to the sediment transport patterns and contaminant dispersion. These potential effects will be dealt with as a continuation of this line of research.

Acknowledgements

This work is part of the project "Assessment of Renewable Energy Resources" (DPI2009-14546-CO2-O2) supported by Spain's Ministry of Science and Innovation (Ministerio de Ciencia e Innovación). Its authors wish to thank P. García, M. Alvarez and M. Ouro for their contribution to the field campaign, as well as the Spanish Oceanographic Institute (Instituto Español de Oceanografía) for the salinity and temperature data obtained within the framework of European Project 0313-RAIA-1-E. During this work M. Sanchez and V. Ramos have been supported by the I2C grants PRE/2011/236 (Plan Galego de Investigación Innovación e Crecemento 2011–2015) of Xunta de Galicia.

References

[1] López I, Andreu J, Ceballos S, Martínez de Alegría I, Kortabarria I. Review of wave energy technologies and the necessary power-equipment. Renew Sustain Energy Rev 2013;27(0):413–34.
[2] Iglesias G, Carballo R. Wave resource in El Hierro—an island towards energy self-sufficiency. Renew Energy 2011;36(2):689–98.
[3] Iglesias G, Carballo R. Wave energy resource in the Estaca de Bares area (Spain). Renew Energy 2010;35(7):1574–84.
[4] Veigas M, Carballo R, Iglesias G. Wave and offshore wind energy on an island. Energy Sustain Develop In Press, Corrected Proof, Available online 11 December 2013
[5] Ramos V, Iglesias G. Wind power viability on a small island. Int J Green Energy 2013.
[6] Sánchez M, Iglesias G, Carballo R, Fraguela JA. Power peaks against installed capacity in tidal stream energy. IET Renew Power Gener 2013;7(6):246–53.

USC UNIVERSIDADE DE SANTIAGO DE COMPOSTELA

[7] Babarit A, Ben Ahmed H, Clément AH, Debusschere V, Duclos G, Multon B, et al. Simulation of electricity supply of an Atlantic island by offshore wind turbines and wave energy converters associated with a medium scale local energy storage. Renew Energy 2006;31(2):153–60.
[8] O Rourke F, Boyle F, Reynolds A. Tidal energy update 2009. Appl Energy 2010;87(2):398–409.
[9] Xia J, Falconer RA, Lin B. Impact of different operating modes for a Severn Barrage on the tidal power and flood inundation in the Severn Estuary, UK. Appl Energy 2010;87(7):2374–91.
[10] Hooper T, Austen M. Tidal barrages in the UK: Ecological and social impacts, potential mitigation, and tools to support barrage planning. Renew Sustain Energy Rev 2013;23(0):289–98.
[11] Lim YS, Koh SL. Analytical assessments on the potential of harnessing tidal currents for electricity generation in Malaysia. Renew Energy 2010;35(5):1024–32.
[12] Brooks DA. The tidal-stream energy resource in Passamaquoddy–Cobscook Bays: a fresh look at an old story. Renew Energy 2006;31(14):2284–95.
[13] Carballo R, Iglesias G, Castro A. Numerical model evaluation of tidal stream energy resources in the Ria de Muros (NW Spain). Renew Energy 2009;34(6):1517–24.
[14] Güney MS, Kaygusuz K. Hydrokinetic energy conversion systems: a technology status review. Renew Sustain Energy Rev 2010;14(9):2996–3004.
[15] Rourke FO, Boyle F, Reynolds A. Marine current energy devices: current status and possible future applications in Ireland. Renew Sustain Energy Rev 2010;14(3):1026–36.
[16] Yavuz T, Koç E, Kaynak B. Hydrodynamics performance of hydrofoil-slat arrangements in 3D analysis. Energy Convers Manag 2013;75(0):44–50.
[17] Faez Hassan H, Karim OA, El-Shafie A. Tidal current turbines glance at the past and look into future prospects in Malaysia. Renew Sustain Energy Rev 2012;16(8):5707–17.
[18] Myers LE, Bahaj AS. Experimental analysis of the flow field around horizontal axis tidal turbines by use of scale mesh disk rotor simulators. Ocean Eng 2010;37(2–3):218–27.
[19] Ramos V, Iglesias G. Performance assessment of tidal stream turbines: a parametric approach. Energy Convers Manag 2013;69(0):49–57.
[20] Work PA, Haas KA, Defne Z, Gay T. Tidal stream energy site assessment via three-dimensional model and measurements. Appl Energy 2013;102(0):510–9.
[21] Neill SP, Jordan JR, Couch SJ. Impact of tidal energy converter (TEC) arrays on the dynamics of headland sand banks. Renew Energy 2012;37(1):387–97.
[22] Neill SP, Litt EJ, Couch SJ, Davies AG. The impact of tidal stream turbines on large-scale sediment dynamics. Renew Energy 2009;34(12):2803–12.
[23] Ahmadian R, Falconer RA. Assessment of array shape of tidal stream turbines on hydro-environmental impacts and power output. Renew Energy 2012;44(0):318–27.
[24] Ahmadian R, Falconer R, Bockelmann-Evans B. Far-field modelling of the hydro-environmental impact of tidal stream turbines. Renew Energy 2012;38(1):107–16.
[25] Sánchez M, Carballo R, Ramos V, Iglesias G. Tidal stream energy impact on the transient and residual flow in an estuary: a 3D analysis. Appl Energy 2014;116(0):167–77.
[26] Ramos V, Carballo R, Álvarez M, Sánchez M, Iglesias G. Assessment of the impacts of tidal stream energy through high-resolution numerical modeling. Energy;61:541–554.
[27] Ramos V, Carballo R, Sanchez M, Veigas M, Iglesias G. Tidal stream energy impacts on estuarine circulation. Energy Convers Manag 2014;80(0):137–49.
[28] Perillo GME. Chapter 2 definitions and geomorphologic classifications of estuaries. Developments in sedimentology: Elsevier. p. 17–47.
[29] Castaing P, Guilcher A. Chapter 4 geomorphology and sedimentology of rias. Developments in sedimentology: Elsevier. p. 69–111.
[30] Pugh DT. Tides, surges, and mean sea-level/a handbook for engineers and scientists; 1996. John Wiley & Sons Inc.
[31] Iglesias G, Sánchez M, Carballo R, Fernández H. The TSE index – a new tool for selecting tidal stream sites in depth-limited regions. Renew Energy 2012;48(0):350–7.
[32] Oceanflowenergy.comhttp://www.oceanflowenergy.com, [accessed 10.07.14].
[33] User manual Delft3D-flow. Delft, The Netherlands: Deltares ed; 2010.
[34] Carballo R, Iglesias G, Castro A. Residual circulation in the Ria de Muros (NW Spain): a 3D numerical model study. J Mar Syst 2009;75(1–2):130.
[35] Iglesias G, Carballo R. Effects of high winds on the circulation of the using a mixed open boundary condition: the Ria de Muros, Spain. Environ Model Softw 2010;25(4):455–66.
[36] Iglesias G, Carballo R. Can the seasonality of a small river affect a large tide-dominated estuary? the case of the Ria de Viveiro, Spain. J Coast Res 2011;27(6):1170–82.
[37] Bolle A, Bing Wang Z, Amos C, De Ronde J. The influence of changes in tidal asymmetry on residual sediment transport in the Western Scheldt. Cont Shelf Res 2010;30(8):871–82.
[38] Hu K, Ding P, Wang Z, Yang SA. 2D/3D hydrodynamic and sediment transport model for the Yangtze Estuary, China. J Mar Syst 2009;77(1–2):114–36.
[39] Iglesias G, Carballo R. Seasonality of the circulation in the Ria de Muros (NW Spain). J Mar Syst 2009;78(1):94–108.
[40] Bahaj AS, Molland AF, Chaplin JR, Batten WMJ. Power and thrust measurements of marine current turbines under various hydrodynamic flow conditions in a cavitation tunnel and a towing tank. Renew Energy 2007;32(3):407–26.
[41] Philips NA. A co-ordinate system having some special advantages for numerical forecasting. J Meteorol 1957;14:184–5.
[42] Lynch DR, Davies AM, Gerritsen H, Mooers CNK. Closure: quantitative skill assessment for coastal ocean models. Quantitative Ski Assess Coast Ocean Models Am Geophys Union 1995;2013:501–6.
[43] Skogseth R, Sandvik AD, Asplin L. Wind and tidal forcing on the meso-scale circulation in Storfjorden. Svalbard Cont Shelf Res 2007;27(2):208–27.
[44] Cheng RT, Casulli V, Gartner JW. Tidal, residual, intertidal Mudflat (TRIM) model and its applications to San Francisco Bay, California. Estuar Coast Shelf Sci 1993;36(3):235–80.
[45] Dias JM, Sousa MC, Bertin X, Fortunato AB, Oliveira A. Numerical modeling of the impact of the Ancão inlet relocation (Ria Formosa, Portugal). Environ Model Softw 2009;24(6):711–25.
[46] Dias JM, Lopes JF. Implementation and assessment of hydrodynamic, salt and heat transport models: the case of Ria de Aveiro Lagoon (Portugal). Environ Model Softw 2006;21(1):1–15.
[47] Smith SD. Wind stress and heat flux over the ocean in gale force winds. J Phys Oceanogr 1980;10(5, May 1980):709–26.
[48] Yelland MJ, Moat BI, Taylor PK, Pascal RW, Hutchings J, Cornell VC. Wind stress measurements from the open ocean corrected for airflow distortion by the ship. J Phys Oceanogr 1998;28(7):1511–26.

USC UNIVERSIDADE DE SANTIAGO DE COMPOSTELA

USC
UNIVERSIDADE
DE SANTIAGO
DE COMPOSTELA

APPENDIX II. PREVIOUS WORKS: DETERMINATION OF LOCATION FOR TIDAL STREAM ENERGY EXPLOITATION IN RIA DE ORTIGUEIRA

In this appendix it is included, as a previous work of the author, the following article:

Title: The TSE index – A new tool for selecting tidal stream sites in depth-limited regions.

Journal: Renewable Energy, Volume 48, December 2012, Pages 350-357

Doi: https://doi.org/10.1016/j.renene.2012.05.012

Impact factor (2012): 2.989

Position (2012): 18/81 in Energy & Fuels category (Q1)

Authors: Gregorio Iglesias (GI), Marcos Sanchez (MS), Rodrigo Carballo (RC), Hernán Fernández (HF),

USC
UNIVERSIDADE DE SANTIAGO DE COMPOSTELA

USC
UNIVERSIDADE
DE SANTIAGO
DE COMPOSTELA

Renewable Energy 48 (2012) 350–357

Contents lists available at SciVerse ScienceDirect

Renewable Energy

journal homepage: www.elsevier.com/locate/renene

The TSE index – A new tool for selecting tidal stream sites in depth-limited regions

G. Iglesias*, M. Sánchez, R. Carballo, H. Fernández

Univ. of Santiago de Compostela, Hydraulic Eng., Campus Univ. s/n, 27002 Lugo, Spain

ARTICLE INFO

Article history:
Received 5 October 2011
Accepted 15 May 2012
Available online 17 June 2012

Keywords:
Tidal power
Tidal stream energy
Hydrodynamics
Ria de Ortigueira
Galicia
Spain

ABSTRACT

In many regions strong tidal flow occurs only in areas with restricted water depths, typically within estuaries or rias. Although in some of these areas the depth constraint may preclude the exploitation of this resource, in others it is exploitable – and substantial. The objective of this work is twofold: (i) to develop a tool, the Tidal Stream Exploitability (TSE) index, to facilitate the selection of tidal power sites in depth-limited zones, and (ii) to demonstrate it with a case study. The TSE index combines the flow and water depth information so that the areas with potential as prospective tidal power sites present large TSE values. On the contrary, areas of lesser interest – of weak flow, too shallow, or both – have small TSE values. In the case study (Ria de Ortigueira, a large estuary in NW Spain) a numerical model of the hydrodynamics is implemented. Once validated based on field data, the model is used to compute the flow velocity and power density in the estuary at different moments of the tide. Two areas present high values of power density. One is unsuitable for a tidal stream power plant due to its shallowness; the other, which does have sufficient water depth, clearly stands out in the TSE map. Thus, the TSE index is shown to facilitate the selection of tidal stream sites in depth-limited regions.

© 2012 Elsevier Ltd. All rights reserved.

1. Introduction

Marine energies, and tidal energy among them, are among the most promising renewables [1–4]. Tidal energy can be exploited in two different ways: by building a tidal barrage so as to impound water and then use its potential energy (much as in a conventional hydropower scheme), or by using the tidal stream itself to drive tidal energy converters (TECs) [5–14]. Both tidal barrage and tidal stream power have a significant advantage relative to other renewables – their high predictability. Tidal flow can be predicted with great accuracy over very long periods, and therefore the power output of a certain tidal plant at a given location can also be accurately predicted – an important point when it comes to the cost-benefit analysis of a project. With respect to tidal barrage schemes, tidal stream energy has two main advantages, both of which stem from its non-requirement of the barrage: lower environmental impact, and lower capital investment [15,16]. With respect to wind energy, the power density available for marine current energy converters will generally be much higher than that for wind energy converters at appropriately rated speeds for both technologies – a result of the much higher density of water, some 800 times that of air [11]. A further advantage of tidal stream energy is the absence of extreme flow velocities that might damage the equipment or, at least, complicate its maintenance. All in all, the advantages of tidal stream power are clear. Its main disadvantage is perhaps its fluctuating nature, due to the relative motions of the Earth, Moon, and Sun. The fluctuations occur in different time scales, from hours (diurnal inequality) to days (fortnightly inequality, i.e. the spring-neap tidal cycle) to months (annual inequality) to years (Metonic cycle) [17]. There are, however, strategies to manage the surplus electricity-production from fluctuating renewable-energy sources [18], which can be applied to integrate tidal power into an energy system. Another fundamental aspect to consider is the environmental impact of tidal stream energy [19,20]. A tidal stream plant can affect the sediment transport, morphodynamics, water quality, and biota of an area, and therefore its impact must be assessed in detail before any decision is taken.

The tide is the result of the lunar and solar attraction on the water particles of the oceans [17]. The tidal wave is subjected to reflection at the land boundaries, Coriolis effects, friction and refraction over the continental shelf, etc.; it can be amplified by resonance in certain bays or estuaries, or merely because the estuary through which it propagates gradually narrows. For these reasons the tidal stream resource presents significant geographical variations, and its characterisation in the region of interest is one of

* Corresponding author. Tel.: +34 982823650; fax: +34 982285926.
E-mail address: gregorio.iglesias@usc.es (G. Iglesias).

0960-1481/$ – see front matter © 2012 Elsevier Ltd. All rights reserved.
doi:10.1016/j.renene.2012.05.012

USC UNIVERSIDADE DE SANTIAGO DE COMPOSTELA

the first steps towards its exploitation [5,8–10,12–15,21–23]. When assessing the tidal stream resource the current velocity is all-important, for the power of a stream varies with its velocity to the cube. Notwithstanding, water depth is also of importance [24] for a number of reasons, among which the fact that a greater water depth allows to install larger (and potentially more cost-effective) TECs. On the other hand, the technological options for shallow areas are rather limited. There are, for instance, few TECs that can operate in water depths of ~5 m. The greater the depth the greater the choice – which can also result in a more cost-effective installation.

Galicia (NW Spain) has a great potential for marine renewables, with a substantial wave resource [25–27]; as for its tidal stream resource, strong currents occur in certain areas within the Galician rias – large estuaries subjected to a tidal range of 4.0–4.5 m. These areas are typically depth-limited, which does not mean that their tidal stream resource must be discarded, but that the variable 'water depth' must be given more attention in the analysis. This is the motivation for the present work, in which a new tool, the Tidal Stream Exploitability (TSE) index, is developed to facilitate the selection of the areas with potential as tidal stream sites in depth-limited zones such as the Galician rias. Based on the power available from a tidal stream per unit width (considering the whole water column), the TSE index synthesises the information on the power density and water depth in a single parameter. A penalty function is applied where the water depth becomes a limiting factor. Moreover, the definition of the TSE index accounts for the possible ebb-flood asymmetries that are common in many estuaries [28], and which were investigated by Neill et al. [29] in the context of tidal stream energy.

This approach has two main advantages. Firstly, its simplicity: the areas with potential as tidal stream sites – considering both the power density and available water depth – are clearly highlighted in a TSE graph. Secondly, in the depth-limited conditions of an estuary, a certain area may well be of greater interest as a tidal stream site than a nearby area with slightly stronger flow but smaller water depths. This cannot be ascertained by considering the flow velocity and the bathymetry separately (the conventional approach), but it can by means of the TSE index. This paper is structured as follows. In Section 2, the definition of the TSE index is explained. In Section 3, the case study in Ria de Ortigueira is presented and the numerical model implemented. Section 4 contains the results and discussion. Finally, conclusions are drawn in Section 5.

2. The TSE index

The flux of kinetic energy that passes through a section perpendicular to the flow direction, i.e. the power available from a tidal stream is,

$$P_A = \frac{1}{2}\rho A v_0^3, \tag{1}$$

where v_0 is the unperturbed fluid velocity, ρ is the water density, and A is the area of the section under consideration. The tidal stream power density, i.e. the flux of kinetic energy per square meter, is

$$p = \frac{1}{2}\rho V^3. \tag{2}$$

The power available from a stream of water per unit width can be defined by considering a vertical area of unit width and height equal to the water depth; if the vertical variation of the water density and velocity are considered, the power per unit width can be written as,

$$P_u = \frac{1}{2}\int_{-h}^{0} \rho(z)[v(z)]^3 \mathrm{d}z, \tag{3}$$

where $v(z)$ and $\rho(z)$ are the unperturbed velocity and water density at the level z, with z the vertical coordinate (negative downwards from the reference plane) and h the water depth. The range of seawater density is 1020–1050 kg/m^3 if the whole range of water depths is considered. Tidal stream power sites, of course, must be located in nearshore areas, so the pertinent range is far smaller (its upper bound is lower). Therefore, with a variability of less than 3%, the density may be considered constant for the purposes of Equation (3). As for the vertical variation of the flow, a depth-mean velocity can be defined as,

$$V = \frac{1}{h}\int_{-h}^{0} v \mathrm{d}z. \tag{4}$$

Introducing this definition into Equation (3) yields,

$$P_u = \frac{1}{2}\alpha\rho V^3 h, \tag{5}$$

where the coefficient α is given by,

$$\alpha = \frac{1}{V^3 h}\int_{-h}^{0} v^3 \mathrm{d}z. \tag{6}$$

The value of α is unity for uniform flow. In other cases it is above unity, for the mean of the cubes of the velocity is greater than the cube of the mean velocity. With the possible exception of layered flow (in which the very notion of depth-mean velocity loses its physical meaning) α can be taken as unity with a small error [30]. (In wide channels, for instance, $\alpha = 1.03$). With this assumption – which is, incidentally, on the conservative side from the standpoint of the resource assessment – the power available from a stream of water per unit width is given by

$$P_u = \frac{1}{2}\rho V^3 h. \tag{7}$$

From Equation (7) it is apparent that the power available from a tidal stream per unit width is proportional to the product V^3h. On this basis, the TSE index is constructed by considering the flow at two moments of the tide (mid-ebb and mid-flood) in order that it can be used to compare areas with ebb-flood asymmetries with others with no asymmetry; by including a function to penalise shallow areas; and by nondimensionalising the resulting expression – as follows.

In many coastal areas, and in particular in shallow estuaries, there is an ebb-flood asymmetry, i.e. the velocities are not the same during the ebb and flood (e.g. [31,32]). Taking the mean spring tide [17] as a reference, if the depth-mean velocities at mid-ebb and mid-flood are denoted by V_e and V_f, respectively, then $V_f > V_e$ in the case of flood dominance, and $V_e > V_f$ in the case of ebb-dominance. In either case it seemed appropriate to consider both values (the mid-ebb and mid-flood velocities), for keeping only one of them would imply either overestimating or underestimating the resource relative to another location with no ebb-flood asymmetry. On these grounds the following function was defined:

$$\varphi = \frac{1}{2}\left(V_f^3 + V_e^3\right)h \tag{8}$$

where h is the local water depth at mid-tide.

Next, a function to penalise shallow areas was introduced in the knowledge that, where the available water depth is small, few TECs

USC UNIVERSIDADE DE SANTIAGO DE COMPOSTELA

can be installed; and where it is very small, the practical exploitation of the tidal stream resource may be impossible.

At present there are TECs in operation in as little as 5 m of water in the Humber Estuary [33], and floating TECs capable of operating in as little as 2 m of water have been developed, such as a floating turbine with a diameter of 1.5 m [34]. Therefore, a minimum water depth $h_1 = 2$ m is assumed for the purposes of this work. In other words, the TSE index will be 0 where the lowest water depth is below 2 m. Further, given that at the time of writing there are no TECs operating in water depths between $h_1 = 2$ m and $h_2 = 5$ m, a linear penalty is introduced for this range, again with reference to the lowest water depth. Thus the penalty function ξ can be written:

$$\begin{aligned}
&\xi = 0 \quad \text{if} \quad h - \frac{\Delta h}{2} \le h_1 \\
&\xi = \frac{1}{h_2 - h_1}\left(h - \frac{\Delta h}{2} - h_1\right) \quad \text{if} \quad h_1 < h - \frac{\Delta h}{2} < h_2, \quad \text{and} \\
&\xi = 1 \quad \text{if} \quad h - \frac{\Delta h}{2} \ge h_2.
\end{aligned} \tag{9}$$

where h is the mid-tide water depth, Δh is the maximum tidal range, and h_1 and h_2 are, respectively, the lower and upper bounds of the penalty range. For the case study that follows, these bounds were set at 2 m (h_1) and 5 m (h_2), respectively, in view of the current state of the technology, as explained. However, it cannot be ruled out that other values may be more appropriate in future due to the technological advance of TECs, or even at present in a different location – for instance, if the developers wish to set a different value for the minimum water depth because they do not want to consider a certain type of turbine. In any case, the focus of this work is not on the numerical values of the bounds of the penalty interval, which can be varied to suit the technological options preferred by the developers or the development of new technologies, but on the TSE methodology.

Introducing the penalty function defined in Equation (9) into Equation (8) yields:

$$\varphi^* = \frac{\xi}{2}\left(V_f^3 + V_e^3\right)h. \tag{10}$$

Finally, the TSE index is obtained by nondimensionalising Equation (10):

$$\mathrm{TSE} = \frac{\xi}{2V_0^3 h_0}\left(V_f^3 + V_e^3\right)h, \tag{11}$$

where V_0 is a characteristic velocity, and h_0 a characteristic water depth. The interest of these characteristic magnitudes lies in their dimensions rather than their numeric values, which need only reflect the order of magnitude of the respective variables.

The physical interpretation of the TSE index is straightforward. A value of TSE = 5, for instance, signifies that the average power (average between mid-flood and mid-ebb) available from the tidal stream per unit width is five times that of a tidal current of V_0 in a water depth of h_0. The values used in this work were $V_0 = 1.5$ m s^{-1} and $h_0 = 5$ m.

3. A case study: Ria de Ortigueira

As a case study, the TSE index defined in the previous section was applied to an estuary in NW Spain, Ria de Ortigueira. In coastal geomorphology the term "ria" denotes a type of estuary in which sedimentation has not kept pace with sealevel rise, so the coastline and bathymetry very much reflect the morphology of the original fluvial valley. In short, rias are drowned river valleys [35]. The coast of Galicia (NW Spain) is characterised by its numerous rias.[1] Galician rias are usually classified into Rias Baixas, Rias Altas, and Cantabrian Rias, each category having its own morphological and tectonic traits [36–39]. With a surface area of 85 km^2, Ria de Ortigueira is one of the largest of the Rias Altas group. Its broad mouth is delimited by two major headlands, Cape Ortegal and Estaca de Bares (Fig. 1). Riverine discharge is very limited – the only river of some import is River Mera, with a mean discharge of 6.77 m^3 s^{-1} – and the ria is a well-mixed estuary.

The period of the tidal oscillation is approximately 12 h 25 min or 24 h 50 min for semidiurnal or diurnal tides, respectively. Whether the tide is semidiurnal or diurnal depends on the relative amplification of the main tidal constituents, which is quantified by means of the tidal form factor,

$$F = \frac{K_1 + O_1}{M_2 + S_2}, \tag{12}$$

where K_1 and O_1 represent the local amplitudes of the principal diurnal constituents, and M_2 and S_2 are the local amplitudes of the principal semidiurnal constituents. If $F < 0.25$ or $F > 3$, the tidal regime is semidiurnal or diurnal respectively; $0.25 < F < 1.5$ implies a mixed, predominantly semidiurnal regime, whereas $1.5 < F < 3$ signifies a mixed, predominantly diurnal regime [5,17]. In Ria de Ortigueira tides are purely semidiurnal, with a form factor $F = 0.0819$. From the perspective of tidal stream energy this is advantageous, for semidiurnal tides give rise to stronger currents, ceteris paribus, than diurnal tides. With a maximum tidal range of 4.5 m, strong tidal flow does occur in certain areas of the estuary. This, and the fact that the available water depth in these areas is limited, make Ria de Ortigueira an appropriate context to apply the TSE approach for selecting prospective tidal stream sites.

A numerical model of the hydrodynamics of Ria de Ortigueira was implemented and validated based on field data. The model, Delft3D–FLOW, is a finite-difference code solving the Navier–Stokes equations. As in previous assessments of the tidal resource [5,40], the depth-mean equations were used in their baroclinic form, so the model takes into account the horizontal density gradients that may be caused by salinity and/or temperature gradients across the ria. The equations are:

$$\frac{\partial \zeta}{\partial t} + \frac{\partial[(d+\zeta)u]}{\partial x} + \frac{\partial[(d+\zeta)v]}{\partial y} = Q \tag{13}$$

$$\left.\begin{aligned}
&\frac{\partial u}{\partial t} + u\frac{\partial u}{\partial x} + v\frac{\partial u}{\partial y} - fv = -g\frac{\partial \zeta}{\partial x} - \frac{g}{\rho_0}\int_{-d}^{\zeta}\frac{\partial \rho'}{\partial x}\mathrm{d}z + \frac{\tau_{sx} - \tau_{bx}}{\rho_0(d+\varsigma)} + \nu_h\nabla^2 u \\
&\frac{\partial v}{\partial t} + u\frac{\partial v}{\partial x} + v\frac{\partial v}{\partial y} + fu = -g\frac{\partial \zeta}{\partial y} - \frac{g}{\rho_0}\int_{-d}^{\zeta}\frac{\partial \rho'}{\partial y}\mathrm{d}z + \frac{\tau_{sy} - \tau_{by}}{\rho_0(d+\varsigma)} + \nu_h\nabla^2 v
\end{aligned}\right\} \tag{14}$$

$$\frac{\partial(\zeta+d)c}{\partial t} + \frac{\partial[(\zeta+d)uc]}{\partial x} + \frac{\partial[(\zeta+d)vc]}{\partial y} = D_h\nabla^2 c - \lambda_d(d+\zeta)c + R \tag{15}$$

Equations (13) and (14) are the equations of conservation of mass and momentum, respectively. Equation (15) is the equation of transport, which is solved both for salinity and temperature. In these equations, d is the local water depth below a horizontal reference plane and ζ is the water level relative to the reference

[1] Indeed, the term comes from the Galician language.

USC UNIVERSIDADE DE SANTIAGO DE COMPOSTELA

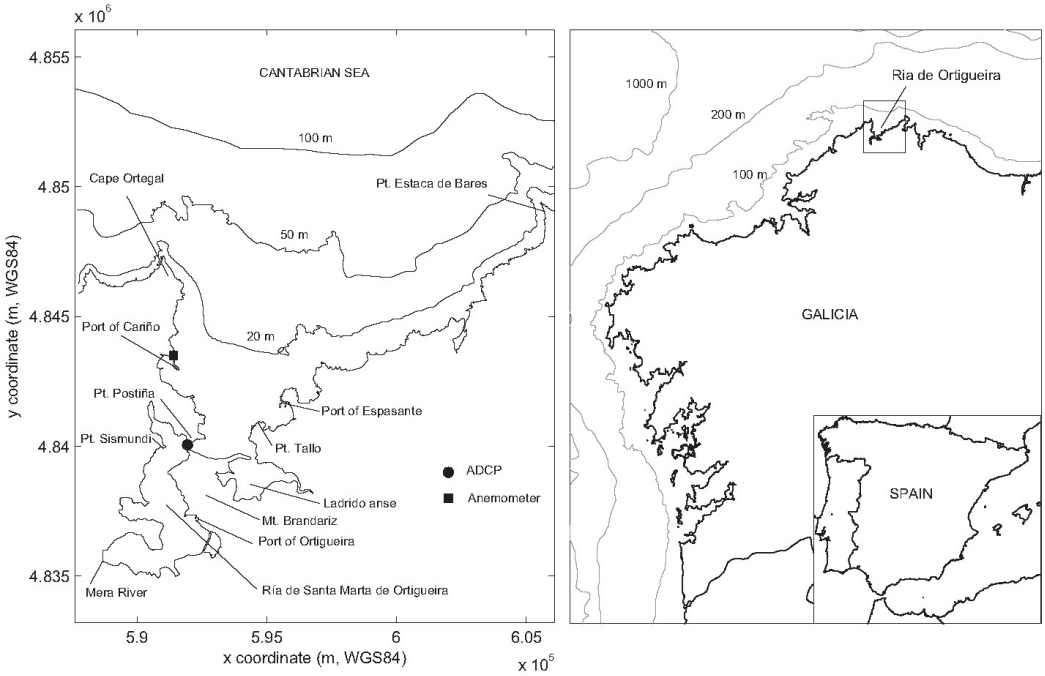


Fig. 1. Ria de Ortigueira (left) in Galicia, NW Spain (right).

plane; u and v are, respectively, the depth-mean flow components in the x- and y-coordinate directions; Q is the mass source intensity; υ_h is the horizontal kinematic eddy viscosity; D_h is the horizontal diffusivity; f is the Coriolis parameter; ρ_0 and ρ are, respectively, the reference and anomaly density; τ_{sx} and τ_{sy} are the wind stress components; τ_{bx} and τ_{by} are the bottom shear stress components; c represents salinity or temperature; λ_d is the first-order decay process; finally, R is the source term.

The computational grid was Cartesian and had its x and y axes aligned with the west–east and south–north directions, respectively. (Thus, the u and v velocity components were eastward and northward components). The cell size in the inner ria, 50 × 50 m, was kept unchanged up to roughly the 25 m contour, from where it gradually increased northward up to the outer boundary, approximately at the 150 m contour, where it reached 50 × 150 m. The bathymetry (Fig. 2) was obtained from nautical charts nos. 408 and 4083 of Spain's Hydrographic Institute. In the intertidal zones of the innermost ria the charts were supplemented with maps nos. 00718d, 00188d and 00281d of the 1:5000 cartography of the Galician Regional Government (Xunta de Galicia). In the numerical model, the process of drying and flooding is represented by removing grid points from the flow domain that become "dry" when the tide falls and by adding grid points that become "wet" when the tide rises, as explained in [41].

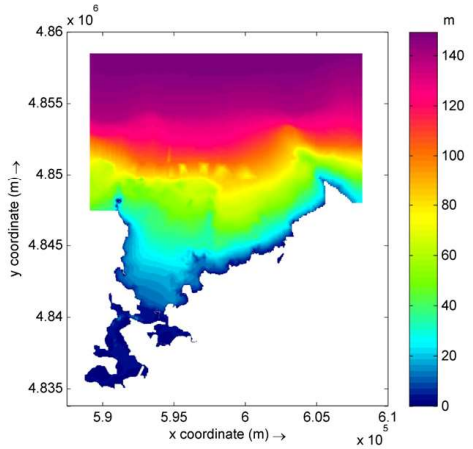


Fig. 2. Bathymetry of Ria de Ortigueira.

Table 1
Main tidal harmonics in Ria de Ortigueira.

Constituent	Amplitude (cm)	Phase (°)
M2	122.79	90.15
S2	42.91	121.08
N2	25.98	70.39
K2	12.03	118.76
K1	7.35	73.49
O1	6.22	324.62
P1	2.22	65.15

USC UNIVERSIDADE DE SANTIAGO DE COMPOSTELA

Table 2
Tidal analysis of the sea level time series recorded by the ADCP [SNR = signal-to-noise ratio].

Tidal constituent	Frequency (cph)	Amplitude (cm)	Amplitude error (cm)	Phase (°)	Phase error (°)	SNR
MSF	0.0028219	10.37	1.3	174.87	8.64	61
M2	0.0805114	132.99	13.3	90.54	5.69	100
S2	0.0833333	32.92	12.5	127.56	20.66	6.9
K1	0.0417807	8.80	1.4	81.43	10.51	38
O1	0.0387307	6.33	1.6	313.61	13.14	16
M4	0.1610228	2.71	2.2	340.97	56.82	1.5
M6[a]	0.2415342	1.52	2.1	298.22	104.03	0.55

[a] The results concerning the M6 overtide are not statistically significant (SNR < 1).

Table 3
Correlation coefficients between observed and computed time series of sea level (R_ζ) and eastward and northward velocity components (R_u and R_v, respectively) for different values of the calibration parameter, the horizontal kinematic eddy viscosity (ν_h).

ν_h ($m^2\ s^{-1}$)	R_ζ	R_u	R_v
50	0.988	0.935	0.915
30	0.989	0.949	0.930
15	0.990	0.957	0.939

At the ocean boundary the sea level was prescribed using the seven main tidal harmonics (Table 1), obtained from the global ocean tide model TPXO 7.2 [42]. Although field data remain indispensable for tuning a coastal numerical model, a global ocean tide model can be used to force a coastal circulation model along its open boundaries [43], and the TPXO model has been shown to produce good results (e.g. [44]). Salinity and temperature at the ocean boundary were imposed using data from Spain's Oceanographic Institute (Instituto Español de Oceanografía) [45]. At the land–water interface the boundary conditions were free slip and null flow.

The numerical model was validated based on field data of tidal level and flow. The validation period comprised 19 days, from 16 December 2010 to 4 January 2011, during which an Acoustic Doppler Current Profiler (ADCP) and an anemometer were deployed in the ria. The ADCP (Sontek Argonaut-XR) measured the tidal level and the velocity and direction of the flow at a point in the inner ria south of Pt. Postiña (Fig. 1), in a water depth of 9.5 m at low tide. The anemometer was installed at a point close to the breakwater of the Port of Cariño, taking advantage of an existing steel structure to support it at a height of approx. 10 m above the mean sea level. In addition to the flow and wind data, the hourly discharge of the River Mera during the validation period was obtained from a gauging station close to its mouth.

A tidal analysis of the sea level time series was carried out assuming a Rayleigh criterion $R = 1$ [46]. The results (Table 2) indicate that the M4 overtide is relatively weak (M4/M2 = 0.02), and hence only minor tidal asymmetry may result from it at the ADCP site [28,47].

The initial condition was the so-called *cold start*, i.e. null surface elevation and flow velocity. The simulation covered a period of 49 days, i.e. 30 days of spin-up plus 19 days of the validation period (the period of interest). The purpose of the spin-up period before the validation period is to adjust dynamically the flow field so that the initial conditions do not influence the numerical results during the period of interest [48].

The calibration parameter was the horizontal kinematic eddy viscosity (ν_h). Three values in the habitual range for this kind of models (15, 30 and 50 $m^2\ s^{-1}$) were tested [49]. The correlation coefficients between observed and computed time series of sea level and flow velocity were very high in all cases (Table 3), and in particular for $\nu_h = 15\ m^2\ s^{-1}$ – the value selected for the validation. The computed and observed time series of tidal level (Fig. 3) show excellent agreement. The same is true of the time series of current velocity (Fig. 4).

4. Results and discussion

After validating the numerical model, it was used to determine the tidal flow on a mean spring tide – the benchmark for the TSE index. For this purpose the model was forced with the seven main tidal harmonics (Table 1) and the mean discharge of the Mera River. As in the validation run, the simulation period was composed of the period of interest preceded by a spin-up period of 30 days. The mid-flood and mid-ebb flow patterns thus obtained are shown in Fig. 5 for the middle and inner ria (the weaker flow of the outer ria is without interest as regards tidal stream power). A tidal asymmetry is apparent, with the flood stronger than the ebb. Tidal asymmetry can be caused by the distortion of the tidal wave as it propagates over the coastal shelf, or by the different geometry of the estuary at different tidal levels [50]. It would appear that both causative factors may be at work in Ria de Ortigueira, although definite conclusions cannot be drawn without the appropriate investigation – which is outside the scope of this work. At any rate, flood dominance has recently been reported in the neighbouring Ria de Viveiro [32].

Of greater interest from the standpoint of the tidal resource, the strongest flow occurs at two constrictions of the inner ria: one to the east, in the passage between the middle ria and the Ladrido Anse, and another to the west, in the channel between the middle ria and the innermost ria, or Ria de Santa Marta (Fig. 5; for reasons of clarity, the velocity vectors represented

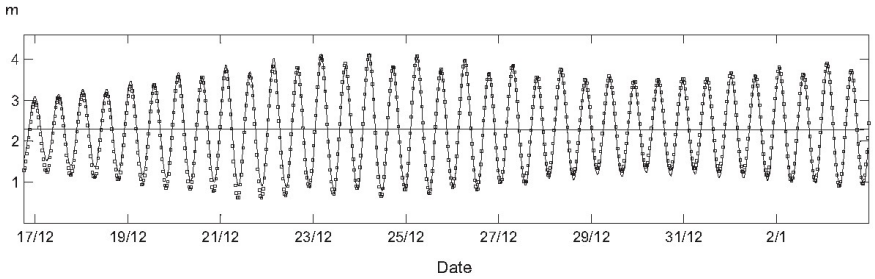


Fig. 3. Computed (–) and observed (·) time series of sea level during the validation period.

USC UNIVERSIDADE DE SANTIAGO DE COMPOSTELA

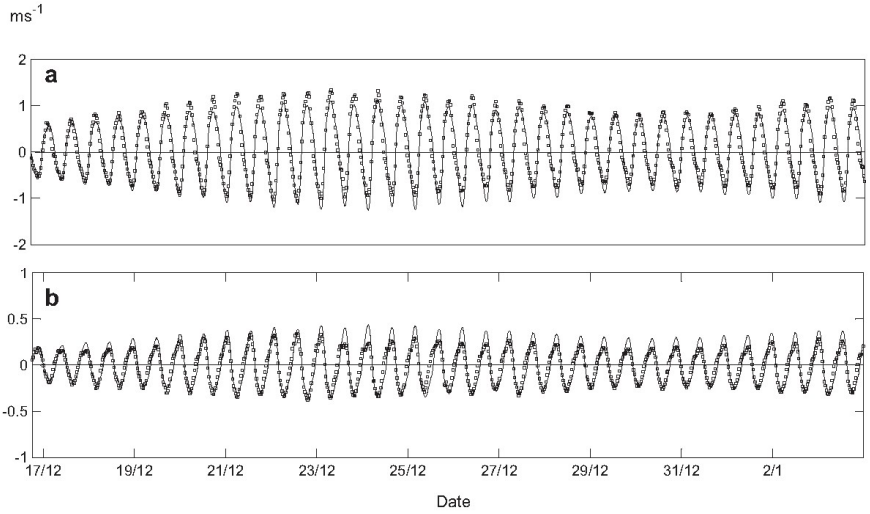


Fig. 4. Computed (–) and observed (") time series of the eastward (a) and northward (b) velocity components during the validation period.

are fewer than those actually computed by the model). The values of power density, computed according to Equation (2), are represented in Fig. 6. The maximum flow velocities, 2.5 and 2.0 m s ^{1}, occur at mid-flood in the passages into the Ladrido Anse and the inner ria, respectively; and the corresponding values of power density are ≈8 and ≈6 kW m ^{2}, also respectively. The areas where these values occur are marked as A and B in Fig. 6.

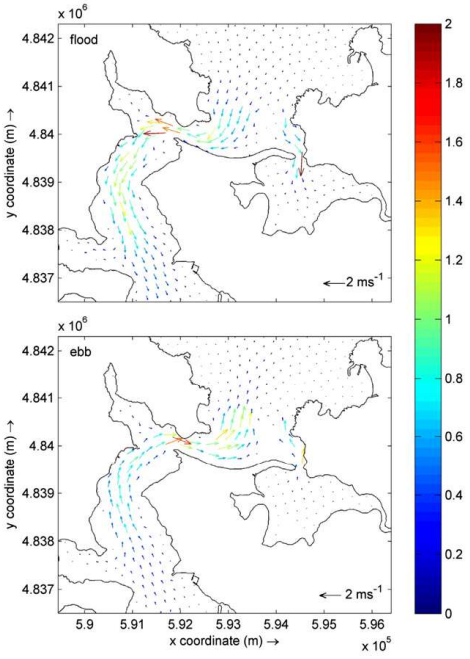


Fig. 5. Mid-flood and mid-ebb flow patterns in the middle and inner ria.

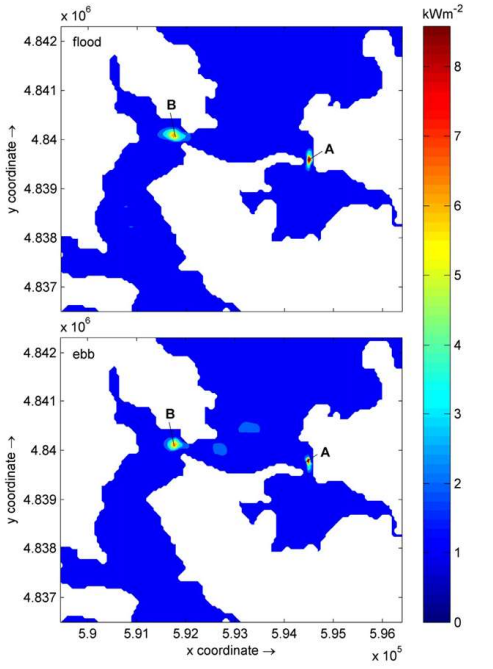


Fig. 6. Mid-flood and mid-ebb values of the power density in the middle and inner ria.

USC UNIVERSIDADE DE SANTIAGO DE COMPOSTELA

Based on these results, the TSE index was determined according to Equation (11) (Fig. 7). The only area that stands out clearly in the graph is area B, with values of approx. 5 over a roughly circular region of 150 m in diameter – a sizeable surface area. With more than 8 m of water depth, area B is a promising tidal stream site. Area A of Fig. 6 is indistinguishable in the TSE graph in spite of its high power density because of its very low water depth (Fig. 8), which makes it unsuitable for a tidal power site. On the other hand, Area C (Fig. 8) represents the opposite situation: sufficient water depth, but weak flow; again, it does not feature in the TSE graph.

To summarise, the tidal stream site with the greatest potential (area B) was highlighted in the TSE graph (Fig. 7), for the TSE index is based on both the flow and water depth information. Areas with strong flow but insufficient water depth, such as area A, or with sufficient water depth but weak flow, such as area C, presented low TSE values. Thus, the case study of Ria de Ortigueira showed how the TSE index facilitates the selection of tidal stream sites in depth-limited areas.

Of course, the TSE approach can be applied elsewhere, and the upper and lower bounds of the penalty interval (h_1 and h_2) need not be the same. The previous values of the index were obtained using $h_1 = 2$ m and $h_2 = 5$ m in Equation (9). The latter, in particular, means that areas with more than 5 m of water depth at lowest low water were not penalised. This threshold could be varied depending on the technical specifications of the TECs to be deployed – and different TSE maps would ensue. If h_2 had been set at 10 m, for instance, area B would be penalised, and the area immediately to its east would possibly have larger TSE values. It is only logical that the areas of greatest interest as potential tidal sites in a depth-limited estuary should depend on the minimum water depth required by the technology under consideration – which is consistent with the fact that TSE values depend on the thresholds of the penalty function. And, as mentioned in the Introduction, the technological evolution of TECs will most likely suggest different values in future. Similarly, the characteristic magnitudes V_0 and h_0 can be varied at will – the only implication being a change in the reference for the physical interpretation of a given TSE value. On these grounds it is clear that the essence of the TSE index lies in the procedure rather than in its actual values in a particular application.

Finally, it is worth mentioning that the TSE approach can also be very useful to investigate possible sites for River Current Energy Conversion Systems (RCECS) [21,51,52], given that the water depth constraint will often play a major role in riverine contexts.

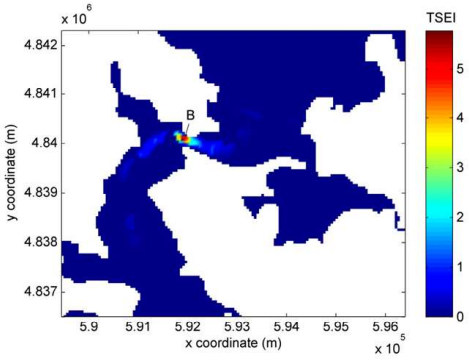


Fig. 7. TSE index in the middle and inner ria.

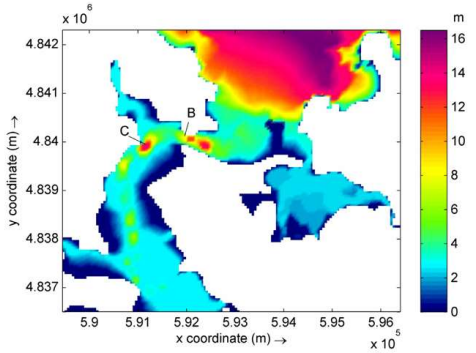


Fig. 8. Detailed bathymetry of the middle and inner ria.

5. Conclusions

In many regions strong tidal flow occurs mainly in semi-enclosed bodies of water open to the ocean, such as estuaries, rias, etc., subjected to a substantial tidal range, and in particular in areas within them in which the coastal morphology and bathymetry combine to produce strong currents. These areas are typically shallow; however, their depth-limited nature should not lead to discarding them a priori as tidal stream power sites, for some do have sufficient water depth – and a substantial resource. In this work a new tool, the Tidal Stream Exploitability (TSE) index, was proposed to facilitate the selection of tidal power sites in depth-limited zones; it is based on the power available from a tidal stream per unit width, determined both at mid-flood and mid-ebb to incorporate possible tidal asymmetries. A penalty function is used to take into account the limitations to the exploitability of the tidal stream resource imposed by small water depths.

A case study in Ria de Ortigueira, a large estuary in NW Spain with a 4.5 m tidal range, was developed to demonstrate the TSE approach. A numerical model of the hydrodynamics was implemented and validated based on observations of tidal level and current velocity. The correlation coefficients between the computed and observed time series were very close to unity, which proved the model's ability to solve the flow in the ria. The model was then applied to determine the tidal currents and power density at mid-flood and mid-ebb on a mean spring tide. A tidal asymmetry was found, with flood dominance; therefore, the fact that the TSE index considers both the mid-flood and mid-ebb velocities was relevant in the case study.

Two areas with high values of power density emerged in the inner ria, corresponding to two narrow passages: the entrance to the Ladrido Anse (area A) and the passage from the middle ria to the Ria de Santa Marta (area B). Area A has a slightly higher power density than area B. However, its TSE values are penalised by its shallowness, which would impose a major constraint for the exploitation of the tidal resource. Area B, though depth-limited like the whole ria, is outside the penalty range – implying that there are TECs currently in operation in similar water depths; for this reason, and for its large power density, it presents large TSE values – the largest in Ria de Ortigueira. Although there are other areas in the estuary that also have sufficient water depth for a tidal power plant, their TSE values are low due to their scanty power density. Only area B has potential for a tidal stream site; and only area B was conspicuous in the TSE graph. Thus, the new index was shown to facilitate the selection of tidal stream sites.

The essence of this work lies in the TSE approach rather than in particular values of the TSE index. These values will change if the

USC UNIVERSIDADE DE SANTIAGO DE COMPOSTELA

bounds of the penalty interval used for its calculation (h_1 and h_2) are modified – for instance, to take into account the evolution of tidal stream power technology. Using different values of h_1 and h_2 will result in different maps of the TSE index, in which the areas with the largest TSE values may also be different. This is consistent with the fact that, in a depth-limited region such as an estuary, the area best suited for a tidal stream plant may well depend on the water depth requirements of the TECs to be installed.

In summary, a new tool to facilitate the selection of tidal stream sites in depth-limited regions, such as estuaries, inlets, etc., was presented, and its usefulness was proven with a case study in Ria de Ortigueira. An area with potential for a tidal stream power plant was found in one of the narrow passages of the inner ria. The interest of this work goes beyond this estuary, for the same methodology – of which the TSE index is the crux – can be applied elsewhere.

Acknowledgements

This work is part of the project "Assessment of Renewable Energy Resources" (DPI2009-14546-C02-02) supported by Spain's Ministry of Science and Innovation (Ministerio de Ciencia e Innovación). Its authors wish to thank P. Otero, M. Ruiz-Villareal, and A. Peliz of Spain's Oceanography Institute (Instituto Español de Oceanografía) for the salinity and temperature data, obtained within the framework of European Project 0313-RAIA-1-E.

References

[1] Bahaj AS. Generating electricity from the oceans. Renewable and Sustainable Energy Reviews 2011;15:3399–416.
[2] CRES. Ocean energy conversion in Europe - recent advancements and prospects. Published in the framework of the "Coordinated Action on Ocean Energy" EU project under FP6 Priority: 6.1.3.2.3; Renewable Energy Technologies with the support of the European Commission directorate-General for Research under contract SES6-CT2004-502701; 2006.
[3] Charlier RH, Finkl CW. Ocean energy: tide and tidal power. Springer; 2008.
[4] Johnstone CM, Nielsen K, Lewis T, Sarmento A, Lemonis G. EC FPVI coordinated action on ocean energy: a European platform for sharing technical information and research outcomes in wave and tidal energy systems. Renewable Energy 2006;31:191–6.
[5] Carballo R, Iglesias G, Castro A. Numerical model evaluation of tidal stream energy resources in the Ria de Muros (NW Spain). Renewable Energy 2009;34:1517–24.
[6] Ahmadian R, Falconer R, Bockelmann-Evans B. Far-field modelling of the hydro-environmental impact of tidal stream turbines. Renewable Energy 2012;38:107–16.
[7] Ahmadian R, Falconer R, Lin B. Hydro-environmental modelling of proposed Severn barrage, UK. In: Proceedings of the Institution of Civil Engineers – Energy, 163; 2010. p. 107–17.
[8] Blunden LS, Bahaj AS. Initial evaluation of tidal stream energy resources at Portland Bill, UK. Renewable Energy 2006;31:121–32.
[9] Myers L, Bahaj AS. Simulated electrical power potential harnessed by marine current turbine arrays in the Alderney Race. Renewable Energy 2005;30:1713–31.
[10] Bahaj AS, Myers L. Analytical estimates of the energy yield potential from the Alderney Race (Channel Islands) using marine current energy converters. Renewable Energy 2004;29:1931–45.
[11] Bahaj AS, Myers LE. Fundamentals applicable to the utilisation of marine current turbines for energy production. Renewable Energy 2003;28:2205–11.
[12] Bryden IG, Couch SJ. ME1—marine energy extraction: tidal resource analysis. Renewable Energy 2006;31:133–9.
[13] Brooks DA. The hydrokinetic power resource in a tidal estuary: the Kennebec river of the central Maine coast. Renewable Energy 2011;36:1492–501.
[14] Grabbe M, Lalander E, Lundin S, Leijon M. A review of the tidal current energy resource in Norway. Renewable and Sustainable Energy Reviews 2009;13:1898–909.
[15] Brooks DA. The tidal-stream energy resource in Passamaquoddy–Cobscook bays: a fresh look at an old story. Renewable Energy 2006;31:2284–95.
[16] Rourke FO, Boyle F, Reynolds A. Marine current energy devices: current status and possible future applications in Ireland. Renewable and Sustainable Energy Reviews 2010;14:1026–36.
[17] Pugh DT. Tides, surges, and mean sea-level/a handbook for engineers and scientists. John Wiley & Sons Inc; 1996.
[18] Lund H, Münster E. Management of surplus electricity-production from a fluctuating renewable-energy source. Applied Energy 2003;76:65–74.
[19] Neill SP, Jordan JR, Couch SJ. Impact of tidal energy converter (TEC) arrays on the dynamics of headland sand banks. Renewable Energy 2012;37:387–97.
[20] Shields MA, Woolf DK, Grist EPM, Kerr SA, Jackson AC, Harris RE, et al. Marine renewable energy: the ecological implications of altering the hydrodynamics of the marine environment. Ocean Coast Management 2011;54:2–9.
[21] Khan MJ, Bhuyan G, Iqbal MT, Quaicoe JE. Hydrokinetic energy conversion systems and assessment of horizontal and vertical axis turbines for river and tidal applications: a technology status review. Applied Energy 2009;86:1823–35.
[22] O'Rourke F, Boyle F, Reynolds A. Tidal current energy resource assessment in Ireland: current status and future update. Renewable and Sustainable Energy Reviews 2010;14:3206–12.
[23] Lim YS, Koh SL. Analytical assessments on the potential of harnessing tidal currents for electricity generation in Malaysia. Renewable Energy 2010;35:1024–32.
[24] Bryden IG, Naik S, Fraenkel P, Bullen CR. Matching tidal current plants to local flow conditions. Energy 1998;23:699–709.
[25] Iglesias G, Carballo R. Wave energy resource in the Estaca de Bares area (Spain). Renewable Energy 2010;35:1574–84.
[26] Iglesias G, Carballo R. Wave energy potential along the Death coast (Spain). Energy 2009;34:1963–75.
[27] Iglesias G, López M, Carballo R, Castro A, Fraguela JA, Frigaard P. Wave energy potential in Galicia (NW Spain). Renewable Energy 2009;34:2323–33.
[28] Friedrichs CT, Aubrey DG. Non-linear tidal distortion in shallow well-mixed estuaries: a synthesis. Estuarine Coastal and Shelf Science 1988;27:521–45.
[29] Neill SP, Litt EJ, Couch SJ, Davies AG. The impact of tidal stream turbines on large-scale sediment dynamics. Renewable Energy 2009;34:2803–12.
[30] Chow VT. Open-channel hydraulics. New York: McGraw-Hill; 1959.
[31] Brown JM, Davies AG. Flood/ebb tidal asymmetry in a shallow sandy estuary and the impact on net sand transport. Geomorphology 2010;114:431–9.
[32] Iglesias G, Carballo R. Can the seasonality of a small river affect a large tide-dominated estuary? The case of the Ria de Viveiro, Spain. Journal of Coastal Research 2011;27:1170–82.
[33] www.pulsetidal.com, 14 December 2011.
[34] www.oceanflowenergy.com, 21 January 2012.
[35] Dyer KE. Estuaries: a physical introduction. New York: John Wiley; 1997.
[36] Díez J, Negro V, Fernández P. Further studies for stabilizing the entry channel to Foz Fishing Port, Lugo. Journal of Coastal Research 2006;22:710–9.
[37] Díez J, Negro V, Fernández P, García JA. Beach nourishment for shore protection by out-back-passing sands. Journal of Coastal Research; 2006:1771–4.
[38] Díez J, Costas Las. Alianza editorial; 1996.
[39] Duck RW, McManus J, Díez J. Comparative study of two largely infilled estuaries: the Eden Estuary (Scotland) and the Ria de Foz (Spain). Netherlands Journal of Aquatic Ecology 1995;29:203–10.
[40] Xia J, Falconer RA, Lin B. Impact of different operating modes for a Severn Barrage on the tidal power and flood inundation in the Severn Estuary, UK. Applied Energy 2010;87:2374–91.
[41] User manual Delft3D-FLOW. The Netherlands: Delft; 2010.
[42] Egbert GD, Bennett AF, Foreman MGG. Topex/Poseidon tides estimated using a global inverse model. Journal of Geophysical Research 1994;99:24821–52.
[43] Sauvaget P, David E, Guedes Soares C. Modelling tidal currents on the coast of Portugal. Coast Engineering 2000;40:393–409.
[44] Gladkikh V, Tenzer R. A comparison of model estimates of ocean-tide loading displacements in New Zealand. Journal of Geodetic Science 2011;1:94–113.
[45] Otero P, Ruiz-Villarreal M, Peliz A. Variability of river plumes off Northwest Iberia in response to wind events. Journal of Marine Systems 2008;72:238–55.
[46] Pawlowicz R, Beardsley B, Lentz S. Classical tidal harmonic analysis including error estimates in MATLAB using T_TIDE. Computers and Geosciences 2002;28:929–37.
[47] Blanton JO, Lin G, Elston SA. Tidal current asymmetry in shallow estuaries and tidal creeks. Continental Shelf Research 2002;22:1731–43.
[48] Carballo R, Iglesias G, Castro A. Residual circulation in the Ria de Muros (NW Spain): a 3D numerical model study. Journal of Marine Systems 2009;75:116–30.
[49] Ramming HG, Kowalik Z. Numerical modelling of marine hydrodynamics: applications to dynamic physical processes. Elsevier Scientific Publications; 1980.
[50] Dronkers J. Tidal asymmetry and estuarine morphology. Netherlands Journal of Sea Research 1986;20:117–31.
[51] Lalander E, Leijon M. In-stream energy converters in a river – effects on upstream hydropower station. Renewable Energy 2011;36:399–404.
[52] Khan MJ, Iqbal MT, Quaicoe JE. River current energy conversion systems: progress, prospects and challenges. Renewable and Sustainable Energy Reviews 2008;12:2177–93.

USC UNIVERSIDADE DE SANTIAGO DE COMPOSTELA

AUTORITATION OF THE PUBLISHER FOR USING THE ARTICLES IN THIS DOCTORAL THESIS

According with the copyright policies of Elservier, publisher of the three articles reproduced in this Doctoral Thesis (two of them included as part of the Thesis per se, and the third included as additional works), the author can include his articles in the thesis, whether in full or in part, without the need for written authorization.

In this vein, the author of this Doctoral Thesis wants to thank the publisher for allowing to use the material for non-commercial purposes.

Elsevier's copyright policy, available on https://www.elsevier.com/about/policies/copyright/permissions, reads:

As an Elsevier journal author, you have the right to include the article in a thesis or dissertation (provided that this is not to be published commercially) whether in full or in part, subject to proper acknowledgment; see the Copyright page for more information. No written permission from Elsevier is necessary.

This right extends to the posting of your thesis to your university's repository provided that if you include the published journal article, it is embedded in your thesis and not separately downloadable.

USC
UNIVERSIDADE DE SANTIAGO DE COMPOSTELA

USC
UNIVERSIDADE
DE SANTIAGO
DE COMPOSTELA

ACEPTATION OF THE COAUTHORS FOR USING THE ARTICLES IN THIS DOCTORAL THESIS

USC
UNIVERSIDADE
DE SANTIAGO
DE COMPOSTELA

USC
UNIVERSIDADE
DE SANTIAGO
DE COMPOSTELA

ESCOLA DE DOUTORAMENTO
INTERNACIONAL (EDIUS)

Document 1: Authorisation of doctor/non-doctor co-authors for the partial or total reproduction of articles in a monographic Doctoral Thesis with total or partial reproduction of publications

The doctoral thesis completed by *D. Marcos Sánchez Carricoba*, titled *INTEGRAL ANALYSIS OF TIDAL STREAM ENERGY IN RIA DE ORTIGUEIRA*, is presented as **monographic with partial or total reproduction of publications**

The PhD student **DECLARES THAT**:

1. The following co-authors of the articles included in their doctoral thesis are non-doctor co-authors:

Publication Title	
Name and Surnames	**University where thesis is developed**

Add as many lines as necessary

2. The following co-authors of the articles included in the doctoral thesis are doctors:

Publication Title
Energy production from tidal currents in an estuary: A comparative study of floating and bottom-fixed turbines
Name and Surnames
Rodrigo Carballo Sánchez
José Víctor Ramos Castro
Gregorio Iglesias Rodriguez
Publication Title
Floating vs. bottom-fixed turbines for tidal stream energy: A comparative impact assessment
Name and Surnames
Rodrigo Carballo Sánchez

USC
UNIVERSIDADE
DE SANTIAGO
DE COMPOSTELA

ESCOLA DE DOUTORAMENTO
INTERNACIONAL (EDIUS)

José Victor Ramos Castro
Gregorio Iglesias Rodriguez

In Santiago de Compostela, in *May 2022*

Firmado por SANCHEZ CARRICOBA, MARCOS (FIRMA) el día 13/05/2022 con un certificado emitido por AC DNIE 005

Signed: *Electronically by Marcos Sánchez Carricoba*

USC UNIVERSIDADE DE SANTIAGO DE COMPOSTELA

ESCOLA DE DOUTORAMENTO
INTERNACIONAL (EDIUS)

The doctoral thesis completed by *Marcos Sánchez Carricoba*, titled *INTEGRAL ANALYSIS OF TIDAL STREAM ENERGY IN RIA DE ORTIGUEIRA*, is presented as **monographic with total or partial reproduction of publications**.

Mr/Ms: *Gregorio Iglesias Rodriguez*, appears as the co-author of the publication(s) stated below:

- *Energy production from tidal currents in an estuary: A comparative study of floating and bottom-fixed turbines.*

- *Floating vs. bottom-fixed turbines for tidal stream energy: A comparative impact assessment*

And declares his/her commitment to identify clearly and unambiguously the contributions from the PhD student, in the case of presenting these publications as an addition to his/her doctoral thesis.

In *Santiago de Compostela, in May 2022*

Signed: *Gregorio Iglesias Rodríguez (Electronically)*

ESCOLA DE DOUTORAMENTO
INTERNACIONAL (EDIUS)

The doctoral thesis completed by *Marcos Sánchez Carricoba*, titled *INTEGRAL ANALYSIS OF TIDAL STREAM ENERGY IN RIA DE ORTIGUEIRA*, is presented as **monographic with total or partial reproduction of publications**.

Mr/Ms: *Rodrigo Carballo Sánchez*, appears as the co-author of the publication(s) stated below:

- *Energy production from tidal currents in an estuary: A comparative study of floating and bottom-fixed turbines.*

- *Floating vs. bottom-fixed turbines for tidal stream energy: A comparative impact assessment*

And declares his/her commitment to identify clearly and unambiguously the contributions from the PhD student, in the case of presenting these publications as an addition to his/her doctoral thesis.

In *Santiago de Compostela, in May 2022*

Signed: *Rodrigo Carballo Sánchez (Electronically)*

USC
UNIVERSIDADE
DE SANTIAGO
DE COMPOSTELA

ESCOLA DE DOUTORAMENTO
INTERNACIONAL (EDIUS)

The doctoral thesis completed by *Marcos Sánchez Carricoba*, titled *INTEGRAL ANALYSIS OF TIDAL STREAM ENERGY IN RIA DE ORTIGUEIRA*, is presented as **monographic with total or partial reproduction of publications**.

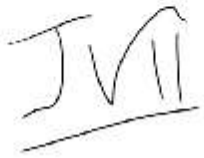
Mr/Ms: *José Victor Ramos Castro*, appears as the co-author of the publication(s) stated below:

- *Energy production from tidal currents in an estuary: A comparative study of floating and bottom-fixed turbines.*

- *Floating vs. bottom-fixed turbines for tidal stream energy: A comparative impact assessment*

And declares his/her commitment to identify clearly and unambiguously the contributions from the PhD student, in the case of presenting these publications as an addition to his/her doctoral thesis.

In *Santiago de Compostela, on 3rd May 2022*



Signed: *José Victor Ramos Castro*

USC UNIVERSIDADE DE SANTIAGO DE COMPOSTELA

USC
UNIVERSIDADE
DE SANTIAGO
DE COMPOSTELA

USC
UNIVERSIDADE
DE SANTIAGO
DE COMPOSTELA

In this Doctoral Thesis several factors involved in the use of tidal energy in the Ría de Ortigueira are studied, including the determination of the most appropriate conversion system, based on the analysis of annual yields and their intra-annual variability, and the impacts derived from energy use on transient and residual circulations. For this purpose, a 3D high-resolution numerical model is implemented for simulating the hydrodynamics of the estuary during different periods, with different combinations of boundary conditions and different tidal power plants. The results achieved allow us to continue advancing in the research and development of renewable energies in Galicia, and more specifically, in marine renewable energies, which have great potential in this territory due to its privileged location.